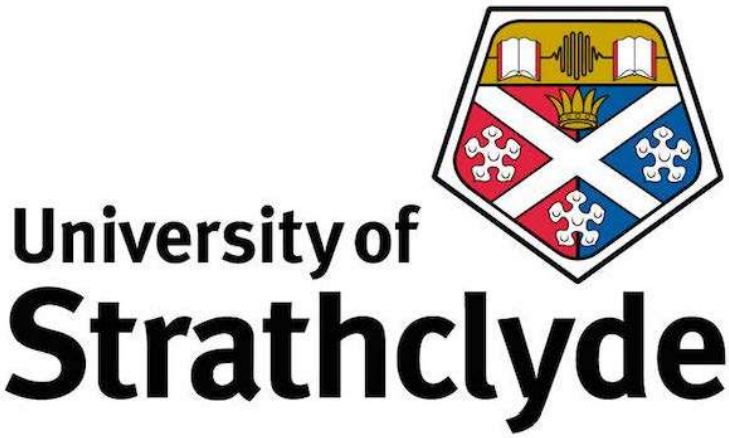

University of Strathclyde

Department of Pure and Applied Chemistry

Detection of Long-chain DNA Fragments and Amplification Products Using Surface Enhanced Raman Spectroscopy and Resonance Raman Spectroscopy

Daniel Macdonald

A thesis submitted to the Department of Pure and Applied Chemistry, University of Strathclyde, in fulfilment of the requirements for the degree of Doctor of Philosophy

2019

This thesis is the result of the author's original research. It has been composed by the author and has not been previously submitted for examination which has led to the award of a degree.

Signed:

Date:

Acknowledgements

Firstly, I would like to thank Professor Duncan Graham and Professor Karen Faulds for providing me with the opportunity to pursue this research project and for all the support, guidance and supervision that you have given along the way. I am also very grateful to Professor Ewen Smith for investing his time in offering Raman tutorials, informative discussions and useful feedback throughout.

I would like to say thank you to the post-docs within the Bionano group (past and present) for helping me to get started, pushing me to get finished, and sharing any knowledge and advice along the pathway to completion. A special thanks to Dr Sam Mabbot for introducing me to the project, Dr Stacey Laing for her resonance Raman advice, and to Dr Will Tipping and Dr Sian Sloan-Dennison for their thesis feedback and support towards the finishing line.

I'd also like to thank everybody within the Bionano group for the good times and memories over the past few years. I am very happy to have met you all and wish you all the best with everything to come. I am especially thankful for having the opportunity to share the duration of the PhD experience with Kirsty C, Anastasia, Amy, Kirsty M and Jenny who have been there from beginning to end and have become my extended PhD family since. A special mention to Dr Pietro Gancitano as well for your friendship and the invitation for a memorable trip to meet the Gancitanos in Sicily!

Most importantly, I would like to thank my mum, gran and aunt for all your words of strength and support over the years and for helping me to become the person I am today. Finally, I would like to thank Daniela and my therapy dog Kai for being with me every step of the way! I am truly grateful for you all.

Abstract

The aim of this research was to progress the application of surface enhanced Raman spectroscopy (SERS) and resonance Raman spectroscopy for the detection of long-chain DNA fragments and amplification products.

The use of SERS for the detection of DNA has significant potential in terms of sensitivity and multiplex target detection from nanoparticles. Current methods are usually performed with short chain, synthetic DNA fragments or require additional separation steps for the detection of longer chain DNA fragments. An integrated method for the rapid and sensitive detection of long-chain DNA fragments (≥ 100-base) with minimal preparation and separation steps was demonstrated. Key to this was the DNA sequence-specific assembly of silver nanoparticles labelled with a Raman tag to provide an enhanced signal from the tag and hence molecular recognition of the target DNA. Effective detection of long-chain DNA was achieved with head-to-head probes and by adding polyethylene glycol 10000 to the hybridisation buffer. This gave a 34-fold discriminatory enhancement factor when applied to a synthetic target. A structured approach toward maximising hybridisation procedures and SERS response has been described, followed by an initial demonstration of SERS detection of a single-stranded DNA target amplified by asymmetric PCR which was used without further separation. This has implications for future developments in using SERS for DNA detection due to the new-found ability to integrate SERS with asymmetric PCR.

Furthermore, an alternative strategy for the detection of a recombinase polymerase amplification (RPA) product was demonstrated using tailed primers, an enzyme-linked reporter conjugate and resonance Raman spectroscopy. The amplification of DNA by RPA could be achieved within 20 minutes and a colorimetric change could be detected using resonance Raman spectroscopy with discriminatory value at the lowest concentration of 100 aM. This demonstrated the first application of resonance Raman spectroscopy for the detection of an RPA amplification product and indicates

significant potential for the integration of resonance Raman spectroscopy with an emerging rapid isothermal nucleic acid amplification technique.

The research described here has successfully demonstrated the sensitive and rapid detection of long-chain DNA fragments and amplification products using both SERS and resonance Raman spectroscopy. Furthermore, the methods presented require minimal sample preparation steps for the detection of the long-chain DNA fragments and amplification products. This indicates significant progression from current literature which commonly describes the detection of short, synthetic DNA fragments or utilises methods requiring complex physical separation or purification steps for the detection of longer DNA fragments. The findings therefore advance the potential for the application of Raman spectroscopy for the detection of biologically relevant nucleic acid target sequences, and it hoped that this will encourage further development of Raman spectroscopy for the application of DNA detection in future.

Abbreviations

A	Adenine
AgNPs	Silver nanoparticles
AuNPs	Gold nanoparticles
Bp	Base-pair
C	Cytosine
DMSO	Dimethyl sulfoxide
DNA	Deoxyribonucleic acid
dNTPs	Deoxynucleotide triphosphates
dsDNA	Double-stranded deoxyribonucleic acid
ELISA	Enzyme-linked immunosorbent assay
G	Guanine
HEG	Hexaethylene glycol
HRP	Horse radish peroxidase
LATE-PCR	Linear-after-the-exponential polymerase chain reaction
LSPR	Localised surface plasmon resonance
MGITC	Malachite green isothiocyanate
$MgCl_2$	Magnesium chloride
miRNA	microRNA
NaCl	Sodium chloride
NC	Non-complementary
NPs	Nanoparticles
NTC	No template control
PBS	Phosphate buffered saline
PCR	Polymerase chain reaction
PEG	Polyethylene glycol
RNA	Ribonucleic acid

rRNA	Ribosomal ribonucleic acid
RPA	Recombinase polymerase amplification
SERS	Surface enhanced Raman spectroscopy
ssDNA	Single-stranded deoxyribonucleic acid
T	Thymine
T_m	Melting temperature
TMB	3,3’,5,5’-Tetramethylbenzidine
UV-Vis	Ultraviolet-visible

Contents

1 Introduction

1.1 The Properties of Deoxyribonucleic Acid (DNA)

1.1.1 A Brief Introduction to DNA

Deoxyribonucleic acid (DNA) is a fundamental biochemical component of all cellular life forms. DNA contains the hereditary genetic information required for the synthesis of proteins that perform the cellular processes required to sustain life. DNA is typically contained within the nucleus of the cell, where it exists in long, condensed strands referred to as chromosomes. The chromosomes may be further sub-divided into shorter sections called genes which provide a blueprint for the expression of proteins. The fundamental role of DNA is to encode for the expression of proteins, which occurs via two steps; transcription into mRNA, and translation of mRNA into proteins.

1.1.2 A Short History of the Discovery of DNA

The discovery of the structure of DNA is widely accredited to the findings of Watson and Crick who first described the secondary structure of the DNA double-helix in 1953.[1] Although Watson and Crick were the first to report the secondary structure of DNA, the DNA molecule was first identified by Miescher in 1869.[2] Miescher described the presence of a molecule named "nuclein" within the nucleus of human white blood cells, noting the unusually high phosphorus content and resistance to proteolysis that distinguished this molecule from the proteins within the cell nucleus. In 1909, Leven described the composition of DNA, identifying that four nucleotides; adenine, cytosine, guanine, and thymine, existed in the order of a base, sugar and phosphate group.[3] In 1950, Chagraff observed that DNA contained varying proportions of the DNA bases, although adenine and thymine, and cytosine and guanine were always present in equal proportions.[4] This is referred to as "Chagraff's rule" and the significance of this observation in relation to the structure of DNA would only be realised at a later stage. Franklin and Gosling provided a key breakthrough for the resolution of the DNA structure in 1953 with the publication of an x-ray

crystallographic image of DNA that was suggestive of a regularly repeating helical conformation (**Figure 1.1**).[5]

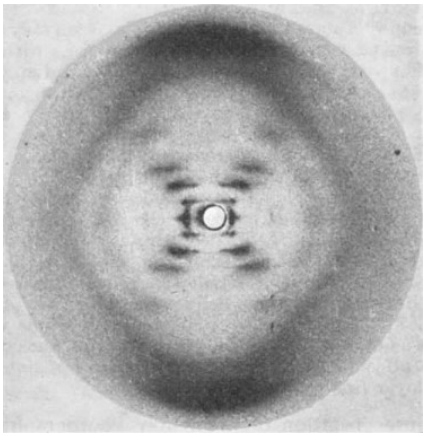

Figure 1.1. *Franklin and Gosling's x-ray crystallographic image of DNA in the helical form. Reprinted from FRANKLIN, R. E.; GOSLING, R. G. Molecular Configuration in Sodium Thymonucleate. Nature 1953, 171 (4356), 740–741, with permission from Springer Nature © 1953.*

Watson and Crick subsequently connected Chagraff's base association rule with Franklin and Gosling's crystal structural image to solve and describe the first account of the DNA helical secondary structure.

1.1.3 Primary Structure of DNA

The primary structure of DNA is composed of four monomer nitrogenous bases including the fused ring purines; adenine (A) and guanine (G), and the single ring pyrimidines; cytosine (C) and thymine (T). Each base is attached to a deoxyribose pentose sugar via a covalent glycosidic bond. A base linked to a sugar is referred to as a nucleoside. A phosphate group is attached to the opposing side of the sugar via a covalent ester bond. A base linked to both a sugar and a phosphate group is referred to as a nucleotide. The chain forms of each nucleotide are shown in **Figure 1.2**.

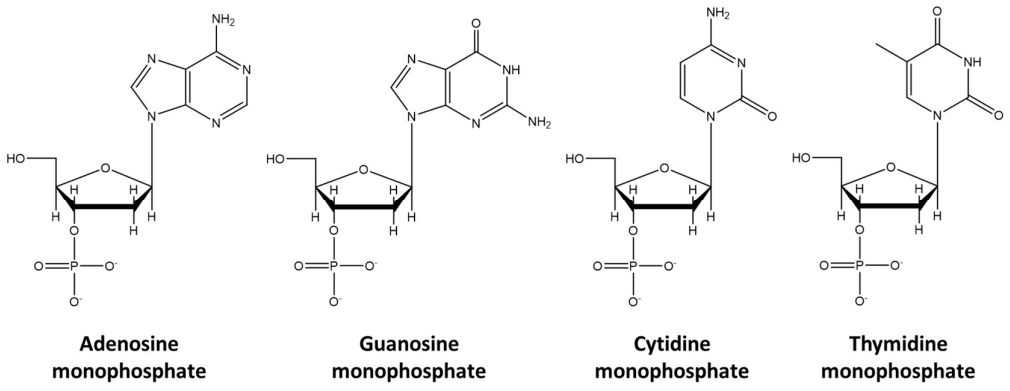

***Figure 1.2**. Molecular structures of each of the DNA nucleotides in their chain form.*

These building blocks are assembled as a linear polymeric strand via a series of phosphodiester bonds, and the polymeric form of repeating monomers is referred to as an oligonucleotide.

1.1.4 Secondary Structure of DNA

The secondary structure of DNA is composed of two strands that are combined in the double-helix formation (**Figure 1.3**).[6]

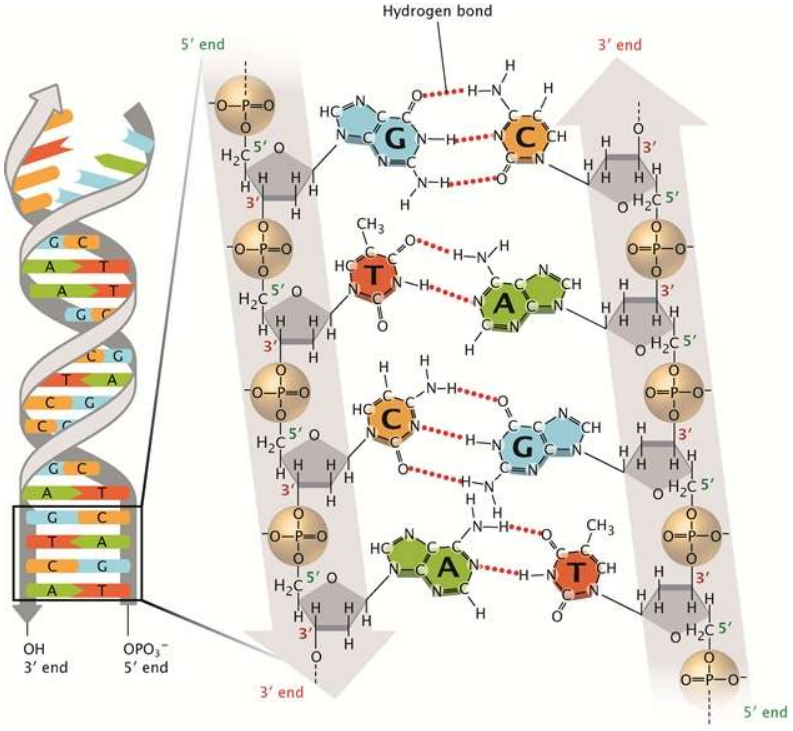

***Figure 1.3.** Schematic representation of the double-helix structure. Reprinted from Nature Scitable with permission from Springer Nature (open access).*

The negatively charged sugar-phosphate backbone is positioned on the outside of the molecule, and the hydrophobic bases are stacked within the intertwined strands of DNA that form the double-helix. This structure is supported by both the base-stacking interactions and the formation of hydrogen bonds between the bases contained within the DNA duplex. The adenine bases pair with the thymine bases via two hydrogen bond interactions, and the cytosine bases pair with the guanine bases via three hydrogen bond interactions. This is referred to as base-pairing and the specificity of these base-pair (bp) interactions explains the mechanism by which one strand can provide a template for the replication of the partner strand. The base-pairing specificity of two strands of DNA is referred to as sequence complementarity.

The two strands of DNA that form the duplex structure of the helix exist in an antiparallel orientation. Each strand has opposite polarity as they run in opposite directions. In simplified terms, a single strand of DNA has two opposing ends referred to as the 5’ and 3’ ends. At the 5’ end exists the primary hydroxyl group which may be free or may be joined to a 5’ phosphate group. At the 3’ end exists the secondary free hydroxyl group. Neither the 5’ or 3’ ends are linked to further nucleotides and these are commonly referred to as the 5’ and 3’ ends of the DNA strand. As the base-pairs form between two strands of DNA in a helix, the 5’ and 3’ ends of each strand are positioned at opposite ends of the duplex structure. It is conventional to describe a DNA strand in the 5’→3’ direction in accordance with direction of DNA replication.

1.1.5 DNA Stability

The stability of the DNA duplex is primarily founded upon the hydrogen bond formations and base-stacking interactions that support the integrity of the helical structure.[7] These are weak, non-covalent interactions and the two strands may be reversibly dissociated. This is fundamental for the replication of DNA *in vivo* and *in vitro*. The dissociation of the double-stranded DNA (dsDNA) duplex is typically performed in the laboratory by heating DNA to approximately 95 °C. This breaks the hydrogen bonds and disrupts the base-stacking interactions, thus producing two strands of single-stranded DNA (ssDNA). The process of dissociation is referred to as

"melting" and occurs over a narrow temperature range. The point at which 50 % of the DNA duplex has dissociated is referred to as the melting temperature (T_m). The unstacked DNA bases of the ssDNA will absorb more UV light at 260 nm than the stacked bases and this effect is called hyperchromism. As the sample is cooled to an ambient temperature, the dissociated ssDNA strands will spontaneously re-associate to reform the dsDNA duplex via the complementary base-pairing interactions. This process is known as hybridisation or annealing. The stacked bases of dsDNA will absorb less UV light at 260 nm than the unstacked bases of ssDNA and this effect is called hypochromism. UV-Vis extinction spectroscopy may be applied for melting curve analysis to identify the associated stability of the DNA melting transitions over a temperature gradient. Upon dissociation, the absorbance value will increase, and upon re-association, the absorbance value will decrease (**Figure 1.4**).[8]

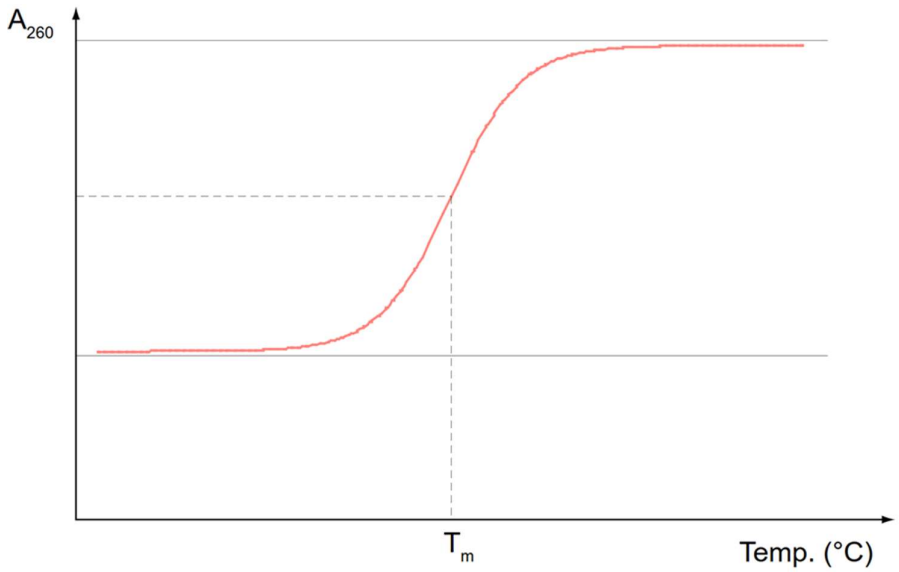

Figure 1.4. *A schematic representation of a DNA melting curve. The melting temperature at which 50 % of the DNA has dissociated is indicated by a dotted line. Reprinted from the Wikimedia Commons media repository with permission from the original creator - Fdardel (CC BY-SA 3.0).*

The melting temperature of DNA is used as a general indicator of the stability of any given DNA duplex structure. There are several factors which can influence the stability of the DNA secondary structure. These include the buffer salt composition,

the length of the DNA and the % GC content which refers to the number of guanine-cytosine base-pairs.[9,10]

Salts are required to neutralise the negative charge associated with the phosphate groups of the DNA backbone and monovalent or divalent cations including Na^+, K^+ or Mg^{2+} are commonly added to buffer solutions to induce hybridisation of complementary DNA sequences. Increasing the concentration of cations is associated with increased melting temperatures and enhanced hybridisation kinetics. Divalent cations such as Mg^{2+} provide a greater degree of stability to the duplex structure as compared to monovalent cations such as Na^+. For instance, as a general empirical rule of thumb, ~ 10 mM Mg^{2+} will provide a comparable degree of duplex stability as ~ 1M of Na^+ ions, although this will be dependent on the properties of the nucleic acid.[11] If no cations are present, the DNA duplex stability will be compromised, and hybridisation will not occur as the negatively charged sugar-phosphate backbone will not be sufficiently neutralised to overcome electrostatic repulsions that prevent duplex formation.

Additionally, as the length of a DNA duplex increases, the associated melting temperature will also increase as the cumulative effects of base-stacking and hydrogen bonding further enhance the dsDNA duplex stability.

Finally, the % GC content is an important consideration. The stability of dsDNA will increase as the % GC content increases. This is often attributed to the presence of the three hydrogen bonds that form between GC base-pairs, whereas only two hydrogen bonds form between AT base-pairs. It is a misconception that the greater number of hydrogen bonds increases duplex stability. The increased melting temperature associated with greater GC content is provided by the greater base-stacking contributions of the GC base-pairs.[7]

1.2 DNA Amplification Techniques

1.2.1 A Brief Introduction to the Polymerase Chain Reaction (PCR)

A primary challenge related to the analysis of DNA is the low concentration of the analyte within biological samples. The polymerase chain reaction (PCR) is an exceptionally powerful technique for the enzymatic amplification of a target DNA sequence *in vitro.* PCR utilises temperature cycles to control two central reactions consisting of reversible DNA melting and enzyme-driven DNA replication. Upon each thermal cycle, the DNA target sequence is replicated by the polymerase enzyme present within the reaction mix. The PCR product is amplified exponentially as the target concentration doubles upon each cycle of replication and millions of copies of the target may be synthesised within a couple of hours of thermal cycling from just a single copy of template DNA.

PCR was first devised by Kary Mullis in the 1980s whilst employed at the Cetus corporation.[12] Mullis considered the potential of applying two oligonucleotide primer sequences and a polymerase enzyme for the exponential amplification of DNA. This was inspired by the research of Kronberg who first described the enzymatic synthesis of DNA using a crude enzyme extract from *E. coli* bacteria in 1956.[13] Kronberg later reported the isolation of the *E. coli* polymerase enzyme and conditions required for the *in vitro* replication of DNA.[14, 15] The polymerase enzyme extended a short oligonucleotide "primer", with the addition of a nucleotide to the 3' end of the primer sequence. The reaction only occurred if the primer was hybridised to a complementary strand of DNA in a solution containing adenine, cytosine, thymine and guanine deoxynucleotide triphosphates (dNTPs) that served as the building blocks for replication of the template strand. These early observations described many of the key components that are essential for the application of PCR.

Mullis built upon these foundations, with the recognition that the application of two oligonucleotide primers would provide the capacity for the exponential replication of DNA, as each primer would replicate the opposing complementary strand of DNA, thus doubling the available template concentration for the next round of

amplification. The first account of the application of PCR was published by Mullis and co-workers in 1985 for the detection of a β-globin gene sequence related to sickle cell anaemia.[16] The method defined the requirement for thermal cycling upon each amplification step. The samples were heated to 95 °C to denature the dsDNA template and cooled to 30 °C to allow the primers to hybridise to the complementary target sequence. The polymerase was then added, and the replication of the template strand occurred as the primer sequence was elongated by the polymerase. This cycle was repeated numerous times and the exponential amplification of the β-globin gene sequence was achieved. The initial method was laborious as the samples had to be manually transferred between heat blocks upon heating and cooling, and the polymerase had to be added for each cycle as the polymerase was denatured upon application of the 95 °C heat step.

Two significant advances led to the automation of the PCR reaction. Mullis originally utilised the same polymerase that was first isolated from *E. coli* by Kronberg. This was later exchanged for a thermostable polymerase that was first isolated from *Thermus aquaticus* in 1976.[17] *Thermus aquaticus* is an extremophile bacteria native to the hot springs of Yellowstone national park. The polymerase isolated from this bacterium is stable at high temperatures which was a key attribute for advancement of the PCR reaction. This polymerase is now commonly referred to as *Taq* polymerase. In 1988, Mullis and co-workers published a PCR method that exploited the use of *Taq* polymerase.[17] The reaction could be performed at higher temperature, increasing the amplification sensitivity and specificity which allowed for the first demonstration of single molecule detection using PCR. The second advancement came with the advent of the thermocycler. The automated programming of the thermal cycle which was combined with the heat stability of the *Taq* polymerase which removed the necessity for human intervention and paved the way for the wide-scale application of PCR.

1.2.2 The Principles of PCR

The PCR reaction mix consists of several key components. These include; a) a buffer solution containing monovalent ions required to neutralise the charge repulsions

associated with the negatively charged backbone of the DNA b) a DNA template strand for replication c) two primer sequences that are complementary to the opposing strands of the template to initiate the replication process d) each of the four deoxyribonucleotide triphosphates (dNTPs) that provide the building blocks for synthesis of a new template strand e) *Taq* polymerase for the enzymatic polymerisation of the dNTPs during replication f) magnesium ions which are an essential cofactor for the activation of the polymerase activity.

The amplification of DNA using PCR requires a thermal cycle to control the process of reversible DNA melting and enzymatic amplification of the target sequence. This generally consists of three steps. The reaction proceeds with an initial denaturation step to allow the dsDNA template strands to dissociate. This is typically performed at 95 – 98 °C. The reaction is then cooled to a temperature within the range of 45 – 65 °C to allow the primers to anneal to their complementary target strand. The precise temperature is defined by the salt concentration, primer sequence length and % GC content of the primer sequences. Finally, the temperature is increased to approximately 70 °C which reflects the optimal temperature for enzymatic replication of the template sequence. This cycle is repeated multiple times to exponentially amplify the target sequence. A simplified depiction of the PCR process is shown in **Figure 1.5**.[18]

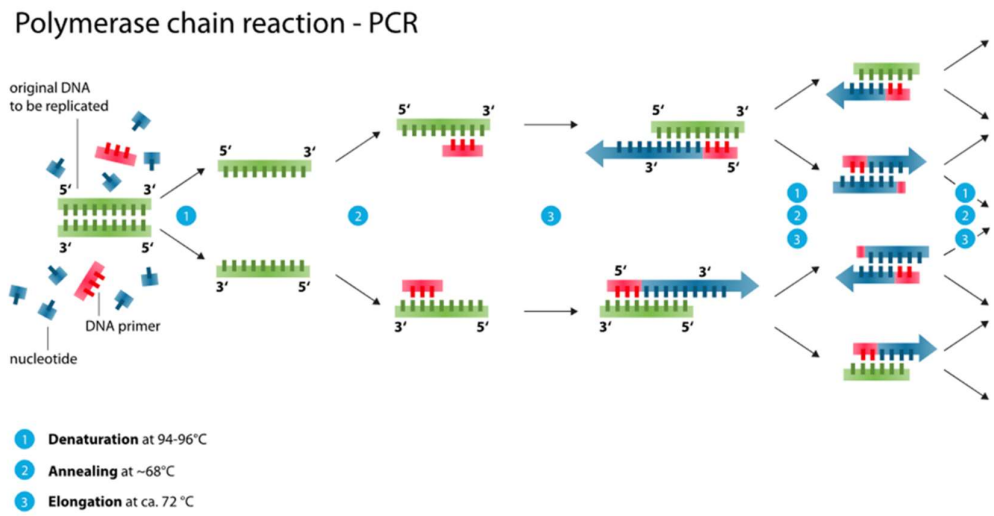

Figure 1.5 *The basic principle of the polymerase chain reaction for the amplification of DNA. Reprinted from the Wikimedia Commons media repository with permission from the original creator - Enzoklop (CC BY-SA 3.0).*

1.2.3 A Brief Introduction to Isothermal Amplification Techniques

PCR has been widely accepted as an effective molecular diagnostic tool for application in both research and clinical settings. However, a major constraint associated with this technique is the requirement for a benchtop thermocycler. This equipment is expensive and bulky, thus requiring laboratory space and the necessity for a mains power supply to operate the energy intensive thermal cycle. Furthermore, the equipment requires a trained operator to perform the technique effectively. Therefore, the application of PCR has been constrained to operation within centralised laboratories with the resources available to acquire the equipment and skilled operators to perform the procedure.

PCR was the first example of a DNA amplification technique and remains the most commonly utilised method, although many alternative isothermal amplification techniques have since been developed. Isothermal amplifications generally operate at a constant temperature, thus eliminating the requirement for a thermocycler. This is significantly advantageous for application in resource-limited settings or at the point-of-need for detection and diagnosis of disease. Therefore, molecular diagnostic

testing may no longer be limited to large, centralised laboratories with the significant resources available to apply such techniques.

There are many examples of isothermal amplification techniques, each operating based upon fundamentally different principles. Examples of some of the most commonly described isothermal amplification techniques include; nucleic acid sequence based amplification (NASBA), transcription mediated amplification (TMA), multiple displacement amplification (MDA), loop-mediated amplification (LAMP), helicase-dependant amplification (HDA), rolling circle amplification (RCA), signal-mediated amplification (SMART), recombinase polymerase amplification (RPA), self-sustained sequence replication (3SR), ramification amplification (RAM) and strand displacement amplification (SDA).[19], [20], [21], [22], [23], [24], [25], [26], [27], [28], [29] Evidently, the development of isothermal amplification techniques is a research field of extensive interest. The general mechanism of the DNA dissociation event (temperature vs. enzyme driven) that drives these reactions, the temperature of operation and the associated reaction times required are listed for comparison in **Table 1.1**.[30]

Table 1.1. *Comparison of isothermal amplification DNA dissociation mechanisms, temperature and times associated with the reactions. Adapted from James, A.; Macdonald, J. Recombinase Polymerase Amplification: Emergence as a Critical Molecular Technology for Rapid, Low-Resource Diagnostics. Expert Rev. Mol. Diagn. 2015, 15 (11), 1475–1489, with permission from Taylor and Francis © 2015.*

Isothermal Technique	DNA Dissociation Mechanism	Estimated Reaction Temperature	Estimated Reaction Time
NASBA	Temperature	41 °C	1.5 h
TMA	Temperature	37 °C	1 – 2 h
MDA	Enzymatic	30 °C	8 – 10 h
LAMP	Enzymatic	65 °C	< 1 h
HDA	Enzymatic	37 °C	2 h
RCA	Enzymatic	23 °C	1 h
SMART	Temperature	41 °C	2 h
RPA	Enzymatic	37 – 42 °C	10 minutes
3SR	Temperature	37 °C	< 1 h
RAM	Enzymatic	35 °C	1 h
SDA	Temperature	37 °C	2 h

Many of these isothermal techniques have removed the necessity of a thermocycler for operation and have advanced the potential for applying molecular diagnostics in resource limited settings or at the point-of-need. However, the uptake of these isothermal techniques has not yet been fully realised. This is generally due to complex reaction mechanisms that prevent practical application, or limits of detection that have not yet matched the sensitivity of PCR.[31] A full and comprehensive review of the mechanisms involved, and the sensitivities achieved is beyond the scope of this report, however, Zhao et al., have recently published an extensive review detailing the nature of the mechanisms that underlie many of these isothermal amplification techniques and the relative sensitivities that have been attained.[31]

This investigation will further focus on the recombinase polymerase amplification (RPA) technique. The RPA technique was first introduced by Piepenburg et al., in

2006.[26] The findings demonstrated that DNA could be amplified from just 10 copy numbers of a gene target sequence within 30 minutes using the RPA isothermal amplification technique. This was approximately equivalent to the sensitivity that may be attained by PCR, and significantly quicker than PCR which generally takes 1-2 hours for amplification. Furthermore, the amplification occurred at a constant temperature of 37 °C which indicated that the reaction may be implemented without the requirement of a thermocycler. The RPA technique displays the inherent sensitivity to match that of PCR, unlike many other isothermal techniques which are often less sensitive.[31] Furthermore, amplification using the RPA technique is significantly faster than alternative isothermal techniques with detectable levels of amplification products produced in less than 30 minutes.[26], [30] These attributes have distinguished the RPA technique as a potential and emergent successor to PCR for the molecular diagnosis of disease, and will likely prove to be key for the future application of molecular diagnostics at the point-of-need or in resource limited settings.

1.2.4 The Principles of RPA

The RPA reaction mechanism differs significantly from the PCR reaction, which typically applies thermocycling conditions to reversibly control the melting of the dsDNA template during replication. More specifically, amplification by RPA is enzyme-driven rather than temperature driven and is founded upon a complex reaction mix consisting of several components. Many of these are the same as those of the PCR reaction including; a) a buffer solution containing monovalent ions required to neutralise the charge repulsions associated with the negatively charged backbone of the DNA b) a DNA template strand for replication c) two primer sequences that are complementary to the opposing strands of the template to initiate the replication process d) each of the four deoxyribonucleotide triphosphates (dNTPs) that provide the building blocks for synthesis of a new template strand e) a polymerase for the enzymatic polymerisation of the dNTPs during replication f) magnesium ions which are an essential cofactor for the activation of the polymerase activity. Insofar, the components listed are the same as those required for

amplification by PCR. However, there are several additional components required for the enzymatic amplification by RPA.

The RPA reaction is reflective of an *in vitro* adaption of the homologous recombination process that occurs in the cell. This process is reliant upon enzymes and associated proteins that catalyse the reaction and an adenosine triphosphate (ATP) based energy-supply system to drive the reaction. These additional reaction components include; a) a recombinase protein (T4 UvsX) b) a recombinase protein loading factor (T4 UvsY) c) single-stranded binding proteins (T4 gp32) d) ATP e) creatine kinase f) creatine phosphate.

The roles that the reaction proteins perform are not entirely distinct, but rather serve to complement each other's function within the recombination process. In brief, the recombinase protein forms a complex with the loading factor protein, which in turn binds to the primers within the reaction mix. This nucleoprotein complex is enzymatically capable of scanning and locating a region of sequence complementarity within the dsDNA template strand, unwinding the dsDNA and displacing the duplex to form a localised D-loop structure. The primer contained within the complex hybridises to its complementary region within one of the strands, whereas the opposing strand is stabilised by the single-stranded binding proteins (SSB) which act cooperatively to prevent interaction with the primer-bound template. As the primer is hybridised, the polymerase may then act to displace the remaining duplex structure as it replicates the template strand. The recombinase protein and loading factor are then released to repeat the process. The enzymatic process is driven by the energy released from the hydrolysis of ATP. The ATP energy source may be replenished by the transfer of phosphate from creatine phosphate, as catalysed by creatine kinase. The principles of this reaction are shown in **Figure 1.6**.[32]

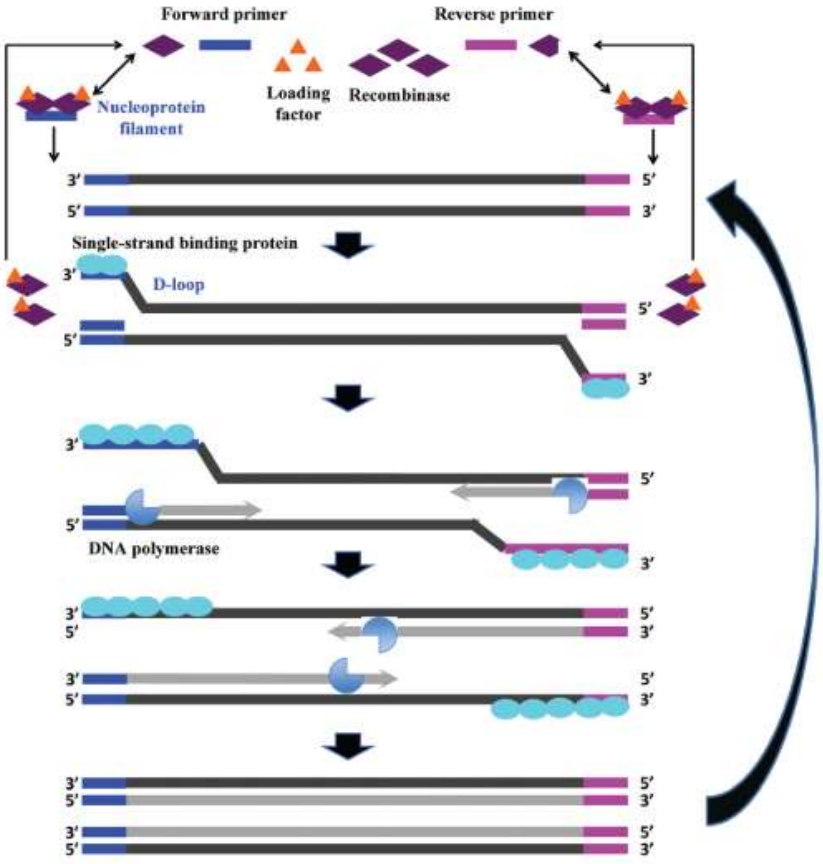

Figure 1.6 *The basic principle of the recombinase polymerase amplification reaction for the amplification of DNA. Reprinted from Li, J.; Macdonald, J.; von Stetten, F. Review: A Comprehensive Summary of a Decade Development of the Recombinase Polymerase Amplification. Analyst 2019, 144 (1), 31–67 with permission from the Royal Society of Chemistry (CC BY 3.0).*

This work emphasises the development of novel Raman spectroscopy-based methods for the detection of long-chain nucleic acids and amplification products that have been synthesised using asymmetric PCR and RPA amplification. A surface-enhanced Raman spectroscopy (SERS) method for the detection of an asymmetric PCR product upon addition of the product to DNA functionalised and dye-coded AgNPs is described in detail. Furthermore, a resonance Raman method for the detection of an RPA amplification product is also described. Therefore, a brief introduction to nanoparticles and Raman spectroscopy will be made in the following section.

1.3 Nanoparticles

1.3.1 A Brief Introduction to Nanoparticles

Nanoparticles (NPs) are typically defined as particles of any shape with one or more dimension within the range of 1-100 nm. NPs are commonly synthesised from metallic elements such as gold, silver and copper. Many of the metallic elements may be used for the synthesis of NPs; however, gold, silver and copper are most commonly utilised due to their distinct colouration which arises due to their interaction with light within the visible range and their associated stabilities.[33] Metallic NPs display unique physical and optical properties as compared to the respective bulk materials. The optical properties associated with NPs are governed by the underlying physical properties including the constituent material, size, shape and polydispersity. These physical properties may be altered for specific applications.

Historically, the distinct optical properties of metallic NPs have been exploited for the application of staining glass. The Romans developed methods to stain glass with the inclusion of small amounts of gold and silver NPs, however the processes by which this was achieved are generally unknown. Perhaps the most famous example is the Lycurgus cup dating from the 4th century (**Figure 1.7**).[34]

Figure 1.7. *Image of the Lycurgus cup containing traces of gold and silver nanoparticles. The cup appears green as light is reflected (left) and red as light is transmitted (right). Reprinted from the British Museum online image gallery with permission from the British Museum (CC BY-NC-SA 4.0).*

The Lycurgus cup contains gold and silver NPs dispersed throughout the glass and appears green as light is reflected from the glass, and red as light is transmitted through the glass.

In 1857, Michael Faraday reported the first scientific account of the synthesis of AuNPs by the aqueous reduction of chloroaurate ($AuCl_4^-$) with phosphorus.[35] Faraday investigated the optical properties of the AuNPs, describing the characteristic ruby red colouration that developed as the AuNPs were formed in solution and the transition to a violet-blue colouration in the presence of salt. Faraday made many shrewd observations, concluding that the ruby red colouration was due to the presence of gold in a "finely divided state" and suggesting that the change in colour to a violet-blue colouration upon addition of salt was due to a "change of the relation of the surface of the particles to the surrounding medium", thus causing the aggregation of the particles in solution. The seminal findings described by Faraday are considered by many to be the birth of nanoscience. Numerous reports have since been published describing a wide variety of methods for the chemical synthesis of NPs in a range of sizes and shapes.

1.3.2 Synthesis of Nanoparticles

NPs are most commonly synthesised by the chemical reduction of dilute metal precursor salts in solution. As the reaction proceeds, the metal ions are reduced to their neutral atomic state. For instance, AuNPs are formed upon the reduction of Au^{3+} to Au^0, and AgNPs are formed upon the reduction of Ag^+ to Ag^0.

A commonly employed method for the synthesis of AuNPs involves the reduction of chloroauric acid ($HAuCl_4$) with citrate. Citrate acts as both a reducing agent and a capping agent for the stabilisation of the AuNPs upon synthesis.

The synthesis of AuNPs by citrate reduction occurs in a three-step process consisting of nucleation, growth and coagulation. Nucleation occurs as the gold ions are coordinated in complexation with the citrate reducing/capping agent. This is followed by reduction to metallic gold, yielding the nuclei which provide a template for further growth. Growth occurs as additional gold particles are added to pre-existing nuclei,

thus increasing the size. The growth process stops when all the gold has reacted. Finally, coagulation will occur as multiple nuclei join to form larger particles. The control of the coagulation stage determines the size, structure and distribution of the NPs in solution. Excess coagulation will compromise the stability of NPs.

The citrate reduction method for the synthesis of AuNPs was first described by Turkevich in 1951.[36] Turkevich described the reduction of chloroauric acid ($HAuCl_4$) with the addition of sodium citrate for the synthesis of AuNPs that were ~ 20 nm in size. The method is relatively simple; the $HAuCl_4$ is dissolved in solution at 100 °C, and sodium citrate solution is added with vigorous stirring. The solution is then left to cool upon the development of the distinctive red colouration associated with AuNPs.

In 1973, Frens reported that a range of AuNP sizes could be synthesised by controlling the molar ratio of gold and citrate salts.[37] This method produced monodispersed AuNPs within the size range of 16-147 nm as a function of the gold/citrate ratio. Frens identified that a reduction in the concentration of citrate could be applied to control the processes of nucleation and growth, thus producing larger AuNPs. This method is commonly applied for the size-dependant synthesis of AuNPs.

The citrate reduction method has also been described for the synthesis of AgNPs. This method was first reported by Lee and Meisel in 1982.[38] Lee and Meisel described the reduction of silver nitrate ($AgNO_3$) with the addition of sodium citrate for the synthesis of AgNPs. The method is comparable to the citrate reduction of AuNPs; the $AgNO_3$ is dissolved in solution at 100 °C, and sodium citrate solution is added with vigorous stirring. The solution is then left to cool upon the development of the distinctive yellow colouration associated with AgNPs. Whilst the citrate reduction method reliably synthesises AuNPs of a spherical nature, the citrate reduction method is associated with the synthesis of AgNPs that can vary widely in both size and shape.[39] This may affect the reproducibility of bulk analysis performed with the AgNPs and cause instability during the conjugation of the AgNPs with biomolecules. Therefore, alternative methods are widely applied.

Numerous alternative methods have been since been described for the synthesis of AgNPs using a variety of reducing agents. These include the borohydride, EDTA and hydroxylamine reduction methods.[40, 41, 42] The hydroxylamine method is particularly favourable as it is fast, simple, can be performed at room temperature and the synthesised AgNPs were found be monodisperse with SERS enhancement properties that were considered equivalent to that of the citrate reduced AgNPs.[42]

1.3.3 Localised Surface Plasmon Resonance

AuNPs and AgNPs display intense plasmon bands within the UV-Vis extinction spectrum that are not present in the spectrum of the bulk material. The characteristic colourations of AuNPs or AgNPs and their associated plasmon bands within the UV-Vis extinction spectrum are due to the phenomenon of localised surface plasmon resonance (LSPR) (**Figure 1.8**).[43]

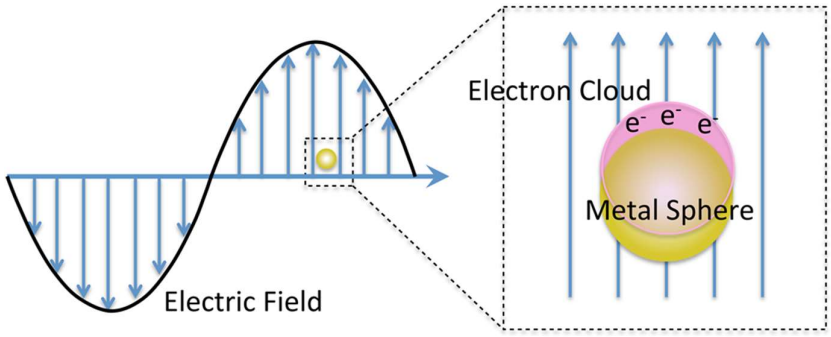

Figure 1.8. *Schematic depicting the localised surface plasmon resonance of a nanoparticle in an oscillating electric field. Reprinted from the Wikimedia Commons media repository with permission from the original creator - Tem5psu (CC BY-SA 3.0).*

The LSPR phenomenon was first described by Gustav Mie in 1908, who identified that the plasmon band of metallic NPs was due to the collective dipole oscillations of free electrons in the conductance band.[44] LSPR occurs when the frequency of the incident light is in resonance with the oscillations of the conduction electrons that are loosely held upon the surface of the NPs. LSPR has two major effects including significant increases in the absorption and scattering (extinction) properties of the NPs and an enhancement of the electromagnetic field upon the surface of the NPs.

The resonant oscillation of electrons generates large increases in the absorption and scattering of light from the NPs as observable by the wavelength-selective plasmon band within the UV-Vis extinction spectrum. The intensity and the peak location of the plasmon band is highly dependent on various factors such as the nanoparticle material, size, shape, interparticle distance and dielectric constant of the surrounding medium. Various strategies have been proposed for the application of high-sensitivity chemical and biological sensors in account of the relationship between the LSPR signal and these influencing factors (**Figure 1.9**).[45]

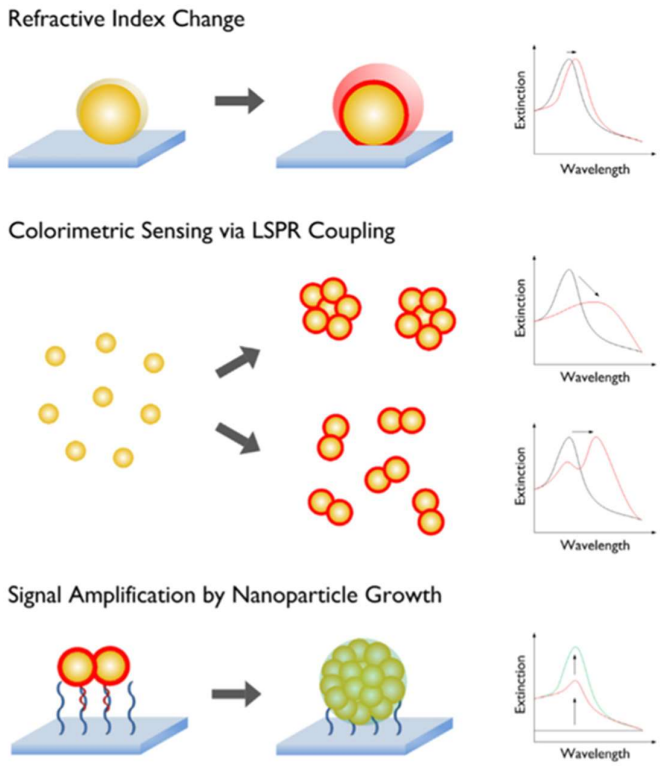

Figure 1.9. *Strategies for analyte sensing based upon the extinction properties of nanoparticles including refractive index changes (top), LSPR coupling (middle) and signal amplification by nanoparticle growth (bottom). Reprinted from Guo, L.; Jackman, J. A.; Yang, H.-H.; Chen, P.; Cho, N.-J.; Kim, D.-H. Strategies for Enhancing the Sensitivity of Plasmonic Nanosensors. Nano Today 2015, 10 (2), 213–239, with permission from Elsevier (CC BY NC ND).*

These detection strategies are often attained by attaching molecular recognition elements such as chemical or biological ligands upon the nanoparticle surface, thereby conferring specificity to the analyte of interest.

Small changes in the dielectric constant of the surrounding medium due to adsorption or binding of the ligands upon the nanoparticle surface may induce measurable redshifts in the extinction spectrum. This is indicative of the presence of an analyte of interest, although the sensitivity of this strategy may be constrained by the limited magnitude of the observable redshift. Therefore, alternative strategies such as LSPR-coupling have been applied. This typically involves the molecular recognition and cross-linking of NPs upon addition of the molecule of interest, thereby decreasing the interparticle distance and inducing near-field coupling. Consequently, the electromagnetic field within the junctions between the coupled NPs is strongly enhanced. LSPR-coupling may be confirmed by a significant redshift and peak dampening in the extinction spectrum and will produce a distinct colour change that is often observable to the naked-eye. A further strategy for enhancing the sensitivity of LSPR sensors involves the amplification of the plasmon signal by nanoparticle growth. This involved a secondary growth step of NPs that have been captured upon a surface following binding to the analyte of interest. This may increase the magnitude of the extinction properties associated with NPs, thereby increasing the detection sensitivity. Furthermore, the enhanced electromagnetic fields that occur on the nanoparticle surface due to LSPR form the basis for the sensing of chemical and biological analytes using surface-enhanced spectroscopy techniques such as surface-enhanced Raman spectroscopy (SERS). Specifically, LSPR-coupling may be applied to control the electromagnetic SERS effect which can dramatically improve the sensitivity of SERS based detection methods.

1.4 Raman Spectroscopy

1.4.1 Raman Spectroscopy

Raman spectroscopy is a vibrational spectroscopy technique which provides molecularly specific fingerprint spectra upon the inelastic scattering of light. The

Raman effect was initially proposed by Smekal in 1923, and first demonstrated experimentally by Raman and Krishnan in 1928.[46, 47]

When incident light is directed at matter, photons interact with the molecules present and may be absorbed, absorbed and emitted (photoluminescence) or scattered. Absorption of a photon will occur if the frequency of the incident light matches the energy gap between the molecular levels, elevating the molecule from the ground electronic state to the excited electronic state. The excited molecule returns to the ground state upon radiative emission of a photon via photoluminescent processes such as fluorescence, or non-radiative processes such as vibrational relaxation or quenching. The loss of energy upon absorption, or the emission of photons may be measured by techniques such as UV-Vis absorption and fluorescence spectroscopy respectively.

Scattering does not require the frequency of the incident light to match the energy gap between molecular levels and is independent of electronic absorption. As light propagates as an oscillating dipole, it interacts with the molecular orbitals that form a molecule's electron cloud. This causes the electrons and nuclei to polarise and the electron cloud is distorted as the light forms a transient complex with the molecule referred to as a "virtual state". The distorted electron configuration is not stable, so the photon is immediately re-radiated and scattered as the electron cloud relaxes. Most photons are scattered at the same frequency as that of the incident light and the energy is therefore conserved in an elastic scattering process referred to as Rayleigh scattering. However, one in every $10^6 – 10^8$ of all scattered photons will lose or gain energy upon transfer to or from the nuclei of the molecule.[48] The frequency of the scattered light shifts by one vibrational unit as the energy transfer corresponds to the change in the vibrational level of the molecule. This is called Raman scattering and is a relatively weak phenomenon when compared to the dominant Rayleigh scattering effect. Raman scattering can occur via one of two potential process; Stokes scattering of anti-Stokes scattering.

If a molecule exists within a ground vibrational state, energy will be gained from the incident photon and the molecule will be promoted to an excited vibrational state. The photon is then re-radiated at a lower frequency and this is called Stokes Raman scattering. Conversely, if a molecule exists within an excited vibrational level, the incident photon will gain energy from the molecule and the molecule will fall to the ground vibrational level. The photon is then re-radiated at a higher frequency and this is called anti-Stokes Raman scattering. The processes of Stokes, anti-Stokes and Rayleigh scattering may be summarised within a Jablonski diagram as depicted in **Figure 1.10**.

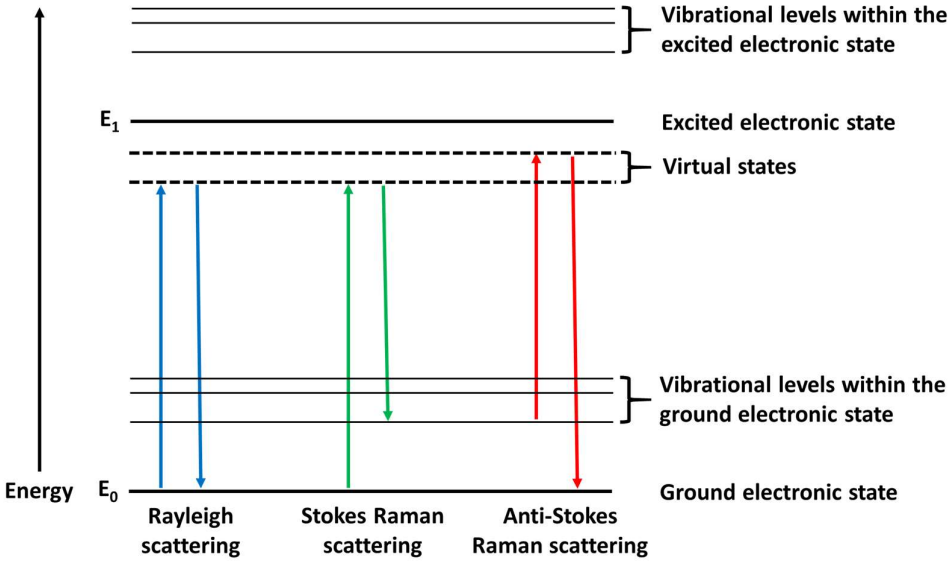

Figure 1.10. *Jablonski diagram depicting the energy transitions that occur for Rayleigh (blue), Stokes (green) and anti-Stokes scattering (red).*

A selection rule for Raman scattering states that the vibrational energy transition may only change by one vibrational unit. The selection rule is summarised as $\Delta\upsilon \pm 1$ for which $\Delta\upsilon + 1$ corresponds to Stokes Raman scattering and $\Delta\upsilon - 1$ corresponds to anti-Stokes Raman scattering.

The ratio of the intensities of the Stokes and anti-Stokes scattering depends upon the proportion of molecules in the ground or excited vibrational levels. This may be summarised using the Boltzmann equation as follows:

$$\frac{N_n}{N_m} = \frac{g_n}{g_m} exp\left[\frac{-(E_n - E_m)}{kT}\right]$$

Where N_n is the number of molecules in the excited vibrational level, N_m is the number of molecules in the ground vibrational level, g is the degeneracy of the levels n and m, $E_n - E_m$ is the difference in energy between the vibrational energy levels, k is the Boltzmann's constant (1.3807×10^{-23} JK $^{-1}$)and T is the temperature. Most molecules exist in the ground vibrational level at room temperature, and therefore Stokes scattering usually provides the most intense scattering that may be observed under typical experimental conditions. At higher temperatures, an increasing number of molecules will exist at the excited vibrational level, and therefore anti-Stokes scattering will become more intense at higher temperatures.

The intensity of the Raman scattering may be summarised in the following equation:

$$I = Kl\alpha^2 v^4$$

Where I is the Raman intensity, K is a constant, l is the laser power, α is the polarizability of the molecule and υ is the frequency of the incident light. Therefore, two operational factors may be controlled to maximise Raman signal intensity. The power of the laser used may be increased as the intensity is directly proportionate to laser power, or a laser with a high frequency may be applied as the intensity is proportionate to the 4th power of the frequency applied. However, the choice of laser frequency requires consideration of the molecular properties as some molecules may absorb light at higher frequencies within the UV region of the spectrum. This can lead to sample degradation or fluorescence emission which are undesirable as sample degradation may affect the accuracy of the results and prevent repetition of the experiment, whereas fluorescence can overlap spectrally and mask the Raman signal obtained. Conversely, a lower frequency within the IR region may be applied to avoid electronic absorption and fluorescence or sample degradation, but the Raman scattering intensity will decrease by the 4th power and therefore, sensitivity will be reduced.

1.4.2 Resonance Raman Spectroscopy

If the frequency of the incident laser wavelength is close to an electronic transition in the molecule of interest, resonance Raman scattering may be observed. Resonance Raman scattering enhances the Raman scattering of the photons in the order of 10^3 - 10^4.[48] Therefore, resonance Raman can be applied to significantly enhance the sensitivity of Raman spectroscopy. Resonance Raman occurs as the molecule absorbs an electron from the incident light, thereby promoting the molecule to a virtual state that exists within the first excited electronic state. As the incident light matches an electronic transition in the molecule of interest, interference from fluorescence can occur depending upon the properties of the molecule. This may be considered as a limitation for the practical application of resonance Raman spectroscopy for the analysis of certain molecules. Fluorescence will occur as the molecule absorbs an electron, promoting the molecule to an excited vibrational level within the excited electronic state. The molecule then decays to the lowest vibrational level within the excited electronic state via non-radiative relaxation. Finally, the molecule will return to the ground electronic state via radiative emission of the photon at a longer wavelength. The process of resonance Raman scattering and fluorescence occur within different timescales with Raman scattering typically occurring in picoseconds or less, whereas fluorescence typically occurs in nanoseconds or more.[49] The processes of resonance Raman scattering and fluorescence emission may be summarised within a Jablonski diagram as depicted in **Figure 1.11**.

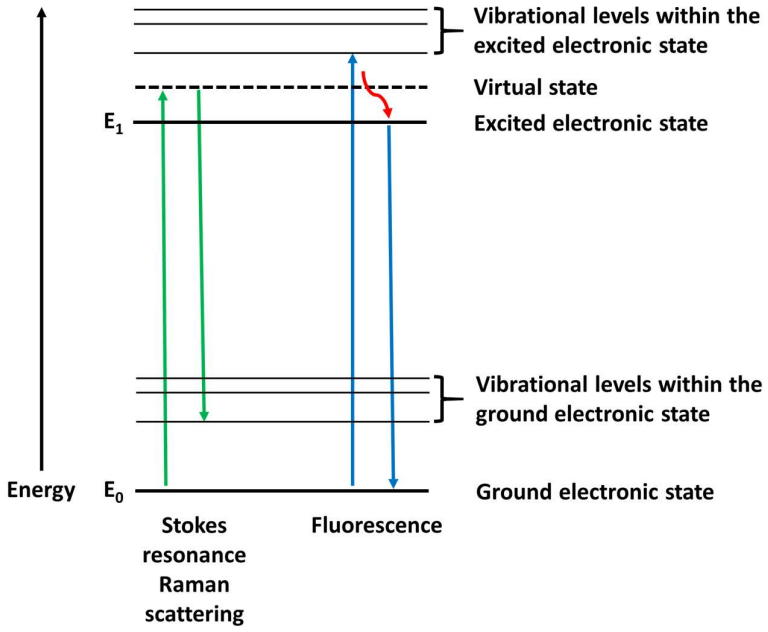

Figure 1.11. *Jablonski diagram depicting the energy transitions that occur for Stokes resonance Raman scattering (green) and fluorescence emission (blue).*

1.4.3 Surface Enhanced Raman Spectroscopy

Raman scattering may be further enhanced by the adsorption of an analyte upon a roughened metal surface and this is referred to as surface enhanced Raman spectroscopy (SERS). SERS provides an enhancement in the scattering efficiency by a factor of approximately 10^6 as compared to conventional Raman scattering.[48] SERS was first observed by Fleischmann et al., in 1974 when analysing pyridine upon the surface of a silver electrode.[50] The authors misattributed the enhanced sensitivity to an increase in the surface area of the electrode due to roughening of the surface by redox cycling, therefore adsorbing higher concentrations of pyridine.

These observations led to further theories describing the nature of the SERS effect. Jeanmarie and Van Duyne proposed that the enhancement was due to the electromagnetic effect, and Albrecht and Creighton proposed that the enhancement was due to a charge-transfer effect.[51, 52]

The electromagnetic effect occurs due to the enhancement of the electric field upon the surface of metallic NPs. The conduction electrons are loosely held upon the metal

surface and will collectively oscillate upon interaction with incident light of a specific frequency. This induces an enhanced localised electric field referred to as localised surface plasmon resonance (LSPR). The enhanced electric field interacts with the electrons of the molecule that is either in near proximity to, or directly adsorbed upon the nanoparticle surface. This increases the polarisation of the molecule, thereby increasing the observable Raman scattering intensity and generates SERS enhancement. The greatest magnitude of electromagnetic SERS enhancement occurs from NPs in near proximity. The junctions between the NPs concentrate the incident electromagnetic field and amplify the near field between the NPs as the LSPRs of the NPs interact. These regions of concentrated electromagnetic activity are referred to as “hotspot” regions and generate intense SERS enhancement.

The charge-transfer effect occurs due to a chemical bond formation between the molecule of interest and the surface of metallic NPs. This creates a new chemical system composed of the metal-molecule complex. The formation of the metal-molecule complex increases the polarizability of the molecule upon interaction with the electrons of the metal, creating new electronic states that are in resonance with the incident light source of a specific frequency. This increases the observable Raman scattering intensity and generates SERS enhancement.

It is generally accepted that the electromagnetic effect provides the greater contribution to SERS enhancement. As stated previously, the most significant electromagnetic SERS enhancement occurs within the junctions or “hotspot” regions of nanoparticles in near proximity. These hotspot regions may be generated by aggregating nanoparticles upon addition of a non-specific aggregating agent such as salt, however the aggregation is challenging to control and the reproducibility of results may be compromised. Therefore, this work emphasised the controlled assembly of DNA functionalised and dye-coded AgNPs based upon the molecular recognition of a target sequence. Such an approach provides the potential to orientate and maximise the SERS response based upon the specificity of molecular recognition and assembly. Therefore, the next section will introduce the concept of DNA detection by the controlled assembly of NPs.

1.5 Nucleic Acid Detection by Nanoparticle Assembly

1.5.1 Non-SERS Detection of Nucleic Acids by the Controlled Assembly of Nanoparticles

In 1996, two groups independently reported the controlled assembly of DNA functionalised AuNPs in solution upon hybridisation to a complementary synthetic DNA target sequence. Mirkin et al., demonstrated that AuNPs could be functionalised with two thiolated oligonucleotide probe sequences, and that addition of a complementary synthetic DNA target sequence could cross-link and assemble the functionalised AuNPs in solution upon hybridisation to the target sequence.[53] The general concept is shown in **Figure 1.12**.[54]

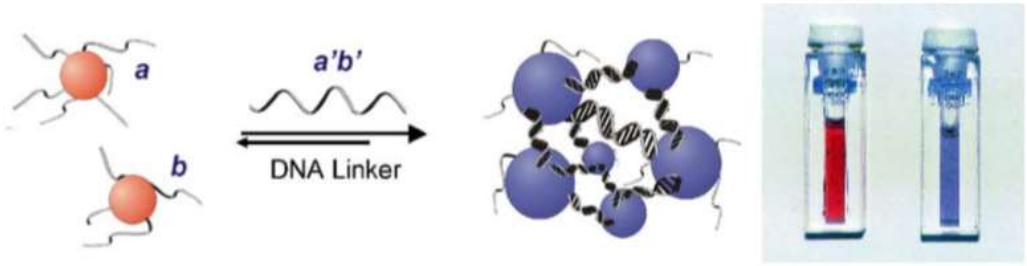

Figure 1.12. *General concept of the controlled assembly of AuNPs in solution (left) and the associated visible colorimetric change from red to blue. Reprinted from Thaxton, C. S.; Georganopoulou, D. G.; Mirkin, C. A. Gold Nanoparticle Probes for the Detection of Nucleic Acid Targets. Clin. Chim. Acta 2006, 363 (1–2), 120–126, with permission from Elsevier © 2005.*

The hybridisation event was confirmed visually by an observable colour change as the LSPR frequency of the AuNP conjugates shifted upon the transition from monodispersed AuNPs to assembled AuNPs. The characteristically red colouration of monodispersed AuNPs in solution changed to a dark blue colouration due to LSPR-coupling, and this transition could be analysed by UV-Vis extinction spectroscopy. The assembly process was shown to be reversible as the temperature was cycled repeatedly between 0 °C and 80 °C, which indicated that the assembly process could be controlled in accordance with the melting properties of the DNA probes used to functionalise the AuNPs.

Alivatatos et al., concurrently reported the functionalisation of AuNPs with thiolated oligonucleotide probes, and further demonstrated that the functionalised AuNPs could be cross-linked and assembled to form discrete dimer and trimer formations upon hybridisation to a complementary synthetic target sequence in solution.[55] These dimer and trimer formations were confirmed and distinguished by transmission electron microscopy (TEM) and could be size discriminated using gel electrophoresis.

These independent reports first demonstrated the potential for the functionalisation of NPs with DNA for biosensing applications. The Mirkin group have continued to publish extensively, reporting many research themes related to the detection of DNA using DNA functionalised AuNPs. These themes included investigation of the melting properties associated with the DNA assembled NPs, and general strategies for the sensitive detection of DNA based upon the assembly of NPs both in solution and upon the surface. [56, 57, 58, 59, 60] One of the striking features associated with the assembled AuNPs are the sharp melting transitions observed upon the application of elevated temperatures. These sharp melting transitions are due to the dense loading of oligonucleotides upon the surface of the NPs. This provides an increased number of binding sites (multivalency) and a cooperative mechanism of assembly in the presence of multiple target strands. These sharp melting transitions have been utilised to assess the melting properties and associated stability of the assemblies and have also been exploited to discriminate DNA targets when applying solution and surface-based detection methods.

The melting properties and stabilities of the assembled AuNPs are determined by several factors including DNA surface density, nanoparticle size, interparticle distance and salt concentration.[56] An increase in the oligonucleotide surface density will stabilise and increase the melting temperature as the cooperative assembly mechanism will be stabilised by a higher number of hybridised target strands. An increase in the nanoparticle size has been associated with increasingly sharp melting transitions, which was attributed to a higher number of hybridised target linkers per particle as the size increased. As the interparticle distance increases, the melting

temperature and stability of the assemblies also increases. This is due to reduced steric repulsions between the NPs as the interparticle distance is increased. Finally, an increase in the salt concentration will further stabilise assembled NPs as evident by an associated increase in melting temperature. This is in accordance with the general properties of DNA as a function of salt concentration. Salt is required to neutralise the negative charge associated with DNA, and therefore increased salt concentrations will increase the stability associated with the hybridised DNA assemblies. Furthermore, increasing the salt concentration will allow larger assemblies to form as the negative charges associated with NPs are screened by the positively charged salt ions.

In addition to the investigation of the melting properties of DNA assembled AuNPs, the Mirkin group have described various strategies for the sensitive detection of synthetic DNA using DNA functionalised AuNPs. These strategies include the solution-based assembly method, and various surface-based assembly methods including the Northwestern spot test method, the scanometric method and the biobarcode method. [57, 58, 59, 60]

Early reports within the Mirkin group identified that the DNA assembled AuNP conjugates displayed sharp melting transitions, and melting curve analysis could be applied to distinguish single-base imperfections such as mismatches, deletions or insertions in the complementary synthetic target sequence in solution.[57], [58] Furthermore, the enhanced colorimetric discrimination of these single-base imperfections could be attained upon spotting the assembled conjugates onto a white, reverse-phase silica surface. This simple test was referred to as the "Northwestern spot test" and provided a straightforward means to obtain a permanent and readily obtainable colorimetric signal. The limit of detection of the Northwestern spot test was ~ 10 fmol. The general concept is shown in **Figure 1.13**.

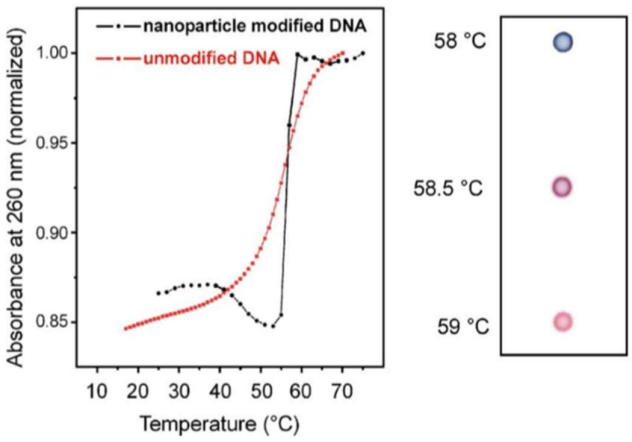

Figure 1.13. *Schematic depicting the sharp melting transitions associated with DNA assembled AuNPs (left) and discriminatory capacity of the Northwestern spot test as a function of melting temperature. Reprinted from Thaxton, C. S.; Georganopoulou, D. G.; Mirkin, C. A. Gold Nanoparticle Probes for the Detection of Nucleic Acid Targets. Clin. Chim. Acta 2006, 363 (1–2), 120–126, with permission from Elsevier © 2005.*

The colorimetric surface-based detection of DNA conjugates was later extended to glass surfaces.[61] A DNA probe was immobilised upon a glass slide and hybridised to a complementary synthetic target sequence. DNA functionalised AuNPs were then hybridised to the complementary target sequence present upon the glass surface, and further additions of target and conjugate could be added in cycles to generate multiple layers of target specific AuNP conjugates. The hybridisation event could be determined visually by the colorimetric change upon accumulation of the AuNP conjugate layers. The characteristically sharp melting transitions of DNA assembled AuNP conjugates were further confirmed upon the surface of the glass slides and heating above the melting temperature of the probes could dissociate the conjugates from the surface due to the reversible melting properties of the DNA probe and target sequences.

These findings provided the basis for a detection method referred to as the "scanometric" method.[59] This method applied a sandwich assay format upon a glass slide combined with detection using a flatbed scanner to obtain a quantitative signal. An oligonucleotide probe was immobilised upon the surface of the glass slide and

hybridised to the complementary synthetic target sequence. DNA-functionalised AuNPs were then hybridised to the complementary target sequence present upon the glass surface. The sensitivity of the method was further enhanced with the reduction of silver ions upon the surface of the hybridised AuNP conjugates which provided a greater signal intensity. The scanometric method was shown to be applicable for the discrimination of single-base mismatches within the target sequence based upon the differential melting transitions associated with the mismatches. The limit of detection of the scanometric test was 50 fM. The general concept is shown in **Figure 1.14**.

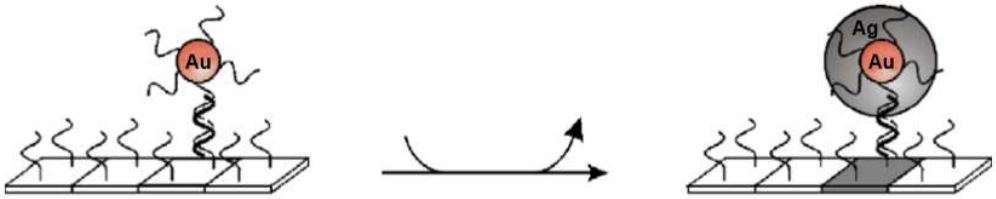

Figure 1.14. *General concept of the scanometric method utilising silver enhanced AuNPs. Reprinted from Thaxton, C. S.; Georganopoulou, D. G.; Mirkin, C. A. Gold Nanoparticle Probes for the Detection of Nucleic Acid Targets. Clin. Chim. Acta 2006, 363 (1–2), 120–126, with permission from Elsevier © 2005.*

The biobarcode assay was subsequently introduced as a target amplification strategy that utilises DNA functionalised AuNPs and DNA functionalised magnetic microparticles.[60] The AuNPs were conjugated with two different oligonucleotide probe sequences, one of which was complementary to the synthetic target sequence, and one of which was complementary to the biobarcode sequence. The biobarcode probe was present upon the surface at an excess concentration as compared to the target specific probe. The magnetic microparticles were conjugated with a further probe sequence which was also complementary to the target sequence. Initially, the DNA-functionalised AuNPs were loaded with an excess of the biobarcode sequence. The AuNP conjugates were then cross-linked to the magnetic microparticles upon hybridisation to the complementary synthetic target sequence. The cross-linked assemblies could then be separated upon application of a magnetic field and heated

to release the excess barcode sequence. A further magnetic separation step left only the biobarcode sequence at a significantly greater concentration than the target sequence used to crosslink the AuNP and magnetic microparticle assemblies. The biobarcode sequence could then be detected using the previously described scanometric method. This target amplification strategy was used to attain a limit of detection of just 500 zM. The pinciples of the biobarcode detection method are shown in **Figure 1.15**.

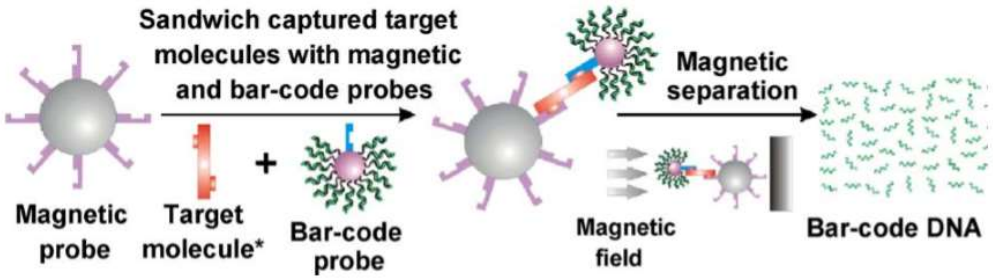

Figure 1.15. *Schematic depicting the principles of the biobarcode target amplification strategy. Reprinted from Thaxton, C. S.; Georganopoulou, D. G.; Mirkin, C. A. Gold Nanoparticle Probes for the Detection of Nucleic Acid Targets. Clin. Chim. Acta 2006, 363 (1–2), 120–126, with permission from Elsevier © 2005.*

A modified biobarcode method was later demonstrated for the multiplex detection of synthetic target sequences that were specific to 10 different viral pathogens.[62] The multiplex detection was achieved in a high density array format upon the surface of a glass slide, and the different target sequences could be specifically discriminated at a concentration of 500 fM.

The detection methods that have been described insofar, have generally utilised short, synthetic nucleic acid target sequences. Further reports have been published describing the detection of biologically relevant nucleic acid target sequences which have generally been applied using surface-based detection methods.

Storhoff et al., reported the detection of unamplified genomic DNA, specific to the methicillin-resistant Staphylococcus aureus (MRSA) *mecA* gene upon spotting of assembled AuNPs upon the surface of a glass slide.[63] The genomic DNA was first

fragmented by sonication and hybridised to DNA functionalised AuNPs in solution. The assembled AuNPs were then spotted upon the glass slide and illuminated using a white light source in the plane of the slide. The target assembled AuNPs provided different scattering colour and intensity when compared to the unassembled AuNPs and the result could be quantified using a CCD colour camera. A limit of detection was established at 33 zmol of genomic target DNA.

The Mirkin group have continued to develop the application of the biobarcode and scanometric methods for the detection of biologically relevant nucleic acid target sequences.

The biobarcode was applied for the detection of unamplified bacterial genomic DNA.[64] This required an increasingly complex detection method to address the issue of detecting double-stranded DNA targets. The bacterial genomic DNA was initially digested using a restriction endonuclease. This was described as necessary to prevent supercoiling of the DNA prior to detection; however, it is also likely that this reduced the size of the target sequence, rendering them more amenable for detection by controlled nanoparticle assembly. The genomic DNA was then heated to 95 °C to denature the double-stranded duplex and cooled in the presence of blocking oligonucleotides that prevented the reformation of double-stranded duplex structure. The target could then be detected using the biobarcode method, and a limit of detection of 2.5 fM was established.

The scanometric was further applied for the multiplex detection of microRNAs (miRNAs) associated with prostate cancer.[65] A limit of detection of 1 fM with single-base mismatch specificity was initially established in a serum sample spike with synthetic miRNA. The multiplex capability of the assay was further validated using synthetic targets and a dynamic detection range was established from 1 nM – 100 fM. The sensitivity of the multiplex assay could be improved to 1 fM with further deposition of gold to increase the size of the hybridised AuNPs prior to scanometric detection. Following validation of the assay using synthetic miRNA, the high-throughput multiplex detection of endogenous miRNA was demonstrated using

miRNA isolated from human cell lines. This indicated that the scanometric method could detect an additional 88% of miRNA species as compared to conventional fluorophore methods. Furthermore, the assay was capable of quantitatively discriminating changes in the expression levels of miRNA in treated cell lines as validated by comparison using qRT-PCR. Collectively, these findings were then applied for the analysis of 706 miRNA expression levels in tissue samples positive for prostate cancer. The findings identified that the expression levels of 109 miRNAs were downregulated and 54 were upregulated. Most recently, the authors have built upon these findings to quantify the expression levels of miRNA biomarkers that can specifically discriminate low-risk forms of prostate cancer from aggressive forms of prostate cancer.[66] These reports demonstrate the potential of applying DNA-functionalised AuNPs in combination with the scanometric method, for the clinical diagnosis of disease.

Much of the literature described has focused on the controlled assembly of DNA-functionalised AuNPs, with relatively little comparative literature describing the application of DNA-functionalised AgNPs. The Mirkin group initially reported difficulties in achieving stable AgNP conjugates upon functionalisation with thiolated DNA, and therefore resorted to synthesising core-shell Ag/Au NPs to provide the unique optical properties associated with silver and the stability associated with gold.[67] As observed for the AuNPs in previous reports, the DNA functionalised core-shell Ag/AuNPs could be cross-linked using a complementary target sequence, and this was observable by a slight darkening in the colouration of the solution. Furthermore, the assembly of the core-shell Ag/Au conjugates also displayed a pronounced redshift and dampening of the UV-Vis extinction spectra due to LSPR coupling of the NPs in solution. The sharp and reversible melting transitions were comparable to that observed with AuNP conjugates, and the enhanced colorimetric discrimination of the target sequence could be achieved using the previously described spot-test.

The group later described the successful conjugation of oligonucleotides modified with terminal cyclic disulfide groups to AgNPs.[68] The use of oligonucleotides that

were modified with polydentate thiol groups provided greater binding affinity and stability than monodentate thiol groups, and this was required to attain the stability required for further experimental application. The AgNP conjugates were functionalised with two probe sequences that were complementary to each other and could be assembled in a conjugate-conjugate formation. This however did not demonstrate the direct detection of a target sequence.

Thompson et al., published the first account of the controlled assembly of DNA-functionalised AgNPs in solution upon addition of a complementary synthetic target sequence.[69] This did not require core-shell modification of the AgNPs, or further stabilisation with polydentate thiol modifications. The AgNPs were demonstrated to be as robust as their AuNP counterparts and could provide greater detection sensitivities due to the higher extinction coefficients associated with AgNPs. The DNA functionalised AgNPs displayed the characteristic red-shift and dampening of the extinction spectra and a darkening in colouration upon hybridisation. Melting curve analysis confirmed the sharp melting transitions associated with nanoparticle assemblies, and these were exploited for the discrimination of a single-base mismatch in the target sequence. Furthermore, the colorimetric discrimination of complementary, non-complementary and single-base mismatch targets sequences could be enhanced with application of a spot-test. A direct comparison of the detection sensitivities of DNA-functionalised AuNPs and AgNPs was investigated, and a limit of detection of 2 nM and 40 pM was established for the AuNPs and AgNPs respectively. This indicated that the application of AgNPs could provide a 50x greater sensitivity than AuNPs for the colorimetric detection of DNA.

The detection of nucleic acids by the controlled assembly of DNA-functionalised NPs has been effectively demonstrated using a variety of both solution and surface-based methods. The detection of the target sequences may be confirmed visually by a colorimetric change in solution, although this is typically limited to monoplex detection strategies as the colour change will not discriminate between multiple target sequences in solution. Therefore, the multiplex detection of nucleic acids based upon the controlled assembly of DNA-functionalised NPs has been limited to

surface-based methods in the form of high-density arrays such as those demonstrated upon the application of the scanometric or biobarcode detection methods.

1.5.2 SERS Detection of Nucleic Acids by the Controlled Assembly of Nanoparticles

Surface enhanced Raman spectroscopy (SERS) has been applied for the detection of nucleic acids using a wide variety of strategies. It is possible to detect nucleic acids directly using SERS, however, due to the structural similarities in the nucleotide composition of differing nucleic acid sequences, it can be particularly challenging to discriminate the order and specificity of a unique target sequence using this approach.[70] Therefore, nucleic acids are commonly detected and distinguished indirectly with the application of Raman reporter dyes. The reporter dye may be used to label the nucleic acid sequences that are specific to the hybridisation event, or alternatively, may be adsorbed directly upon the surface of the DNA-functionalised NPs. Either of these approaches provides the potential for SERS detection of the reporter dye which is indicative of the target specific hybridisation of the DNA-functionalised NPs to the complementary target sequence.

The use of Raman reporter dyes offers significant potential for the multiplex detection of DNA.[70] Conventional methods for the detection of DNA are often based upon the fluorescence emission of molecular fluorophore dyes. However, there are limitations associated with the detection of DNA by fluorescence emission. The overlapping features associated with the broad emission spectra of fluorophores limits the capacity for multiplex detection. Specifically, fluorescence emission spectra are limited to between 2 and 5 resolvable colours due to featureless spectral peaks that span ~ 1500 cm^{-1}.[71] Furthermore, fluorophores are prone to degradation by photobleaching which can compromise detection sensitivity and accuracy. Conversely, Raman reporter dyes display narrow spectral features which significantly extends the potential for multiplex detection. Specifically, the narrow spectral features span ~ 10 cm^{-1}, thereby greatly increasing the potential for multiplex analysis.[71]. With the application of SERS, both fluorescent and non-fluorescent dye

molecules may be utilised as reporter dyes for SERS as fluorescence will be quenched upon the surface of metallic nanoparticles. Therefore, a wide range of Raman reporter molecules may be applied for the multiplex SERS detection of DNA. In principle, the indirect SERS detection of DNA with application of Raman reporter dyes has significant potential for multiplexing. However, in practice, effective methods to realise this potential have yet to be well defined. This is due to the complexities associated with combining the assembly of DNA-functionalised NPs, in a manner that reproducibly maximises the SERS intensity gained from the nanoparticle assemblies. Various strategies to progress toward the realisation of this potential have been proposed.

The Mirkin group reported the potential for the multiplex SERS detection of six synthetic DNA targets specific to viral pathogens upon the surface of a glass slide, however it should be noted that this was not a true multiplex method due to the requirement for spatial separation.[72] The method utilised the same sandwich assay format as applied for detection of DNA using the scanometric method, however further modifications were made for the purpose of SERS detection. An oligonucleotide probe was immobilised upon the surface of the glass slide and hybridised to a solution containing a mixture of each of the six synthetic target sequences. The DNA-functionalised AuNPs were then added and hybridised to the complementary target sequence. The thiolated probe sequences used to functionalise the AuNPs were covalently labelled with Raman reporter dyes. Each probe sequence was specific to a different viral pathogen sequence and modified with a unique Raman reporter dye. The reduction of silver ions upon the surface of the hybridised AuNP conjugates provided electromagnetic enhancement of the Raman reporter dyes which could then be detected using SERS. The results demonstrated that virtually no cross-hybridisation occurred upon analysis of the solution containing each of the six target sequences. Furthermore, the Raman spectra of each reporter dye could be attributed to the corresponding target sequence, and each sequence could be clearly discriminated upon the surface. A limit of detection of 20 fM was established.

Braun et al., described an alternative surface-based method for the SERS detection of DNA.[73] This method utilised a smooth Ag film that was modified with a surface bound Raman reporter dye. An oligonucleotide probe was immobilised upon the surface of the Ag film and hybridised to the complementary synthetic target sequence. DNA-functionalised AgNPs were then hybridised to the complementary target sequence present upon the surface of the smooth film. Hybridisation of the AgNPs created hotspot regions at the junctions between the smooth film and AgNPs, and the resulting electromagnetic enhancement of the surface-bound Raman reporter confirmed the hybridisation and detection of the complementary synthetic DNA target sequence.

The described methods demonstrated the SERS detection of DNA by the controlled assembly of NPs using Raman reporter dyes, however, these methods were initially constrained to detection upon the surface rather than in solution.

Graham et al., first demonstrated the controlled assembly of DNA functionalised and dye-coded AgNPs for the SERS detection of DNA in solution.[74] AgNPs were functionalised with two thiolated oligonucleotide probes, and addition of a complementary synthetic DNA target cross-linked and assembled the AgNPs in solution upon hybridisation to the target sequence. The DNA-functionalised AgNPs were modified by dye-coding the AgNPs with the addition of a Raman reporter dye. Upon assembly of the AgNPs in solution, hotspot regions were created between the junctions of the assembled NPs, and electromagnetic enhancement of the surface-bound Raman reporter confirmed the hybridisation and detection of the target sequence. The principle of this detection strategy is shown in **Figure 1.16**.[75]

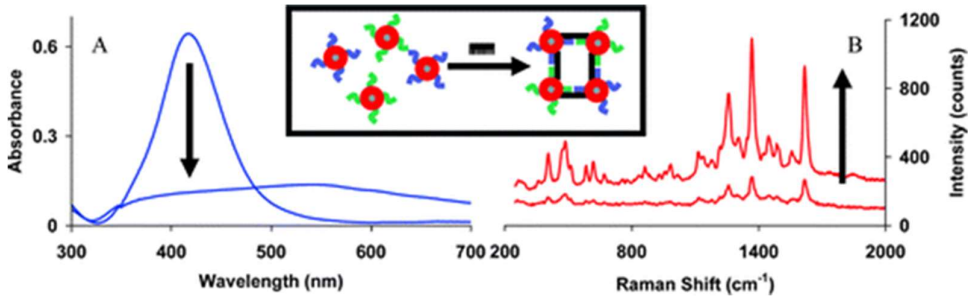

Figure 1.16. *Principles of the controlled assembly of DNA functionalised and dye-coded AgNPs for the SERS detection of DNA. As the AgNPs are assembled in solution, LSPR-coupling occurs (left) and this is accompanied by an increase in the SERS signal intensity. Reprinted from Graham, D.; Stevenson, R.; Thompson, D. G.; Barrett, L.; Dalton, C.; Faulds, K. Combining Functionalised Nanoparticles and SERS for the Detection of DNA Relating to Disease. Faraday Discuss. 2011, 149, 291–299, with permission from the Royal Society of Chemistry © 2011.*

If the complementary target sequence was present, the AgNPs were assembled and SERS was switched on. If the complementary target sequence was not present, the AgNPs were not assembled and SERS remained switched off. The assembly of DNA-functionalised AgNPs and resulting SERS enhancement was shown to be sequence-specific and provided selective enhancement of the Raman reporter dye based upon the complementarity of the target sequence. Importantly, the enhancement of two Raman reporter dyes was demonstrated in a one-pot reaction, with modification of two different conjugate probe sequences with two different Raman reporter dyes. The SERS enhanced Raman spectra displayed narrow spectral peaks that were characteristic of the assembly of both conjugate probe sequences in a single reaction. This was particularly significant as the result confirmed the potential for the multiplex detection of DNA target sequences in solution, within a single sample containing multiple target sequences.

The authors subsequently applied the same solution-based assembly method for the SERS detection of every possible single-base mismatch in synthetic complementary target sequences.[76] If the target sequence contained an internal base-pair mismatch, the controlled assembly of the DNA functionalised and dye-coded AgNPs did not

occur and therefore the electromagnetic SERS enhancement remained switched off. The SERS enhancement would only occur if the target sequence was fully complementary, and therefore the solution-based SERS detection method displayed the potential for the discrimination of single nucleotide polymorphisms in biologically relevant target sequences.

Further work within the group has exploited the controlled assembly of DNA functionalised and dye-coded AgNPs to investigate the magnitude of the electromagnetic SERS response as a function of the interparticle distance.[77] This study utilised the rigid properties of triplex DNA formations to tune the interparticle distance between the junctions of the DNA functionalised and dye-coded AgNPs upon hybridisation and assembly. The interparticle distance was controlled by introducing regions of non-complementarity between the probe and target sequences which were extended by 0, 5, 10 and 15 base-pairs respectively. The results indicated that the magnitude of the SERS enhancement decreased exponentially as the interparticle distance was increased. Therefore, the positioning of NPs in the closest possible proximity may be considered crucial for the maximisation of the electromagnetic SERS response upon the controlled assembly of DNA functionalised and dye-coded NPs in solution.

Following the publication of the initial findings of Graham et al., others have demonstrated similar methods for the assembly-based SERS detection of DNA using DNA functionalised and dye-coded NPs in solution. Qian et al., reported the SERS detection of synthetic DNA using DNA functionalised and dye-coded AuNPs based upon the same solution-based assembly principles as described by Graham et al. [78] The AuNP assemblies were also shown to be capable of discriminating single-base mismatches within the complementary target sequence. The electromagnetic SERS enhancement was only switched on if the target sequence was fully complementary to the probe sequences used to functionalise the AuNPs.

Zhang et al., described the triplex detection of synthetic target sequences in solution using DNA functionalised and dye-coded AgNPs.[79] A single AgNP conjugate was

functionalised with three different DNA probe sequences that were complementary to each of the target sequences investigated. A further three batches of AgNP conjugates were synthesised upon functionalisation with three different DNA probe sequences that were complementary to each of the target sequences. The three batches of conjugates were dye-coded with a unique Raman reporter with distinct spectral features. The controlled assembly of these conjugates occurred upon addition of the complementary target sequences in solution and SERS was switched on due to electromagnetic SERS enhancement. The selective enhancement of the SERS detection method was confirmed using different combinations of target sequences, and the triplex detection could be confirmed by identification of the unique spectral features of the Raman reporter dyes within the spectra obtained from a sample containing all three of the target sequences.

Whilst, the assembly and SERS detection of DNA functionalised and dye-coded NPs has been demonstrated for the monoplex and multiplex detection of target sequences with single-base mismatch sensitivity, the concept has still to be extensively applied to biological target sequences, which presents further challenges.

1.6 Detection of Long-chain Nucleic Acids by the Controlled Assembly of Nanoparticles

To date, most reports describing the detection of nucleic acids based upon the controlled assembly of DNA-functionalised NPs have utilised short-chain, synthetic target sequences. The detection of short, synthetic target sequences has been widely applied for both non-SERS and SERS-based detection methods, either in solution or upon the surface. These short target sequences provide an idealised model for the detection of DNA by the controlled assembly of NPs as they typically match the combined length of the two complementary probes used to detect the target in the sandwich assay format. These sequences are therefore an ideal size for cross-linking and assembling the NPs prior to detection. Furthermore, the synthetic DNA targets are readily synthesised in the single-stranded form, and as such, the targets are directly accessible for hybridisation, assembly and detection.

Comparatively, there are far fewer reports describing the detection of DNA by the controlled assembly of DNA-functionalised NPs using long-chain target sequences. This is an important consideration, as long-chain targets sequences are generally more reflective of biologically relevant targets. There are exceptions, such as miRNA, which naturally exist as short-chains of single-stranded RNA. Therefore, miRNA provides an attractive target for detection of nucleic acids by nanoparticle assembly using the principles that have been established previously using short, synthetic DNA target sequences. However, the challenges associated with the detection of biologically relevant long-chain nucleic acid fragments requires further investigation.

The detection of biologically relevant genomic DNA by the controlled assembly of NPs presents multiple challenges that have not been thoroughly addressed within the literature. Genomic DNA exists as extensive polymer sequence that is many thousands of nucleotides in length and is only present in low quantities within the cell. As such, the detection of genomic DNA is most commonly preceded by the amplification of long-chain fragments using techniques such as PCR. This generates high concentrations of a specific long-chain fragment of DNA which is more readily detectable than that of the unamplified genomic DNA. These amplification products are generally longer than the short synthetic target sequences that have previously been detected by the assembly of NPs.

Therefore, this raises the primary research question; is it possible to apply SERS for the detection of long-chain DNA fragments by the controlled assembly of DNA functionalised and dye-coded NPs in solution? If so, this would provide a foundation for the progression towards the SERS detection of biologically relevant genomic DNA sequences.

A further challenge associated with the detection of biologically relevant genomic DNA sequences relates to the secondary structure of the target sequence. Genomic DNA exists in the double-stranded form and this is also typically true for products amplified by techniques such as PCR, which generally synthesises double-stranded amplification products. The previously described reports have typically utilised short,

synthetic DNA target sequences that are conveniently synthesised in the single-stranded form. If a target sequence exists within the double-stranded form, the DNA-functionalised NPs will not be able to readily hybridise to the target recognition sequence due to presence of the complementary strand in the double-stranded amplification product.

This raises the secondary research question; is it possible to amplify a long-chain DNA fragment that is single-stranded and detectable by SERS based upon the controlled assembly of DNA functionalised and dye-coded NPs in solution? If so, this would greatly simplify the detection method, without requirement of increasingly complex methods for the generation of single-stranded DNA such as alkali treatment, enzymatic digestion or magnetic bead separation.

The detection of long-chain DNA fragments by the controlled assembly of NPs in solution has previously been investigated within the group. These investigations are directly related in principle to the experiments performed and described within this report, and therefore the findings and limitations of these investigations will be described in further detail. For reference, a simple depiction of the head-to-head, head-to-tail and tail-to-tail probe orientations investigated by the authors is shown in **Figure 1.17** in the order of increasing interparticle distance. These probe orientations are discussed in further detail and context within section 2.9.

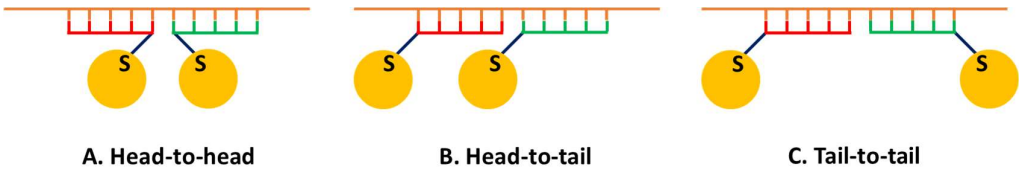

Figure 1.17. *Simplified schematic of the probe orientations in order of decreasing interparticle proximity.* ***A.*** *Head-to-head orientation* ***B.*** *Head-to-tail orientation* ***C.*** *Tail-to-tail orientation.*

Donnelly et al., investigated the hybridisation properties that affect the controlled assembly of DNA-functionalised AgNPs in solution using long-chain synthetic DNA targets.[80] The hybridisation and assembly kinetics were investigated as a function of target length, buffer composition, probe length and probe orientation. Furthermore,

the assembly melting properties were investigated as a function of probe length and orientation. All experiments were performed and analysed using UV-Vis extinction spectroscopy.

The target length was initially investigated using targets that were 24, 48, 96 and 144 bases in length. All experiments were performed using probes positioned in the head-to-tail probe orientation. The assembly kinetics were significantly reduced and occurred to a lesser extent as the target length increased from 24 to 48 bases. As the target increased to 96 bases, no hybridisation or assembly was observed. This was attributed to various potential factors including; reduced diffusion rates as the target length increased, increased steric hindrances and electrostatic repulsions associated with longer targets, and potential secondary structures forming within the long-chain target sequence.

The buffer composition was investigated due to the reduced rate of assembly observed for the longer target sequences. The assembly kinetics were not improved by simply increasing the salt concentration. Therefore, molecular crowding agents including dextran sulfate and polyethylene glycol (PEG) 10000 were added separately to the buffer at concentrations of 3 %, 5 % and 7 % (w/v). The addition of either of these crowding agents significantly enhanced the assembly kinetics upon addition of the 144 base target sequence, although the underlying effect of these crowding agents was not directly described. Some conjugate instability was observed as the concentration increased beyond 3 % (w/v), and therefore, subsequent experiments were performed using dextran sulfate at this concentration.

The probe length was investigated using 12, 18, 24 and 30 base probes. The findings identified that the assembly rate increased as a function of probe length, although reduced hybridisation rates were observed as the probe length increased to 30 bases. This trend was observed in both the tail-to-tail and head-to-tail orientations. This trend was attributed various factors including; greater stability associated with a higher number of DNA duplex base-pair formations, a reduction of electrostatic repulsions due to the greater interparticle distances associated with longer probe

sequences, and shorter target overhangs as the probe length increased. The reduced hybridisation rate observed for the 30 base probes was not conclusively explained. The hybridisation and assembly rate also occurred more rapidly and to a greater extent in the tail-to-tail orientation as compared to the head-to-tail orientation. The interparticle distance is greater in the tail-to-tail orientation than the head-to-tail orientation, and the enhanced assembly kinetics in the tail-to-tail orientation was attributed to reduced electrostatic repulsions as compared to the head-to-head orientation.

The melting temperatures of the assemblies were also investigated as a function of probe length and orientation. As the probe length increased, the melting temperature of the assemblies also increased, and this was observed in both the tail-to-tail and head-to-tail orientations. This was attributed to increased base-stacking interactions as the probe length increased. Furthermore, higher melting temperatures were associated with the tail-to-tail orientation as compared to the head-to-tail orientation. This was attributed to reduced steric hindrances and electrostatic repulsions associated with greater interparticle distance in the tail-to-tail orientation as compared to the head-to-tail orientation.

The investigation by Donnelly et al., identified many of the challenges associated with the controlled assembly of NPs using long-chain DNA fragments in solution. However, all experiments were limited to analysis by UV-Vis extinction spectroscopy, and therefore it remains unclear as to how the findings may be related to the SERS detection of DNA. Important findings were described, including the necessity of molecular crowding agents for the hybridisation and assembly of DNA-functionalised NPs in solution upon addition of a long-chain DNA fragment. Additionally, probe lengths may be increased to enhance the assembly rate and increase the melting temperatures of the assemblies. Furthermore, increasing the interparticle distance in the tail-to-tail orientation as compared to the head-to-tail orientation was associated with enhanced assembly rates and increased melting temperatures. This was due to the increased interparticle distance which reduces steric hindrances and electrostatic repulsions. However, in terms of electromagnetic SERS enhancement, it is favourable

to assemble NPs in the closest possible proximity.[77] In theory, the head-to-head probe orientation should provide the closest proximity which may be advantageous for maximising SERS intensities, although this orientation was not described within the investigation.

Mabbot et al., subsequently investigated the SERS detection of synthetic long-chain DNA fragments and PCR products by the controlled assembly of DNA functionalised and dye-coded AgNPs in solution.[81] The SERS discriminatory value was initially investigated as a function of target length and buffer composition using long-chain synthetic DNA targets, prior to the detection of a PCR product. As described previously, the assembly of the DNA functionalised and dye-coded AgNPs generates electromagnetic SERS enhancement as the Raman reporter molecules are positioned in the hotspot regions of the assembled NPs. If the complementary target sequence was present, the AgNPs were assembled and SERS was switched on. If the complementary target sequence was not present, the AgNPs were not assembled and SERS remained switched off. Mabbot et al., compared the relative SERS intensity of the spectral peaks associated with the Raman reporter dye upon addition of complementary and non-complementary target sequences. The resulting SERS intensity could then be compared as a SERS on: off ratio to measure the discriminatory value of the assembly-based method.

The target length was initially investigated using synthetic target lengths of 24, 48, 96 and 144 bases. The AgNPs were functionalised with 12 base probe sequences and the controlled assembly of the DNA functionalised and dye-coded AgNPs was performed in the head-to-tail probe orientation. The SERS intensity decreased significantly as the complementary target length increased, and the relative SERS on: off discriminatory ratios were approximately 3: 1, 2:1, < 2: 1 and < 2:1 for each of the respective target lengths investigated as compared to non-complementary target. This was attributed to the tendency for longer single-stranded targets to form internal secondary structures.

The buffer composition was investigated due to the reduced discriminatory value observed for the longer target sequences. Dextran sulfate was added to the buffer at concentrations of 3 % and 6 % (w/v) and the SERS intensities obtained upon addition of the 144 base target were compared to a control sample that did not contain dextran sulfate. The SERS intensity increased upon addition of dextran sulfate and relative SERS on: off discriminatory ratios were approximately 1:1, 3:1 and 3:1 for the samples containing 0 %, 3 % and 6 % dextran sulfate respectively. The improved discriminatory value was attributed to the volume exclusion effect of the molecular crowding agent minimising the diffusion rate of the target sequence.

The detection of a 380 base-pair PCR amplification product was also investigated. As the PCR product was double-stranded, target denaturation was performed by alkali treatment using sodium hydroxide solution prior to hybridisation. The controlled assembly of the DNA functionalised and dye-coded AgNPs was performed in the tail-to-tail orientation for the detection of the PCR product, although the reasoning for this change was not clearly defined. Initially, the SERS discrimination of the PCR product could not be obtained using the previously optimised conditions. This was attributed to various possible factors including; the extensive length of the PCR product impeding hybridisation and the possibility of a low concentration or poor viability of the single-stranded DNA following alkali treatment.

The probe length was increased from 12 bases to 18 bases to improve the discriminatory value, although this was not initially successful. The dextran sulfate concentration was increased to 10 % and this provided some SERS discrimination in combination with the longer probe sequences. Discrimination of 10 µL of PCR product was obtained, although the relative SERS on: off discriminatory ratio was < 2: 1. The detection of a volumetric range of PCR product was investigated using 5 µL, 2 µL, 1 µL, 0.5 µL, 0.2 µL and 0.1 µL volumes of PCR product, however, the relative SERS on: off discriminatory ratios were all typically < 2: 1.

The investigation by Mabbot et al., demonstrated that the SERS detection of long-chain DNA fragments by the controlled assembly of DNA functionalised and dye-

coded could be achieved, however, the relative SERS on: off discriminatory ratios were typically 3: 1 or less upon addition of a 144 base synthetic DNA target and less than 2: 1 for 380 base-pair PCR product. Important findings were described, such as the necessity of a molecular crowding agent which was required for the SERS detection of the 144 base synthetic DNA target and PCR product. This was comparable to the findings of Donnelly et al. Furthermore, the alkali treatment of the PCR product was described as a potential method for the detection of the double-stranded PCR product, however it was stated that this method may not produce satisfactory concentrations of viable single-stranded DNA for subsequent detection by SERS. Finally, the authors described the concept of the tail-to-tail, head-to-tail, and head-to-head probe orientations. The tail-to-tail orientation provides the greatest interparticle distance. The interparticle distance is reduced in the head-to-tail orientation as compared to the tail-to-tail orientation. Finally, the head-to-head orientation provides the most proximate of all three of the probe orientations. The SERS detection of the 144 base target was performed in the head-to-tail orientation, whereas the SERS detection of the PCR product was performed in the tail-to-tail orientation. The reasons for the selection of these orientations was not described in detail. As stated previously, it is favourable to assemble the NPs in closest possible proximity to obtain the maximum electromagnetic SERS enhancement of the Raman reporter dye upon the controlled assembly of the NPs.[77]. However, the potential of the head-to-head orientation was not demonstrated.

To summarise, prior research within the group has explored the potential for detecting long-chain DNA targets and PCR products using both non-SERS and SERS methods. However, the SERS detection of long-chain DNA targets has yet to be convincingly demonstrated based upon the controlled assembly of DNA functionalised and dye-coded NPs in solution. Prior work did not exploit the potential of maximising the SERS intensity and discriminatory value of the method using the probe head-to-head orientation, thus providing an opportunity for further investigation. Furthermore, the detection of PCR products is hindered by the double-stranded nature of the PCR product. Therefore, there was further opportunity to

define a strategy for the generation of a single-stranded amplification product for detection without requirement for complex methods such as alkali denaturation.

Two key research questions formed the basis of this investigation:

- Is it possible to apply SERS for the detection of long-chain DNA fragments by the controlled assembly of DNA functionalised and dye-coded AgNPs in solution?
- Is it possible to amplify a long-chain DNA fragment that is single-stranded and detectable by SERS based upon the controlled assembly of DNA functionalised and dye-coded AgNPs in solution?

2 A Proof-of-principle Investigation for the SERS Detection of a Long-chain Synthetic DNA Target by the Controlled Assembly of DNA Functionalised and Dye-coded AgNPs in Solution

2.1 Aim of the Proof-of-principle Assay

The aim of the proof-of-principle investigation was to demonstrate the sequence-specific SERS detection of a long-chain (100-base) synthetic DNA target in solution, using DNA functionalised and dye-coded AgNPs. A 100 base synthetic target was chosen as this was comparable in size to a DNA amplification product, and if the proof-of-principle was to be proven feasible, the findings were to be applied to a biologically relevant amplification product at a later stage. A *Candida krusei* specific target was chosen as this was aligned with the research activities of the commercial project sponsor to recognise an unmet clinical need for the rapid molecular detection of fungal pathogens.[82]

Fungal pathogens are ubiquitous, opportunistic, and invasive infectious pathogens that are responsible for many serious health related complications and fatalities globally. Two of the most commonly identifiable genera of fungi present in clinical environments are *Candida* and *Aspergillus* species, the causative agents of *Candidiasis* and *Aspergillosis* respectively.[83] Neither *Candida* nor *Aspergillus* pose a significant risk to healthy individuals with strong immune systems to prevent infection. However, invasive fungal infections cause approximately 1.5 million fatalities each year in immuno-compromised patients worldwide and are associated with high mortality rates.[84] Global estimates for the rate of life-threatening *Candidiasis* are >400,000 whilst estimated *Aspergillosis* rates are >200,000.[84] The respective mortality rates are estimated to be between 46-75% and 30-90% dependant on geographical location, socio-economic factors and underlying health condition. [84] Whilst *Candida albicans* has been identified as the predominant *Candida* pathogen in the past, other species such as *Candida krusei* have recently become increasingly common, potentially due to an inherent resistance to common

antifungal drugs such as fluconazole.[85] Therefore, in addition to *Candida albicans*, drug resistant species such as *Candida krusei* also require improved diagnosis and treatment options.

Traditionally, fungal pathogens have been detected using techniques such as microscopy, culture and histology which serve as the current gold standard although such methods are time consuming and lack sensitivity.[86, 87] However, molecular methods such as PCR have the potential to enhance the detection sensitivity and speed, thereby improving patient outcomes. Currently, widespread implementation of molecular methods for the diagnosis of fungal infections have not been achieved due lack of assay standardisation and validation. Therefore, further development and commercial validation of molecular detection methods may be translated into better healthcare outcomes for patients if detection times and sensitivities may be improved with the application of emerging molecular detection methods.

Renishaw Diagnostics Limited (RDL), the commercial sponsor of the project, have developed a semi-automated platform for the SERS detection of PCR amplification products specific to fungal pathogens.[82] This method was originally developed by Graham et al., and later adapted for commercial application by RDL.[88] The commercialised method requires a complex multi-step process prior to SERS detection. PCR products are amplified using biotinylated primers, hybridised to probes covalently modified with a Raman reporter dye, purified using streptavidin magnetic beads, washed, eluted into a colloidal suspension and detected by SERS upon addition of an external aggregating agent to the colloidal suspension. The method is effective, however the inclusion of biotinylated primers, covalently modified probe sequences, magnetic bead separations and wash steps inevitably increases both the cost and time required for detection. Other research groups have recently described the ongoing development and application of variations of this method for the multiplex SERS detection of PCR products. Li et al., have applied this method for multiplex detection of mutations associated with lung cancer, colorectal cancer and thalassemia respectively, substituting magnetic bead separation for spin-column purification.[89, 90, 91] Alternatively, Wee a developed a comparable method for

the multiplex detection of melanoma associated mutations in circulating tumour DNA, omitting addition of a non-specific aggregation agent in favour of enrichment and SERS detection directly upon the surface of magnetic-beads.[92] This was achieved using a biotinylated reverse primer for magnetic bead capture, and a forward primer modified with an internal spacer and 5' overhang for direct hybridisation to DNA functionalised and dye-coded NPs. However, each of these methods still require physical separation or sample purification. Therefore, it was desirable to identify an alternative, faster and simplified method for the SERS detection of DNA sequences specific to *Candida* fungal pathogens.

Further research within the group has demonstrated that the sequence-specific SERS detection of DNA may be achieved without requirement of such a complex detection strategy. As described previously, Graham et al., reported the SERS detection of DNA in solution based upon the controlled assembly of DNA functionalised and dye-coded AgNPs.[74] By using AgNPs that were modified using a suitable Raman reporter dye, covalent modification of probe sequences with reporter dye molecules could be eliminated. Furthermore, as the SERS signal was relative to the molecular assembly of the AgNPs in solution, magnetic bead separation and addition of external aggregating agents could be avoided. The feasibility of this SERS detection method was demonstrated, although the investigation utilised short-chain (18-base) targets that were not representative of a biological nucleic acid amplification product.

Further investigation was necessary to identify if the assembly-based SERS detection method could be extended to long-chain DNA targets. If this principle could be proven using a synthetic DNA target, the investigation could progress toward the solution-based assembly and SERS detection of a biologically relevant amplification product. This would demonstrate significant potential for the simplification of the SERS detection method applied by RDL and provide further progression towards the application of SERS for clinical diagnostic purposes.

2.2 Introduction to the Assay Principles

The SERS detection of DNA sequences related to *Candida* fungal pathogens was founded upon the controlled assembly of DNA functionalised and dye-coded AgNPs in solution upon hybridisation to the complementary target sequence. To achieve this, AgNPs were functionalised with probe sequences that were complementary to the synthetic *Candida krusei* target sequence. Two probe sequences were designed to hybridise to separate complementary regions that were positioned directly next to each other within the target sequence. Upon hybridisation, the complementary target cross-linked the AgNP conjugates in an assembled formation that was dependent on the sequence-specificity of the probes used to functionalise the AgNPs. As the probe hybridisation regions were positioned directly next to each other within the target sequence, the hybridisation of the conjugates to the target sequence positioned the AgNPs in proximity to each other as the nanoparticle assemblies formed. Hybridisation thereby reduced the interparticle distance and induced LSPR coupling which could be observed using UV-Vis extinction spectroscopy. SERS hotspot regions were also formed in the junctions between the assembled AgNP conjugates as a result of LSPR coupling. The Raman reporter dye present upon the surface of the dye-coded AgNPs was subjected to an increase in the electromagnetic field. This generated SERS enhancement of the signal which was indicative of target recognition. If the target sequence was complementary to the conjugate probe sequence, the AgNPs were assembled to create hotspot regions and SERS was "switched on". If the target sequence was non-complementary, the AgNPs remain dispersed in solution and SERS remained "switched off". The discriminatory value of the detection methodology could be calculated by comparing the Raman reporter peak intensities for complementary and non-complementary target sequences. This provided an on: off SERS ratio to assess the discriminatory value of the detection methodology. A simplified depiction of this concept is provided in **Figure 2.1**.

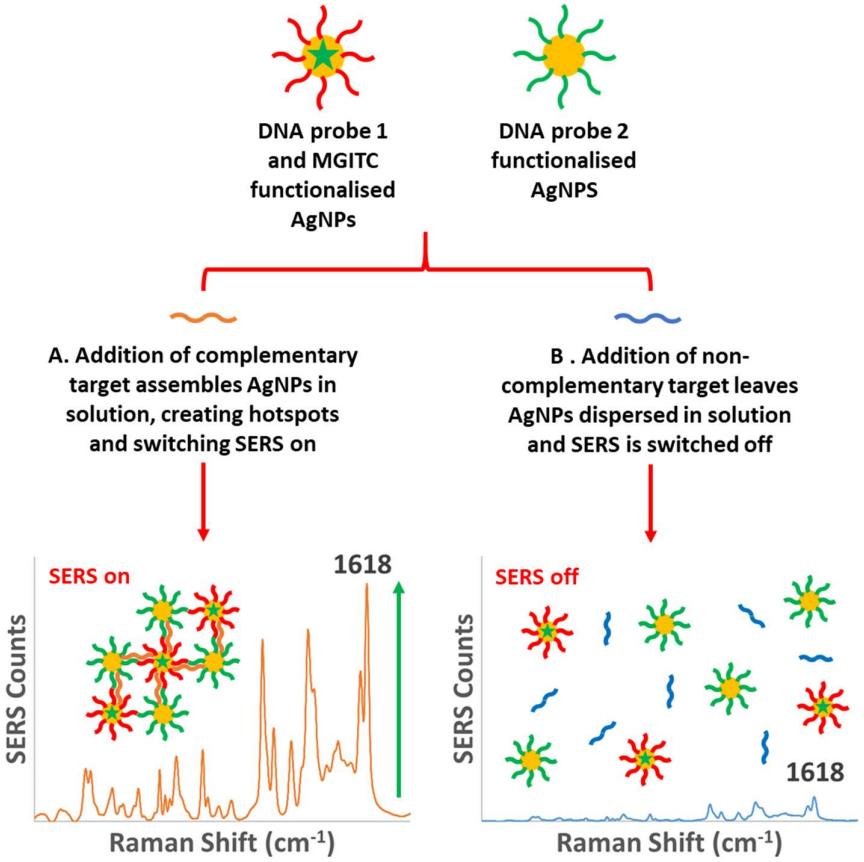

***Figure 2.1**. Simplified schematic depicting principles of the SERS DNA detection methodology in solution upon; **A.** Addition of complementary DNA which switches SERS on **B.** addition of non-complementary DNA leaving SERS switched off. The on: off discriminatory ratio may then be calculated by comparing the Raman reporter (MGITC) peak intensities at 1618 cm^{-1}.*

The detection methodology applied here is therefore an example of indirect or extrinsic DNA detection as the measured SERS response relates to the spectral enhancement of the reporter dye rather than that of the target DNA sequence.

2.3 Nanoparticle Synthesis

The detection methodology utilised AgNPs as AgNPs have a molar extinction coefficient that is 100x greater than that of AuNPs and therefore greater detection sensitivities may be attained when performing analysis by UV-Vis absorption spectroscopy.[69] Furthermore, AgNPs have been experimentally demonstrated to

support greater SERS enhancement factors than that of AuNPs at mid-optical wavelengths.[93] AgNPs and AuNPs may both scatter and absorb light, although AgNPs display a favourable scattering-to-absorbance ratio as compared to AuNPs. The greater scattering-to-absorbance ratio of AgNPs and the greater polarizeabilty of the electrons associated with AgNPs favour their application as a substrate for SERS enhancement.[93]

AgNPs were synthesised using the hydroxylamine reduction method as reported by Leopold and Lendl.[42] The advantages of the hydroxylamine synthesis method include a short synthesis time (20 minutes) and simple procedure that allows for the reproducible synthesis of monodisperse AgNPs at room temperature. Other common methods for the synthesis of AgNPs include the Lee and Meisel citrate reduction method although this requires boiling and vigorous stirring for 1 hour.[38] Alternatively, the Creighton borohydride reduction method may be used, however this requires ice-cold incubation and stirring as the reaction proceeds.[94] Following the synthesis, the hydroxylamine AgNPs were filtered to remove impurities and stored in the dark at room temperature.

2.4 Nanoparticle Characterisation

Following the synthesis, the AgNPs were characterised by UV-Vis extinction spectroscopy and dynamic light scattering. The extinction spectrum for hydroxylamine AgNPs is shown in **Figure 2.2**.

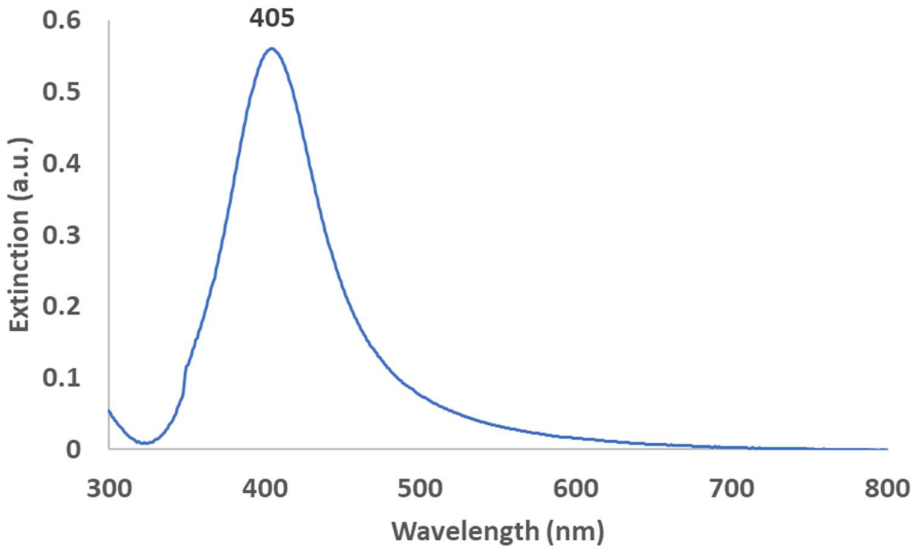

Figure 2.2. *UV-Vis extinction spectrum of hydroxylamine AgNPs following synthesis with an extinction maximum at 405 nm.*

The spectrum displayed a single, prominent extinction peak maximum at 405 nm which was typical for monodisperse AgNPs within the UV-Vis range.[33] The size and zeta potential of the AgNPs was estimated using dynamic light scattering. Three replicate sample readings were taken using DLS for the size and zeta potential. The readings obtained are described in **Table 2.1**

Table 2.1. *Dynamic light scattering size (nm) distribution and zeta potential (mV) data used to estimate size and stability of nanoparticles in suspension.*

	Size (nm)	Zeta potential (mV)
Reading 1	53.43	-40.2
Reading 2	52.72	-44.2
Reading 3	52.78	-40.4
Mean	52.98	-41.6
Standard deviation	0.39	2.25

The average AgNP size was calculated to be 53.0 nm ± 0.4 nm and the average zeta potential was -41.6 mV. AgNPs with a zeta potential charge of ± 30 mV are strongly cationic or anionic and due to electrostatic repulsions are considered to be highly stable.[95, 96] The concentration of hydroxylamine AgNPs was estimated to be 209 pM using the Beer-Lambert law and the extinction coefficient 537 x 10^8 M^{-1} cm^{-1} for 50 nm AgNPs.[97] The hydroxylamine AgNPs were functionalised without further dilution following synthesis and filtration.

2.5 Selection of DNA Oligonucleotide Probe and Target Sequences

The aim of the assay was to detect a 100-base sequence specific to the invasive fungal pathogen *Candida krusei.* Two oligonucleotides probes that were 18 bases in length were designed to be specific for a complementary region of the 18s ribosomal RNA (rRNA) gene sequence of *Candida krusei*. The 18s rRNA gene sequence was selected as the rRNA genes of fungal species evolve slowly, and the conserved nature of these sequences provide an ideal target for phylogenetic discrimination at the genus and species level.[98] The 18s, 5.8s and 28s rRNA genes or ITS1 and ITS2 internal transcribed spacer regions are most commonly targeted sequences for detection and are referred to as multi-copy targets as there are 50-100 copies within a single genome, providing a further advantage for maximising detection sensitivities.[86] There are numerous examples of PCR assays that have been designed for the detection and discrimination of *Candida* species based upon the 18s rRNA gene sequence.[99, 100, 87] Therefore, a

100-base region of the 18s rRNA gene was selected as the target. A 100-base sequence, complementary to the target sequence was used as a negative control sequence. This did not contained regions that were complementary to the probe sequences and could therefore be used as a suitable negative control target.

Two probes were designed for complementarity to a *Candida krusei* specific region of the 18s rRNA target sequence for species-specific discrimination, and were checked for specificity using the NCBI BLAST sequence database.[101] The probes were checked for homo-dimer, hetero-dimer and hairpin formations using the OligoAnalyzer application.[102] Dimers form if there is self-complementarity between the probes and this can cause non-specific aggregation of functionalised NPs, whereas hairpin formations occur if a probe hybridises within itself and this may prevent target hybridisation if the probe is blocked. The probes were screened to ensure that the free energy (ΔG) values were greater than -9 units to reduce the likelihood of probe dimer and hairpin formations, in line with recommended design criteria.[103] The probe and synthetic target sequences applied for the species-specific detection of *Candida krusei* are shown in **Table 2.2**.

Table 2.2. *Probe and target sequences designed for the species-specific detection of the Candida krusei 18s rRNA gene. Probe 1 is highlighted in red, probe 2 is highlighted in green, and the corresponding hybridisation regions within the complementary target are highlighted in red and green respectively.*

Sequence Name	Sequences (all in 5' – 3' direction)
Probe 1	5' – AGG TAG ACC GTC CGC CCA – 3'
Probe 2	5' – CGC AAC AGT GCT TAC CAT – 3'
Complementary target	5' – TCC AGC TCC AAT AGC GTA TAT TAA AGT TGT TGC AGT TAA AAA GCT CGT AGT TGA ACT TTG GGC CTG GGC GGA CGG TCT ACC TAT GGT AAG CAC TGT TGC G – 3'
Non-complementary target	5' – CGC AAC AGT GCT TAC CAT AGG TAG ACC GTC CGC CCA GGC CCA AAG TTC AAC TAC GAG CTT TTT AAC TGC AAC AAC TTT AAT ATA CGC TAT TGG AGC TGG A – 3'

2.6 Inclusion of a Spacer for Optimal Hybridisation Efficiency

The 18 base probes used to functionalise the AgNPs contained a triple hexaethylene glycol (HEG) spacer which is important for several reasons. The use of a spacer is advantageous due to; a) prevention of electrostatic interactions between the nucleobases of the probe and nanoparticle surface which would render them inaccessible for hybridisation b) reduction of inter-strand steric repulsions that would limit the surface coverage upon DNA loading and c) reduction of steric congestion around the hybridisation region, thus increasing free volume for improved hybridisation efficiencies.[104, 105]

Demers et al., previously reported that inclusion of a polyA spacer between the terminal thiol and DNA probe recognition sequence used to functionalise AuNPs improved hybridisation efficiencies by approximately ten-fold when compared to the equivalent probe sequences with no spacer.[104] The polyA spacer prevented nucleobases within the probe recognition sequence from interacting electrostatically with the nanoparticle surface and provided greater free volume for hybridisation to occur. However, the polyA spacer also interacted with the nanoparticle surface, lying planar rather than perpendicular, which reduced the loading coverage. This issue was partially negated with the use of a polyT spacer which interacted with the surface to a lesser degree than the polyA equivalent. Further investigation by Hurst et al., compared the use of a polyethylene glycol (PEG) spacer with polyA and polyT spacers for maximising the loading of thiolated DNA onto the surface of AuNPs.[105] It was concluded that the maximum loading efficiency could be obtained with use of a PEG spacer as PEG is non-ionic and therefore inter-strand repulsions were minimised, and the issue of electrostatic nucleobase interactions with the nanoparticle surface could be eliminated.

Based upon these findings, a triple hexaethylene glycol (HEG) spacer was selected as this would provide the benefits of reduced probe-particle interactions, reduced inter-strand repulsions and increased volume for hybridisation, whilst avoiding the complications of nucleobase spacers lying planar on the nanoparticle surface.

2.7 Functionalisation of AgNPs with Thiolated DNA

The conjugation of DNA oligonucleotides to NPs is challenging due to the negative charges associated with both the sugar-phosphate backbone of DNA and the nanoparticle surface. This leads to electrostatic repulsion which prevents spontaneous adsorption of DNA onto NPs, and therefore Mirkin's group introduced the concept of salt-aging to overcome this issue.[57, 58] Typically, this process takes days as thiolated oligonucleotides are added to AuNPs in solution without salt and incubated for 16 hours. NaCl is then added incrementally to a final concentration of 0.1 M and "aged" for a further 40 hours. The Na^+ ions screen the negative charges associated with DNA phosphate groups allowing the thiolated oligonucleotides to gradually adsorb onto the nanoparticle surface. The authors later demonstrated that an optimal surface coverage could be achieved by further increasing the final NaCl concentration within the range of 0.7 M - 1 M.[104, 105]

Although the salt-aging method is effective, there are disadvantages associated with this approach. Care must be taken to ensure that salt is not introduced to the suspension too rapidly, as this irreversibly aggregates the NPs if an insufficient quantity of DNA has adsorbed to the surface to ensure protection. Furthermore, the time required (approximately 2 days) is impractical for routine implementation. Finally, the authors reported that the salt-aging method was not readily transferable to AgNPs, as sufficient conjugate stability could not be achieved for further analysis using typical hybridisation conditions.[67]

Zhang et al., observed that the adsorption of DNA onto AuNPs significantly increased as the buffer pH was decreased, with approximately 90 % of DNA adsorbed at pH 3.5 and less than 20% of DNA adsorbed at pH 7.6 following 5 minutes of incubation.[106] The authors translated this finding for the rapid functionalisation of AuNPs with thiolated DNA.[107] Approximately 80 % of thiolated DNA oligonucleotides adsorbed to the AuNP surface within 2 minutes of adding the sodium citrate buffer adjusted to pH 3.0. The conjugates could be resuspended in pH neutral conditions, indicating that pH adjustment was only required for DNA attachment. This method was also

effective for the functionalisation of AgNPs with thiolated DNA.[108] Similar results were obtained, although adsorption kinetics were reduced when compared to AuNPs, with surface coverage achieved after 20 minutes, and the pH adjusted citrate buffer had to be introduced incrementally which was not required for AuNPs. This method has also been applied for the efficient adsorption of non-thiolated DNA to surface of AuNPs.[109] The surface coverage was comparable to thiolated DNA, and the passively adsorbed DNA retained its hybridisation functionality as the terminal probe nucleobases anchored the sequence to the surface, whilst the remaining sequence was positioned in an upright orientation allowing for hybridisation to occur. The authors of the pH adjusted method have associated the significantly improved DNA adsorption kinetics on to the surface of AuNPs or AgNPs with the protonation of the DNA bases.[110] Specifically, adenine and cytosine which have pK_a values of 3.5 and 4.2 respectively may be protonated at pH 3.0. This minimises the electrostatic repulsion between the DNA and nanoparticle surface, and further reduces interstrand repulsions that limit coverage, thus providing rapid adsorption and optimal coverage.

The pH adjusted method is quick and can be reproducibly implemented within minutes rather than hours, the procedure requires less salt and DNA for functionalisation than traditional salt-aging and is applicable to both AuNPs and AgNPs. For these reasons, this method was selected for the functionalisation of AgNPs throughout this investigation.

2.8 Selection of the Raman Reporter Dye

The assay is based on the increase in SERS signal upon AgNP assembly which is achieved by using a Raman reporter and Malachite green isothiocyanate (MGITC) was selected for application in this investigation. MGITC generates intense Raman signals with the potential for resonant Raman contributions due to electronic transitions in the visible region.[111] Furthermore, MGITC has been demonstrated to provide enhancement factors that are approximately 200-fold higher than that of malachite green (MG) on the surface of AuNPs.[112] This was attributed to the reactive isothiocyanate group (-N=C=S) which provides stronger electronic coupling on the

nanoparticle surface and an improved capacity for chemical enhancement with higher overall enhancement factors than MG. The Raman spectra for MGITC displayed prominent peaks at 1172 cm^{-1}, 1365 cm^{-1} and 1618 cm^{-1} which relate to the dye-specific vibrational modes of the reporter molecule. Whilst no thorough peak assignments for MGITC are readily available in the literature, tentative assignments have been made for MG which displays a highly comparable Raman spectrum.[113] The peaks at 1172 cm^{-1}, 1365 cm^{-1} and 1618 cm^{-1} have been assigned to in-plane C-H bends, N-phenyl stretching, and N-phenyl and C-C stretching respectively. The molecular structure and corresponding SERS spectra are displayed in **Figure 2.3**.

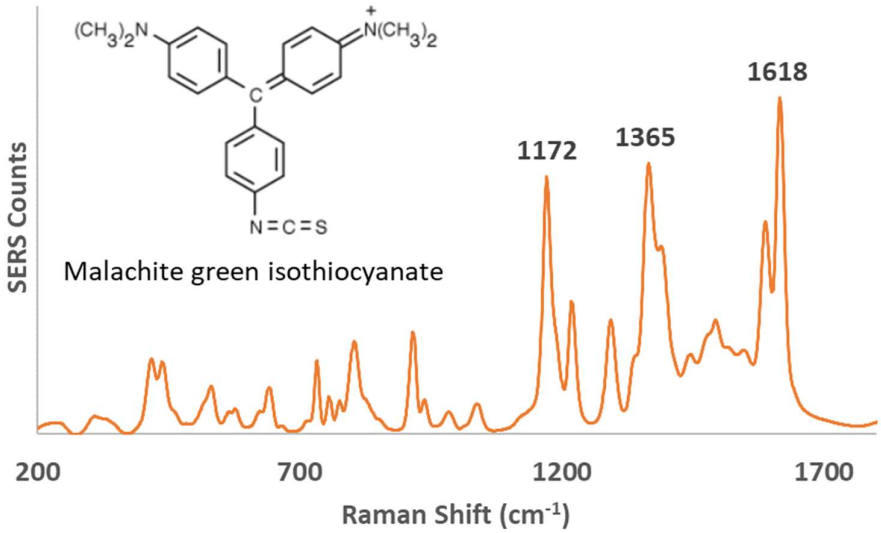

Figure 2.3. *SERS spectrum of malachite green isothiocyanate (MGITC) with distinct peaks at 1172 cm^{-1}, 1365 cm^{-1} and 1618 cm^{-1}. Spectra accumulated using 532 nm laser. Inset shows the molecular structure of MGITC.*

The application of DNA functionalised and dye-coded AgNPs for the SERS detection of DNA in solution was first demonstrated by Graham et al., as described previously.[74] In this instance, the Raman reporter was added to the NPs prior to functionalisation with DNA. A benzotriazole monoazo dye was specifically selected as the Raman reporter contained a negatively charged phenolic group which prevented nanoparticle aggregation prior to further stabilisation with thiolated DNA. Therefore, by adding a Raman reporter to the nanoparticle surface for dye-coded detection,

costly dye-labelling of the probe or target sequences could be avoided. McKenzie et al., later demonstrated that the NPs could be dye-labelled after the functionalisation of NPs with DNA.[114] As the NPs were stabilised with the DNA prior to dye addition, the issue of non-specific aggregation upon dye addition was minimised, thus allowing for a greater degree of freedom for dye selection.

This investigation utilised MGITC as the Raman reporter of choice due to the characteristically intense Raman signals and capacity to adsorb efficiently onto the nanoparticle surface via the isothiocyanate group. MGITC was added to the AgNPs following functionalisation with DNA and therefore dye-induced aggregation could be avoided whilst significant Raman signal could still be attained.

2.9 Interparticle Distance and Probe Orientations

The interparticle distance is a crucial consideration for maximisation of SERS signal due to the requirement for LSPR coupling of the NPs and subsequent generation of electromagnetic SERS enhancement due to the creation of hotspot regions within the interparticle junctions. Guerrini et al., investigated the electromagnetic SERS response of AgNPs as a function of interparticle distance, by altering the length of rigid triplex DNA formations that cross-linked NPs within a range of 0 – 15 bases in length.[77] The SERS response was reduced by more than 50 % as the interparticle distance increased from 0 bases to 15 bases as determined by the addition of bases between the probe hybridisation regions. Therefore, it is crucial to attain the closest possible proximity for the maximisation of the electromagnetic SERS response upon hybridisation.

Mabbot et al., investigated a model in which selective modification of either the 5' or 3' ends of the probe sequences with a thiol group could be applied to assemble NPs in a head-to-head, head-to-tail or tail-to-tail orientation upon hybridisation to a complementary target sequence.[81] The concept of each of these orientations in summarised in **Figure 2.4**.

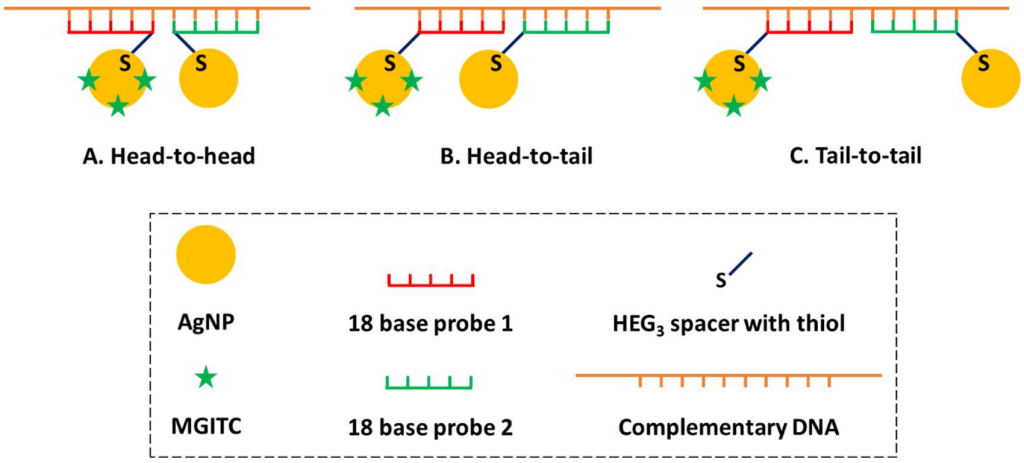

***Figure 2.4**. Simplified schematic depicting the probe orientations investigated based upon selective combinations of 5' or 3' modifications of the probe sequences. **A.** Head-to-head orientation **B.** Head-to-tail orientation **C.** Tail-to-tail orientation. Key describing conjugate components displayed below.*

In theory, the tail-to-tail orientation should produce lower SERS enhancement due to the largest interparticle separation, thus reducing the plasmonic coupling required for enhancement within hotspot regions. Conversely, a head-to-head orientation should provide the closest proximity and greatest SERS enhancement, although steric hindrances were considered to potentially undermine the hybridisation event and limit the associated SERS response due to the proximity of this orientation. A head-to-tail orientation should provide a compromise by which SERS discrimination may be attained as the NPs are proximate enough to generate a SERS response, whilst distant enough to avoid steric hindrances. This description was not thoroughly concluded experimentally by Mabbot et al., and therefore this investigation compared the SERS response of the probes in each orientation to further test this theory.

As the head-to-head orientation was hypothesised to produce the maximum SERS intensity, the investigation began by exploring the conditions required to attain hybridisation in this orientation despite the possibility of steric hindrances interfering. If hybridisation within the head-to-head orientation could be attained, the relative discriminatory value of each of the three orientations could then be

compared. The probe sequences and 5' and 3' modification combinations applied for the different orientations are described within **Table 2.3**.

Table 2.3. *Probe sequences and combinations of 5' and 3' modifications used for the head-to-head, head-to-tail and tail-to-tail orientations. All orientations use the same probe 1 (red) and probe 2 (green) sequences. The positions of the triple HEG (HEG_3) spacer and monothiol modifications differ for each orientation.*

Probe Orientation	Probe Sequences (all in 5' – 3' direction)
Head-to-head orientation	5' – SH – HEG_3 – AGG TAG ACC GTC CGC CCA – 3'
	5' – CGC AAC AGT GCT TAC CAT – HEG_3 – SH – 3'
Head-to-tail orientation	5' – SH – HEG_3 – AGG TAG ACC GTC CGC CCA – 3'
	5' – SH – HEG_3 – CGC AAC AGT GCT TAC CAT – 3'
Tail-to-tail orientation	5' – AGG TAG ACC GTC CGC CCA – HEG_3 – SH – 3'
	5' – SH – HEG_3 – CGC AAC AGT GCT TAC CAT – 3'

2.10 Confirmation of DNA Functionalisation and MGITC Adsorption on the NP Surface

Hydroxylamine AgNPs where functionalised with the thiolated DNA probes specific for *Candida Krusei* using the pH adjusted method at an excess concentration to ensure conjugate stability in the buffer conditions used for analysis. The thiolated probes were added at a DNA to AgNP molar concentration ratio of 7500: 1. If insufficient DNA was added, the AgNPs would aggregate upon addition of the pH adjusted citrate buffer or following resuspension in 0.1 M PBS. This would occur if the surface of the AgNPs was not sufficiently protected by a monolayer of thiolated DNA upon the surface, and therefore the negative charge associated with AgNPs would be screened upon addition of the Na^+ ions in the citrate buffer or 0.1 M PBS thereby inducing aggregation. Following DNA functionalisation, MGITC was added to the conjugates at a concentration that provided a strong Raman signal and significant SERS enhancement upon aggregation. The MGITC Raman reporter was added at a 2500: 1 dye to nanoparticle molar concentration ratio. Upon addition of MGITC to

the DNA functionalised AgNPs, sonication was applied for 3 minutes to allow the MGITC to adsorb onto the surface. Following the addition of the MGITC Raman reporter, the conjugates were resuspended in 0.1 M PBS. This allowed the conjugates to equilibrate in ionic conditions prior to further analysis, with subsequent hybridisation experiments typically performed in 0.3 M PBS.

Agarose gel electrophoresis was preformed to ensure that the thiolated DNA probes were attached upon the surface of the AgNPs and to confirm the stability of the conjugates. Gel electrophoresis separates the analyte of interest (such as AgNP conjugates or DNA products) based upon size and charge. As the electric field is applied to the gel, the negatively charged AgNP conjugates migrate towards the positively charged anode. The AgNP conjugates are inversely separated by size in accordance with the size of the ligands used to functionalise the AgNPs. Smaller ligands will migrate faster, whereas larger ligands will migrate slower. Bare AgNPs were compared to AgNPs functionalised with thiolated DNA and AgNPs functionalised with thiolated DNA with the further addition of the MGITC Raman reporter. A comparison was made with AgNPs stabilised by the passive adsorption of 0.1% polyvinylpyrrolidone (PVP), and AgNPs stabilised with 10 µM of carboxy-PEG_{12}-thiol ($CT(PEG)_{12}$) which adsorbs via the thiol group. The results are shown in **Figure 2.5**.

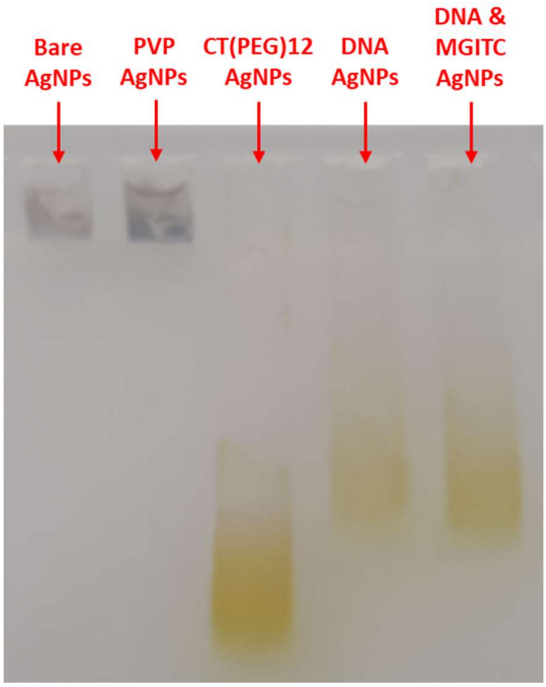

Figure 2.5. *Agarose gel electrophoresis image comparing electrophoretic mobility of bare AgNPs with the mobility of AgNPs functionalised with differing surface ligands immobilised via passive adsorption or a thiol-silver bond.*

As the bare AgNPs were unprotected, they aggregated rapidly after being added to the 0.5x tris-borate-EDTA running buffer. The AgNPs that were stabilised with 0.1 % PVP remained stable upon addition to the well containing the 0.5x TBE buffer. However, as the electrical current was applied, the PVP stabilised AgNPs began to aggregate gradually which suggested that the passively adsorbed PVP was displaced from the surface. The AgNPs that were stabilised with $CT(PEG)_{12}$ or thiolated DNA were stable in the 0.5x TBE buffer and upon application of the electrical current. This indicated that the modification of the AgNP surface with thiolated ligands provided greater stability than passive adsorption. The $CT(PEG)_{12}$ coated AgNPs migrated further than the DNA functionalised AgNPs. This was expected as the $CT(PEG)_{12}$ surface ligand is smaller than that of the 18 base probes present on the surface of the DNA functionalised AgNPs. It was concluded that the thiolated DNA probes had successfully attached to the surface of the hydroxylamine AgNPs via the thiol group following implementation of the pH adjusted conjugation method.

To ensure that the MGITC Raman reporter was present upon the surface and further assess the potential for discrimination of the aggregated vs. non-aggregated SERS signal, the reporter conjugate was analysed by SERS using a 532 nm laser excitation wavelength following non-specific aggregation of the conjugates with $MgCl_2$. The conjugate was diluted to a concentration of 10 pM in 0.1 M PBS and remained dispersed following dilution. For comparison, an identical sample was prepared and spiked with 5 mM of $MgCl_2$ which aggregated following salt addition. The SERS intensity was monitored until it peaked after 5 minutes. The SERS spectra generated from the reporter conjugate with and without addition of $MgCl_2$ are shown in **Figure 2.6**.

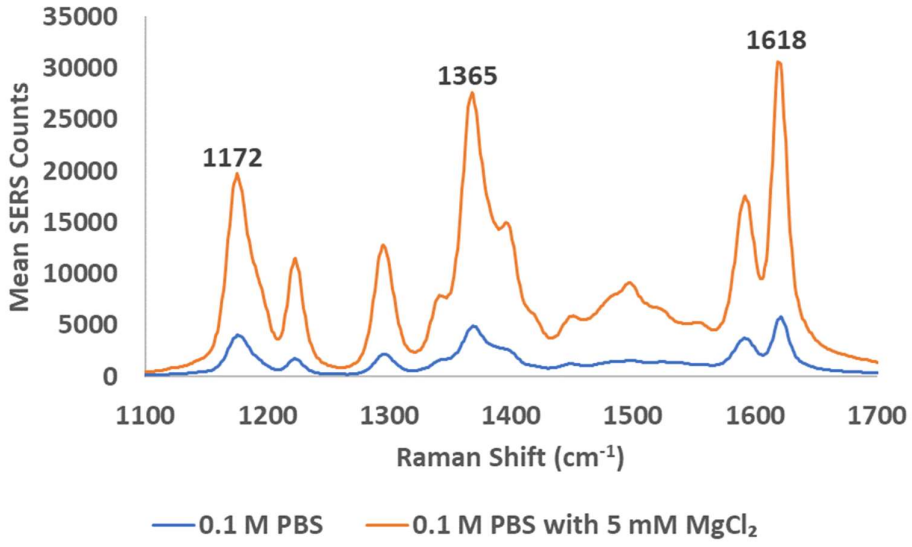

Figure 2.6. *SERS spectra of MGITC dye-coded reporter conjugate (10 pM) in 0.1 M PBS with and without the addition of 5 mM $MgCl_2$.MGITC added at a dye: AgNP molar ratio of 2500: 1. Spectra accumulated with a 532 nm laser, 1 second acquisition time and 10 % (5 mW) laser power.*

The spectra indicated that upon aggregation, the AgNP conjugate generated a significantly enhanced signal due to the SERS enhancement of the MGITC reporter dye which was present within the hotspot regions of the aggregates. The dispersed AgNPs also displayed some inherent SERS signal. The non-specific aggregation of the DNA functionalised and dye-coded AgNPs provided a maximum SERS on: off ratio of

6: 1 demonstrating the potential for SERS enhancement. Further experimentation was required to confirm if this on: off ratio could be attained or exceeded by the controlled assembly of the conjugates following hybridisation to a complementary target sequence.

2.11 Optimisation of Hybridisation Kinetics for the Assembly of DNA Functionalised AgNPs by UV-Vis Extinction Spectroscopy

The head-to-head orientation was assumed to produce the greatest SERS intensity as the NPs are positioned within the closest possible proximity, although steric hindrances have been identified as a potential limitation of this orientation. Therefore, suitable hybridisation conditions were investigated to identify if the head-to-head orientation could be achieved.

The hybridisation conditions were established by monitoring the UV-Vis extinction kinetics of the DNA functionalised NPs in suspension upon addition of a 100-base complementary target sequence. An additional sample was prepared under identical conditions, but with the addition of a 100-base non-complementary sequence. This provided a negative control to ensure that any shift in the extinction spectrum was due to the species-specific hybridisation to the complementary DNA sequence. Each sample used for the UV-Vis extinction kinetics experiments consisted of 10 pM of each conjugate and 10 nM of target sequence. These were diluted in 0.3 M PBS for the purpose of hybridisation. If the DNA functionalised AgNPs hybridised to the complementary target sequence, the extinction maximum would decrease and an increase was observed at higher wavelengths, most prominently at 500 nm. This corresponded to the LSPR-coupling of the assembled AgNPs. The aggregation kinetics could then be displayed as an extinction maximum / extinction 500 nm ratio which provided a means to directly compare the dispersity of NPs in suspension upon the addition of complementary or non-complementary DNA. The investigation of hybridisation conditions began with the addition of the complementary and non-complementary target sequences to conjugates in suspension at room temperature for 1 hour (**Figure 2.7**).

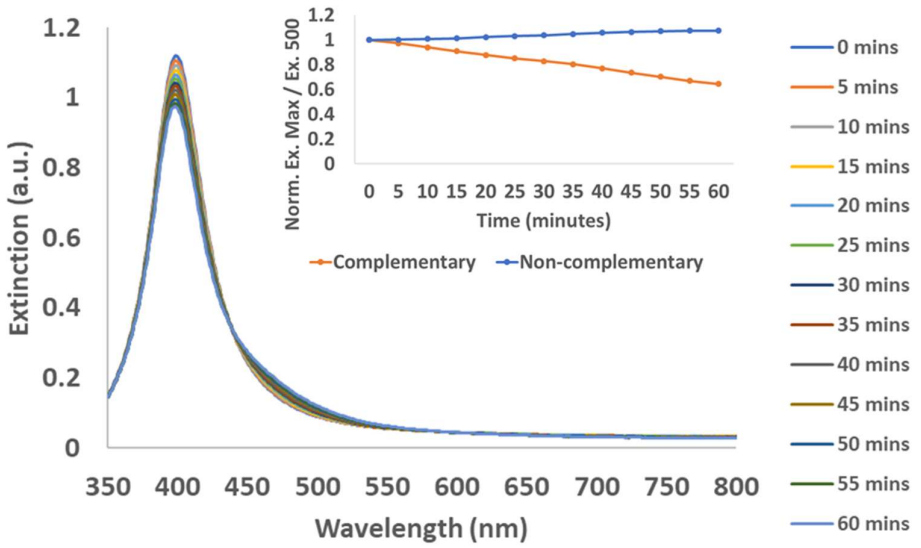

Figure 2.7. *Extinction spectrum of AgNP conjugates (10 pM of each conjugate) upon addition of 10 nM complementary DNA at room temperature for 1 hour. Inset shows the normalised extinction maximum / extinction 500 nm ratio for complementary (orange) and non-complementary (blue) target sequences.*

It was evident from the UV-Vis extinction spectra that hybridisation did occur as the addition of complementary DNA induced assembly, as visible by a decrease in the extinction maximum and a slight increase at 500 nm. This did not occur upon addition of the non-complementary DNA, for which a slight increase in extinction maximum occurred. This was attributed to an increase in the dispersion of the AgNPs upon dilution within the 0.3 M PBS buffer. The extinction maximum / extinction 500 nm ratio indicated that the negative sample containing non-complementary DNA remained stable, whilst the positive complementary sample assembled gradually, as shown by the linear decrease. This was continuous for the 1-hour experiment and potentially could have continued beyond this time limit. However, for practical application it was desirable to achieve a greater degree of assembly within a 1-hour time frame. Therefore, further investigation was required.

The extended length of the 100-base target sequence was considered to have the potential to form internal secondary structures that would effectively block or reduce the hybridisation rate due to limited accessibility to the probe hybridisation region.

Therefore, an elevated temperature was applied to minimise secondary structures, whilst maintaining probe specific hybridisation. The elevated temperature has the capacity to denature the weak and non-specific base-pair interactions within the target sequence. The elevated temperature provides the positive change in free energy required to dissociate the non-specific secondary structure interactions, whilst maintaining the potential to allow specific hybridisation of the probe sequences to the target. This was achieved by increasing the temperature to 45 °C which remained below the probe melting temperatures, thus ensuring that target hybridisation was not inhibited.

Secondary structures may be predicted *in silico* using the MFold application which determines the likelihood of secondary structure formation based upon the sequence, ionic concentration and temperature conditions.[115] The 100-base target sequence was analysed using salt adjusted parameters reflective of the buffer concentration (0.3 M NaCl) and the structures were compared at room temperature and 45 °C. The predicted structures are shown in **Figure 2.8**.

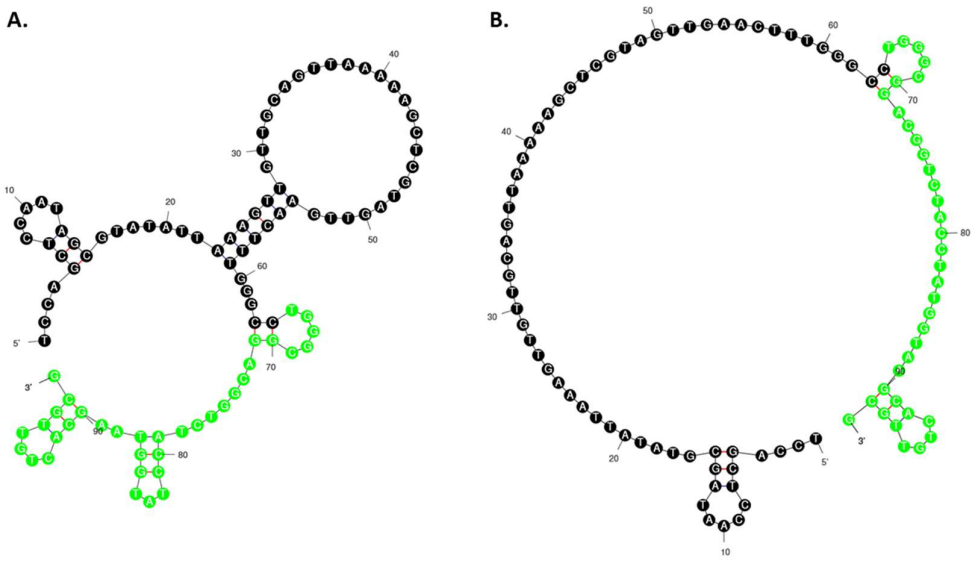

Figure 2.8. *Target secondary structures as predicted using MFold.* ***A.*** *Secondary structure at room temperature* ***B.*** *Secondary structure at 45 °C. Probe hybridisation region is highlighted in green.*

It was evident that the increased temperature significantly reduces the secondary structure formation, providing greater accessibility for probe hybridisation. The hybridisation kinetics investigation was repeated at 45 °C to identify if this improved the rate of hybridisation. The results are shown in **Figure 2.9**.

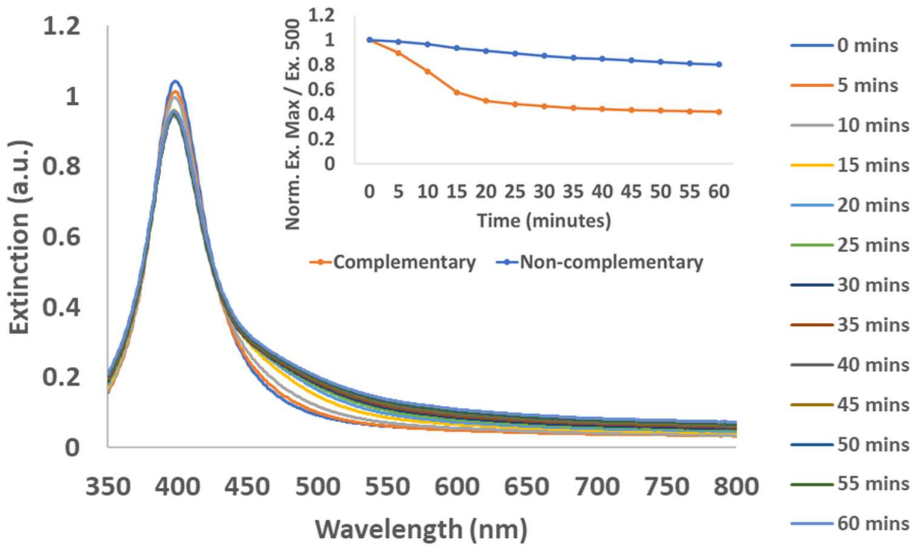

Figure 2.9. *Extinction spectrum of AgNP conjugates (10 pM of each conjugate) upon addition of 10 nM of complementary DNA at 45 °C for 1 hour. Inset shows the normalised extinction maximum / extinction 500 nm ratio for complementary (orange) and non-complementary (blue) target sequences.*

As observed previously, the extinction peak was dampened and an increase occurred at higher wavelengths, indicative of target recognition and assembly. However, the increase at 500 nm was more pronounced than observed at room temperature. Furthermore, the extinction maximum / extinction 500 ratio shows a non-linear trend, with the greatest extent of assembly occurring within the first 20 minutes. Following 20 minutes, the assembly plateaus and only a slight decrease is observable for the remaining 40 minutes. This indicated that the assembled NPs were stable in solution following assembly. The negative control sample showed a slight decrease in stability, although it was clearly distinct from the positive sample. It was possible the NPs were destabilised upon heating due to the disruption of non-specifically adsorbed probe nucleobases on the nanoparticle surface. Mirkin's group demonstrated that heating may be applied during conjugation to increase loading densities by disruption of non-specific nucleobase adsorption on the nanoparticle surface.[105] It is possible that during the conjugation procedure applied here, some of the probes were non-specifically adsorbed, and upon heating this was disrupted thus

deprotecting the NPs from salt-induced aggregation, however, further investigation would be required to confirm this hypothesis.

Molecular crowding agents have been shown to increase the rate of hybridisation and assembly of nanoparticle in solution. Storhoff et al., demonstrated that the addition of dextran sulfate was critical for the detection of a PCR fragment using DNA functionalised AuNPs, with no hybridisation evident without the addition of dextran sulfate.[63] Moreover, Zhang et al., have identified that the addition of high molecular weight polyethylene glycol (PEG) could increase the hybridisation efficiency of DNA functionalised AuNPs to a complementary target by 50 - 100 %.[116] Whilst the term "molecular crowding" is commonly applied, it is likely that a number of synergistic effects underlie the increased hybridisation rates observed upon addition of molecules such as dextran sulfate or PEG. These include volume exclusion, decreased molecular diffusion rates, changes in solution properties such as the dielectric constant and changes to biomolecular equilibrium constants.[117, 118]

High molecular weight PEG was selected for application in this investigation due to its commercial availability, variable molecular weight range, low-cost, non-ionic properties and biologically inert status. High molecular weight PEG 6000 was specifically selected as low molecular weight PEG has been shown to destabilise DNA duplexes, whereas high molecular weight PEG increases the stability of DNA duplexes.[119], [120] The hybridisation kinetics were investigated with the addition of 5 % PEG 6000 to the 0.3 M PBS buffer at room temperature (**Figure 2.10**).

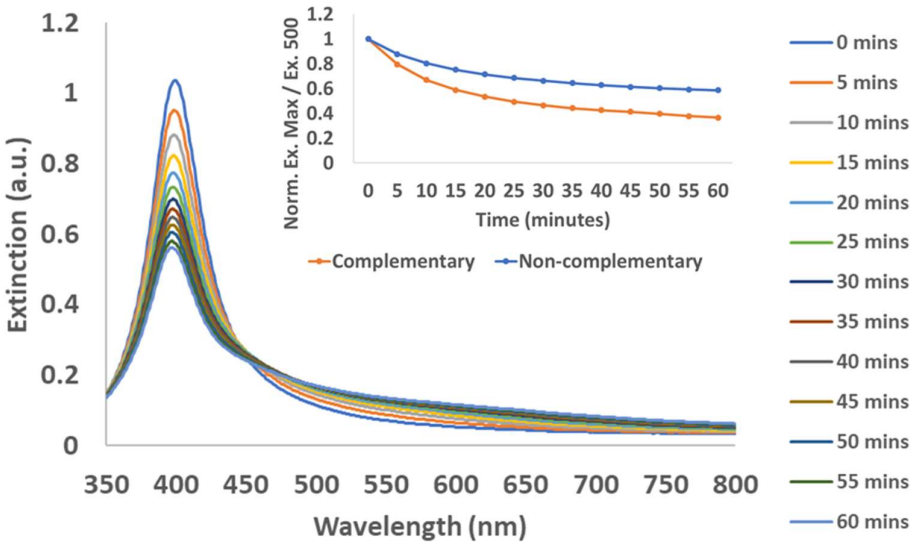

Figure 2.10. *Extinction spectrum of AgNP conjugates (10 pM of each conjugate) upon addition of 10 nM of complementary DNA at room temperature for 1 hour, with 5 % PEG 6000 added to the hybridisation buffer. Inset shows the normalised extinction maximum / extinction 500 nm ratio for complementary (orange) and non-complementary (blue) target sequences.*

Upon addition of 5 % PEG 6000 to the hybridisation buffer, both the complementary and non-complementary samples began to aggregate, as indicated by the extinction maximum / extinction 500 ratio. This loss of specificity was attributed to the crowding reagent instigating non-specific dimerization between the probe sequences, and the aggregation appeared to slow over time.

The previous experiment had indicated that the hybridisation kinetics may be improved upon hybridisation at 45 °C. This was attributed to the melting of target secondary structures which increased the accessibility to the probe hybridisation regions. As the addition of high molecular weight PEG induced non-specific interactions between the probe conjugates, it was considered that hybridisation at 45 °C may also prevent these interactions in addition to minimising target secondary structures. The experiment was repeated at 45 °C with the addition of a slightly reduced PEG concentration of 3 % to ensure specificity (**Figure 2.11**).

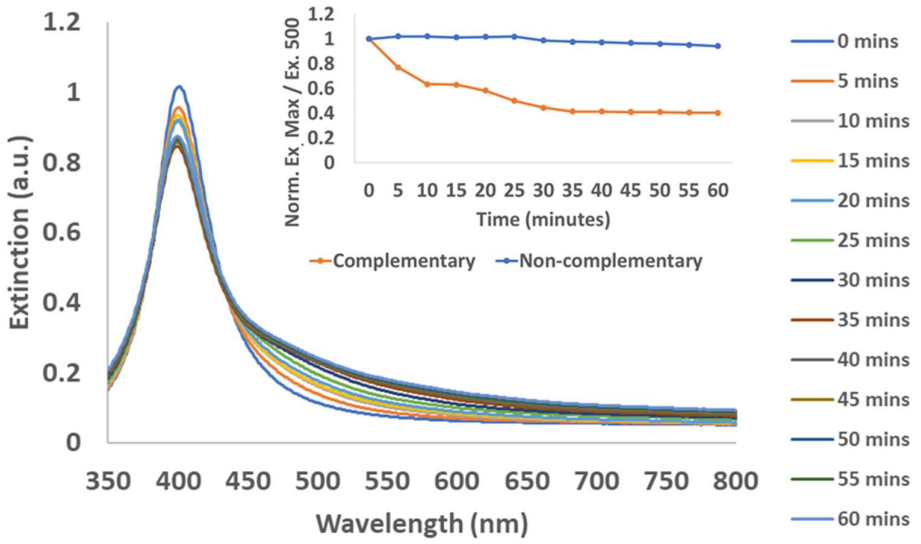

Figure 2.11. *Extinction spectrum of AgNP conjugates (10 pM of each conjugate) upon addition of 10 nM of complementary DNA at 45 °C for 1 hour, with 3 % PEG 6000 added to the hybridisation buffer. Inset shows the normalised extinction maximum / extinction 500 nm ratio for complementary (orange) and non-complementary (blue) target sequences.*

Upon addition of 3 % PEG 6000 and hybridisation at 45 °C, specificity was maintained, and good discrimination was achieved as indicated by the extinction max / extinction 500 ratio for complementary and non-complementary DNA. The results obtained were comparable to those achieved at 45 °C without the addition of PEG 6000. The negative control appeared to be more stable at 45 °C with the addition of PEG. This may be due to the PEG adsorbing to the surface and blocking any salt induced aggregation at 45 °C. This is supported by the findings of Zhang et al., who proposed the use of non-thiolated PEG as a blocking agent due to its capacity to adsorb onto the surface of bare AuNPS.[116] As the hybridisation kinetics were not significantly improved upon with the addition of 3 % PEG 6000, the concentration was increased to 5 % PEG 6000 and the experiment was repeated at 45 °C (**Figure 2.12**).

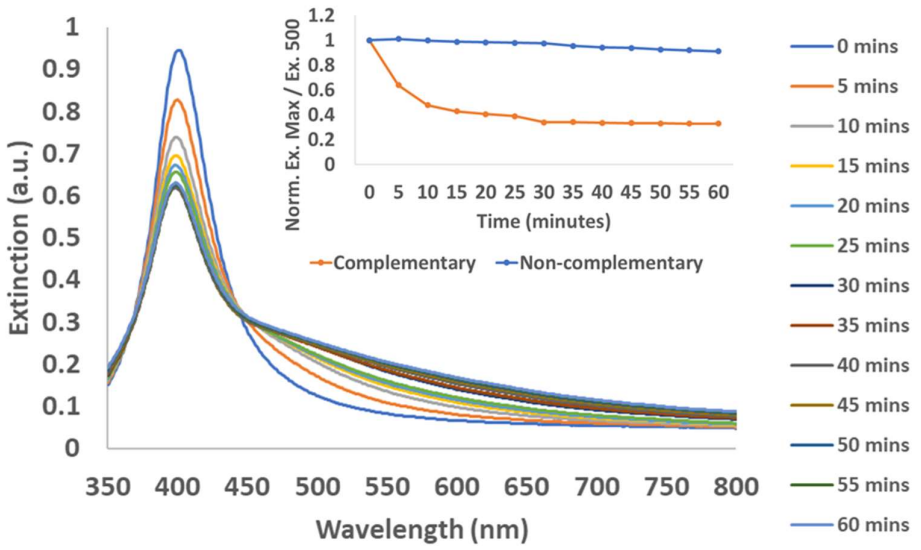

Figure 2.12. *Extinction spectrum of AgNP conjugates (10 pM of each conjugate) upon addition of 10 nM of complementary DNA at 45 °C for 1 hour, with 5 % PEG 6000 added to the hybridisation buffer. Inset shows the normalised extinction maximum / extinction 500 nm ratio for complementary (orange) and non-complementary (blue) target sequences.*

By increasing the concentration of PEG 6000 to 5 %, the rate and extent of assembly was significantly improved and crucially, the specificity was maintained. The extinction spectrum for the positive, complementary sample showed that the extinction maximum decreased to a much greater extent than the prior experiment without addition of PEG at 45 °C. This was accompanied by a distinct increase at 500 nm. The extinction maximum / extinction 500 ratio indicated that most of the assembly occurred within 10 minutes and that the negative, non-complementary sample was stable and therefore the AgNP assembly was DNA sequence specific.

As the hybridisation kinetics were improved by increasing the PEG concentration to 5 % whilst maintaining specificity, a further increase in concentration to 7 % was investigated to see if the crowding effect could be further optimised (**Figure 2.13**).

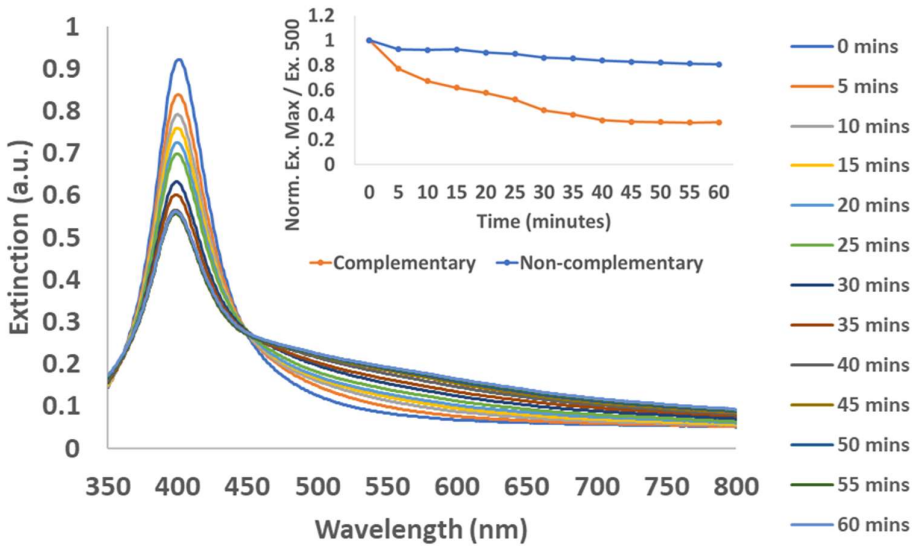

Figure 2.13. *Extinction spectrum of AgNP conjugates (10 pM of each conjugate) upon addition of 10 nM of complementary DNA at 45 °C for 1 hour, with 7 % PEG 6000 added to the hybridisation buffer. Inset shows the normalised extinction maximum / extinction 500 nm ratio for complementary (orange) and non-complementary (blue) target sequences.*

As observed previously, a significant decrease in the extinction maximum occurred with a significant increase at 500 nm. However, the extinction maximum / extinction 500 ratio indicated that the rate of assembly was reduced with the increase to 7 % PEG 6000. As stated previously, the addition of molecular crowding agents may have an effect via more than one mechanism including volume exclusion, decreased molecular diffusion rates, changes in solution properties such as the dielectric constant and changes to biomolecular equilibrium constants.[117], [118] It is likely that the improved hybridisation kinetics observed using 5 % PEG 6000 occurred due to volume exclusion. As the PEG concentration increased, the solution becomes more viscous and it is possible that decreased molecular diffusion began to decrease the rate of assembly. Furthermore, the increase to 7 % PEG 6000 began to induce non-specific interactions between the conjugate probes, as indicated by the decrease in the extinction maximum / extinction 500 ratio for the negative, non-complementary sample. Therefore, it was concluded that optimal hybridisation assembly kinetics

could be achieved with addition of 5 % PEG 6000 at 45 °C. To ensure the reproducibility of the optimised conditions, the experiment was repeated in triplicate with a new batch of AgNPs (**Figure 2.14**).

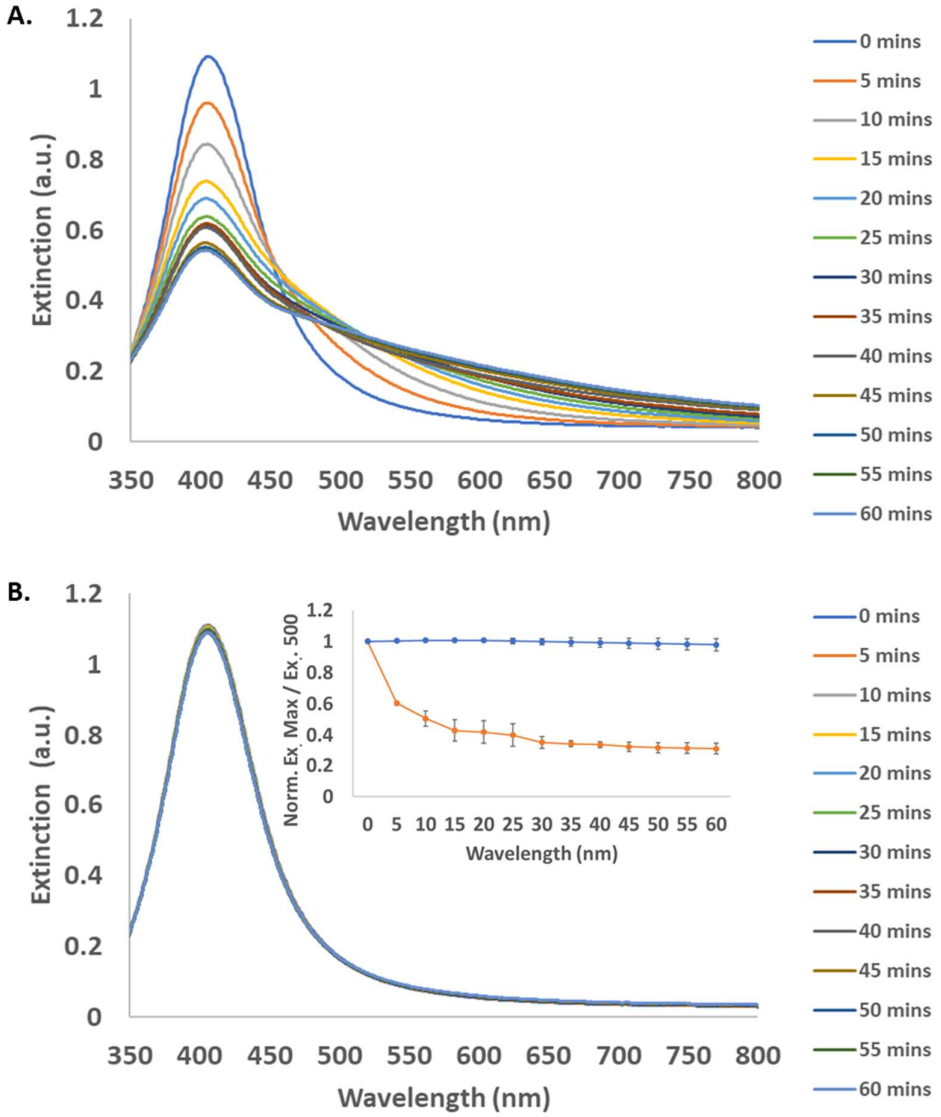

Figure 2.14. *Extinction spectra of AgNP conjugates (10 pM of each conjugate) upon the addition of 10 nM of complementary or non-complementary DNA at 45 °C for 1 hour, with 5 % PEG 6000 added to the hybridisation buffer.* ***A.*** *Complementary DNA* ***B.*** *Non-complementary DNA. Inset shows the normalised mean (n=3) extinction maximum / extinction 500 nm ratio for complementary (orange) and non-complementary (blue) target sequences.*

The results were highly comparable to the previous data and any deviation between samples was minimal as indicated by the error bars of the extinction maximum / extinction 500 nm ratio. The greatest deviation occurred during the assembly process which was to be expected as the AgNPs changed from dispersed to assembled formation.

2.12 Optimisation of the SERS Response Upon the Assembly of DNA Functionalised AgNPs

Following the optimisation of the buffer hybridisation conditions and successful UV-Vis analysis, SERS analysis was implemented to identify if the assembly of AgNP conjugates in solution generated the expected electromagnetic SERS response upon creation of hotpot regions within the nanoparticle assemblies. All experiments were performed with 10 pM of each conjugate and 10 nM of target sequence. The conjugates were hybridised for one hour in 0.3 M PBS with the addition of 5 % PEG 6000 at 45 °C as optimised previously, and following hybridisation, the samples were immediately transferred to a black 96-well plate and analysed by SERS. The samples required immediate analysis, as removal from the heat-block induced non-specific interactions in the negative sample as the solution cooled. This was undesirable as non-specific interactions can significantly increase the SERS intensity, producing a false-positive signal. The SERS analysis was performed using a 532 nm wavelength and 10 % (5 mW) laser power for all experiments performed. Each experiment was repeated in triplicate.

The SERS investigation began with the analysis of conjugates assembled in the tail-to-tail, head-to-tail and head-to-head orientations. A colour change was observable upon hybridisation in each of these orientations, however SERS analysis was required to confirm that the AgNPs were assembled in near enough proximity to generate electromagnetic SERS enhancement for discrimination of the target DNA sequences. Initially, the tail-to-tail orientation was analysed (**Figure 2.15**).

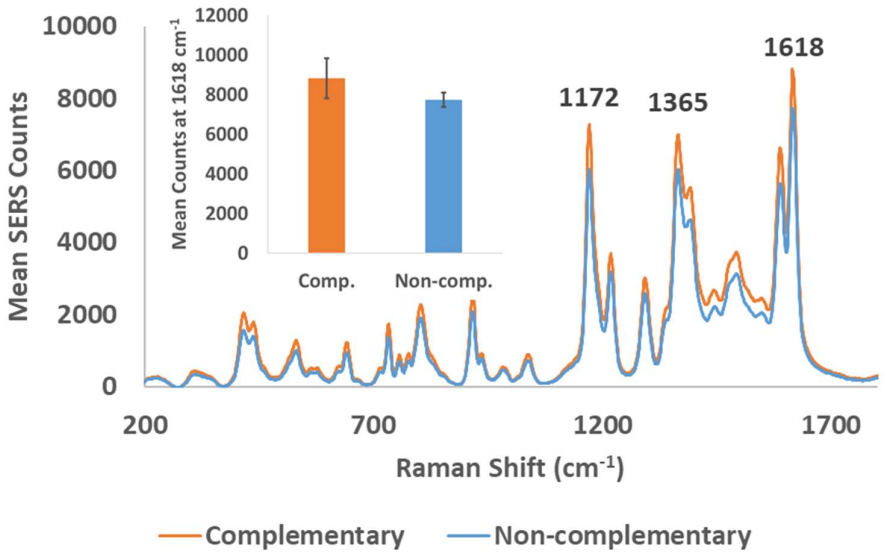

Figure 2.15. *Mean (n=3) SERS spectra of AgNP conjugates (10 pM of each conjugate) hybridised in the tail-to-tail orientation upon the addition of 10 nM of complementary or non-complementary DNA at 45 °C for 1 hour, with 5 % PEG 6000 added to the hybridisation buffer. Inset shows an on: off ratio of 1: 1 for peak comparison at 1618 cm^{-1}. Spectra accumulated with a 532 nm laser, 1 second acquisition time and 10 % (5 mW) laser power.*

As this orientation coordinated the conjugates in the least proximate position of the three orientations investigated here, it was expected that this would generate minimal electromagnetic enhancement and by association, a poorer discriminatory value. It was confirmed by SERS analysis that the tail-to-tail orientation did not generate significant SERS enhancement for the discrimination of complementary from non-complementary DNA target sequences upon assembly. With comparison of the peak at 1618 cm^{-1} for complementary and non-complementary DNA, an on: off ratio of approximately 1: 1 was observed and therefore target discrimination was not achieved. Following analysis of the tail-to-tail orientation, the head-to-tail orientation was investigated (**Figure 2.16**).

As the head-to-tail orientation positions the conjugates in a closer proximity than the tail-to-tail orientation upon hybridisation, it was expected that this would generate a greater magnitude of SERS enhancement. The results indicated that the head-to-

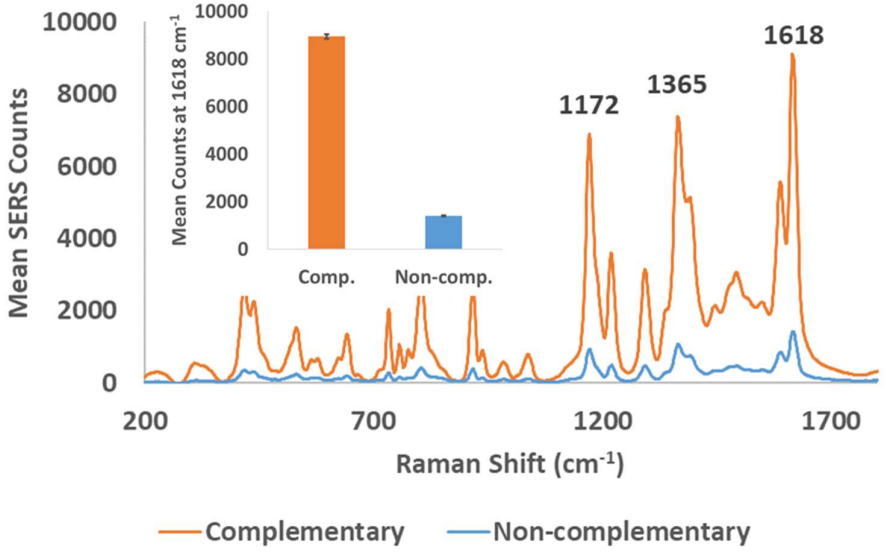

Figure 2.16. *Mean (n=3) SERS spectra of AgNP conjugates (10 pM of each conjugate) hybridised in the head-to-tail orientation upon the addition of 10 nM of complementary or non-complementary DNA at 45 °C for 1 hour, with 5 % PEG 6000 added to the hybridisation buffer. Inset shows an on: off ratio of 6: 1 for peak comparison at 1618 cm^{-1}. Spectra accumulated with a 532 nm laser, 0.1 second acquisition time and 10 % (5 mW) laser power.*

head orientation induced significant electromagnetic enhancement of the SERS signal upon hybridisation. The AgNP conjugates that were assembled in the presence of the complementary target sequence provided an on: off ratio of 6:1 which was a significant improvement in discrimination as compared to the tail-to-tail orientation. Finally, the head-to-head orientation was analysed (**Figure 2.17**).

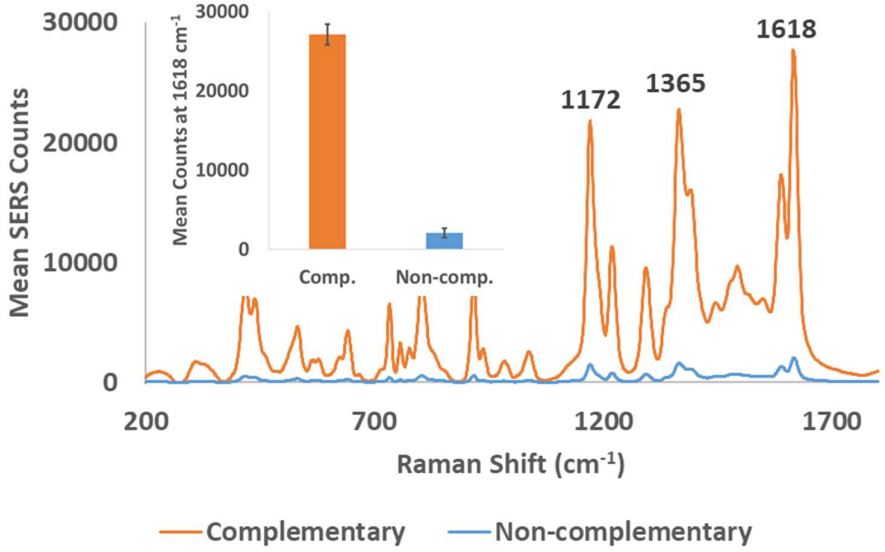

***Figure 2.17**. Mean (n=3) SERS spectra of AgNP conjugates (10 pM of each conjugate) hybridised in the head-to-head orientation upon the addition of 10 nM of complementary or non-complementary DNA at 45 °C for 1 hour, with 5 % PEG 6000 added to the hybridisation buffer. Inset shows an on: off ratio of 13: 1 for peak comparison at 1618 cm^{-1}. Spectra accumulated with a 532 nm laser, 0.1 second acquisition time and 10 % (5 mW) laser power.*

As this orientation positioned the AgNP conjugates in closest possible proximity, it was expected that this would induce the maximum enhancement of the three orientations investigated. The results confirmed that head-to-head orientation produced the greatest SERS enhancement of all three orientations when hybridised to the complementary target sequence and an on: off discriminatory ratio of 13: 1 was achieved. It was concluded that the electromagnetic SERS response that is indicative of target hybridisation, may be tuned to generate an optimal signal by positioning conjugates in the head-to-head orientation.

Upon identification of the head-to-head orientation being the optimal condition for SERS discrimination of the target sequence, further consideration was given to the optimisation of the PEG molecular weight for maximisation of the SERS intensity and discriminatory value. Spink and Chaires have previously identified that PEG may

affect the stability of DNA as a function of concentration and molecular weight, with low molecular weight PEG destabilising duplex formations and high molecular weight PEG stabilising duplex formations.[119] In this instance, PEG 1000 had no effect on duplex stability, whereas duplexes were increasingly destabilised as the PEG molecular weight decreased below this threshold. Conversely, duplex formation was increasingly stabilised by PEG as the molecular weight was increased above this threshold. Further investigation by Knowles et al., delineated these opposing effects and determined that low molecular weight PEG preferentially interacts with the nucleobases of DNA and destabilises the duplex, whereas high molecular weight stabilises DNA duplexes by volume exclusion.[121] Importantly, whilst high molecular weight stabilised duplex DNA formation, it did not stabilise intra-strand hairpin formations. This suggests that high molecular weight PEG may stabilise probe-target hybridisations without stabilising target secondary structures which may reduce hybridisation efficiency.

Therefore, the PEG molecular weight investigation utilised high molecular weight PEG to ensure that the results were related to the beneficial effect of volume exclusion, rather than the direct DNA interaction and destabilisation that may occur with application of low molecular weight PEG. PEG 2000, PEG 6000 and PEG 10000 were added separately to the 0.3 M PBS buffer at a standard concentration of 5 % and the samples were hybridised at 45 °C for 1 hour prior to SERS analysis. The sample containing PEG 2000 was analysed initially (**Figure 2.18**).

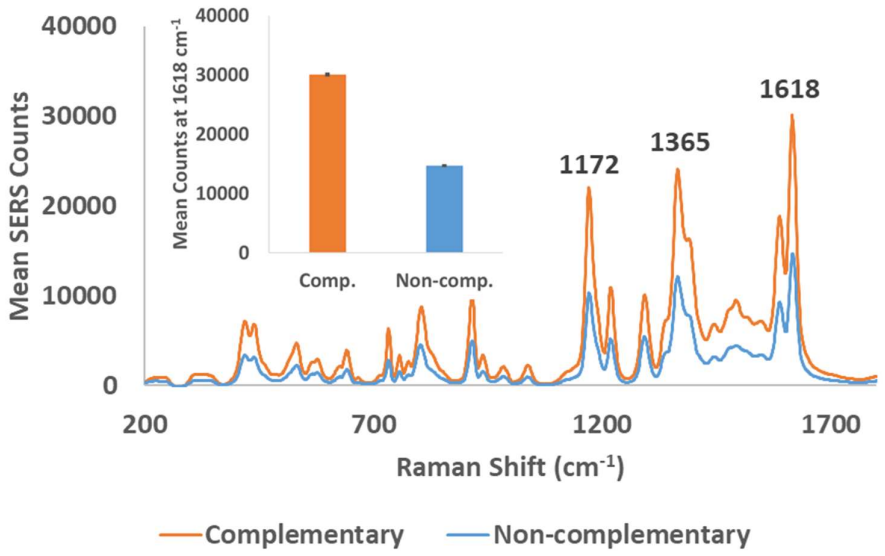

Figure 2.18. *Mean (n=3) SERS spectra of AgNP conjugates (10 pM of each conjugate) hybridised in the head-to-head orientation upon the addition of 10 nM of complementary or non-complementary DNA at 45 °C for 1 hour, with 5 % PEG 2000 added to the hybridisation buffer. Inset shows an on: off ratio of 2: 1 for peak comparison at 1618 cm^{-1}. Spectra accumulated with a 532 nm laser, 0.1 second acquisition time and 10 % (5 mW) laser power.*

With the addition of PEG 2000 to the 0.3 M PBS buffer, it was evident that discrimination of the complementary and non-complementary target sequences could be achieved, however the on: off ratio of 2: 1 was lesser than that previously observed with the use of PEG 6000. The experiment was repeated to ensure the reproducibility of the previous result obtained using PEG 6000, and for further comparison with PEG 2000 and PEG 10000 using the same conjugate batch (**Figure 2.19**).

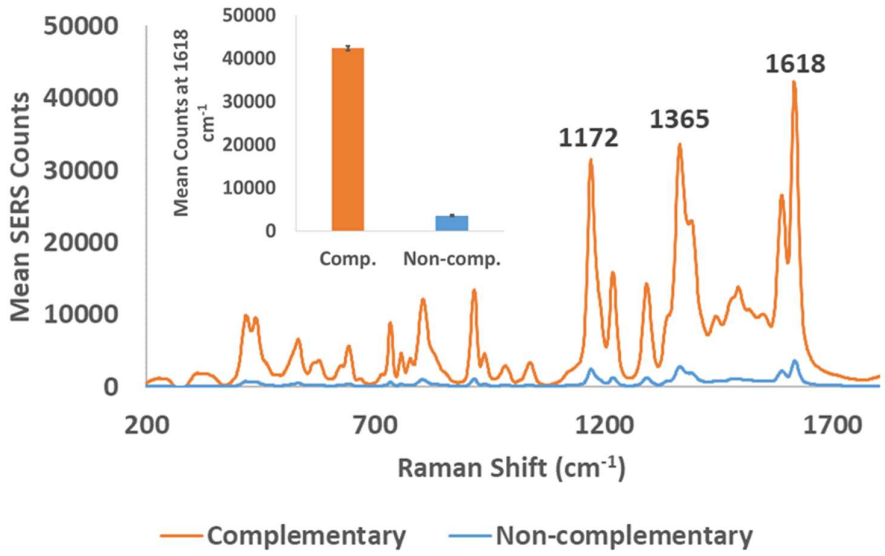

Figure 2.19. *Mean (n=3) SERS spectra of AgNP conjugates (10 pM of each conjugate) hybridised in the head-to-head orientation upon the addition of 10 nM of complementary or non-complementary DNA at 45 °C for 1 hour, with 5 % PEG 6000 added to the hybridisation buffer. Inset shows an on: off ratio of 12: 1 for peak comparison at 1618 cm^{-1}. Spectra accumulated with a 532 nm laser, 0.1 second acquisition time and 10 % (5 mW) laser power.*

The addition of 5 % PEG 6000 displayed significantly improved discrimination as compared to PEG 2000 with an on: off ratio of 12:1. This was highly comparable to the discrimination ratio achieved previously with addition of PEG 6000 which produced an on: off ratio of 13:1. This suggested that the assembly process was highly reproducible with use of a new batch of NPs and fresh aliquot of MGITC reporter dye. Finally, the addition of 5 % PEG 10000 to the hybridisation buffer was analysed by SERS (**Figure 2.20**).

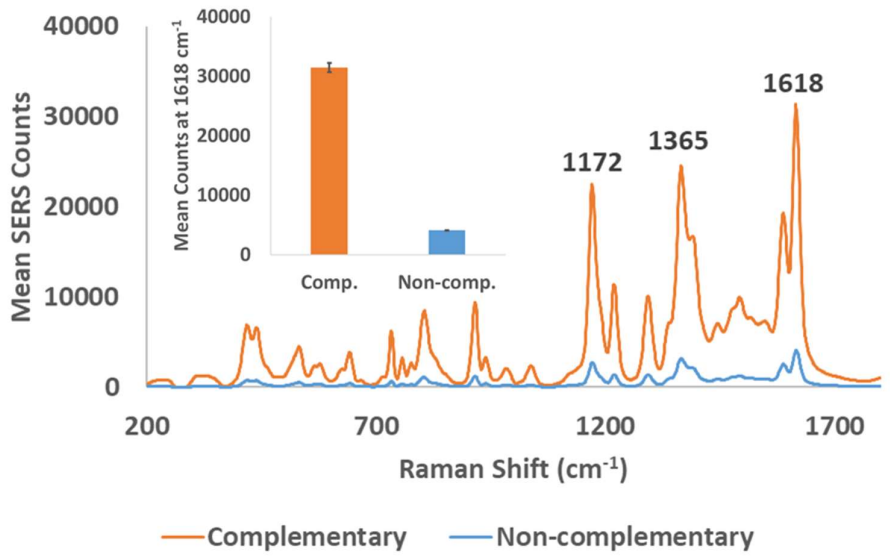

Figure 2.20. *Mean (n=3) SERS spectra of AgNP conjugates (10 pM of each conjugate) hybridised in the head-to-head orientation upon the addition of 10 nM of complementary or non-complementary DNA at 45 °C for 1 hour, with 5 % PEG 10000 added to the hybridisation buffer. Inset shows an on: off ratio of 8: 1 for peak comparison at 1618 cm^{-1}. Spectra accumulated with a 532 nm laser, 0.05 second acquisition time and 10 % (5 mW) laser power.*

Upon addition of 5 % PEG 10000 to the hybridisation buffer, there was clear discrimination between the complementary and non-complementary samples, with an on: off ratio of 8: 1 achieved. This was significantly better than the 2: 1 discriminatory ratio achieved using PEG 2000, although the discriminatory value was lesser than the 12: 1 discriminatory value obtained using PEG 6000. It was noted that the addition of PEG 6000 provided better discrimination, however, the addition of PEG 10000 provided greater SERS intensity. The acquisition time was reduced from 0.1 seconds (as applied for the PEG 2000 and PEG 6000 conditions) to 0.05 seconds to prevent signal saturation. Therefore, the reduced discriminatory value of PEG 10000 as compared to PEG 6000 was due to an increase in SERS intensity gained from the non-complementary negative control sample, rather than a decrease in signal from the complementary, positive sample.

It was considered that the volume exclusion effect of high molecular weight PEG increased as the molecular weight increased. Whilst this effect generated exceptionally high SERS intensities for the samples assembled with complementary DNA, it also appeared to instigate dimerization of AgNP conjugates in the negative sample, thus increasing the intensity observed in this sample. To investigate this theory, a low concentration of Tween 20 was added to reduce the non-specific interactions which occurred with the addition of PEG 10000. Tween 20 is non-ionic and therefore should not cause any aggregation. If the non-specific interactions could be reduced whilst maintaining the target sequence specificity, it was thought that the exceptional SERS intensity could be maintained, and the discriminatory value could be improved. The experiment was repeated with the addition of 5 % PEG 10000 and further addition of 0.1 % Tween 20 (**Figure 2.21**).

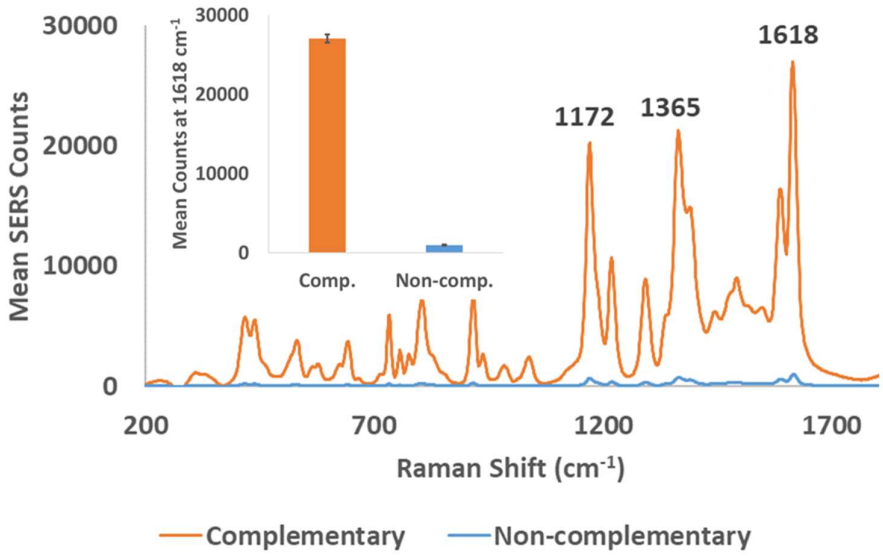

Figure 2.21. *Mean (n=3) SERS spectra of AgNP conjugates (10 pM of each conjugate) hybridised in the head-to-head orientation upon the addition of 10 nM of complementary or non-complementary DNA at 45 °C for 1 hour, with 5 % PEG 10000 and 0.1 % Tween 20 added to the hybridisation buffer. Inset shows an on: off ratio of 28: 1 for peak comparison at 1618 cm^{-1}. Spectra accumulated with a 532 nm laser, 0.05 second acquisition time and 10 % (5 mW) laser power.*

With addition or 0.1 % Tween 20 to the hybridisation buffer containing PEG 10000, it was confirmed that significant improvement could made to the discriminatory value of the detection method, whilst maintaining significant SERS intensity. The further optimisation of the buffer conditions with addition of 0.1 % Tween 20 generated an on: off ratio of 28: 1 which was significantly better than any of the discriminatory ratios that were obtained previously. Whilst the Tween 20 served to reduce the non-specific interactions, the surfactant doesn't discriminate between specific and non-specific interactions, and the SERS intensity appeared to be reduced for both the complementary and non-complementary samples. Therefore, the Tween 20 concentration was further reduced to 0.05 % to identify if the lower concentration could further improve the discriminatory value (**Figure 2.22**).

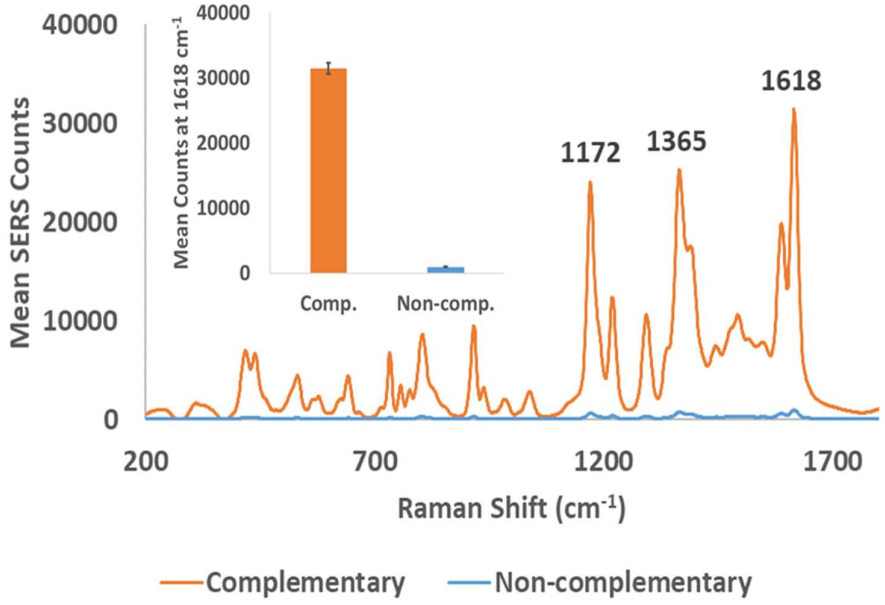

Figure 2.22. *Mean (n=3) SERS spectra of AgNP conjugates (10 pM of each conjugate) hybridised in the head-to-head orientation upon the addition of 10 nM of complementary or non-complementary DNA at 45 °C for 1 hour, with 5 % PEG 10000 and 0.05 % Tween 20 added to the hybridisation buffer. Inset shows an on: off ratio of 34: 1 for peak comparison at 1618 cm^{-1}. Spectra accumulated with a 532 nm laser, 0.05 second acquisition time and 10 % (5 mW) laser power.*

Following the reduction of Tween 20 concentration to 0.05 %, the optimal hybridisation conditions were obtained and an on: off ratio of 34: 1 was achieved. The greatest SERS intensity was provided with the addition of 5 % PEG 10000, whilst the interference from non-specific interactions could be eliminated with addition of 0.05 % Tween 20 without reducing the intensities observed upon sequence-specific target recognition.

2.13 Conclusion of the Proof-of-Principle Investigation

Upon completion of the proof-of-principle investigation, it was concluded that DNA functionalised and dye-coded AgNPs could be effectively applied for the species-specific detection of a 100-base *Candida krusei* target sequence in solution. This required careful consideration of probe design criteria and hybridisation conditions to ensure that the maximum discrimination could be obtained. Specifically, probe sequences were designed with an emphasis on avoiding probe dimer and hairpin formations, as even weak dimer interactions between probe sequences could cause the conjugates to aggregate and fall out of suspension prior to target recognition. These undesirable interactions could be exacerbated by the same conditions used to optimise target specific hybridisation such as an increase in the buffer salt concentration or addition of molecular crowding agents. Therefore, designing probe sequences to strictly avoid the potential for non-specific dimerization was essential for optimal assay performance.

Furthermore, as the ssDNA target increases in length and complexity, it may be assumed that the likelihood of intra-strand secondary structures such as hairpin formations will also increase. Ideally, the target should be designed to minimise secondary structure formations that may inhibit the hybridisation of probe conjugates. However, target sequences cannot be designed at will for the purpose of detecting biologically representative sequences, as the sequence must be sourced from a conserved region of the species genome. Therefore, experimental conditions were optimised to negate the issues associated with secondary structure formation. By increasing the probe annealing temperature to just below that of the probe

melting temperature, probe hybridisation was maintained, whilst secondary structure formations were minimised.

Additionally, the magnitude of the electromagnetic SERS response was tuned by altering the interparticle distance with selective thiol modification of the 3' and 5' ends of the probe sequences. The results produced from this investigation concluded that the head-to-head orientation could be applied to maximise the SERS intensity upon hybridisation. This was to be expected, however there was uncertainty as to whether steric hindrances would inhibit this orientation. As demonstrated, the head-to-head orientation hybridised effectively, and this offered significant advantages for the maximisation of SERS intensity.

Finally, the addition of cosolutes such as molecular crowding agents or surfactants to the hybridisation buffer were investigated to control the hybridisation properties without having to significantly alter the buffer salt concentration. Whilst increasing the salt concentration aided hybridisation by neutralising the negative charge associated with the sugar-phosphate backbone, this approach can also have disadvantages. For instance, increasing the salt concentration too much can cause aggregation by screening the negative charge associated with the NPs. The addition of increased salt concentrations will also stabilise non-specific dimer interactions which can increase the background signal and reduce discrimination. Furthermore, secondary structure formation in the target strand will be more complex and increasingly stable therefore inhibiting target hybridisation. Addition of high molecular weight PEG allowed for improved hybridisation efficiency, without significantly altering the ionic properties of the buffer.

The significant SERS intensity observed with a SERS on: off ratio of 34: 1 using optimised hybridisation conditions, demonstrated significant progression from prior work within the group for the discrimination of long-chain DNA target sequences in solution. Previous work by Mabbot et al.[81] achieved SERS on: off ratios of approximately 3: 1, 2:1, < 2: 1 and < 2:1 for target sequences that were 24, 48, 98 and 144 bases in length respectively. Furthermore, dextran sulfate was utilised within this

investigation as a molecular crowding agent which improved discrimination of the 144-base target, although the discriminatory value of the assay was only slightly improved with an on: off ratio of approximately 2: 1. Therefore, the optimised SERS on: off ratio of 34: 1 achieved represented a greater than 16-fold improvement in the discriminatory value, as compared to the previously obtained SERS on: off ratios for the detection of long-chain DNA fragments of comparable length.

The results produced from the work presented here, identified several key conditions that could be applied to improve the sensitivity of the detection method. For example, the application of an appropriate probe annealing temperature was not previously identified. Additionally, the advantages of applying the head-to-head orientation for maximisation of SERS intensity was not achieved previously due to steric hindrances. This was shown here to be achievable with the application of suitable hybridisation conditions. Moreover, the use of high molecular weight PEG as an alternative to dextran sulfate has been confirmed as an effective molecular crowding agent for the efficient generation of stable AgNP assemblies in solution. Further addition of a non-ionic surfactant for the reduction of background signal generated from the negative control may also be applied to improve the discriminatory value of the assay.

These findings have provided significant progression for the SERS detection of clinical fungal pathogens using DNA functionalised and dye-coded AgNPs in solution. The proof-of-principle investigation concluded that the detection of long-chain DNA sequences may be achieved, and that the conditions identified here should be applied to a biologically relevant amplification sequence in solution.

2.14 Experimental

Nanoparticle Synthesis: AgNPs were synthesised using the method previously published by Leopold and Lendl with reagent quantities adjusted proportionately for a 300 mL batch volume.[42] Final concentrations for each reagent were as follows; 1. 5 mM of hydroxylamine hydrochloride, 3 mM of sodium hydroxide and 10 mM of silver nitrate. The hydroxylamine hydrochloride and sodium hydroxide were dissolved in a

conical flask containing 270 mL of MQ water. Silver nitrate was dissolved separately in 30 mL of MQ water, then added to the reaction mixture and left to stir vigorously for 15 minutes at room temperature. The AgNPs were then filtered and stored in the dark at room temperature. All synthesis reagents were supplied by Sigma-Aldrich Ltd., Dorset, UK.

Oligonucleotide Probe and Synthetic Target Design and Preparation: A 100 base synthetic target sequence was selected from the 18S rRNA gene sequence for *Candida krusei* (also referred to as *Pichia kudriavzevii*), as identified by the GenBank accession number KP202859.1. HPLC purified 100 base oligo synthetic target sequence was ordered from ATDBio (Southampton, UK). Lyophilised oligo synthetic target sequence was briefly centrifuged and resuspended in MQ water to a final concentration of 100 µM and frozen for long-term storage. Probes were designed and evaluated *in silico* using the OligoAnalyzer 3.1 web application.[102] Probes were designed based upon recommended criteria for minimisation of secondary structure formations.[103] Hairpin, self-dimer and hetero-dimer structures were identified and accounted for by maintaining a minimum delta G threshold ≥ -9 kcal/mol to reduce the likelihood of secondary structure formation.[103] The probes were checked for specificity using the NCBI BLAST sequence database.[101] HPLC purified oligo probes were ordered from ATDBio (Southampton, UK). The probe sequences were modified with 3x hexaethylene glycol (HEG) spacer and a terminal dithiol. Lyophilised oligo probes were briefly centrifuged and resuspended in MQ water to a final concentration of 100 µM and frozen for long-term storage.

Buffer preparation: 0.1 M PBS was prepared using 0.1 M of sodium chloride and 10 mM of phosphate buffer powder and 0.3 M PBS was prepared using 0.3 M of sodium chloride and 10 mM of phosphate buffer powder. Both 0.1 M and 0.3 M PBS was adjusted to pH 7.4 and filtered prior to use. If required, further additives such as high molecular weight PEG or Tween 20 were added to the 0.3 M PBS at the appropriate w/v and v/v % concentrations and dissolved with gentle stirring prior to application. 250 mM citrate buffer was prepared using 250 mM of trisodium citrate and adjusted

to pH 3.0 using concentrated hydrochloric acid. All buffer reagents were supplied by Sigma-Aldrich Ltd., Dorset, UK.

Conjugate Preparation: AgNP concentrations were approximated using the Beer-Lambert law ($A = \varepsilon \times l \times C$) and extinction coefficient 537 x 108 M^{-1} cm^{-1} for 50 nm AgNPs.[97] Extinction spectra were gathered using a Varian Cary 300 Bio UV-Vis spectrophotometer (Agilent, California, USA). Conjugates were prepared using the pH adjusted method as published by Zhang et al.[108] The AgNP stock was dispensed in 900 µL volumes followed by the addition of oligo probes at a DNA: AgNP molar concentration ratio of 7500: 1, based upon a final conjugate volume of 1 mL. Samples were vortexed and left to equilibrate for 1 hour following addition of the oligo probes. This was followed by two stepwise additions of 250 mM citrate buffer (pH 3.0). Initially 30 µL of citrate buffer (pH 3.0) was added and shaken for 15 minutes. A further 30 µL of citrate buffer was added, and the total conjugate volume was increased to a volume of 1 mL with the addition of MQ water and left to equilibrate for 45 minutes without shaking. Following probe immobilisation, conjugates were centrifuged at 6000 rpm for 20 minutes and the supernatant was removed. The conjugate without addition of a Raman reporter was then resuspended in 500 µL of 0.1 M PBS (pH 7.4) for a 2x working stock. Addition of a Raman reporter was required for one of the conjugate probes. The reporter conjugate was resuspended in 900 µL of MQ water following DNA functionalisation, and the concentration calculated as previously. Malachite green isothiocyanate (MGITC) was added from a 100 µM stock solution at a MGITC: AgNP ratio of 2500: 1, based upon a final conjugate volume of 1 mL. The total reporter conjugate volume was increased to a volume of 1 mL with the addition of MQ water and sonicated for 3 minutes to facilitate adsorption of the MGITC onto the AgNP surface. The reporter conjugate was then centrifuged at 6000 rpm for 20 minutes and the supernatant was removed. The reporter conjugate was then resuspended in 500 µL of 0.1 M PBS (pH 7.4) for a 2x working stock.

Gel electrophoresis of the AgNP conjugates: 1 % agarose gels were cast using molecular biology grade agarose (Bioline Reagents Ltd., London, UK) dissolved in 1x

TBE buffer. Gel electrophoresis of the AgNP conjugates was performed using 1 % agarose gels run at 80 volts for 90 minutes in 1x TBE buffer.

Hybridisation Assay in Solution: Conjugates were hybridised in Eppendorf tubes containing 0.3 M PBS with inclusion of further additives such as high molecular weight PEG or Tween 20 at the appropriate w/w and v/v % concentrations if required. Eppendorfs were placed in a heat-block that was preheated to 45 °C prior to the addition of the reagents. The final volume for each sample was 500 µL per replicate. The 0.3 M PBS buffer and additives were initially aliquoted, followed by addition of 10 pM of each conjugate and 10 nM of the target sequence. Samples were briefly removed from the heat-block, vortexed and replaced within the heat-block prior to hybridisation. The samples were then hybridised for 1 hour at a constant temperature of 45 °C.

UV-Vis Kinetics Analysis: UV-Vis kinetics analysis was performed using a Varian Cary 300 Bio UV-Vis spectrophotometer and temperature controller (Agilent, California, USA). The kinetics data was collected using the scanning kinetics application. 500 µL of each sample was used for analysis.

SERS Analysis: SERS analysis was performed using a Snowy Range Instrument - Sierra 2.0 Raman Spectrometer (Wyoming, USA). All data was gathered using a 532 nm laser wavelength and 10 % (5 mW) laser power. The analysis was performed in a black 96 well plate placed upon an adjustable platform. The optimal plate distancing was calibrated using an absolute ethanol standard prior to sample analysis. 250 µL of each sample was used for analysis. Spectra were gathered in 5x accumulations and averaged using the proprietary software. The integration time was adjusted in accordance with sample signal intensity. Spectral data was baseline corrected using the SpectraGryph optical spectroscopy software.[122] Each spectrum was baseline corrected using the default adaptive baseline correction settings.

3 A Proof-of-principle Investigation for the SERS Detection of a PCR Product by the Controlled Assembly of DNA Functionalised and Dye-coded AgNPs in Solution

3.1 Aim of the Investigation

The proof-of-principle investigation concluded with the establishment of suitable hybridisation conditions for the species-specific detection of a complementary *Candida krusei* synthetic DNA target in solution using DNA functionalised and dye-coded AgNPs. This target was specifically chosen as the extended length of the target was reminiscent of the size of a typical DNA amplification product. As the assay principle was proven to be feasible, the investigation progressed toward the detection of a biologically relevant DNA amplification product. The aim of this investigation was to demonstrate the SERS detection of a polymerase chain reaction (PCR) amplification product specific to *Candida krusei*, using the same assay format established within the proof-of-principle investigation.

PCR is widely applied for the amplification and detection of DNA, although typically this amplifies DNA in its double-stranded form. This presents an obstacle for the direct detection of an amplification product using DNA functionalised NPs as the probe hybridisation regions are occupied by the presence of the complementary strand. Mabbot et al., have previously attempted to address this issue by application of sodium hydroxide alkali denaturation of the double-stranded amplification product prior to hybridisation with the DNA functionalised AgNPs.[81] This provided some discriminatory value, although the on: off ratio was typically less than 2: 1. Whilst sodium hydroxide may be used to denature DNA in to single-stranded form, both of the complementary strands remain in solution. Therefore, upon addition to a suitable hybridisation buffer, the complementary strands will compete for hybridisation with the DNA functionalised NPs. For this reason, it was necessary to

identify an alternative approach for the amplification of a ssDNA product for SERS detection.

Gyllensten and Erlich first reported the amplification of ssDNA by asymmetric PCR, using a single-step amplification procedure that incorporates a primer concentration imbalance.[123] The reaction mix contains one primer present at an excess concentration, and another primer is present at a lower, limited concentration. As the reaction proceeds, both primers are present, and dsDNA is amplified exponentially as per standard PCR. Following the initial amplification cycles, the concentration limited primer is depleted upon incorporation into the amplification product, leaving the reaction to proceed in the presence of the excess primer. The excess primer continues with the linear amplification of ssDNA from the dsDNA that was amplified in the initial cycles of the reaction. This produces a high concentration of DNA amplification product containing both dsDNA and ssDNA. The ssDNA may then be directly detected using hybridisation probes.

A refined set of primer design criteria were later published with the advent of linear-after-the-exponential PCR (LATE-PCR), which improved the efficiency of ssDNA synthesis by asymmetric PCR.[124, 125] The authors identified that the reduction in concentration of the limiting primer also reduces the melting temperature of this primer, and this reduces the reaction efficiency of the reaction as the primer melting temperature drops below the reaction annealing temperature. If the reaction annealing temperature is reduced to allow the limiting primer to anneal more efficiently, this encourages mis-priming and non-specific amplification by the excess primer. Therefore, it is essential to ensure that the primers used for LATE-PCR are designed based upon the concentration adjusted melting temperatures. The concentration adjusted melting temperature of the limiting primer (T_m^L) should be equal to or higher than that of the excess primer (T_m^X) which may be summarised as follows:

$$\mathbf{T_m^L - T_m^x \geq 0}$$

The LATE-PCR methodology was selected for application in this investigation, as the defined design criteria allow for the efficient synthesis of ssDNA in a one-pot reaction, producing a target that should be accessible for direct hybridisation without competition from the complementary strand.

3.2 PCR Primer and Probe Sequences

The PCR assay that was implemented in this investigation amplified a 383 bp region of the 18s rRNA gene sequence, and the primer sequences used were pre-designed by a commercial sponsor of this project. The primers were not specifically designed for the purpose of asymmetric PCR and careful consideration was required to ensure that the LATE-PCR criteria could be met. Specifically, the limiting primer should have a concentration adjusted melting temperature that is equal to or above that of the excess primer. The primer sequences used in this investigation are described within **Table 3.1**.

Table 3.1. *Candida krusei PCR primer sequences used for the amplification of a 383 bp region of the 18s rRNA gene.*

Primer Name	Sequences (all in 5' – 3' direction)
Forward primer	5' – GAC AAT AAA TAA CGA TAC AGG G – 3'
Reverse primer	5' – CGT CCC TAT TAA TCA TTA CGA T – 3'

It was noted that the forward primer contained a single-base mismatch that was not complementary to the *Candida krusei* target strand. This mismatch is underlined and highlighted in red in **Table 3.1**. The single base mismatch formed an adenine-adenine base pair rather than a thymine-adenine base-pair. This was important as single base mismatches reduce duplex stability and by association, the melting temperature of the primer. This needed to be accounted for when calculating the primer melting temperatures *in silico*.

The OligoAnalyzer application was used to calculate the primer melting temperatures as this allowed for the adjustment of monovalent and divalent salt concentrations, and further accounted for the effect of mismatches within the duplex structure.[102]

The salt concentrations were adjusted to reflect the composition of the PCR buffer mix which contained 50 mM of potassium and 1.5 mM of magnesium. The magnesium concentration was increased to 3.5 mM as further addition of magnesium was found to be optimal for the amplification of dsDNA using the standard PCR conditions recommended by the commercial sponsor. The oligonucleotide concentration was adjusted to 0.8 µM as this was the primer concentration used for the standard PCR amplification of dsDNA.

The melting temperature of the forward primer was calculated using the standard PCR conditions described above, with and without the acknowledgment of the single-base mismatch to identify if this significantly reduced the melting temperature of the forward primer. The melting temperature of the reverse primer was calculated using the standard PCR conditions described above. This was then recalculated using a reduced primer concentration of 0.08 µM, which represented the concentration adjusted primer imbalance used within the asymmetric PCR assay. The predicted melting temperatures are described within **Table 3.2**.

Table 3.2. *Candida krusei PCR primer melting temperatures predicted using the OligoAnalyzer application.*

Sequence Name	Melting Temperature
Forward primer	59.1 °C
Forward primer with mismatch adjustment	55.5 °C
Reverse primer	60.1 °C
Reverse primer with concentration adjustment	57 °C

The *in silico* prediction of primer melting temperatures confirmed that both the sequence mismatch and concentration adjustment significantly affected the primer melting temperatures. The forward primer had a predicted melting temperature of 59.1 °C, although the inclusion of a single base mismatch reduced this to 55.5 °C. The reverse primer had a melting temperature of 60.1 °C, although a ten-fold reduction in concentration reduced this to 57 °C. The most important consideration was the

significant reduction in melting temperature due to the mismatch in the forward primer. With consideration of the internal mismatch, the forward primer had a melting temperature that was 1.5 °C below the melting temperature of concentration adjusted reverse primer. Using this information, the LATE-PCR criteria could be fulfilled. The reverse primer was designated as the limiting primer and the forward primer was designated as the excess primer. Using the mismatch and concentration adjusted melting temperatures for these primers respectively, the simple equation could be solved as follows:

$$\mathbf{T_m^L\ (57\ °C) - T_m^x\ (55.5\ °C) = 1.5\ °C}$$

Whilst the *in silico* prediction of melting temperature was useful for interpreting the effects of primer mismatches and concentration dependence, the OligoAnalyzer application appeared to underestimate the expected melting temperatures for the primer sequences. The pre-developed assay conditions recommended a primer annealing temperature of 58 °C which is above the predicted melting temperature of the forward primer containing a single base mismatch. The PCR assay was found to amplify DNA efficiently using an annealing temperature of 58 °C, suggesting an underestimation from the predicted values. Other applications were considered and provided some variation in predicted values, although many did not allow for the inclusion of mismatches when calculating melting temperatures. Therefore, the predicted values were considered as an approximation, and experimental validation was required for further optimisation of the asymmetric PCR assay.

3.3 Optimisation of Standard PCR Assay

The PCR conditions for the amplification of a 383 bp dsDNA product were optimised prior to implementation within this investigation and the temperature cycle conditions were pre-determined. Two proprietary polymerase enzymes were evaluated in parallel to assess their performance for amplification by PCR. Hot Start Taq was selected for specificity and OneTaq was selected for sensitivity. Each of the PCR optimisation experiments amplified DNA from template plasmid DNA supplied by the commercial sponsor (Renishaw Diagnostics). This was diluted from 10^9 copy

numbers to 10^4 template copy numbers prior to amplification unless stated otherwise. Initially, the magnesium concentration was titrated to ensure optimal amplification efficiency as confirmed by endpoint gel electrophoresis (**Figure 3.1**).

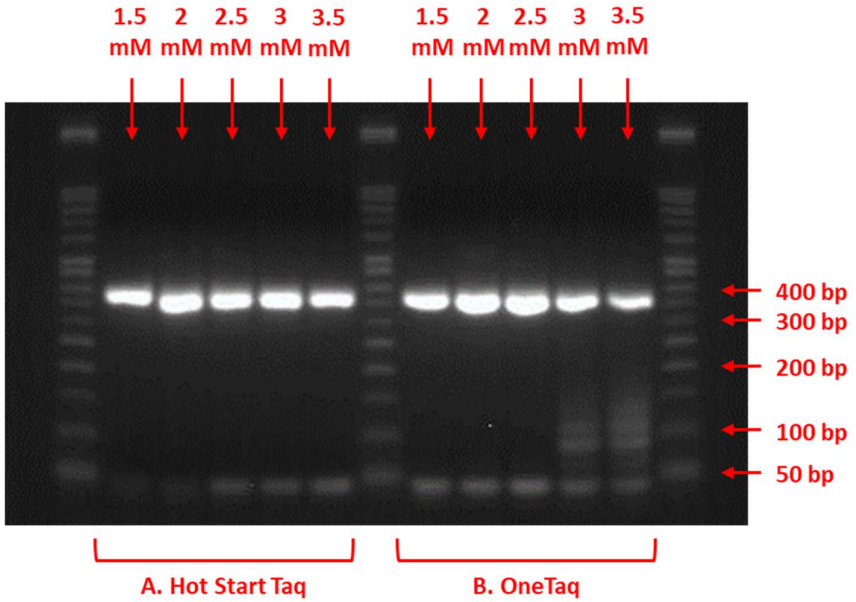

Figure 3.1. *Gel electrophoresis image of PCR product following titration of magnesium concentration.* ***A.*** *Hot Start Taq* ***B.*** *OneTaq.*

The PCR product was amplified using 10^4 copy numbers of plasmid template DNA and amplified a product of the expected size as confirmed by comparison to a 50 bp DNA ladder. The 383 bp product displayed clear amplification bands that could be visualised using GelRed nucleic acid gel stain. The specific PCR product was located between the 350 bp and 400 bp bands of the 50 bp DNA ladder that was used for size comparison. The optimal magnesium concentrations were 2 mM and 2.5 mM for Hot Start Taq and OneTaq respectively, as indicated by the band intensity. Some non-specific smearing was evident for the OneTaq amplification at increased magnesium concentrations, suggesting lower specificity. Following optimisation of the magnesium concentration, the lowest visually observable concentration was identified as shown in **Figure 3.2**.

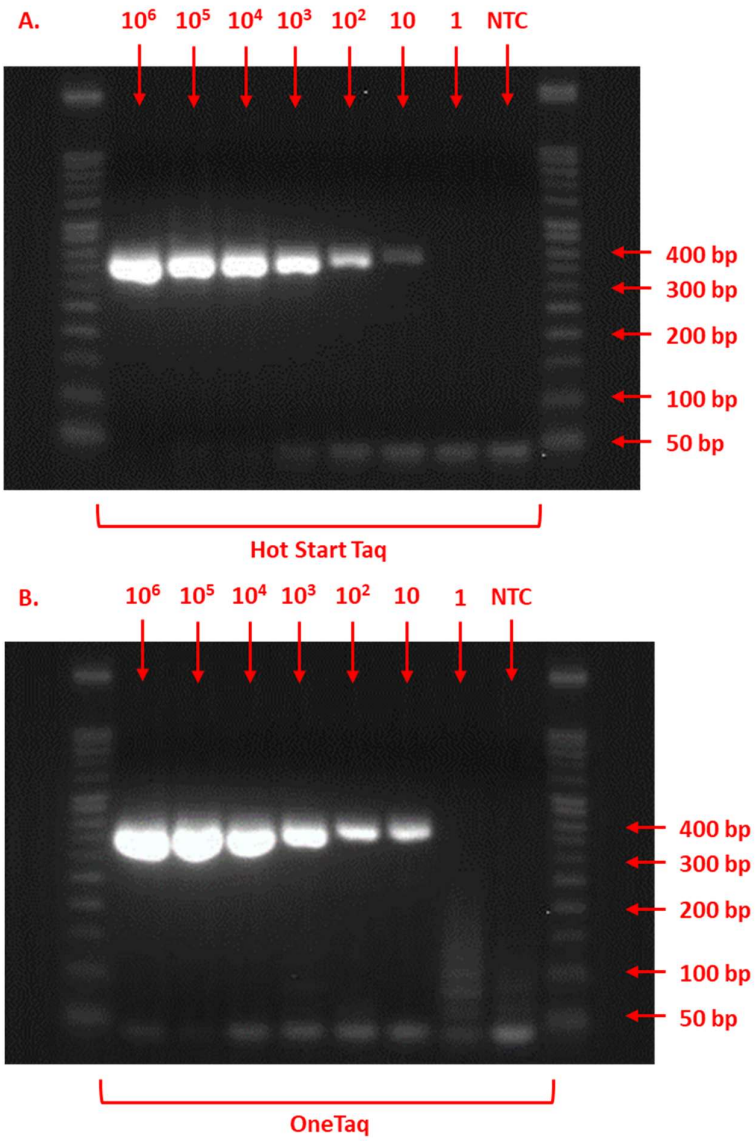

Figure 3.2. *Gel electrophoresis image of PCR product following serial dilution of template copy number range.* ***A.*** *Hot Start Taq* ***B.*** *OneTaq.*

The visually observable concentration range included a no template control (NTC) to ensure specificity. The lowest visually observable concentration was established at 10 copy numbers for each polymerase investigated. The OneTaq polymerase appeared to amplify the target more efficiently as evident by the brighter band at 10 copy numbers when compared to the Hot Start polymerase, suggesting a higher degree of sensitivity. Both the Hot Start Taq and OneTaq produced some primer-dimers which produced the faint bands below the 50 bp marker of the DNA ladder.

Primer-dimer formations occur as the primers self-recognise, producing non-specific amplification products. The amplification of these primer-dimers was further evident when analysing the real-time amplification curves generated with the inclusion of SYBR Green dye in the reaction mix **(Figure 3.3**).

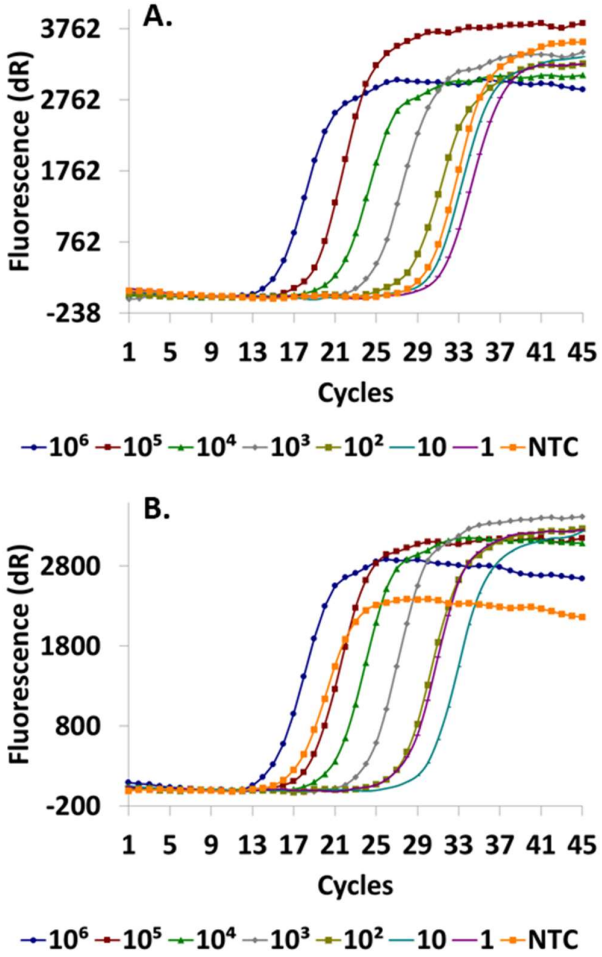

***Figure 3.3**. SYBR Green PCR amplification curves following serial dilution of template copy number range. **A.** Hot Start Taq **B.** OneTaq.*

The SYBR Green amplification curves confirmed the synthesis kinetics of the dsDNA product in real-time. SYBR Green preferentially interacts with DNA duplex formations by intercalation, electrostatic interactions and extended contact with the minor groove of the DNA helix, which subsequently increases the fluorescence intensity by approximately 1000-fold.[126] The amplification curves displayed in **Figure 3.3** show that as the template copy numbers decreased, the number of cycles required to

exponentially amplify the target increased. The formation of primer-dimers produced a false-positive amplification curve as the SYBR Green dye does not discriminate between specific and non-specific amplifications products. This was particularly evident when observing the fluorescence generated for the no template control samples. The Hot Start Taq began to amplify primer-dimers after approximately 30 cycles, whereas the OneTaq amplified primer-dimers after approximately 17 cycles. This confirmed that the Hot Start Taq polymerase had a higher degree of specificity than the OneTaq polymerase.

3.4 Optimisation of Asymmetric PCR Assay

Following the optimisation and establishment of the lowest visually observable concentration for the PCR assay, the amplification conditions were adapted for the synthesis of ssDNA by asymmetric PCR. Prior to optimisation of the asymmetric PCR assay, an aliquot of the double-stranded PCR product was enzymatically digested using lambda exonuclease to produce a ssDNA product (**Figure 3.4**).

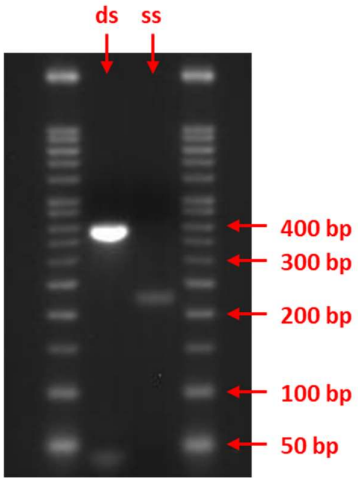

Figure 3.4. *Gel electrophoresis image of PCR product amplified with comparison of dsDNA product (ds) and lambda exonuclease digested ssDNA product (ss).*

When comparing the dsDNA PCR product and the digested ssDNA PCR product by gel electrophoresis, it was evident that the ssDNA migrated further than the dsDNA product, although both products were the same length. This comparison was necessary as it provided a reference for sizing of the asymmetric PCR product at a

later stage, thus ensuring the specificity of the asymmetric ssDNA product. Whilst the undigested dsDNA product was located just below the ladder band at 400 bp, as expected for the 383 bp PCR product, the ssDNA PCR product migrated further and was located just below the 250 bp band of the DNA ladder. This position was then used for confirmation of the desired ssDNA PCR product by asymmetric PCR. The band intensity was significantly reduced for the digested ssDNA product. This was attributed to the GelRed dye which will fluoresce with approximately 50 % less intensity upon interaction with ssDNA as compared to the dsDNA equivalent, according to manufacturer guidelines. Therefore, the band intensities could not be compared directly for an estimation of yield following amplification and digestion.

Following the identification of both the dsDNA and ssDNA products by gel electrophoresis, the optimisation of the asymmetric PCR assay was implemented. This began with the identification of the optimal excess: limiting primer ratio required for ssDNA amplification. The excess primer was maintained at the same concentration used for standard PCR, whereas the limiting primer was reduced in concentration accordingly. The amplification products for each ratio investigated are displayed within **Figure 3.5**.

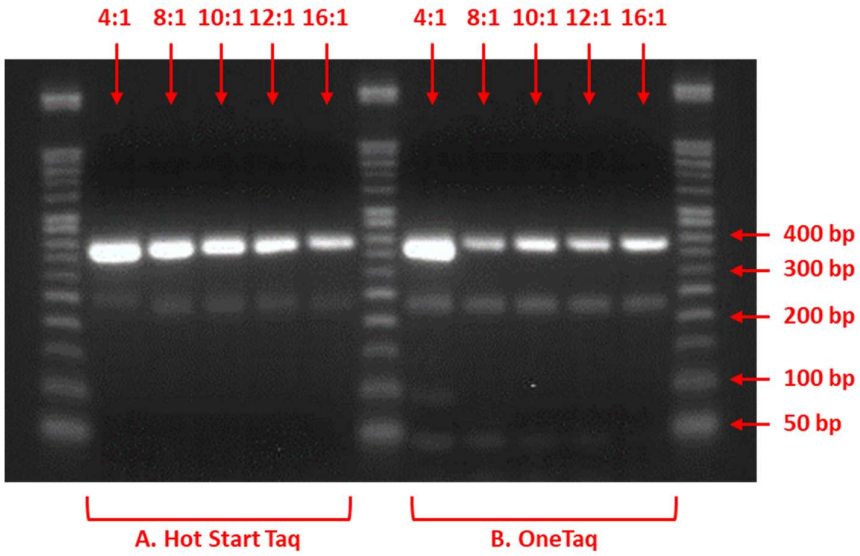

Figure 3.5. *Gel electrophoresis image of asymmetric PCR product following titration of the excess: limiting primer ratios.* ***A.*** *Hot Start Taq* ***B.*** *OneTaq.*

With the introduction of a primer imbalance, both the Hot Start Taq and OneTaq polymerases amplified the dsDNA and ssDNA product within a one-pot reaction, as indicated by the double band present for each primer ratio investigated. These corresponded to the same positions identified within the previous experiment and indicated that asymmetric PCR successfully synthesised the desired ssDNA target. When comparing the activity of both polymerases, it was clear that the OneTaq appeared to amplify the ssDNA more efficiently as the bands displayed a greater intensity. The relative intensities for each ratio were not immediately distinguishable from the image as the fluorescence obtained from ssDNA is not particularly intense, however, direct observation of the gel indicated that a 10: 1 primer ratio appeared to produce the optimal yields of ssDNA. As the primer concentrations had been adjusted, the magnesium content was re-titrated to confirm that the optimal yield of ssDNA was being obtained (**Figure 3.6**).

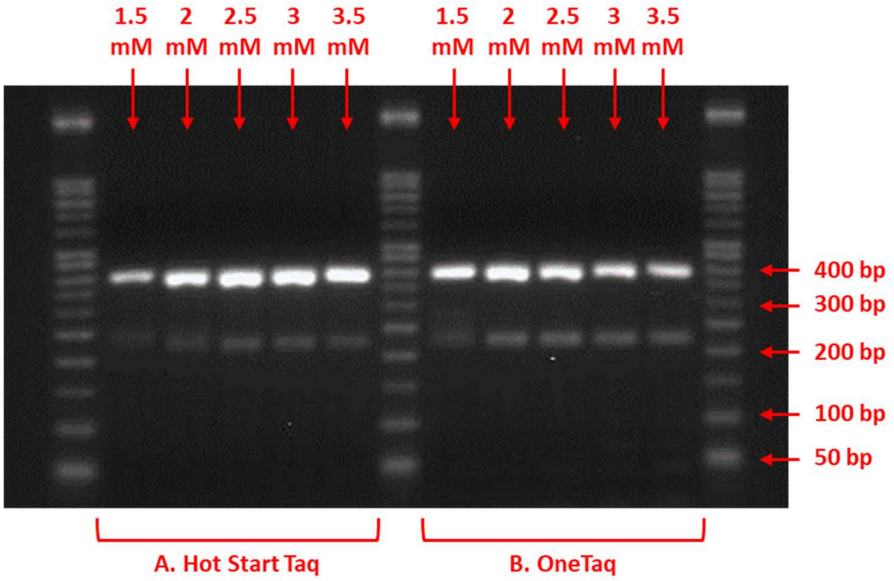

Figure 3.6. *Gel electrophoresis image of asymmetric PCR product following titration of magnesium concentration.* ***A.*** *Hot Start Taq* ***B.*** *OneTaq.*

The results indicated that 2.5 mM of magnesium was optimal for both the Hot Start Taq and OneTaq. Therefore, the magnesium concentration was increased from 2 mM to 2.5 mM for optimal amplification using Hot Start Taq following adaptation from

standard PCR to asymmetric PCR. The magnesium concentration remained at 2.5 mM for optimal amplification using OneTaq and did not require further adjustment. Upon adjustment of the magnesium conditions for asymmetric PCR, the lowest visually observable concentration was investigated and identified. Both polymerases were assessed for their sensitivity and specificity for the amplification of ssDNA. The results obtained are shown in **Figure 3.7**.

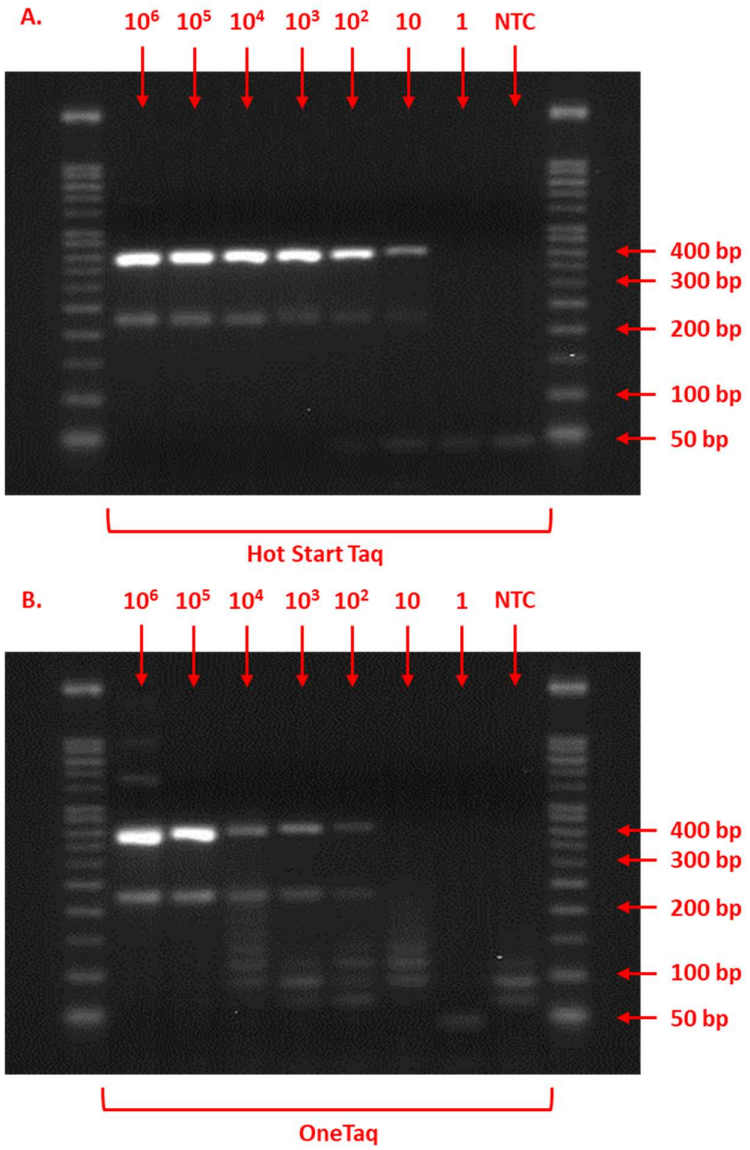

Figure 3.7. *Gel electrophoresis image of PCR product following serial dilution of template copy number range.* ***A.*** *Hot Start Taq* ***B.*** *OneTaq.*

The results indicated that the Hot Start Taq successfully amplified the ssDNA, with a at the lowest visually observable concentration of 10 copy numbers. This demonstrated that the asymmetric PCR could achieve the same lowest visually observable concentration as the standard PCR assay, without requirement for additional amplification cycles. The OneTaq polymerase amplified the ssDNA, although it was evident that this polymerase was less specific than the Hot Start Taq.

This was indicated by the presence of multiple bands as the template copy number was reduced below 10^4 copy numbers. These were non-specific amplification products, and the amplification of these products subsequently reduced the sensitivity of the assay. The lowest visually observable concentration was 10^2 copy numbers with use of the OneTaq polymerase. The amplification kinetics were analysed in real-time as SYBER Green was incorporated within the reaction mix (**Figure 3.8**).

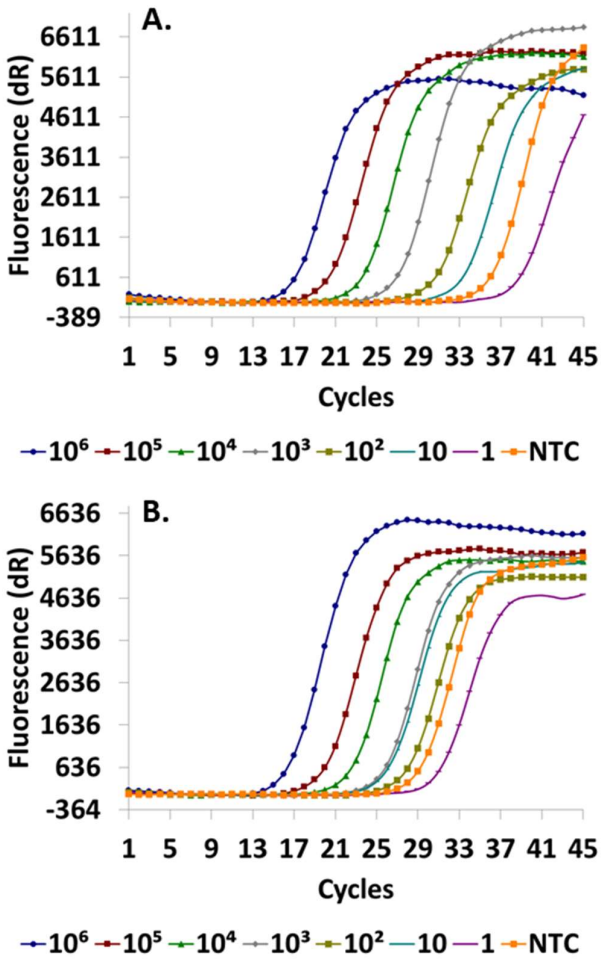

Figure 3.8. *SYBR Green asymmetric PCR amplification curves following serial dilution of template copy number range.* ***A.*** *Hot Start Taq* ***B.*** *OneTaq.*

The amplification curves observed for the Hot Start Taq were evenly distributed, with lower template concentrations requiring a greater number of cycles to amplify the DNA. The single copy number sample and no template control indicated some

amplification of primer-dimers as observed for the standard PCR assay, although these were greatly reduced as the primer imbalance was introduced. This did not interfere with the target specific amplification curves which all occurred prior to primer-dimer amplification. The OneTaq polymerase amplified numerous non-specific products, and this interfered with the results obtained using SYBER Green. At 10 copy numbers, amplification of the specific product did not occur. However, the amplification of the non-specific product produced a distinct curve after approximately 25 cycles. This highlighted the limitations of using SYBER Green for real-time PCR. If primers-dimers form or non-specific products are amplified, this will produce false-positive results.

A lowest visually observable concentration was established for each polymerase investigated, and it was concluded that the Hot Start Taq polymerase was significantly more specific than the OneTaq polymerase, and therefore more suitable for application by asymmetric PCR. The OneTaq appeared to produce more intense bands than the Hot Start Taq whilst optimising the assay performance using high template copy numbers, however as the template concentration was reduced, specificity was lost, and this also reduced the detection sensitivity. Therefore, the Hot Start Taq was selected as the polymerase of choice. Furthermore, SYBER Green could be used for the real-time analysis of amplification, although this was compromised by amplification of non-specific products and primer-dimers.

As the SYBER Green dye had the potential to interfere with SERS detection at a later stage, this was removed from the amplification mix. This also reduced the sensitivity of the asymmetric PCR assay. The previously attained lowest visually observable concentration threshold of 10 copy numbers increased to 10^2 copy numbers (**Figure 3.9**).

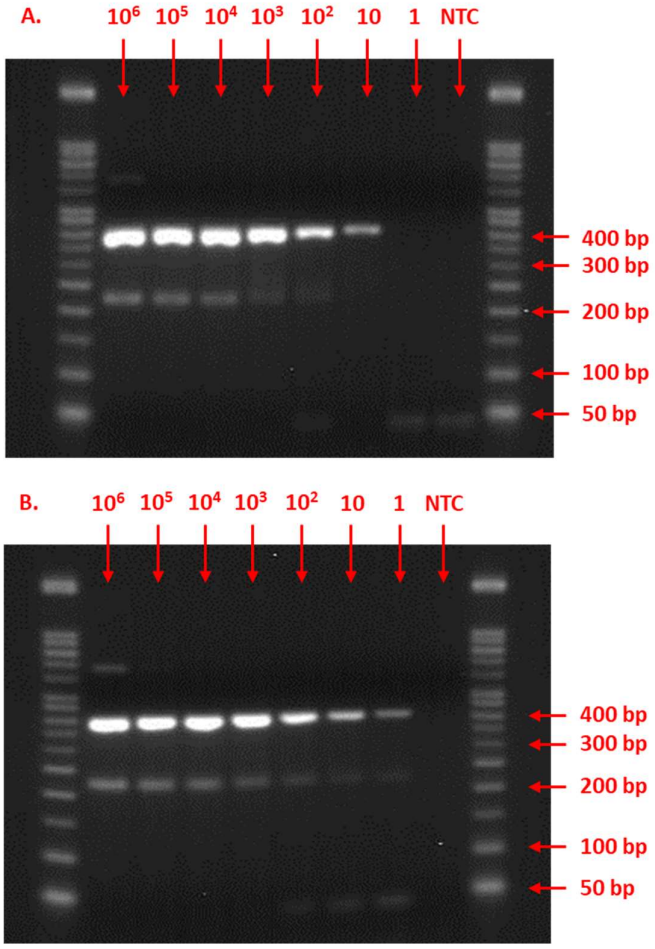

Figure 3.9. *Gel electrophoresis image of PCR product following serial dilution of template copy number range and omission of SYBER Green.* ***A.*** *58 °C annealing temperature* ***B.*** *57 °C annealing temperature.*

This was attributed to the SYBER Green dye stabilising the DNA duplex and increasing the melting temperature of the primer-target formations.[127] As the SYBER Green dye was omitted, the primer melting temperature was reduced to a sub-optimal temperature. To test this theory, the primer annealing temperature was reduced from 58 °C to 57 °C. This significantly improved the sensitivity of the assay and a new lowest visually observable concentration of 1 copy number was established (**Figure 3.9**).

3.5 Selection of Oligonucleotide Probe Sequences

The aim of this investigation was to demonstrate the SERS detection of a DNA amplification product specific to *Candida krusei*, using the same assay format that was established within the proof-of-principle investigation. The asymmetric PCR assay successfully amplified a 383-base target that was specific to the *Candida krusei* 18s rRNA gene sequence. The PCR amplicon incorporated the same sequence that was detected in the proof-of-principle investigation, although the target was more than 3-fold longer in length. The probe sequences were redesigned to increase the probe melting temperature as this would allow the hybridisation to be implemented at a higher temperature, with the aim of reducing interference from secondary structure formation. Whilst the probe sequences differed from those used in the proof-of-principle investigation, the probe length (18 bases) and spacer (triple HEG) modifications were the same as those applied previously.

The probes were selected to hybridise to a region of the target that included single nucleotide polymorphisms (SNPs) specific to *Candida krusei,* as this would ensure species-specific discrimination. This was achieved by performing a sequence alignment of closely related *Candida* species and identifying regions of sequence variation. The sequence alignment was performed using the Jalview sequence analysis tool and MUSCLE alignment server as shown in **Figure 3.10**.[128]

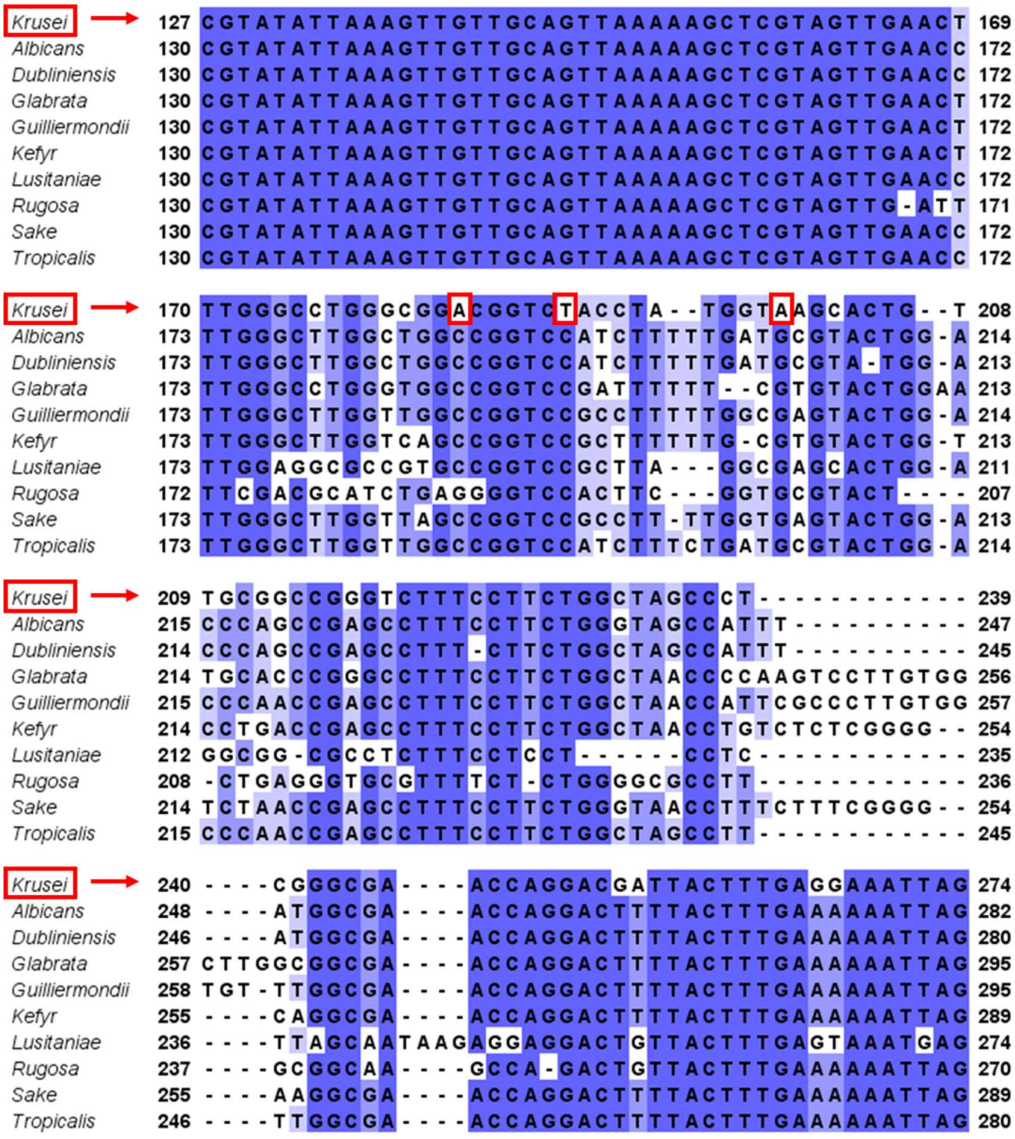

Figure 3.10. *Sequence alignment of the 18s rRNA gene for ten Candida species. The species names are listed on the left and the Candida krusei sequence is encircled in red. The Candida krusei single nucleotide polymorphisms are also encircled in red. Conserved regions are coloured in dark blue, partially conserved regions are coloured in light blue and non-conserved regions are white.*

The 18s rRNA gene sequences of ten closely related *Candida* species were aligned to differentiate regions that were highly conserved from regions with species-specific variability. Following alignment, the sequences were coloured based upon % identity. Conserved regions were highlighted in dark blue, partially conserved regions were

highlighted in light blue and non-conserved regions could be identified without colouration. The *Candida krusei* target sequence and corresponding SNPs were circled in red. The asymmetric PCR target contained mostly conserved sequence homology as indicated by the uniform regions in dark blue. However, it was evident that the target contained a highly variable region in the middle of the target sequence. The SNPs that were unique to *Candida krusei* were identified and the probe sequences were selected for complementarity to this region.

The probe sequences were checked for homo-dimer, hetero-dimer and hairpin formations and the free energy (ΔG) values were maintained at a value greater than -9 kcal/mol to reduce the likelihood of secondary structure formation within the probe sequences.[103] These criteria were the same as those applied in the proof-of-principle investigation and were calculated using the OligoAnalyzer application.[102] The probe sequences and the complementary asymmetric PCR target sequence used in this investigation are shown in **Table 3.3**.

Table 3.3. *Probe and asymmetric PCR target sequences designed for the species-specific detection of the Candida krusei 18s rRNA gene. Probe 1 is highlighted in red, probe 2 is highlighted in green, and the corresponding hybridisation regions within the complementary target are highlighted in red and green respectively.*

Sequence Name	Sequences (all in 5' – 3' direction)
Probe 1	5' – SH – HEG_3 – ATA GGT AGA CCG TCC GCC– 3'
Probe 2	5' – GCC GCA ACA GTG CTT ACC – HEG_3 – SH – 3'
Complementary asymmetric PCR target	5' – GAC AAT ATA TAA CGA TAC AGG GCC TTT GGT CTT GTA ATT GGA ATG AGT ACA ATG TAA ATA CCT TAA CGA GGA ACA ATT GGA GGG CAA GTC TGG TGC CAG CAG CCG CGG TAA TTC CAG CTC CAA TAG CGT ATA TTA AAG TTG TTG CAG TTA AAA AGC TCG TAG TTG AAC TTT GGG CCT GGG CGG ACG GTC TAC CTA TGG TAA GCA CTG TTG CGG CCG GGT CTT TCC TTC TGG CTA GCC CTC GGG CGA ACC AGG ACG ATT ACT TTG AGG AAA TTA GAG TGT TCA AAG CAG GCC TTT GCT CGG ATA TAT TAG CAT GGA ATA ATA GAA TAG GAC GCA TGG TTC TAT TTT GTT GGT TTC TAG GAC CAT CGT AAT GAT TAA TAG GGA CG – 3'

The target sequence shown in **Table 3.3** is the same as that used within the sequence alignment shown in **Figure 3.10**, however the sequence alignment begins at nucleotide 127 and finishes at nucleotide 274 within the section of the alignment shown in **Figure 3.10**.

3.6 SERS Detection of the *Candida Krusei* Asymmetric PCR Product

Following the optimisation of the asymmetric PCR assay and the design of probe sequences that were specific to the discriminatory regions of the *Candida krusei* 18s rRNA gene, SERS analysis was performed. The conjugates were synthesised using the same procedures applied within the proof-of-principle investigation, and conjugates were hybridised in the head-to-head orientation as this had been demonstrated to produce the optimal SERS response. The hybridisation buffer consisted of 0.3 M PBS and 5 % PEG 10000 as this had been previously optimised to maximise the rate and

extent of hybridisation. The experiments were performed using 10 pM of each conjugate as applied previously. The SERS analysis was performed using a 532 nm wavelength and 10 % (5 mW) laser power.

The concentration of the asymmetric PCR product following amplification was unknown. This was due to the composition of the PCR product which contained both ssDNA and dsDNA. Ordinarily, the concentration of the PCR product may be calculated by analysing the UV-Vis extinction spectra of the sample at 260 nm. The Beer-Lambert law may then be applied to calculate the concentration of the sample. In this instance, the asymmetric PCR amplified both ssDNA and dsDNA within a single reaction, and both ssDNA and dsDNA absorb at 260 nm. Therefore, it was not possible to distinguish the ssDNA from the dsDNA present within the amplification product. Alternatively, quantitative DNA ladders are commercially available for estimation of DNA concentration by comparing band intensities following gel electrophoresis, although these are typically applied for comparing dsDNA products. As the GelRed nucleic acid stain used in this investigation fluoresces less efficiently for ssDNA products, a quantitative DNA ladder would be inaccurate for the purpose of quantifying asymmetric PCR products.

As the asymmetric PCR product concentration was unknown, a volumetric range of PCR product was applied for SERS analysis. All experiments were performed using asymmetric PCR product amplified from 10^4 template copy numbers. A template concentration of 10^4 copy numbers was selected as the high template concentration ensured a high yield of PCR product. If the detection could be achieved at a relatively high template concentration, the sensitivity could be optimised at a later stage for the detection of low template copy numbers. Initially, the hybridisation experiment was performed using an annealing temperature of 50 °C. This was 5 °C higher than the annealing temperature used in the proof-of-principle investigation, and the probe sequences were redesigned with a higher melting temperature to account for this. A no template control was included as the negative control sample. The results are shown in **Figure 3.11**.

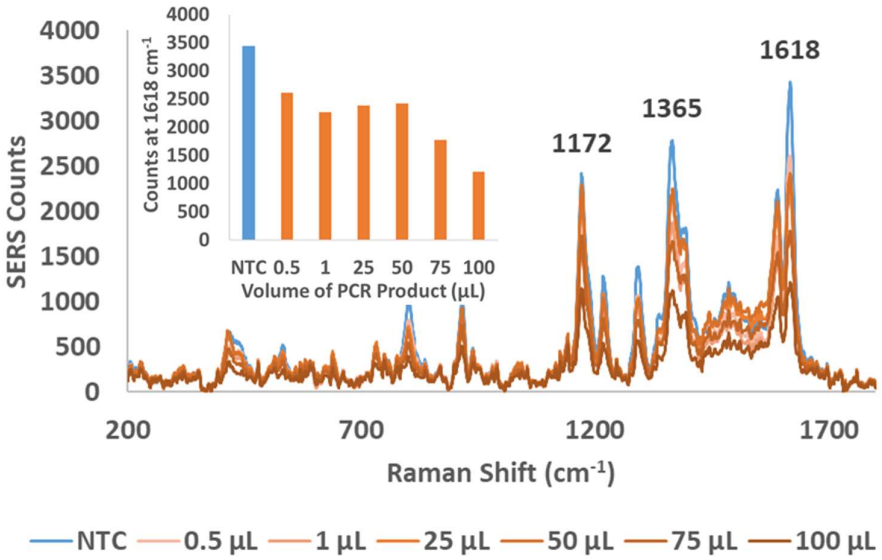

Figure 3.11. *SERS spectra of AgNP conjugates (10 pM of each conjugate) hybridised in the head-to-head orientation upon the addition of a volumetric range of asymmetric PCR product at 50 °C for 1 hour, with 5 % PEG 10000 added to the hybridisation buffer. Inset shows an on: off ratio for peak comparison at 1618 cm^{-1}. Spectra accumulated with a 532 nm laser, 1 second acquisition time and 10 % (5 mW) laser power.*

It was evident from the results in **Figure 3.11** that the hybridisation was unsuccessful as the no template control displayed a higher SERS intensity than all of the positive samples included within the volumetric range. The sample with the maximum volume of PCR product displayed the lowest SERS intensity, whereas the negative control gave the highest intensity. It was likely that the amplified DNA in the PCR reaction mix could passively interact with the nanoparticle surface providing greater stability and increased dispersity in solution. The hybridisation event that was required for the electromagnetic enhancement of the Raman signal did not occur and further investigation was required.

The concept had previously been proven feasible using the same conjugate chemistry and buffer conditions. However, the synthetic target was 100 bases in length and the asymmetric PCR product was 383 bases in length. The potential for the asymmetric PCR product to develop secondary structure formations was further assessed using the MFold application and salt conditions that were representative of the hybridisation buffer.[115] The generated structures are shown in **Figure 3.12**.

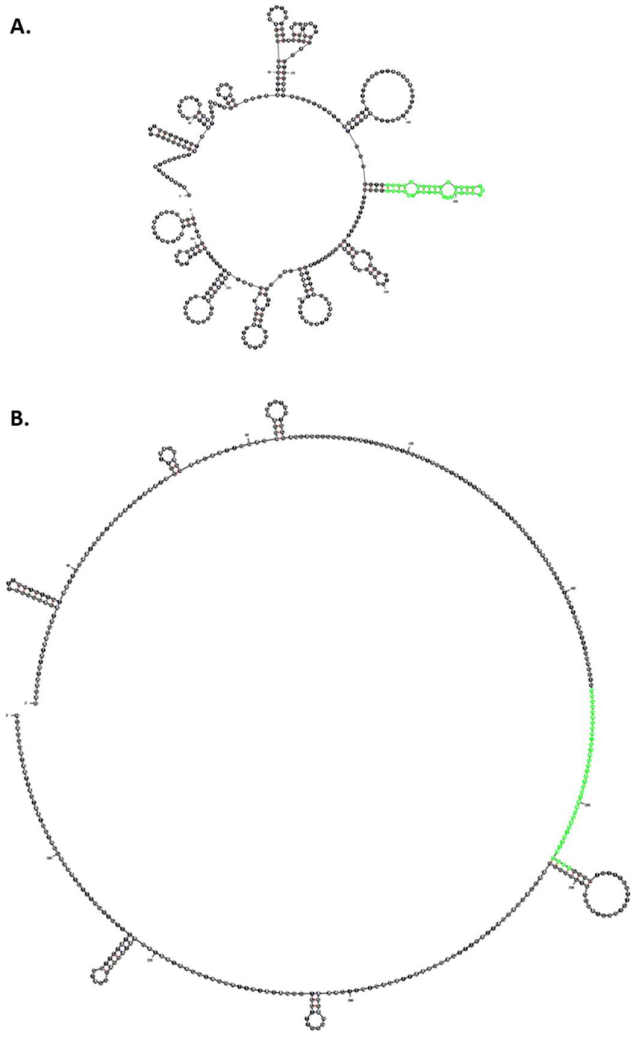

Figure 3.12. *Target secondary structures as predicted using MFold.* ***A.*** *Secondary structure at room temperature* ***B.*** *Secondary structure at 50 °C. Probe hybridisation region is highlighted in green.*

At room temperature, the ssDNA target was predicted to form a complex series of hairpin formations. At 50 °C, the predicted secondary structures were significantly reduced although a significant hairpin formation remained. The secondary structure formation partially overlapped with the region that the conjugate probe 2 sequence was designed to hybridise to. It was possible that the secondary structure formation may have inhibited the hybridisation of probe 2 to the target sequence. The MFold predictions indicated that this structure persisted until the temperature exceeded 70 °C (data not shown), although the stability of this structure was reduced as the temperature increased. To test the theory that secondary structures were inhibiting the hybridisation of the conjugate probe sequences to the target sequence, the annealing temperature was increased by 5 °C and SERS analysis was performed (**Figure 3.13**).

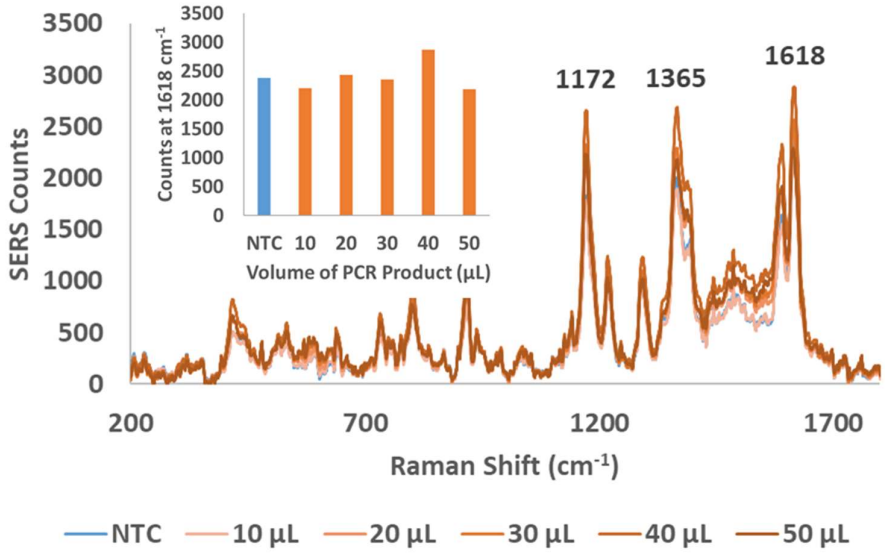

***Figure 3.13**. SERS spectra of AgNP conjugates (10 pM of each conjugate) hybridised in the head-to-head orientation upon the addition of a volumetric range of asymmetric PCR product at 55 °C for 1 hour, with 5 % PEG 10000 added to the hybridisation buffer. Inset shows an on: off ratio for peak comparison at 1618 cm^{-1}. Spectra accumulated with a 532 nm laser, 1 second acquisition time and 10 % (5 mW) laser power.*

This did not significantly improve the results and hybridisation did not occur. The no template control displayed a reduced intensity that was generally equivalent to the positive samples. This was attributed to the increased temperature reducing the non-specific interactions between the probe sequences. If the samples were left at room temperature, the conjugates would aggregate. This was due to the high salt concentration and PEG crowding agent within the buffer inducing probe dimerization. As the temperature increased, the non-specific interaction of the probes decreased. Following SERS analysis of the samples hybridised at 55 °C, the annealing temperature was increased to 60 °C to identify if this could improve the SERS response (**Figure 3.14**).

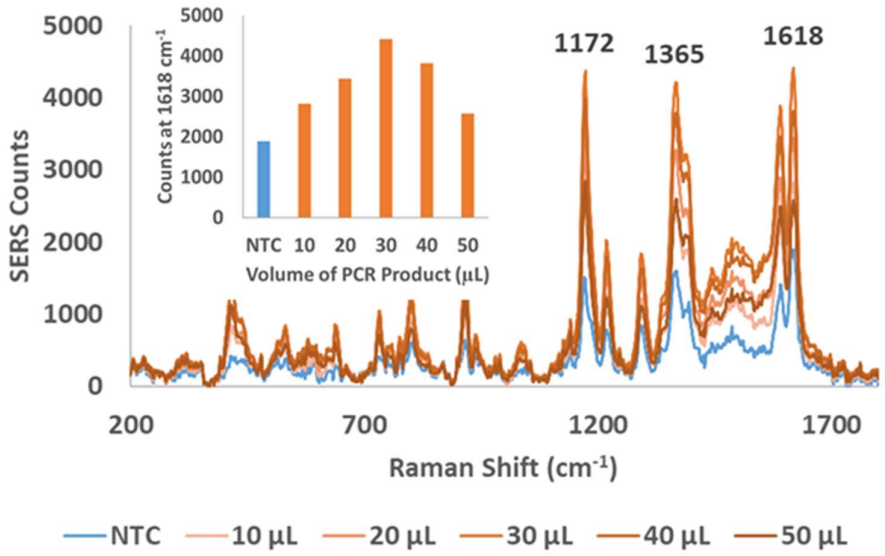

Figure 3.14. *SERS spectra of AgNP conjugates (10 pM of each conjugate) hybridised in the head-to-head orientation upon the addition of a volumetric range of asymmetric PCR product at 60 °C for 1 hour, with 5 % PEG 10000 added to the hybridisation buffer. Inset shows an on: off ratio for peak comparison at 1618 cm^{-1}. Spectra accumulated with a 532 nm laser, 1 second acquisition time and 10 % (5 mW) laser power.*

At 60 °C, the probes appeared to hybridise to the target sequence as each volume of PCR product added displayed a greater SERS intensity than observed for the no template control. There was a linear increase in the SERS intensity as the volume of

PCR product was increased from 10 µL to 30 µL, although the SERS intensity appeared to decrease as the volume of PCR product increased beyond 30 µL. This provided an indication of the "hook effect" occurring. The hook effect is commonly observed in immunoassays performed in the sandwich format when the analyte is present in high concentration.[129] A high number of analyte molecules bind to both the immunoassay capture and detection antibodies, thereby preventing the formation of the sandwich complexes, and this may present itself as a decrease in the signal response at high concentrations within a calibration curve range. This may lead to a misleadingly low target concentration when the target analyte is in fact present in higher concentrations. This effect appeared to present itself in the AgNP hybridisation assay upon addition of the PCR product as evident in **Figure 3.14**.

The increased annealing temperature did appear to improve the discrimination of the assay and an on: off ratio of 2: 1 was achieved with the addition of 30 µL of PCR product. The annealing temperature could not be increased further as this exceeded the probe melting temperature and SERS discrimination would not be achieved. An alternative method was therefore applied.

The samples were heated to 95 °C for 3 minutes to melt any secondary structure formations, and immediately cooled to 55 °C for 1 hour to allow the probes to hybridise to the target (**Figure 3.15**).

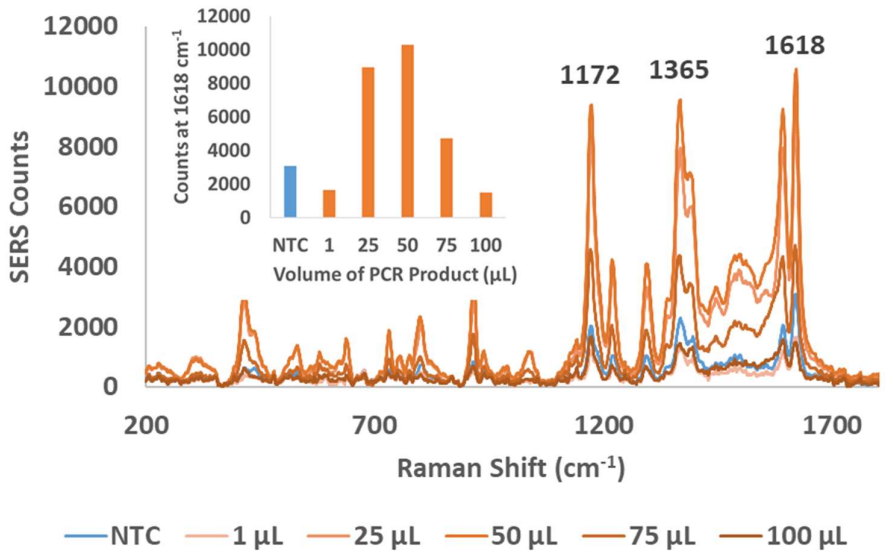

Figure 3.15. *SERS spectra of AgNP conjugates (10 pM of each conjugate) hybridised in the head-to-head orientation upon the addition of a volumetric range of asymmetric PCR product heated to 95 °C and immediately cooled to 55 °C for 1 hour, with 5 % PEG 10000 added to the hybridisation buffer. Inset shows an on: off ratio for peak comparison at 1618 cm^{-1}. Spectra accumulated with a 532 nm laser, 1 second acquisition time and 10 % (5 mW) laser power.*

The application of a heat-and-cool step further improved the discriminatory value of the assay. The addition of 50 µL of PCR product generated a SERS on: off ratio of 3: 1. As the volume of PCR product increased beyond 50 µL the SERS response decreased which indicated that the hook effect was occurring. This was observed previously, although the hook effect occurred using a higher volume of PCR product than observed on the previous occasion. Furthermore, discrimination could not be achieved using 1 µL of PCR product. This indicated that the assay had a limited dynamic range. The experiment was repeated, and the samples were cooled gradually over 1 hour to identify if the discriminatory value could be further improved (**Figure 3.16**).

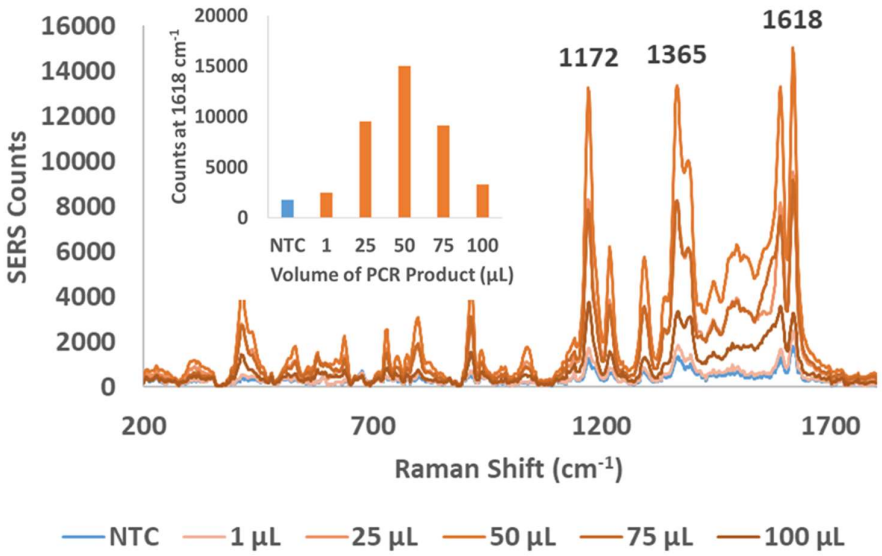

Figure 3.16. *SERS spectra of AgNP conjugates (10 pM of each conjugate) hybridised in the head-to-head orientation upon the addition of a volumetric range of asymmetric PCR product heated to 95 °C and gradually cooled to 55 °C over 1 hour, with 5 % PEG 10000 added to the hybridisation buffer. Inset shows an on: off ratio for peak comparison at 1618 cm^{-1}. Spectra accumulated with a 532 nm laser, 1 second acquisition time and 10 % (5 mW) laser power.*

Upon heating the samples to 95 °C and cooling gradually to 55 °C over 1 hour, the discriminatory value of the assay was further improved and an on: off discriminatory ratio of 8: 1 was achieved with the addition of 50 µL of PCR product. The SERS intensity observed with the addition of 1 µL of PCR product was marginally above that of the no template control and continued to increase linearly until the maximum discriminatory value was observed with the addition of 50 µL of PCR product. As observed previously, the SERS intensity decreased as the volume was increased beyond this threshold due to the hook effect. Therefore, the optimal discrimination of the PCR product was generated upon heating to 95 °C and cooling to 55 °C over 1 hour, and the volumetric detection range was limited between 1 µL and 50 µL of PCR

product. The experiment was repeated in triplicate and the asymmetric PCR product was added in 10 µL increments to a maximum volume of 50 µL (**Figure 3.17**).

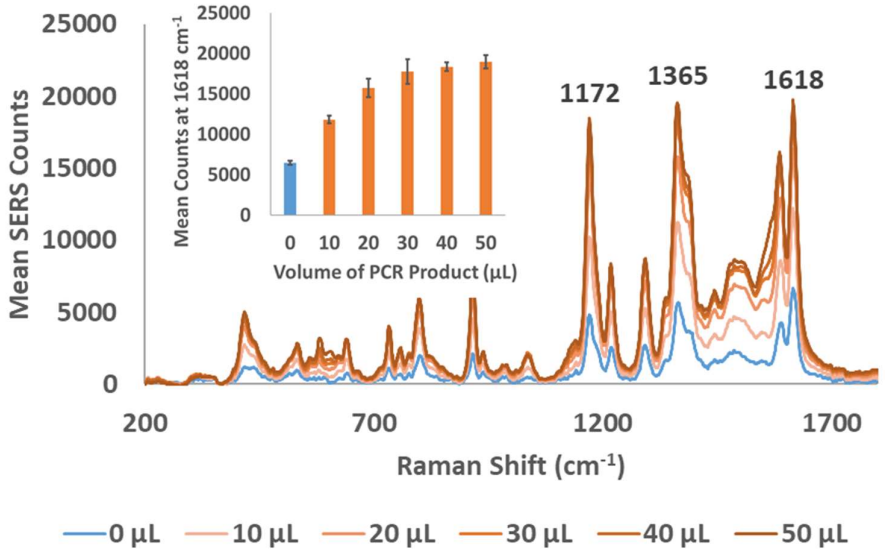

Figure 3.17. *Mean (n=3) SERS spectra of AgNP conjugates (10 pM of each) hybridised in the head-to-head orientation upon the addition of a volumetric range of asymmetric PCR product heated to 95 °C and gradually cooled to 55 °C over 1 hour, with 5 % PEG 10000 added to the hybridisation buffer. Inset shows an on: off ratio for peak comparison at 1618 cm^{-1}. Spectra accumulated with a 532 nm laser, 1 second acquisition time and 10 % (5 mW) laser power.*

The results indicated that each volume of asymmetric PCR product could be discriminated from the no template control and that the SERS response increased in intensity as the volume of asymmetric PCR increased. The increase in SERS intensity began to plateau as the volume increased beyond 30 µL as observed previously. The maximum discriminatory value was generated using 50 µL of asymmetric PCR product and an on: off ratio of 3: 1 was achieved. The on: off ratio of 3:1 was less significant than the 8: 1 ratio previously observed using the same conditions, and this was attributed to an increase in the intensity observed for the no template control. As the samples were removed from the heat-block prior to analysis, the negative control samples would quickly begin to aggregate, and the discriminatory value would be reduced. Whilst great care was taken to analyse the samples as quickly as possible,

the transfer of samples from the heat-block to a 96-well plate for analysis inevitably resulted in variability between experiments. The heat-and-cool approach had demonstrated that discrimination could be achieved, and this was attributed to the reduction of secondary structures which may inhibit the hybridisation efficiency.

A further attempt was made to improve the sensitivity of the assay and 5 % dimethylsulfoxide (DMSO) was added to the hybridisation buffer. DMSO has been shown to improve PCR amplification efficiency of DNA sequences containing complex secondary structures when added at concentrations equal to or above 5 % (w/v).[130] The experiment was repeated using identical conditions, but with the further addition of 5 % DMSO to the hybridisation buffer (**Figure 3.18**).

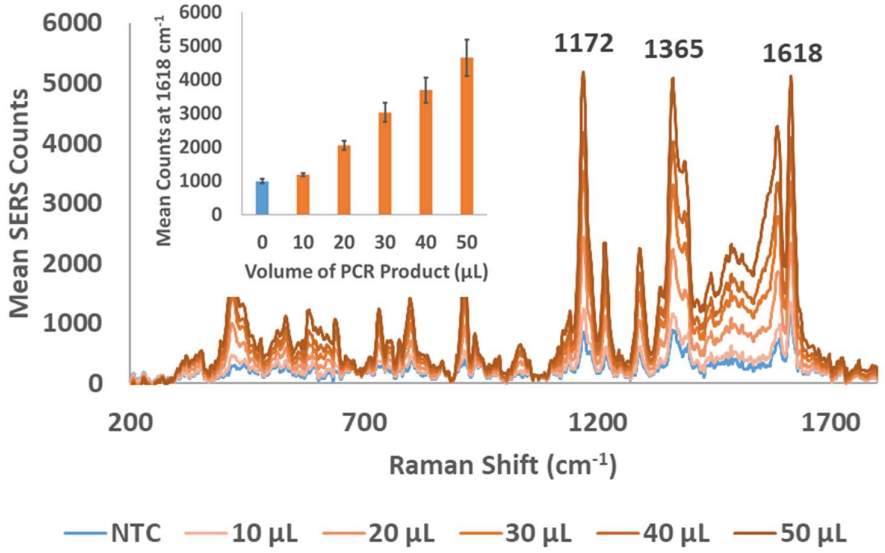

Figure 3.18. *Mean (n=3) SERS spectra of AgNP conjugates hybridised in the head-to-head orientation upon the addition of a volumetric range of asymmetric PCR product heated to 95 °C and gradually cooled to 55 °C over 1 hour, with 5 % PEG 10000 and 5 % DMSO added to the hybridisation buffer. Inset shows an on: off ratio for peak comparison at 1618 cm^{-1}. Spectra accumulated with a 532 nm laser, 1 second acquisition time and 10 % (5 mW) laser power.*

The results indicated a linear trend of increasing SERS intensity as the volume of PCR product increased. Target saturation did not occur with the addition of the maximum volume of PCR product as observed previously. This was attributed to reduced

hybridisation efficiency which prevented target saturation as the overall SERS intensity appeared to be significantly lower than observed previously. This effect was also observed for the no template control which also displayed a lower SERS intensity. Therefore, it was likely that the addition of DMSO prevented non-specific interactions between the probe sequences used to functionalise the conjugates, thus improving the dispersity of the conjugates in solution and reducing the background signal obtained. It could not be concluded that DMSO improved the discriminatory ratio by minimising secondary structure formation. An on: off ratio of 5: 1 was achieved with the addition of 50 µL of PCR product to the hybridisation mix.

3.7 Conclusion of the Investigation

Following completion of the investigation, it was concluded that asymmetric PCR could be applied effectively to amplify ssDNA in a one-pot reaction using the defined LATE-PCR criteria. The asymmetric PCR procedure did not require additional amplification cycles to attain single-digit copy number detection limits. The application of asymmetric PCR for the amplification of ssDNA is advantageous when compared to alternative methods such as sodium hydroxide denaturation as the complementary strand is not present to compete for hybridisation with the AgNP conjugate probes. The ssDNA product was detected using DNA functionalised and dye-coded AgNPs. However, the sensitivity was significantly lower than that obtained using the synthetic target, due to the detection method being more complex than that of the proof-of-principle investigation. Satisfactory discrimination could only be obtained using the heat-and-cool approach. This compromise was required due to the complexity of the amplified target sequence which did not readily hybridise when maintained at a constant temperature.

The difficulties encountered for the detection of the asymmetric PCR product can be attributed to multiple factors. Firstly, the quantification of the ssDNA product in the amplification was not readily achievable due to the heterogenous nature of the reaction product which contained both dsDNA and ssDNA. As described previously, this prevented the quantification using UV-Vis spectroscopy or quantitative DNA

ladders. To accurately quantify the concentration of ssDNA in the asymmetric PCR product, more complex methods would be required. The authors of the LATE-PCR method have demonstrated that fluorescent molecular beacons may be applied to analyse the linear amplification of the ssDNA in real-time. [124, 125] It is therefore possible that a molecular beacon may be designed to hybridise to the ssDNA product following amplification. This would not hybridise to the dsDNA product as the complementary strands would exist as a duplex formation, preventing hybridisation of the beacon to the dsDNA product. Furthermore, the fluorescence intensity would need to be related to the intensity of known target concentrations to deduce the concentration of the ssDNA product. This would require the formulation of a calibration curve using complementary synthetic DNA of a known concentration. In summary, to calculate the concentration of ssDNA in an asymmetric PCR product, a fully quantitative PCR assay would need to be designed based upon the fluorescence generated from hybridisation of a molecular beacon to the ssDNA product.

The second potentially limiting factor that may have contributed to the reduced sensitivity obtained was related to the substantially longer nature of the PCR amplification product and the potential for secondary structure formation. The proof-of-principle investigation utilised a 100-base target, whereas the asymmetric PCR product was 383 bases in length and the potential for a ssDNA strand to form secondary structures increased as the length increased. The effect of target secondary structures on nanoparticle assembly in solution has not been described within the literature. This is presumably due to the common application of short linker DNA sequences that provide an idealised assembly model for studying the properties of the assembled NPs, thus avoiding the complications of detecting longer target sequences. Gao et al., investigated the effect of target hairpin structures on DNA hybridisation kinetics in solution and on the surface of a gold film, using UV-Vis extinction spectroscopy and surface plasmon resonance respectively.[131] The hybridisation kinetics of a target containing no secondary structures was compared to a target containing 3 bp and 4 bp hairpin formations. The hybridisation kinetics were significantly reduced both in solution and on the surface upon introduction of

an internal hairpin structure within the target strand. The kinetics were further reduced as the number of base-pairs within the hairpin structure increased. Ideally, the probes should target a region without evidence of secondary structures, however if this was to be applied within this investigation, the specificity of the probe sequences to the *Candida krusei* specific region of the target would have to be compromised.

The third potentially limiting factor that could have reduced the sensitivity of the asymmetric PCR assay relates to the presence of target overhangs which may inhibit hybridisation and assembly of the NPs. Smith et al., have previously shown that as the length of overhangs increases, the hybridisation efficiency and melting temperature of DNA functionalised AuNP assemblies decreases.[132] This was attributed to steric effects limiting duplex formation and stability. The position of the hybridisation region within the target sequence may have had an impact on hybridisation efficiency. The probes utilised in the proof-of-principle investigation hybridised to a position at the 3' end of the complementary target sequence. This meant that probe 1 had a target overhang of 64 bases, whereas probe 2 had no target overhang. The probes utilised in the asymmetric PCR investigation hybridised to a position in the centre of the target strand. Probe 1 had a target overhang of 178 bases, whereas probe 2 had a target overhang of 169 bases. If probe 1 used for the proof-of-principle investigation could hybridise with a target overhang of 64 bases, this suggested that hybridisation to longer target sequences could be achieved. However, further investigation would be required to confirm an appropriate threshold at which target overhangs effectively prevent target hybridisation.

In consideration of the factors described above, it may be required to return to investigation of a synthetic target sequence to delineate the effects of target secondary structures and overhangs on the assembly of NPs in solution, prior to detecting asymmetric PCR products. Alternatively, it may be possible to avoid these complications by redesigning an asymmetric PCR assay for amplification of a significantly shorter target sequence. To ensure that an optimal concentration of PCR

product is applied, a fully quantitative asymmetric PCR assay should be designed with the application of a molecular beacon fluorescent probe.

The investigation applied here did however provide some discrimination of the amplification product. Due to the application of a heat-and-cool approach, the reproducibility was compromised, and the results were variable between experiments. The reduced sensitivity meant that fluctuations in signal obtained from the no template control significantly affected the discriminatory value. An optimal discriminatory on: off ratio of 5: 1 was obtained with the addition of 5 % DMSO to the hybridisation buffer. This was a demonstrable improvement upon the result obtained by Mabbot et al., for the SERS detection of the same PCR product following sodium hydroxide denaturation. The results reported by Mabbot et al., described a SERS on: off discriminatory ratio of less than 2: 1., and therefore the on: off ratio of 5: 1 achieved within this investigation represented an improvement in the discriminatory value of more than two-fold. However, the full potential of the assembly-based method applied here for the SERS detection of asymmetric PCR products may still be significantly improved, as demonstrated by the results obtained within the proof-of-principle investigation.

3.8 Experimental

Polymerase Chain Reaction: PCR reactions were performed on a Stratagene Mx3005P thermocycler (Agilent, California, USA) using Hot Start Taq polymerase and OneTaq polymerase (New England Biolabs, Hitchin, UK). HPLC purified oligo primers were ordered from ATDBio (Southampton, UK). Reactions were performed in 50 µL volumes. The standard PCR reaction mastermix consisted of 1x PCR buffer, 0.8 mM of the dNTPs, 0.8 µM of the forward primer, 0.8 µM of the reverse primer and 2.5 U of either the Hot Start Taq or OneTaq polymerase. The magnesium chloride concentration was optimised for each polymerase and the optimal concentration was identified to be 2 mM and 2.5 mM for the Hot Start Taq and OneTaq polymerases respectively. The mastermix was spiked with 1 µL of *Candida krusei* plasmid DNA. The *Candida krusei* plasmid DNA was supplied by the commercial sponsor (Renishaw

Diagnostics, Glasgow, UK) at a concentration of 10^9 copy numbers. The PCR reaction mix was then increased to a total volume of 50 µL with the addition of MQ water following addition of plasmid template. PCR was performed with 45x cycles of melting at 94°C for 30 seconds, annealing at 58 °C for 30 seconds and elongation at 72 °C for 30 seconds. A final elongation step was then implemented at 72 °C for 7 minutes following the 45x amplification cycles. The asymmetric PCR reactions were performed using the same conditions as described for the standard PCR assay with slight modification. The reverse (limiting) primer was reduced in concentration to 0.08 µM. The optimal magnesium concentration was identified to be 2.5 mM for both the Hot Start Taq and OneTaq polymerases. The annealing temperature was reduced from 58 °C to 57 °C.

Lambda Exonuclease Treatment of PCR Product: Lambda exonuclease (Thermo Fisher Scientific, Massachusetts, USA) was used to digest PCR product into ssDNA form using the manufacturer recommendations. Enzymatic digestion was performed in a 50 µL reaction volume. 10 U of lambda exonuclease was added for every 2 µg of DNA added to the reaction mix, and left to digest at 37 °C for 30 min. The digestion was then stopped by heating at 80 °C for 10 min.

Nanoparticle Synthesis: AgNPs were synthesised using the same method as detailed within the experimental section of the *Candida krusei* proof-of-principle investigation (section 2.14).

Oligonucleotide Probe Design and Preparation: Oligo probes were designed and prepared using the same methods as detailed within the experimental section of the *Candida krusei* proof-of-principle investigation, with further inclusion of a sequence alignment step to confirm species-specificity. The probe sequences were redesigned based upon complementarity to the *Candida krusei* specific single nucleotide polymorphisms contained within the asymmetric PCR amplification product. These were identified by performing a sequence alignment of closely related *Candida* species. Sequence alignments were performed using the Jalview sequence analysis

tool and MUSCLE alignment server.[128] HPLC purified oligo probes were ordered from ATDBio (Southampton, UK)

Buffer preparation: Buffers were prepared using the same methods as detailed within the experimental section of the *Candida krusei* proof-of principle investigation (section 2.14).

Conjugate Preparation: The conjugates were prepared using the same methods as detailed within the experimental section of the *Candida krusei* proof-of principle investigation (section 2.14).

Gel electrophoresis of the PCR amplification products: 2 % agarose gels were cast using molecular biology grade agarose (Bioline Reagents Ltd., London, UK) dissolved in 1x TBE buffer. GelRed™ nucleic acid stain (Biotium, California, USA) was added at a 1x concentration following dissolution of the agarose in the 1x TBE buffer**.** 10 µL of PCR product was mixed with 2 µL of 6x blue loading dye (Qiagen, Manchester, UK) prior to dispensing into the wells of the gel. The size of the product was compared using a DirectLoad™ 50 bp DNA ladder (Sigma-Aldrich Ltd., Dorset, UK). 12 µL of DNA ladder was added to the well for size comparison. Gel electrophoresis was performed using 2 % agarose gels run at 180 volts for 45 minutes in 1x TBE buffer. The gel images were collected using a BioDoc-It™ imaging system (UVP, Cambridge, UK).

Hybridisation Assay in Solution: The hybridisations were performed using the same method as detailed within the experimental section of the *Candida krusei* proof-of-principle investigation, with slight modification. As the concentration of ssDNA within the asymmetric PCR product was unknown, volumetric ranges of the asymmetric PCR product target sequence were aliquoted for hybridisation. The optimal temperature for hybridisation required a heat-and-cool approach and the heat-block was pre-heated to 95 °C, and gradually cooled to 55 °C over 1 hour. The cooling was initiated 3 minutes after sample addition.

SERS Analysis: SERS analysis was performed using the same method as detailed within the experimental section of the *Candida krusei* proof-of-principle investigation (section 2.14).

4 An Investigation for the Detection of a *Legionella pneumophilia* Recombinase Polymerase Amplification Product using Raman Spectroscopy

4.1 Aim of the Investigation

The aim of the investigation was to detect a recombinase polymerase amplification (RPA) product specific to *Legionella pneumophila* using Raman spectroscopy. A *Legionella pneumophila* serogroup 1 specific target was chosen as this was closely aligned with the research of project collaborators to fulfil an unmet requirement for the point-of-need detection of *Legionella* bacteria in resource limited settings (work unpublished).

Legionellae are gram negative, rod-shaped bacteria (bacilli) that comprise of over 48 species that can be further divided into 65 serogroups, most of which are ubiquitously present within aquatic environments but harmless to humans.[133, 134] A minority of *Legionella* species are pathogenic to humans and the most predominant of these species is *Legionella pneumophila*, the causative agent of an often-fatal form of pneumonia referred to as Legionnaires' disease. [134] *Legionella pneumophila* bacilli are ubiquitously present within both natural freshwater environments and man-made hot water systems[134, 135] Legionnaires disease develops as the bacteria present within aerosols are inhaled into the lungs, followed by replication within the alveolar macrophages and the onset of severe pneumonia within the infected host.[134] There are approximately 250-400 confirmed cases of legionellosis in the UK each year and *Legionella pneumophila* serogroup 1 accounts for approximately 90 % of these cases.[136] Legionnaires disease is typically diagnosed by traditional microbiological culturing methods which can take as long as 8 days for confirmation. Furthermore, the sensitivity is reliant upon the physiological state of the cells and samples may contain viable but non-culturable cells thus leading to erroneous results and diagnosis.[137] Therefore, it is of great importance to improve the diagnosis of Legionnaires disease and further develop rapid and accurate molecular assays for the

detection of the disease. Molecular diagnostics may provide shorter turn-around times as compared to conventional culturing, improved specificity based upon DNA sequence-specific design criteria and furthermore, may eliminated the issue of cell viability associated with culturing thus providing a greater degree of certainty in diagnosing the disease.

Whilst PCR has traditionally been applied as the molecular diagnostic technique of choice for the diagnosis of infectious disease, emerging isothermal techniques offer the potential to eliminate the requirement for a thermocycler and allow for application of molecular diagnostic technology at the point-of-use or within resource limited settings. In this instance, RPA was selected as the isothermal amplification method of choice due to rapid amplification that occurs within 20 minutes and a sensitivity which may be compared to that of the PCR. The detection of RPA products using Raman spectroscopy has not been investigated widely within the published literature. Therefore, the most appropriate method for detecting the amplification product remained to be determined, and both solution and surface-based approaches were investigated.

4.2 Introduction to the Assay Principles

The RPA assay amplifies a *Legionella pneumophilia* specific product in the dsDNA conformation. The asymmetric amplification of ssDNA has not yet been demonstrated using RPA. As the enzymatic mechanism of the RPA reaction differs significantly from thermally controlled PCR reaction, it is likely that asymmetric amplification of ssDNA using RPA is not readily achievable. Therefore, the detection method employed previously was not applicable.

The assay method applied here utilised tailed primers which provide a means to detect the product following amplification. Tailed primers consist of a primer sequence modified with an internal carbon spacer which is linked to a single-stranded tail recognition sequence. The primer is incorporated within the amplification product, whereas the carbon spacer blocks the elongation step during amplification, leaving a single-stranded tail recognition region at the end of the amplification

product. If both primers are tailed, this amplifies a double-stranded product, flanked by a carbon spacer and single-stranded recognition sequence at each end of the amplification product. A simplified schematic of this concept is shown in **Figure 4.1**.

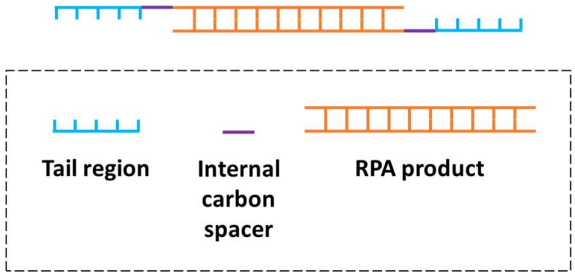

***Figure 4.1**. Simplified schematic depicting the concept of an RPA amplification product with single-stranded tailed regions.*

The single-stranded recognition sequences at each end of the amplification product may then be exploited for hybridisation and detection. The concept of tailed primers was introduced by Joda et al., who reported the electrochemical detection of PCR amplification products related to coeliac disease using tailed-primers captured on the surface of an electrode array.[138] The tailed primer on one end of the amplification product hybridised to a complementary capture probe on the electrode surface, and the tailed primer on the opposing end of the amplification product hybridised to a complementary reporter probe that was conjugated to horseradish peroxidase (HRP). The conversion of the HRP substrate produced an electrochemical signal that confirmed the presence of the amplification product. This investigation was later extended for the electrochemical detection of RPA amplification products related to coeliac disease using the same assay format.[139] Further studies have demonstrated that tailed primers may also be integrated with lateral flow devices for the detection of RPA amplified aptamer and DNA sequences.[140, 141] The tailed regions of the primer sequences have no functionality in the amplification process and do not need to be designed for species-specificity as this is conferred by the primer sequence. Therefore, the tailed regions may be designed without constraint and different tail sequences may be used for different amplification products, which is significantly advantageous for multiplexing purposes.

The assay format proposed here utilised a tailed RPA amplification product which was to be detected in a sandwich format on the surface of a 96 well plate. A simplified schematic of the assay format is displayed in **Figure 4.2**.

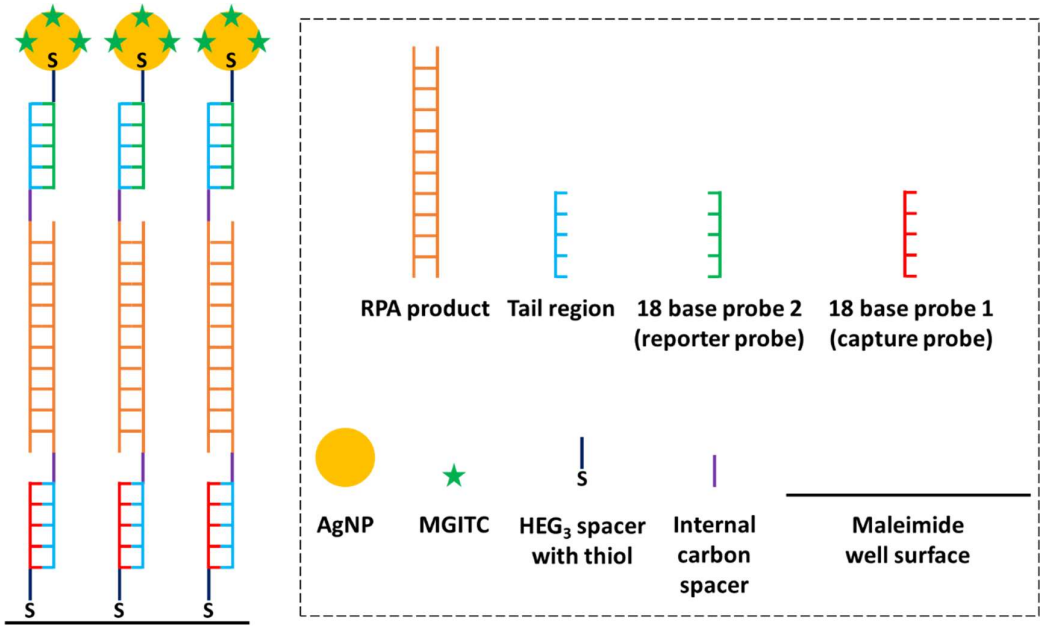

Figure 4.2. *Simplified schematic depicting the principles of the proposed SERS DNA detection methodology on the surface of a maleimide activated 96-well plate. The tailed RPA products act as a cross-linker between the capture probe immobilised upon the well surface and the AgNP reporter conjugate probe. If the RPA product was not present, the conjugate would remain in solution and would be removed during the wash step and no SERS signal would be obtained.*

The 96 well plate contained an activated maleimide surface coating for the immobilisation of thiolated DNA probes. As the thiolated probes are added to the well, the maleimide double-bond undergoes an alkylation reaction with the thiol group to form a stable thioether bond.[142]. The probe sequence that was immobilised on the well surface was complementary to the tailed region at one end of the RPA amplification product. This was designated as the capture probe. Upon addition of the complementary tailed RPA product, the tailed region hybridised to the capture probe. The RPA product contained a further tailed region at the opposing end of the product, and this could be hybridised to a reporter probe. The reporter probe could

be conjugated to an AgNP and dye-coded with a Raman reporter for SERS detection, or alternatively could be conjugated to HRP to produce a colour change upon the addition of a substrate such as 3,3',5,5'-Tetramethylbenzidine (TMB). In the first instance, the reporter probe was conjugated to AgNPs that were dye-coded with MGITC. If the RPA amplification product was present, the reporter probe would hybridise to the captured RPA product and generate a SERS signal. If the RPA was not present, the reporter probe would be removed during the wash step, and no SERS signal would be obtained.

4.3 Nanoparticle synthesis, characterisation and functionalisation

AgNPs were synthesised using the hydroxylamine method as applied previously. The NPs were characterised and sized using UV-Vis spectroscopy. It was noted during the previous investigation that dynamic light scattering produced highly variable size data from batch-to-batch, whereas the UV-Vis data was highly reproducible from batch-to-batch. Therefore, the nanoparticle size was estimated to be 30 nm based upon an excitation maximum at 405 nm using UV-Vis extinction spectroscopy.[97] The nanoparticle concentration was approximated to be 772 pM using the Beer-Lambert law and the extinction coefficient 145 x 108 M^{-1} cm^{-1} for 30 nm AgNPs.[97] The hydroxylamine AgNPs were functionalised without further dilution following synthesis and filtration. The AgNPs were functionalised using the pH adjusted method and MGITC was utilised as the Raman reporter.

4.4 Selection of Oligonucleotide Primer and Probe Sequences

The primer and probe sequences used within this assay had been previously designed by project collaborators for specificity to *Legionella pneumophila* serogroup 1. The RPA primers amplified a 118 bp region of the *Legionella pneumophila wzm-1* gene. The *wzm-1* gene has been associated with a gene cluster encoding for lipopolysaccharide synthesis and is uniquely present within the genome of *L. pneumophila* serogroup 1.[143] Therefore, this gene sequence provides a serogroup-specific genetic biomarker and this specificity has been demonstrated previously by

PCR analysis.[137] The probe and primer sequences used within this investigation are listed within **Table 4.1**.

Table 4.1. *Probe and primer sequences designed for the serogroup-specific detection of L. pneumophila serogroup 1. Probe 1 is highlighted in red and probe 2 is highlighted in green and the corresponding hybridisation regions within the tailed primers are highlighted in red and green respectively.*

Sequence Name	Sequences (all in 5' – 3' direction)
Probe 1 (capture probe)	5' – GTC GTG ACT GGG AAA AC – HEG_3 – SH – 3'
Probe 2 (reporter probe)	5' – ACT GGC TGT CGT TTT ACA – HEG_3 – SH – 3'
Forward primer	5' – GTT TTC CCA GTC ACG AC / iSpC3 / GCT GTT AAT CCA TTA TCT CTT GTT ATC ACC – 3'
Reverse primer	5' – TGT AAA ACG ACA GCC AGT / iSpC3 / CCA CAA GGA AAG TTA TAA TTG CCA TAC C– 3'

4.5 Optimisation of the Conjugation of DNA and AgNPs

The pH adjusted conjugation method for the functionalisation of AgNPs with thiolated DNA was optimised to ensure that full surface coverage was achieved with the addition of the reporter probe sequence. The conjugation utilised different probe sequences to those applied previously and therefore further optimisation was required. Thiolated DNA was added to the AgNP suspension using a range of DNA: AgNP molar ratios and left to equilibrate for 1 hour. This was followed by the addition of 30 µL of 250 mM sodium citrate buffer (pH 3.0) and the suspension was left to shake for 15 minutes. A further 30 µL of citrate buffer was then added and left for 45 minutes without shaking, and the conjugates were centrifuged prior to resuspension in 0.1 M PBS. If an insufficient concentration of DNA was added, the conjugates would aggregate upon addition of citrate buffer or following the centrifuge cycle and resuspension. The reporter probe was added at DNA: AgNP molar ratios of 50: 1, 100: 1, 500: 1, 1000: 1 and 1500: 1. The stability of the AgNPs during the conjugation

process could be assessed by the colour of the conjugates during each stage of the process as shown in **Figure 4.3**.

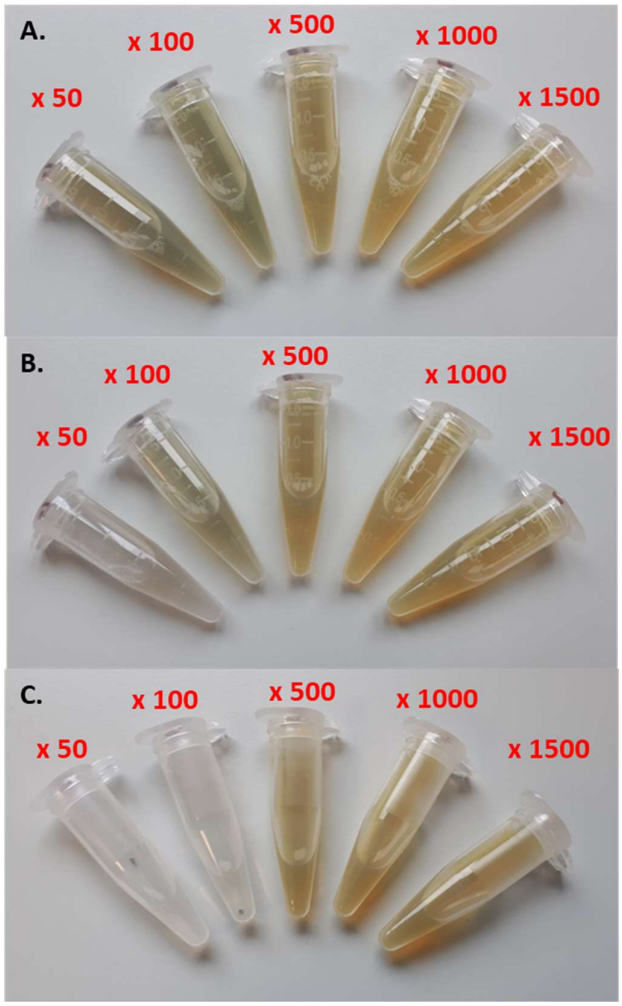

Figure 4.3. *Images of conjugates during functionalisation using the pH adjusted method.* ***A.*** *Following first addition of citrate buffer* ***B.*** *Following second addition of citrate buffer* ***C.*** *Following centrifugation and resuspension in 0.1 M PBS.*

Following the first addition of citrate buffer, the conjugates with DNA at ratios of 50: 1 and 100: 1 began to aggregate. This was evident by the colour change as the conjugates changed from yellow to grey. Upon the second addition of citrate buffer, the conjugate functionalised at a ratio of 50: 1 completely aggregated and turned transparent as the AgNPs were no longer in suspension. The conjugate functionalised at a ratio of 100: 1 remained partially aggregated. Upon centrifugation and

resuspension in 0.1 M PBS, the conjugates functionalised at ratios of 50: 1 and 100: 1 had aggregated irreversibly. The conjugates functionalised at ratios of 500: 1, 1000: 1 and 1500: 1 remained stable throughout the conjugation process and were successfully resuspended without indication of any aggregation as confirmed by UV-Vis extinction spectroscopy (**Figure 4.4**).

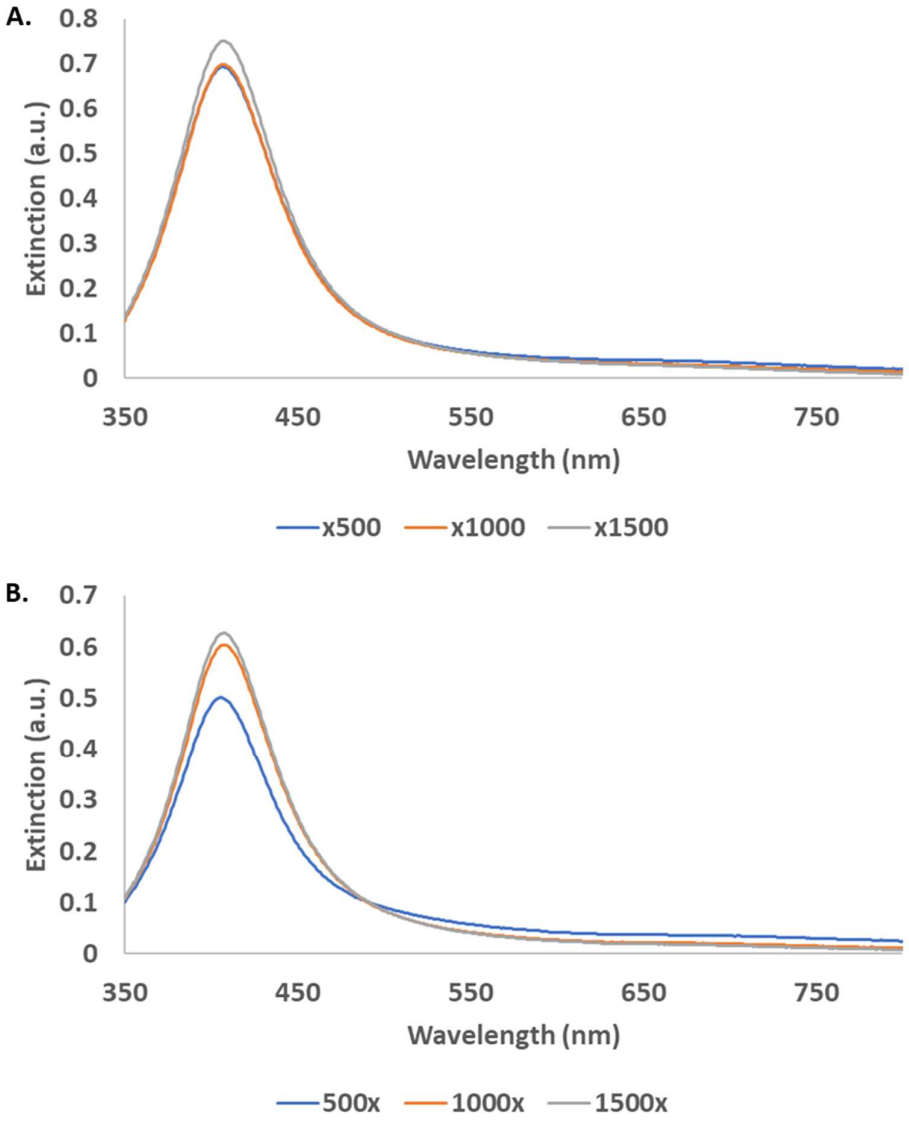

Figure 4.4. *Extinction spectra of AgNP conjugates (1 in 20 dilution of stock solution) following functionalisation and resuspension in 0.1 M PBS buffer.* ***A.*** *After conjugation* ***B.*** *After 5 days of storage at 4 °C.*

Conjugate stability was achieved using a DNA: AgNP ratio of 500: 1. This correlated with the findings of Zhang et al., who demonstrated that full surface coverage could be obtained at a DNA: AgNP ratio of approximately 500: 1.[108] To ensure that the conjugates remained stable over time, UV-Vis extinction spectroscopy was performed following 5 days of storage at 4 °C (**Figure 4.4**).

Each of the conjugates displayed some reduction in the extinction value although this was most significant for the conjugate that was functionalised at a ratio of 500: 1. The slight increase at higher wavelengths suggested that this conjugate had begun to partially aggregate. Whilst the conjugate seemed stable following functionalisation, it was likely that full surface coverage had not been attained and the sodium ions present within the resuspension buffer had induced slight aggregation. Therefore, a DNA: AgNP molar ratio of 1000: 1 was selected as the optimal condition for functionalisation of AgNPs.

4.6 Optimisation of the Raman Reporter Concentration for Maximum SERS Intensity

Following the optimisation of the DNA conjugation procedure, a dye concentration study was performed to identify the optimal concentration of Raman reporter to be used to generate the maximum SERS intensity. MGITC was selected and added after functionalisation with the thiolated DNA. Initially, a wide range of MGITC: AgNP molar ratios were investigated with the assumption that greater dye concentrations would produce greater SERS signal intensities. The MGITC: AgNP ratios investigated were 5: 1, 50: 1, 500: 1, 5000: 1 and 50000: 1. After the addition of the Raman reporter, the conjugates were sonicated for 3 minutes, centrifuged and resuspended in 0.1 M PBS. The UV-Vis extinction spectra of the conjugates were then analysed (**Figure 4.5**).

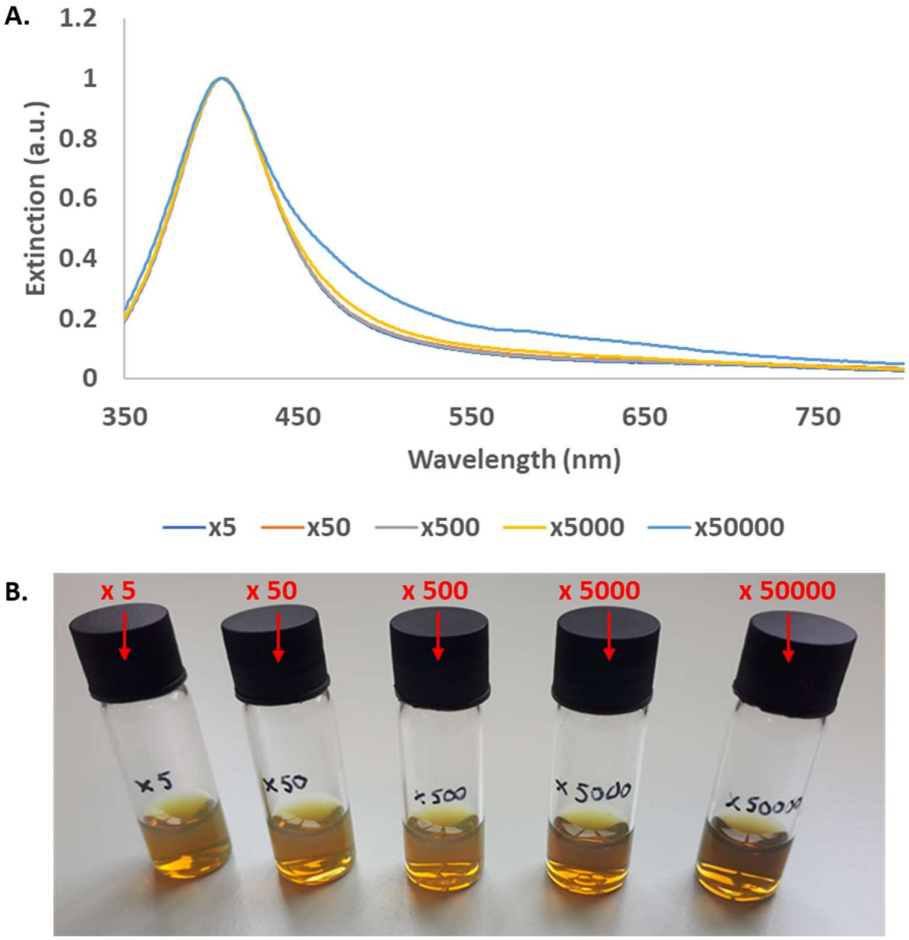

Figure 4.5. *Normalised extinction spectra of AgNP conjugates (1 in 20 dilution of stock solution) following addition of MGITC Raman reporter and resuspension in 0.1 M PBS buffer.* ***A.*** *Normalised extinction spectra* ***B.*** *Image of conjugates following dye*

The conjugates were stable upon addition of each concentration of MGITC, although some partial aggregation appeared to occur with the addition of MGITC at a ratio of 50000: 1 as indicated by the increased extinction values at the higher wavelengths. The conjugate remained stable enough for SERS analysis and any aggregates were left to settle out of solution prior to SERS analysis to ensure that the aggregated NPs would not contribute to an increase in electromagnetic SERS enhancement. The SERS analysis was performed in 0.1 M PBS and the results are shown in **Figure 4.6**.

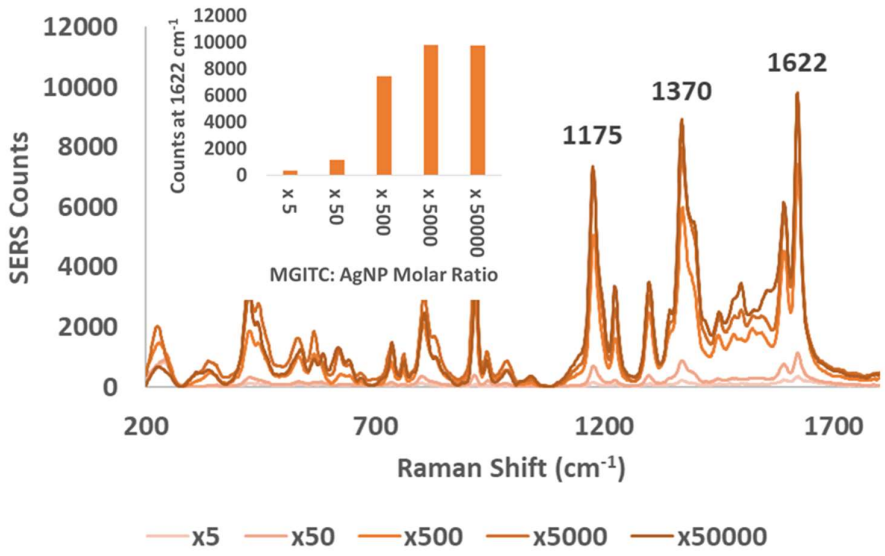

Figure 4.6. *SERS spectra of AgNP conjugates (100 pM) following addition of MGITC Raman reporter and resuspension in 0.1 M PBS. Inset shows peak intensity at 1622 cm^{-1} for each dye ratio investigated. Spectra accumulated with a 532 nm laser, 1 second acquisition time and 10 % (5 mW) laser power.*

It was evident that as the MGITC Raman reporter concentration increased, the SERS intensity also increased. The SERS intensity was weak at low concentrations as indicated by the dye ratios investigated at 5: 1 and 50: 1. The intensity then increased significantly as the dye concentration increased at the ratios of 500: 1 and 5000: 1. The maximum concentration of MGITC investigated at a ratio of 50000: 1 generated a SERS intensity that was approximately equivalent to the intensity observed at a ratio of 5000: 1. This indicated that the addition of MGITC at a ratio above 5000: 1 was not beneficial for the purpose of maximising SERS intensities due to saturation. The experiment was repeated using a reduced concentration range and performed in triplicate to ensure reproducibility. The MGITC dye concentration was investigated at MGITC: AgNP ratios of 50: 1, 500: 1, 1000: 1, 2000: 1, 3000: 1, 4000: 1 and 5000: 1. The UV-Vis extinction spectra were acquired and this indicated that there was no aggregation observable for each of the concentrations investigated (**Figure 4.7**).

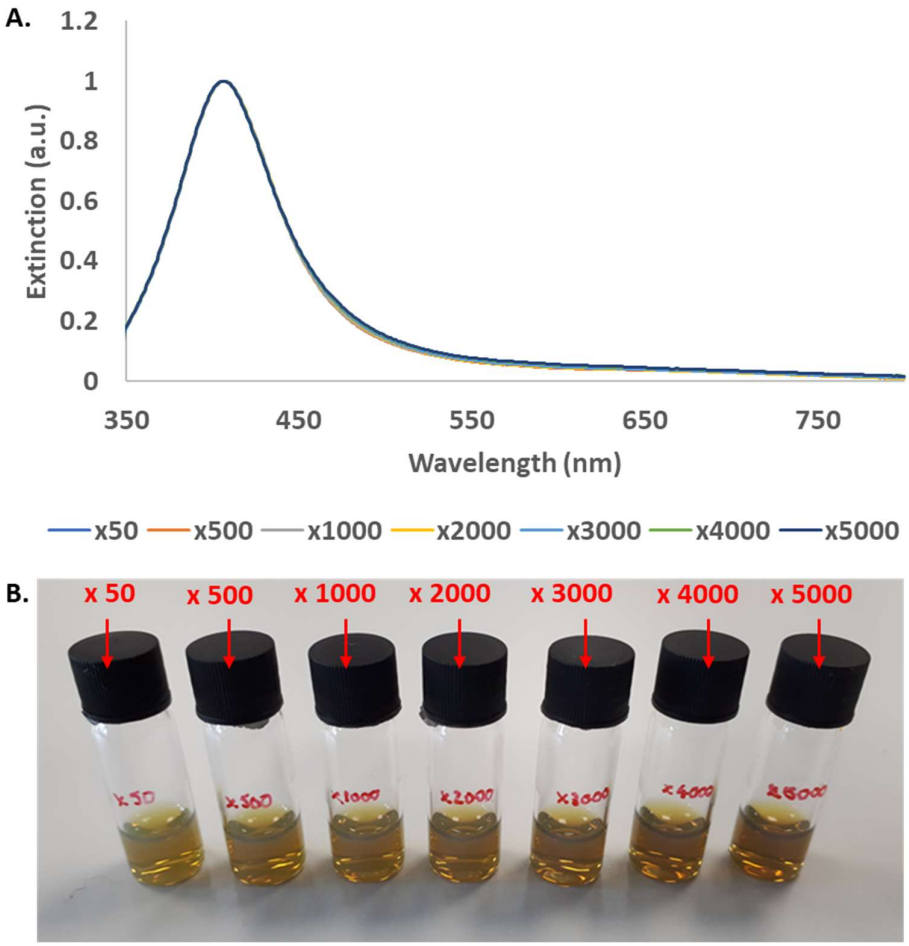

Figure 4.7. *Normalised extinction spectra of AgNP conjugates (1 in 20 dilution of stock solution) following addition of MGITC Raman reporter and resuspension in 0.1 M PBS buffer.* ***A.*** *Normalised extinction spectra* ***B.*** *Image of conjugates following dye*

Following analysis by UV-vis extinction spectroscopy, the SERS spectra of the conjugates at each dye ratio were investigated as shown in **Figure 4.8**.

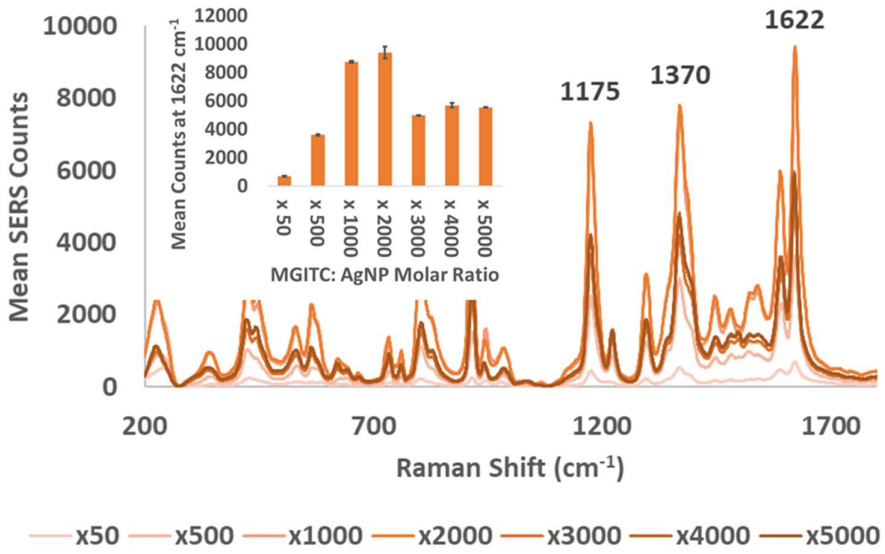

Figure 4.8. *Mean (n=3) SERS spectra of AgNP conjugates (100 pM) following addition of MGITC Raman reporter and resuspension in 0.1 M PBS. Inset shows peak intensity at 1622 cm^{-1} for each dye ratio investigated. Spectra accumulated with a 532 nm laser, 1 second acquisition time and 10 % (5 mW) laser power.*

As the dye ratio increased in concentration from 50: 1 to 1000: 1, the SERS intensities also increased. The SERS intensity plateaued as the ratio increased from 1000: 1 to 2000: 1, and the intensity then decreased significantly as the ratio increased from 2000:1 to 3000: 1. At the dye ratios of 3000: 1, 4000: 1 and 5000: 1, the SERS intensities generated were approximately equivalent. This indicated that the SERS intensity increased beyond the conditions identified in the previous investigation, which did not identify optimal SERS intensity within the MGITC: AgNP range of 1000: 1 to 2000: 1. The decrease in the SERS intensity beyond this range suggested that the dye surface chemistry had changed beyond the ratio of 2000: 1. It was possible that the dye orientation had changed as the concentration increased beyond the limit required for monolayer coverage although further investigation would be required to confirm this.

Following 5 days of storage at 4 °C, the conjugate with MGITC added at a ratio of 2000: 1 had begun to aggregate as evident by the increase in extinction values at higher wavelengths (**Figure 4.9**).

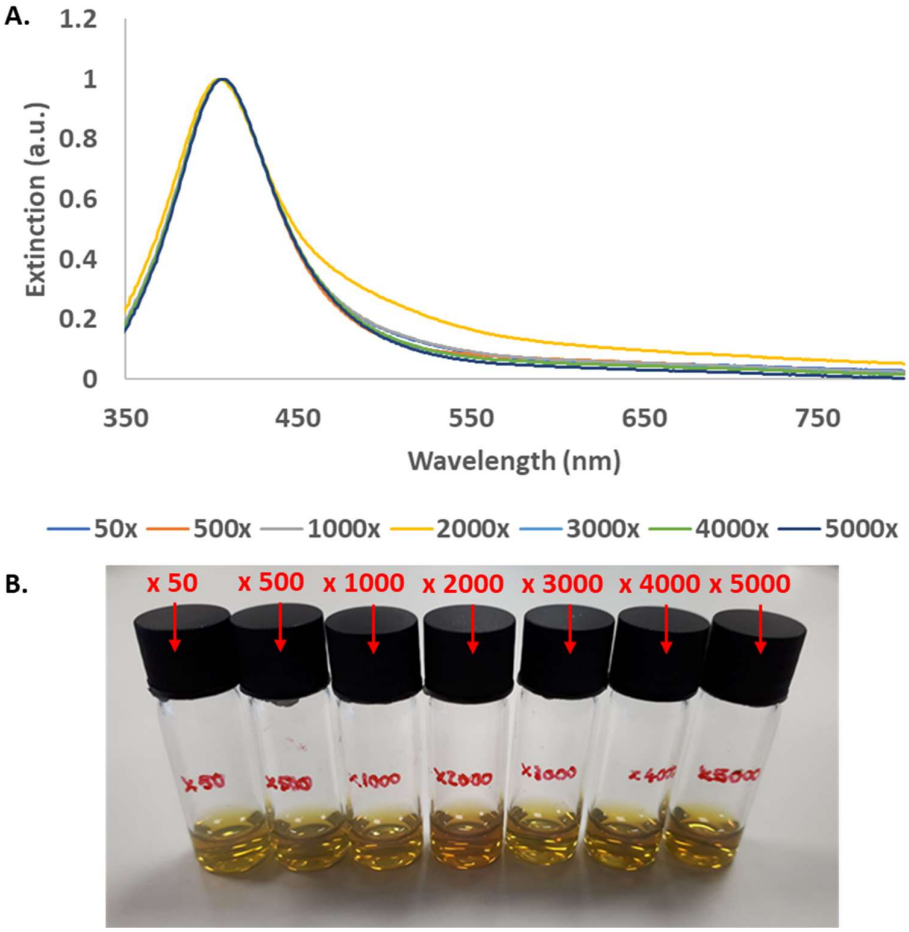

Figure 4.9. *Normalised extinction spectra of AgNP conjugates (1 in 20 dilution of stock solution) following addition of MGITC Raman reporter and resuspension in 0.1 M PBS buffer.* ***A.*** *Normalised extinction spectra* ***B.*** *Image of conjugates following dye addition.*

This was also evident visually, as the conjugate appeared to be darker in colour as compared to the other dye ratios investigated. This supported the theory that the MGITC underwent a change in orientation at higher concentrations with a dye ratio of 2000: 1 indicative of the concentration threshold at which this process occurs. This appeared to destabilise the conjugates in suspension as apparent by the aggregation that occurred uniquely at this concentration. The SERS intensity generated using a MGITC: AgNP ratio of 1000: 1 was approximately equivalent to that obtained using a ratio of 2000: 1 and did not show any indication of aggregation. Therefore, the

optimal Raman reporter concentration was established at a MGITC: AgNP ratio of 1000: 1.

4.7 Optimisation of the RPA Assay

The RPA assay applied within this investigation had been developed by project collaborators previously and did not require further optimisation. The assay was performed using a kit supplied by a commercial supplier (TwistDx) and has been highly standardised to simplify operation by the end user. The kit contains three main components including lyophilised reaction pellets, a rehydration buffer solution for the resuspension of the pellet and magnesium acetate solution that is added to the reaction mix to initiate the reaction (**Figure 4.10**).

Figure 4.10. *RPA kit components including the lyophilised reaction pellets (bottom), rehydration buffer (top left) and magnesium acetate solution (top right).*

Much of the assay optimisation has been predefined by the manufacturer. The assay conditions that are defined by the end user include the selection and addition of primer and target template sequences which may vary in length and composition, the assay temperature which is maintained at a constant temperature within the range of 37 °C and 42 °C, and the assay time which generally requires just 10 – 30 minutes for detection of targets with PCR-comparable sensitivity and specificity.[30, 32] Unlike PCR, the RPA reaction does not require careful optimisation of the primer or magnesium concentrations for optimal assay performance. The primers were added at a standard concentration of 420 nM for each primer, and magnesium was added

at a standard concentration of 14 mM. The template material utilised for the RPA amplification was a plasmid (pUCIDT-AMP) containing the *wzm-1* gene within an 852 bp region of the *Legionella pneumophila* serogroup 1 lipopolysaccharide biosynthesis gene cluster as supplied by the project collaborator. The template material was diluted from a 50 μg/mL stock solution prior to amplification to the required reaction template concentration. The assay conditions that were determined by the operator (primer and target sequences, temperature and assay time) were pre-optimised by the project collaborators (work unpublished), and therefore the assay was performed using these conditions to ensure reproducibility and to establish the lowest concentration with discriminatory value. The RPA assay was performed at 37 °C for 20 minutes and the samples were analysed by gel electrophoresis following amplification as shown in **Figure 4.11**.

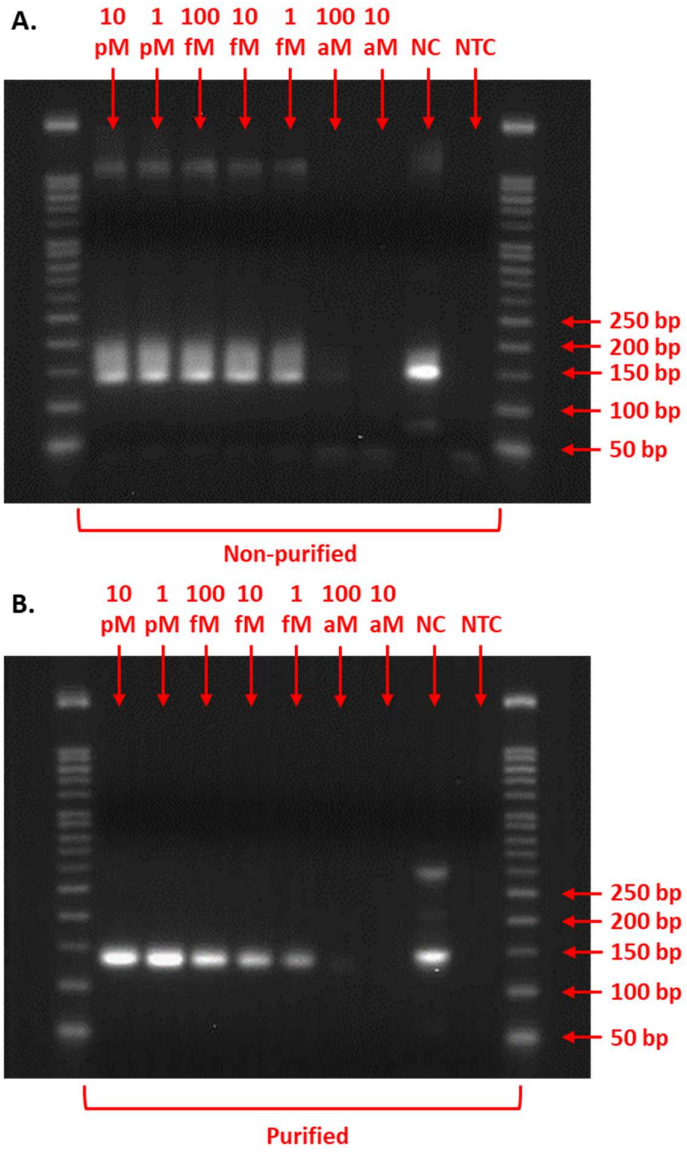

***Figure 4.11**. Gel electrophoresis image of RPA product following serial dilution of template concentration range. **A.** Non-purified product range **B.** Purified product range.*

The non-purified amplification product range was compared to the purified amplification product range as the commercial manufacturer recommends a purification clean-up step prior to gel electrophoresis. A no template control (NTC) was included to ensure specificity and a positive control was included to ensure that the assay amplification occurred as expected. This was designated the non-complementary (NC) control as the product could be used as a non-complementary

negative control for the plate-based assay at a later stage. The NC positive control was amplified using and independent primer set and positive control template material as supplied with the kit provided by the commercial manufacturer.

The results indicated that the amplification was reproducible, and both non-purified and purified amplification products could be visualised by gel electrophoresis. The amplified product was positioned between the 100 bp and 150 bp DNA ladder size markers, which was expected for the product which was 118 bp in length. The non-purified product displayed significant smearing when visualised by gel electrophoresis. This was attributed to the complex reaction mix which contains various macromolecules including recombinase proteins, ssDNA binding proteins and high molecular weight PEG which acts as molecular crowding agent.[32] It is likely that one or more of these reaction components was complexed with the DNA product, producing the smearing effect. This was eliminated with purification. It was also noted that the assay produced some primer-dimers at the lower template concentrations, as indicated by the faint bands below the 50 bp DNA ladder marker in the non-purified product. This was significant as the non-specific products contained both tailed primer hybridisation regions and would therefore have the capacity to generate a non-specific signal when applied for detection using the complementary probes. The primer-dimers could be eliminated by purification due to the small size of the non-specific products. The RPA assay efficiently amplified the expected product within the range of 10 pM – 1 fM as indicated by the intense product bands. A fainter band was still observed at 100 aM and therefore the detection limit was established at 100 aM. The band intensities were difficult to distinguish using the non-purified product, however the purified product indicated that the brightest band was observed at 1 pM. This suggested that reaction was saturated at the maximum template concentration of 10 pM. Following the successful amplification of the RPA product, the SERS analysis of the RPA product was investigated using the plate-based assay and optimised AgNP conjugates.

4.8 SERS Detection of the *L. pneumophila* RPA Product

Prior to SERS analysis, the maleimide activated plate was functionalised with the capture probe and blocked with 6-mercapto-1-hexanol. The RPA product was dispensed into the 96-well plate that had been functionalised using the capture probe that was complementary to one of the tail regions of the RPA product. Following the addition and hybridisation of the of the RPA product, the wells were washed with 0.1 M PBS-Tween 20 buffer to remove any excess RPA product following hybridisation. The DNA functionalised and dye-coded AgNP reporter conjugate was diluted in 0.1 M PBS and added to the well. The conjugates were functionalised using the reporter probe sequence that was complementary to the remaining tail region of the RPA product. The plate was then washed with 0.1 M PBS-Tween 20 following the addition of the reporter conjugate to remove excess, non-hybridised reporter conjugate. If the RPA product and AgNP reporter conjugate successfully hybridised, the reporter conjugate would remain within the well and a SERS signal would be generated. If the hybridisation had not occurred, the AgNP conjugates would be removed during the wash step and no SERS signal would be generated. The RPA product was amplified using 10 pM of template DNA as this represented the highest concentration of template DNA within the detection range, and confirmation of the hybridisation event was required prior to the optimisation of the sensitivity at the lower template concentrations. The concentration of reporter conjugate required to generate a SERS signal was unknown, and therefore the conjugate was added at concentrations of 100 pM, 250 pM, and 500 pM. A no template control was included to ensure the specificity of the result and this was analysed using the highest concentration of reporter probe at 500 pM. The samples were then analysed by SERS using a 532 nm laser wavelength and 10 % (5 mW) laser power (**Figure 4.12**).

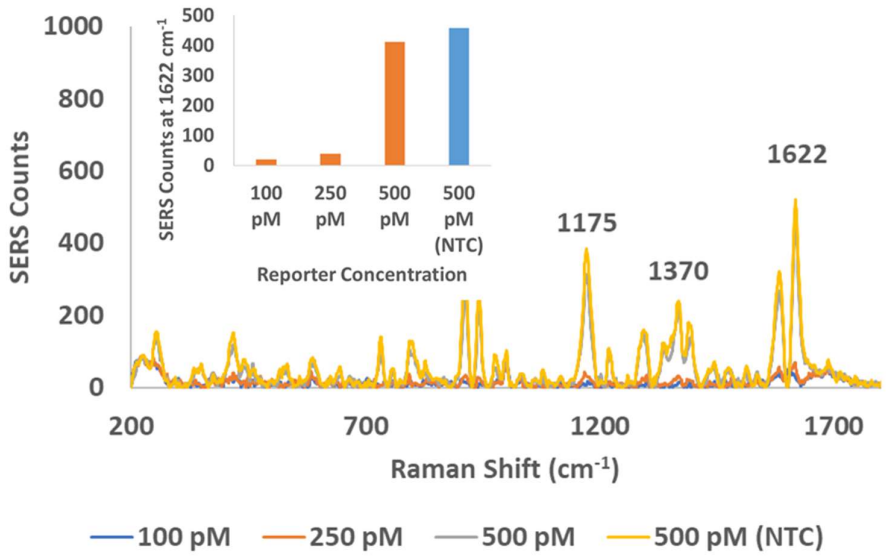

Figure 4.12. *SERS spectra of AgNP reporter conjugate concentration range upon hybridisation to 40 μL of the complementary RPA product within a 96 well plate. Inset shows the peak comparison at 1622 cm^{-1} for each concentration of reporter conjugate investigated. Spectra accumulated with a 532 nm laser, 1 second acquisition time and 10 % (5 mW) laser power.*

The results indicated that almost no SERS signal was generated upon application of the reporter conjugate at 100 pM and 250 pM. The SERS intensity increased as the reporter conjugate concentration increased to 500 pM, however the no template control that was analysed using 500 pM of reporter conjugate indicated that the signal generated was non-specific and did not confirm the specificity of the hybridisation event. It was possible that the RPA product may not have hybridised to the respective probes due to steric repulsions on the surface of the well or alternatively, an insufficient density of capture probe on the well surface may have limited the capacity to generate a SERS response upon hybridisation of the RPA target and AgNP reporter probe.

The detection strategy had previously been validated using a reporter probe conjugated to horse-radish peroxidase (HRP) which produced a colour change upon addition and conversion of a TMB substrate.[141] The primer and target sequences differed from this investigation, however the tailed sequences and complementary

probe sequences were the same as those applied within this investigation. Therefore, it was most likely that assay did not produce a signal due to steric repulsions or insufficient capture probe density on the well surface. However, to confirm this theory, further investigation was required to ensure that the capture and reporter probes could hybridise to the respective complementary tail regions of the RPA target.

Initially, this was investigated in solution. Both the reporter probe and capture probe were conjugated to AgNPs, diluted in 0.1 M PBS, and the RPA product was added to the conjugates in solution. The aim of the experiment was to cross-link the AgNP conjugates in a manner that was analogous to the method applied within the *Candida krusei* investigation. UV-Vis extinction spectroscopy could then be applied to identify if an LSPR shift could be induced to confirm the hybridisation event and further validate the probe sequences used within the investigation. This method was investigated with the addition of 40 μL of RPA product amplified from 10 pM of template DNA to 50 pM of each AgNP conjugate. The analysis was performed in a 0.1 M PBS hybridisation buffer. A no template control RPA product was included as the negative control to ensure the specificity of the result. The results are shown in **Figure 4.13**.

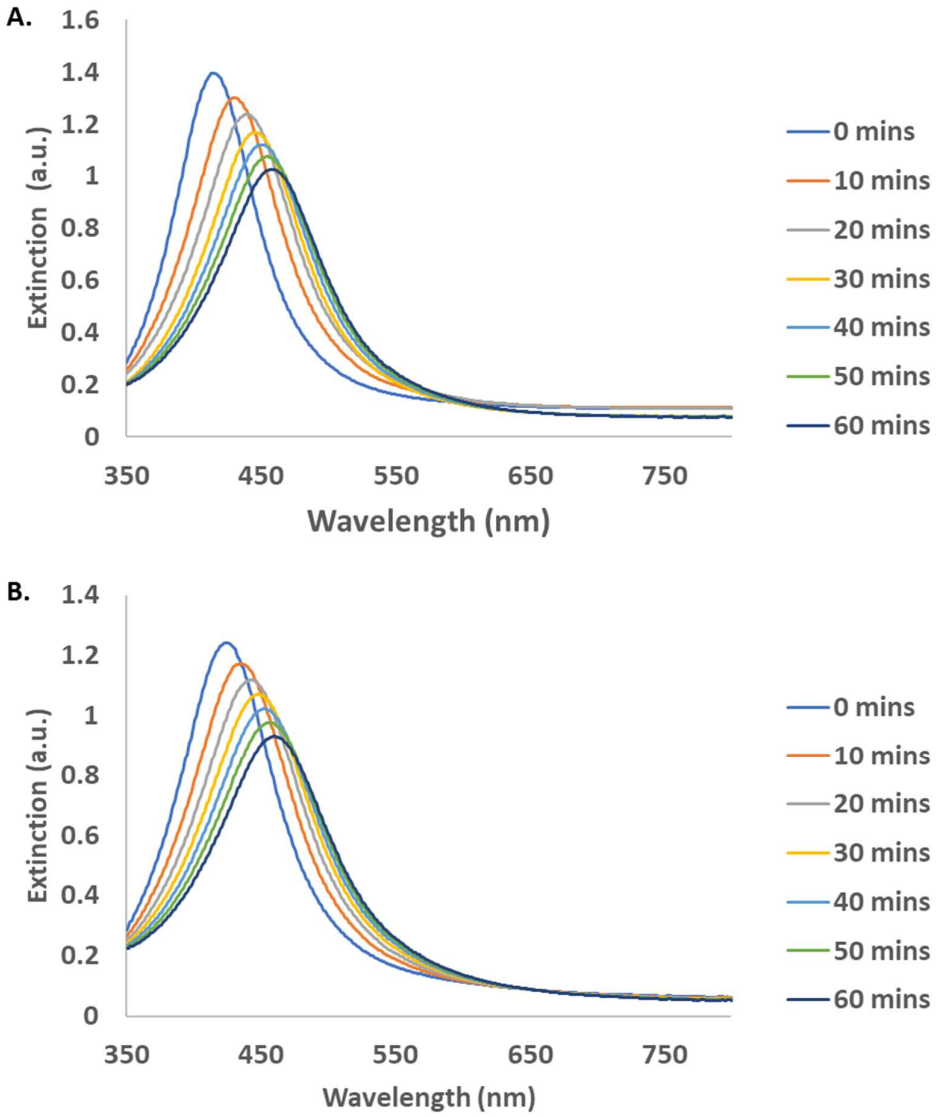

Figure 4.13. *Extinction spectra of AgNP conjugates (50 pM of each) upon the addition of 40 μL of a complementary RPA sample and no template control RPA sample at room temperature for 1 hour.* ***A.*** *Complementary RPA product* ***B.*** *No template control RPA product.*

The results indicated a comparable trend for both the complementary RPA product and the no template control. There was an LSPR shift that occurred gradually and continually over time. This was accompanied by a clearly observable change in colour of the conjugates in suspension, which changed from a yellow colouration to an amber colouration. Evidently, this LSPR shift and colour change was not specific to a

hybridisation event as it occurred in a highly comparable manner for the no template control sample. The cause of this trend was unknown and SERS analysis was performed immediately after a 1 hour incubation step to identify if any SERS enhancement had occurred (**Figure 4.14**).

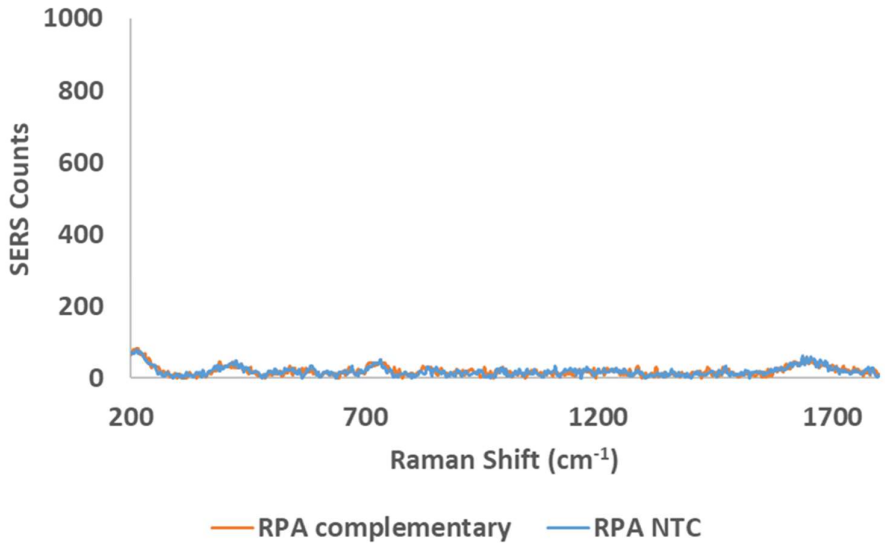

Figure 4.14. *SERS spectra of AgNP conjugates (50 pM of each) upon the addition of 40 μL of a complementary RPA sample and no template control RPA sample following incubation at room temperature for 1 hour.*

The SERS analysis of the conjugates following 1 hour of incubation did not generate a SERS response. Furthermore, the expected MGITC spectra was eliminated entirely upon addition of the RPA product. Therefore, the addition of the RPA product to the AgNP conjugates caused a gradual LSPR shift that was independent of the DNA target sequences, and the causative factor also eliminated the SERS signal obtained. It was likely that one of the many reagents contained within the RPA buffer or pellet had contributed to this effect, although further investigation was required to identify this. The experiment was repeated with further conditions investigated. A positive RPA sample was amplified from 10 pM of template DNA, and a series of controls were also included. A non-complementary DNA control and no template control were included to further confirm that the trend was independent of the DNA target sequence. An RPA positive sample that had been pre-heated to 95 °C was included as

the heating step would denature the recombinase and single-stranded binding proteins contained within the RPA reaction mix. If the RPA reaction enzymes and proteins were denatured, this would confirm that the proteins were not interfering with the nanoparticle surface chemistry or causing non-specific hybridisation or aggregation. A further negative control was included without the addition of the magnesium acetate which is required to initiate the RPA reaction. This would ensure that the presence of divalent ions was not the causative factor. Finally, an RPA negative control was included and consisted of the conjugates resuspended in 0.1 M PBS without the addition of any RPA product. This would confirm that the conjugates were stable, and SERS active. The UV-Vis kinetics were analysed as a ratio of the extinction maximum at 0 minutes / extinction maximum at each time point (*n* minutes) which provided a means to directly compare the dispersity of NPs in suspension upon the addition of the RPA samples (**Figure 4.15**).

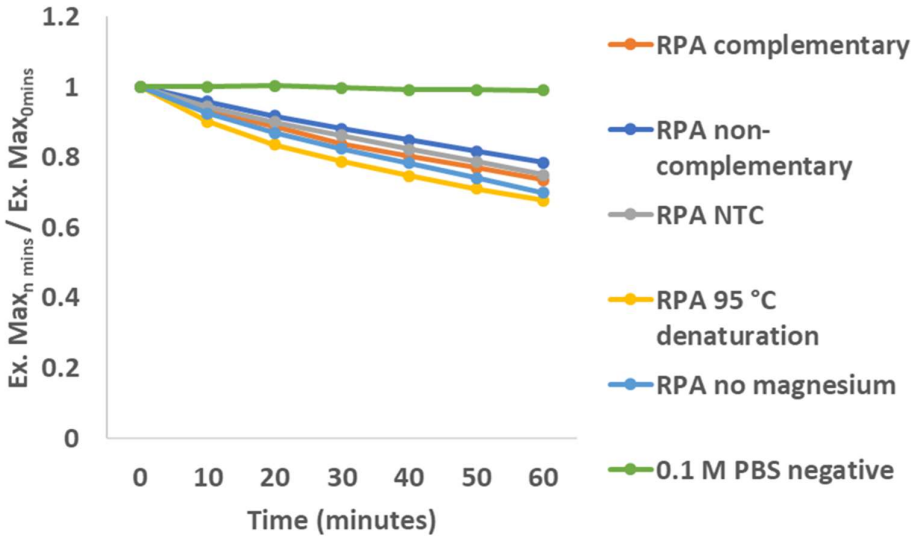

Figure 4.15. *Extinction maximum (*n *mins) / extinction maximum (0 mins) ratio of AgNP conjugates (50 pM of each) upon addition of 40 μL of the RPA samples at room temperature for 1 hour.*

The results indicated that the aggregation event occurred as observed previously for all samples analysed, except for the sample containing the AgNP conjugates resuspended in 0.1 M PBS without addition of any RPA product. This could be

confirmed visually by the distinct colour change observed for the conjugates in solution (**Figure 4.16**).

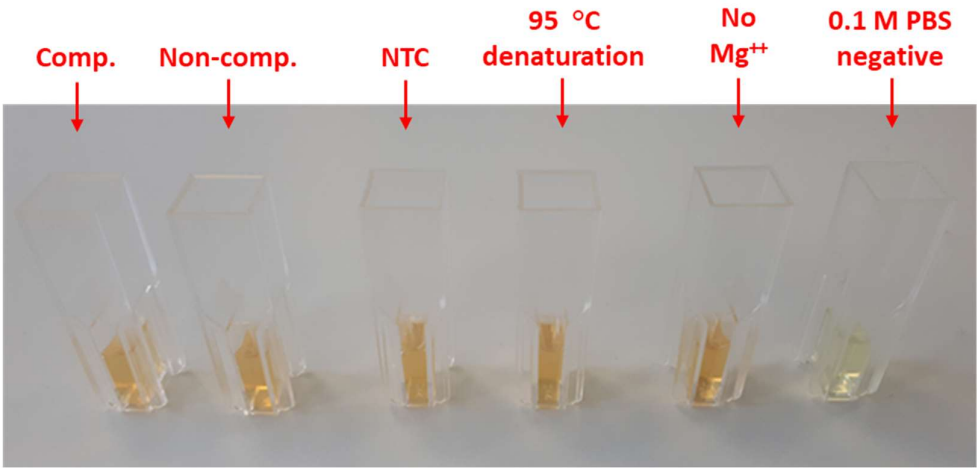

Figure 4.16. *Image of AgNP conjugates (50 pM of each) upon addition of 40 µL of the RPA samples and following incubation at room temperature for 1 hour.*

The absence of an LSPR shift and colour change confirmed that the conjugates were stable in the 0.1 M PBS buffer. The results also confirmed that LSPR shift observed was independent of the DNA target sequence, proteins contained within the RPA reaction mix and the magnesium acetate added to initiate the RPA reaction. SERS analysis was performed to confirm if the RPA product was eliminating the SERS signal (**Figure 4.17**).

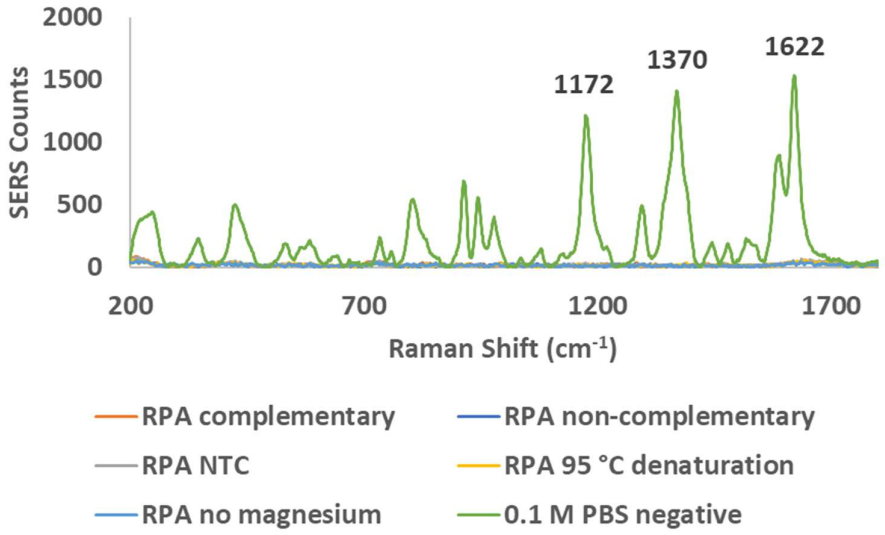

Figure 4.17. *SERS spectra of AgNP conjugates (50 pM of each) upon addition of 40 μL of the RPA samples and following incubation at room temperature for 1 hour. Spectra accumulated with a 532 nm laser, 1 second acquisition time and 10 % (5 mW) laser power.*

The results demonstrated that the RPA product did eliminate the SERS signal, and that the conjugates remained Raman active when resuspended in the 0.1 M PBS buffer. As the LSPR shift, colour change and reduced SERS activity of the conjugates was not related to the target sequence, RPA reaction proteins or magnesium acetate present within the reaction mix, it was concluded that either the RPA reaction buffer or lyophilised pellet must contain a reagent that was incompatible with the conjugate chemistry applied within this investigation. To confirm this theory, the AgNP conjugates were resuspended in a buffer containing the lyophilised pellet dissolved in PBS rather than the commercially supplied rehydration buffer. Furthermore, another sample was prepared in which the AgNP conjugates were resuspended in the rehydration buffer without the reaction pellet. This would identify if the causative factor was contained within either of the commercially supplied kit components. Initially, the UV-Vis extinction kinetics were investigated (**Figure 4.18**).

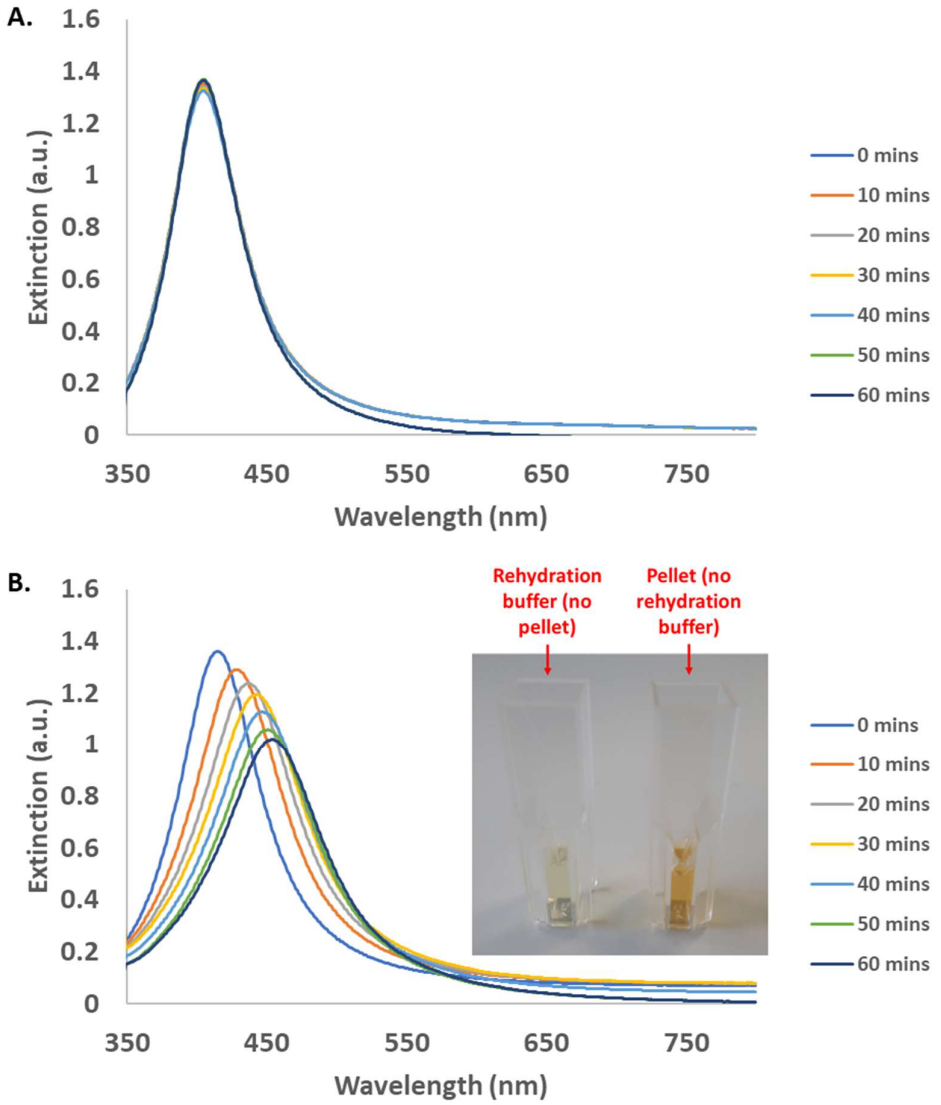

Figure 4.18. *Extinction spectra of AgNP conjugates (50 pM of each) upon addition of 40 μL of rehydration buffer without the pellet or 40 μL of the pellet without the rehydration buffer at room temperature for 1 hour* ***A.*** *Rehydration buffer only* ***B.*** *Pellet only.*

The results demonstrated that the LSPR shift did not occur upon addition of the rehydration buffer to the AgNP conjugates resuspended in 0.1 M PBS. However, the LSPR shift did occur as observed previously when the pellet that was dissolved in 0.1 M PBS was added to the AgNP conjugates resuspended in the 0.1 M PBS buffer. This was accompanied by a distinct colour change that only occurred in the sample

containing the dissolved pellet. Therefore, it was confirmed that the lyophilised RPA reaction pellet contained the reagent that was inducing the LSPR shift and visual colour change. To ensure that this was also eliminating the SERS response, SERS analysis was performed immediately following UV-Vis analysis (**Figure 4.19**).

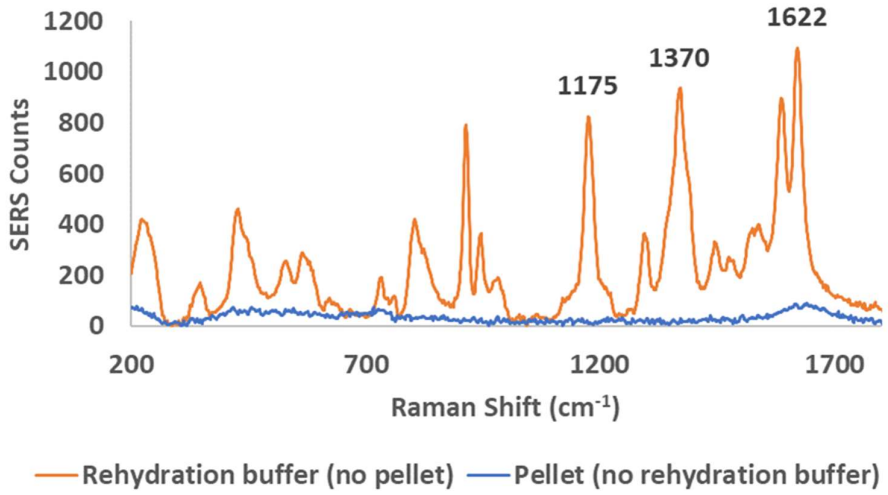

Figure 4.19. *SERS spectra of AgNP conjugates (50 pM of each) upon addition of 40 μL of rehydration buffer without the pellet or 40 μL of the pellet without the rehydration buffer following incubation at room temperature for 1 hour. Spectra accumulated with a 532 nm laser, 1 second acquisition time and 10 % (5 mW) laser power.*

The sample that contained the rehydration buffer generated the expected SERS response, whereas the sample containing the pellet did not. It was concluded that the RPA reaction pellet must contain an unknown reagent that was eliminating the SERS activity of the AgNP conjugates in solution. To further understand the cause of this effect, the contents of the RPA reaction pellet needed to be identified. The precise formulation of the RPA reaction formulation was not readily available within the published literature at the time of investigation, and therefore the reagent formulations were sourced from the commercial patent that described the reaction pellet formulation.[144] The kit components are listed within **Table 4.2**.

Table 4.2. *RPA lyophilised pellet formulation listing reaction components and concentration.*

Component	Concentration
PEG 35,000	2.28 % (w/v)
Trehalose	5.7 % (w/v)
UvsX recombinase protein	260 ng/µL
UvsY protein	88 ng/µL
Gp32 protein	254 ng/µL
Sau polymerase protein	90 ng/µL
ATP	2.5 mM
dNTPs	240 µM
Tris buffer	25 mM
DTT	5 mM
Phosphocreatine	50 mM
Creatine kinase	100 ng/µL

The lyophilised pellet contained a complex combination of reagents that had been commercially developed for the optimal amplification of DNA during the RPA reaction. The presence of dithiothreitol (DTT) within the pellet formulation was suspected to be causative reagent that had induced the LSPR shift and eliminated the SERS signal upon addition to the AgNP conjugates in solution. DTT has previously been shown to displace thiolated DNA from the surface of AuNPs.[145], [146] It was likely that the DTT present in the RPA reaction pellet was gradually displacing the thiolated DNA probes and MGITC present on the surface of the AgNP conjugates used within this investigation. Therefore, the MGITC was removed from the surface of the AgNPs and no SERS signal could be obtained, and as the oligonucleotide probes dissociated from the surface, the NPs partially aggregated as evident from the LSPR shift and colour change.

Due to the poor stability of the conjugates upon addition of the RPA product, an alternative detection method was required. The previous attempt at detecting the RPA product using the plate-based assay had been unsuccessful, possibly due to steric repulsions preventing the AgNP conjugates from hybridising upon the well surface, or possibly due to insufficient capture probe density limiting the capacity to generate a SERS response. The plate-based method had previously been demonstrated using an HRP conjugated DNA reporter probe for the colorimetric detection of a DNA target sequence.[141] Therefore, the AgNP reporter conjugate was substituted for an HRP reporter conjugate to investigate if the biological interaction could be confirmed with the production of a colour change upon addition of the TMB substrate. A simplified schematic of the resonance Raman detection strategy is shown in **Figure 4.20**.

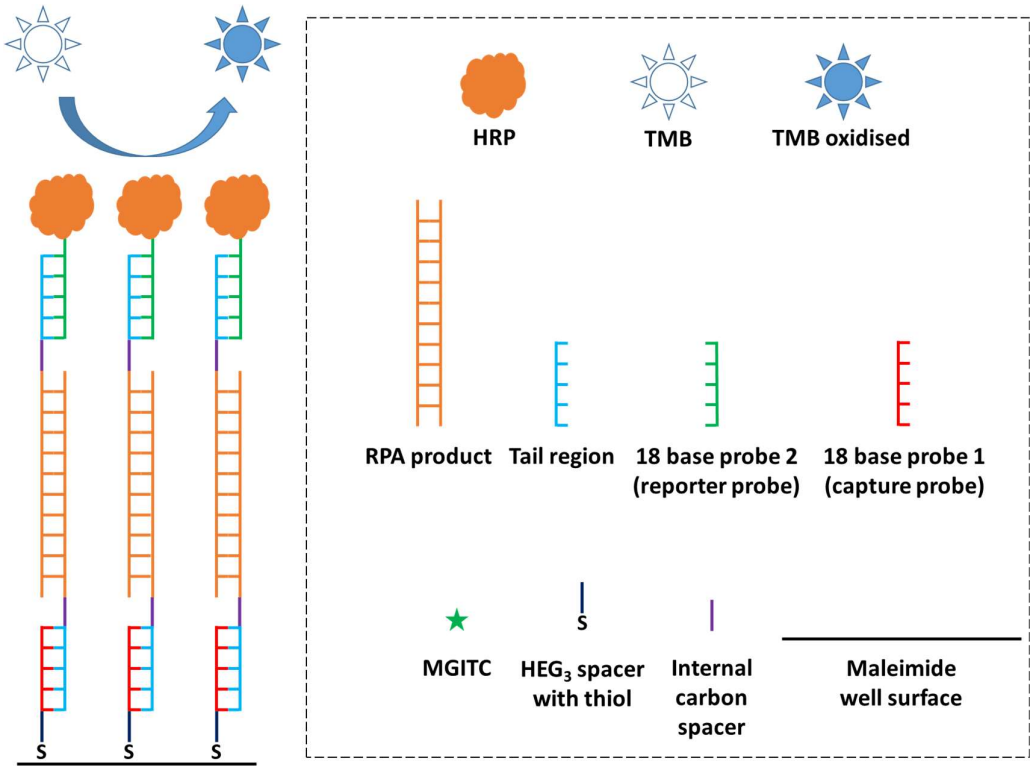

Figure 4.20. *Simplified schematic depicting the principles of the proposed resonance Raman DNA detection methodology on the surface of a maleimide activated 96-well plate. The tailed RPA products act as a cross-linker between the capture probe immobilised upon the well surface and the HRP reporter conjugate probe. If the RPA product was not present, the HRP conjugate would remain in solution and would be removed during the wash step and no resonance Raman signal would be obtained as no colour change would occur.*

If a colour change was produced, the signal could be quantified using resonance Raman spectroscopy. Laing et al., have previously reported a quantitative resonance Raman enzyme-linked immunosorbent assay (ELISA) for the detection of human tumour necrosis factor α.[147] HRP catalysed the oxidation of TMB by hydrogen peroxide, which occurs as result of two successive one-electron oxidisation events. As the first oxidisation event occurs, the colour changes to blue, and as the second oxidisation step occurs, the colour changes to yellow. The first oxidisation step generates a charge transfer complex with an absorbance maximum at approximately 650 nm. Therefore, resonance Raman spectroscopy may be applied using a 633 nm

laser wavelength to achieve resonant detection of the one electron TMB charge transfer complex. This detection strategy was emulated within this investigation for the detection of the *L. pneumophila* RPA target sequence.

4.9 Resonance Raman Detection of the *L. pneumophila* RPA Product

The plate-based assay was performed as previously with described minor changes. The capture probe contained a polyT spacer rather than a triple HEG spacer and the HRP reporter probe was hybridised in 1x PBS rather than 0.1 M PBS as this was consistent with the prior work of the project collaborators.[141] Prior to resonance Raman analysis, the maleimide activated plate was functionalised with the capture probe and blocked with 6-mercapto-1-hexanol as previously implemented. The RPA product was added to the well containing the capture probe and washed with 1x PBS-Tween 20 following hybridisation. The HRP reporter conjugate was diluted in 1x PBS, added to the well and washed again with 1x PBS-Tween 20 following hybridisation. If the target had successfully hybridised, the HRP conjugate remained within the well, and a colour change was produced upon addition of the TMB substrate and hydrogen peroxide. If the target was not present, the HRP reporter conjugate would not hybridise and would be removed following the wash step. A stop solution was added 30 minutes after the addition of the TMB substrate to ensure that the colour change was terminated prior to resonance Raman analysis. The RPA product was amplified using the previously established visually observable concentration range with the lowest concentration of 100 aM of template DNA. A non-complementary (NC) and no template control (NTC) were included as negative controls to confirm the specificity of the result. The successful amplification of the RPA product was confirmed by gel electrophoresis prior to resonance Raman analysis. Furthermore, the colorimetric detection of the RPA product could be confirmed visually as the solution changed from transparent to blue colouration as the reaction proceeded (**Figure 4.21**).

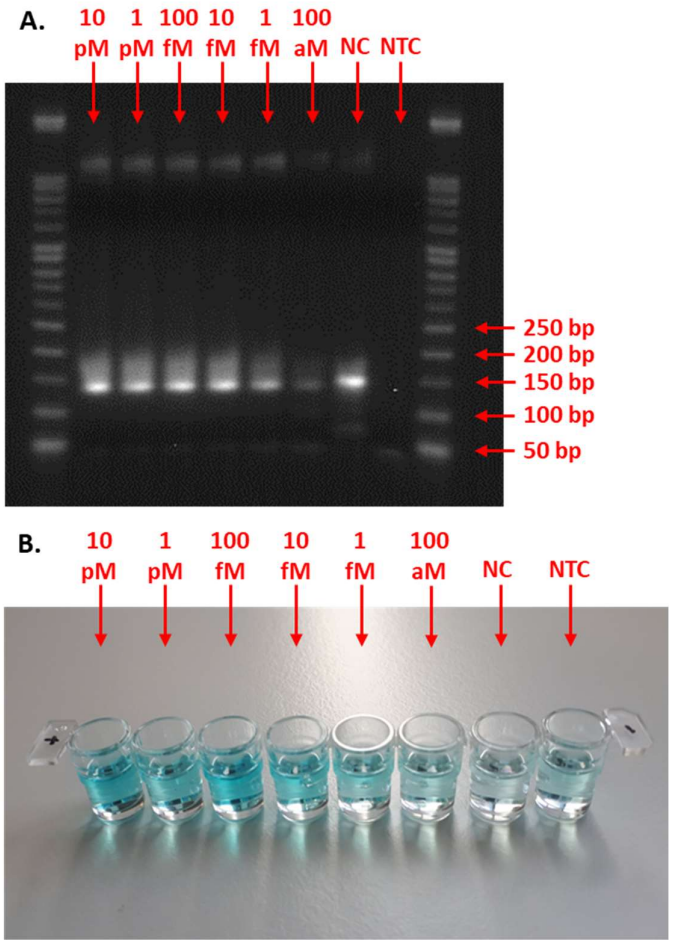

Figure 4.21. *Visual detection of the RPA product.* ***A.*** *Gel electrophoresis image of detection range* ***B.*** *Image of colourimetric change upon addition of TMB substrate.*

The detection range that was established previously was reproduced successfully, and the band that indicated the RPA product amplification from 100 aM of template DNA was slightly more intense than observed in the prior example. When applied to the plate-based assay, a significant colour change was observed. A gradient colour change was apparent, with the most significant colour change occurring upon addition of the RPA samples that were amplified from the higher concentrations of template DNA. However, the most significant colour change occurred for the sample that was amplified from 100 fM of template DNA. This suggested that the RPA amplification may have generated a greater yield of RPA product upon addition of 100 fM of template DNA than at the higher template concentrations of 1 pM or 10 pM. It was notable that the no template control produced a colour change. This was

attributed to the non-specific amplification of primer-dimers as confirmed by gel electrophoresis. This was evident from the band that was visible in the no template control lane and was located just below the 50 bp DNA ladder marker. The primer-dimers are non-specific amplification products that are generated due to low-level self-recognition of the primer sequences. These non-specific products will contain the tail regions that are complementary to the capture and reporter probe sequences, and therefore will have the capacity to hybridise and generate a non-specific colour change. To quantify the colour change, resonance Raman analysis was performed (**Figure 4.22**).

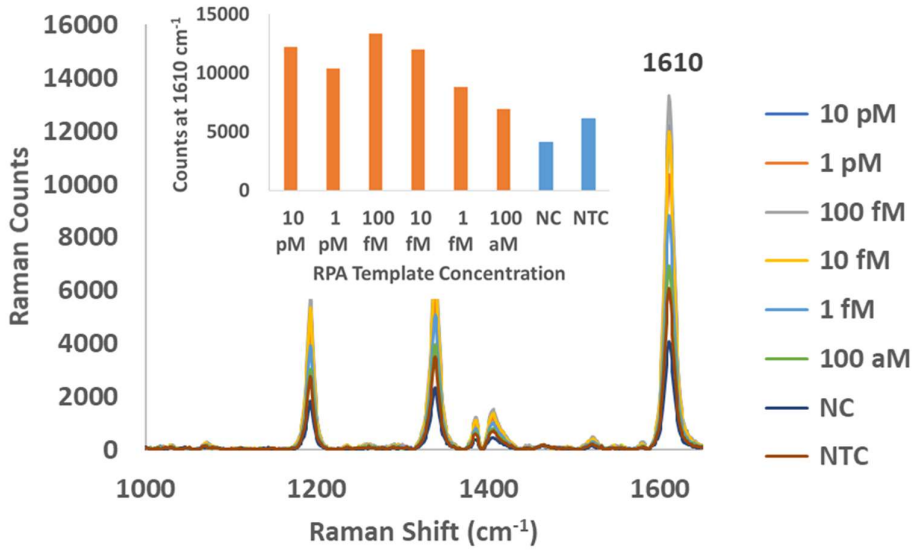

Figure 4.22. *Resonance Raman spectra of oxidised TMB following hybridisation of the HRP conjugate probe to 40 μL of RPA product amplified from a range of initial RPA template concentrations. Spectra accumulated with a 633 nm laser, 20 second acquisition time and 100 % (50 mW) laser power.*

The results indicated that the RPA product could be detected and quantified using the resonance Raman assay. The intensity of the resonance Raman signal increased linearly as the RPA template concentration increased from 100 aM to 100 fM. However, the signal decreased as the RPA template concentration increased to 1 pM and 10 pM. This correlated with the visually observed result and may have indicated that the RPA amplification was saturated at higher concentrations. The positive

samples all generated a greater signal than that obtained from the negative control samples, however, the no template control signal was almost equivalent to the 100 aM template positive sample. Therefore, the presence of the primer-dimers lessened the discriminatory value of the assay at lower template concentrations. The non-complementary control also displayed some Raman signal, and this suggested that there may have been some non-specific binding of the HRP reporter conjugate. The non-complementary control did not utilise the tailed-primers and was amplified from primers supplied by the manufacturer. Therefore, the signal obtained could only be generated by non-specific adsorption. Following the immobilisation of the capture probe, the surface was blocked with 6-mercapto-1-hexanol. Furthermore, the wash steps were included to minimise the likelihood of non-specific adsorption. This did not prevent the non-specific signal and further investigation of alternative blocking agents may be required for future application. The experiment was repeated to identify if the result was reproducible and confirm that a reduced signal at higher template concentrations was reflective of the assay conditions or due to operational error. Gel electrophoresis confirmed the detection range, and the colour change occurred as previously (**Figure 4.23**).

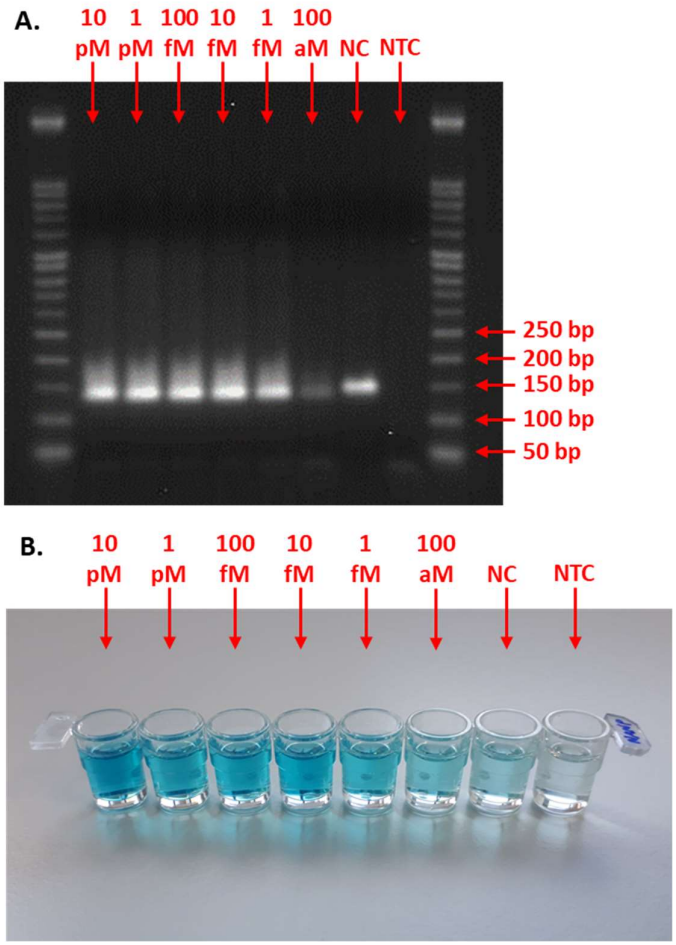

Figure 4.23. *Visual detection of the RPA product.* ***A.*** *Gel electrophoresis image of detection range* ***B.*** *Image of colourimetric change upon addition of TMB substrate.*

Following the observed colour change, the resonance Raman analysis of the samples was performed as shown in **Figure 4.24**.

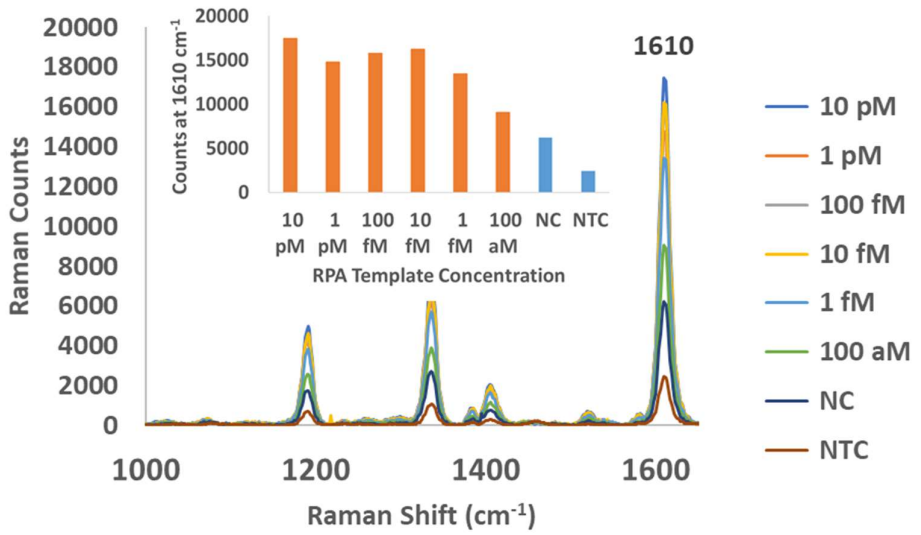

Figure 4.24. *Resonance Raman spectra of oxidised TMB following hybridisation of the HRP conjugate probe to 40 µL of RPA product amplified from a range of initial RPA template concentrations. Spectra accumulated with a 633 nm laser, 20 second acquisition time and 100 % (50 mW) laser power.*

The resonance Raman signal obtained for the detection range was highly comparable to the results obtained in the prior experiment. The positive samples generated a resonance Raman signal that was greater than that obtained from the non-complementary and no template control samples. The signal increased linearly as the template concentration increased from 100 aM to 10 fM. As the template concentration increase beyond 10 fM, the signal decreased slightly before increasing again at 10 pM. This trend was comparable to the prior results and provided further evidence that the RPA reaction plateaued at higher concentrations of template DNA and therefore a linear detection range was not attained. The no template control displayed significantly less signal than observed previously. This may have been due to operational procedure, as great care was taken to ensure that samples were heated to 37 °C immediately after the addition of magnesium acetate to the reaction mix and then stored in the fridge straight after the reaction occurred. This minimised the exposure of the samples to room temperature before and after the reaction, thus limiting the capacity of the reaction to occur at sub-optimal conditions which may be a contributing factor to the amplification of primer-dimers. The non-complementary

sample generated some non-specific signal that was comparable to that observed previously, and this confirmed that further optimisation of the blocking step may be required. The manufacturer guidelines suggest that the efficiency of the RPA reaction may be further improved with the inclusion of an agitation step as the reaction proceeds. After 4 minutes, the samples may be removed from incubation at 37 °C and manually mixed by inverting the samples prior to continuation of the amplification at 37 °C. It was hoped that this step would improve the detection of products at low template concentrations. The experiment was repeated with the inclusion of an agitation step to identify if this could improve the sensitivity of the assay. The samples were amplified and assessed visually as performed previously (**Figure 4.25**).

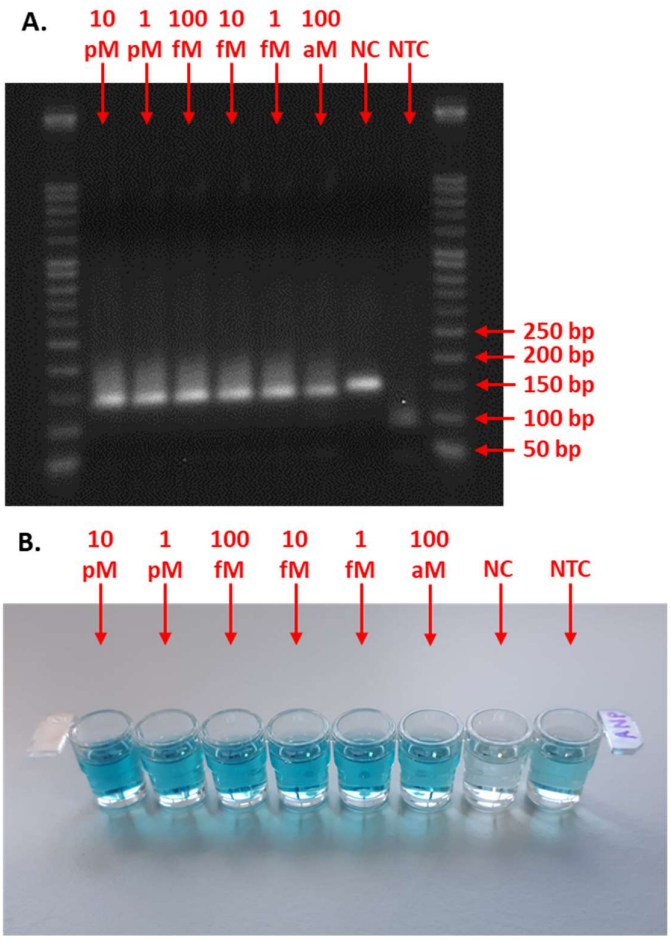

Figure 4.25. *Visual detection of the RPA product amplified with the inclusion of an agitation step.* ***A.*** *Gel electrophoresis image of detection range* ***B.*** *Image of colourimetric change upon addition of TMB substrate.*

With the inclusion of an agitation step, the band intensity obtained from the sample amplified using 100 aM of template DNA appeared to be significantly more intense than that observed without the inclusion of the agitation step. This suggested that the agitation step could be applied to improve the sensitivity of the assay, however it was also noted that the agitation step appeared to induce the amplification of a non-specific product in the no template control. This was evident from the band located at the same position as the 100 bp DNA ladder marker. This product was therefore larger than the primer-dimer products observed in the prior experiments. The non-specific product contained the tail recognition regions and therefore also had the capacity to generate a non-specific Raman signal. Upon addition to the wells

a significant colour change was observed. However, the gradient was less apparent, and the colour change appeared to be uniform for all the positive samples. The non-complementary control did not produce a significant colour change although the no template control generated a false-positive colour change. This was attributed to the non-specific product that was amplified upon inclusion of the agitation step and identified by gel electrophoresis. Resonance Raman analysis was performed to quantify the signal obtained from the sample detection range (**Figure 4.26**).

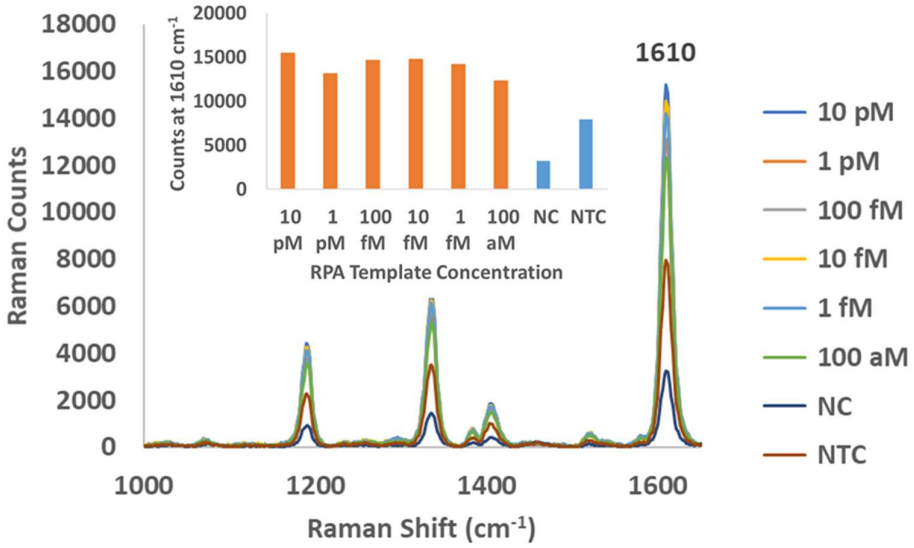

Figure 4.26. *Resonance Raman spectra of oxidised TMB following hybridisation of the HRP conjugate probe to 40 µL of RPA product amplified from a range of initial RPA template concentrations. RPA samples amplified with the inclusion of an agitation step. Spectra accumulated with a 633 nm laser, 20 second acquisition time and 100 % (50 mW) laser power.*

The results indicated that the positive samples generated a near uniform signal. The agitation step had improved the detection sensitivity at the lowest template concentration of 100 aM, however this generated a signal that was generally equivalent for all the template concentrations investigated. This appeared to be due to the amplification process rather than the detection strategy. This was supported by the gel electrophoresis visualisation which showed amplification bands that were highly comparable in intensity. Therefore, it is possible that the agitation step

effectively improved the distribution of the reaction components within the reaction mix following 4 minutes of amplification and maximised the amplification efficiency for the remaining duration of the amplification process. It is possible that a lower detection limit may have been attained with agitation, however this was not investigated as this also instigated the amplification of a non-specific amplification product in the no template control which would reduce the discriminatory value of the assay. The assay detection method successfully discriminated between the positive samples and negative control samples; however, the presence of non-specific amplification products reduced the discriminatory value of the assay.

The no template control samples displayed primer-dimer amplification products without agitation, and a non-specific product that was approximately 100 bp in size when the agitation step was included. The primer-dimer products could be eliminated from the product following purification due to the small size of the non-specific fragments. Therefore, the RPA samples were amplified without agitation and were purified. The experiment was repeated using the purified samples to identify if the discriminatory value could be improved. Gel electrophoresis confirmed that product was still detectable at each concentration investigated following purification as shown in **Figure 4.27**.

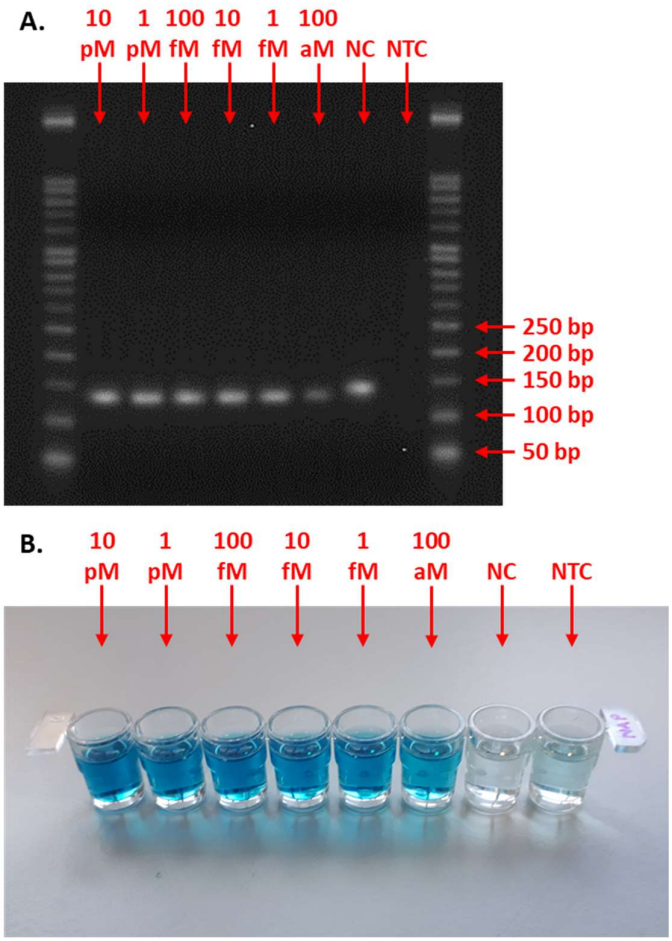

Figure 4.27. *Visual detection of the RPA product following the inclusion of a purification step.* ***A.*** *Gel electrophoresis image of detection range* ***B.*** *Image of colourimetric change upon addition of TMB substrate.*

There were no non-specific products present and the primer-dimers had been eliminated as indicated by the lack of bands below the 50 bp DNA ladder marker. The RPA product was purified using a commercial spin-column kit and eluted in a buffer of unknown composition. The samples were therefore diluted further in 1x PBS to ensure that the product contained an adequate ionic concentration to achieve hybridisation. Following addition to the wells, an intense colour change occurred, and this indicated significant discrimination of the positive samples from the negative control samples. The colour change was more significant than observed previously and this was likely due to the change in buffer conditions. The no template control

displayed some colour change it was possible that the purification process did not remove all the primer-dimers, however these would have to be present at a very low concentration as there was no indication of their presence within the gel image. The non-complementary control remained transparent and there was no indication of non-specific interactions. Resonance Raman analysis was performed to quantify the signal obtained (**Figure 4.28**).

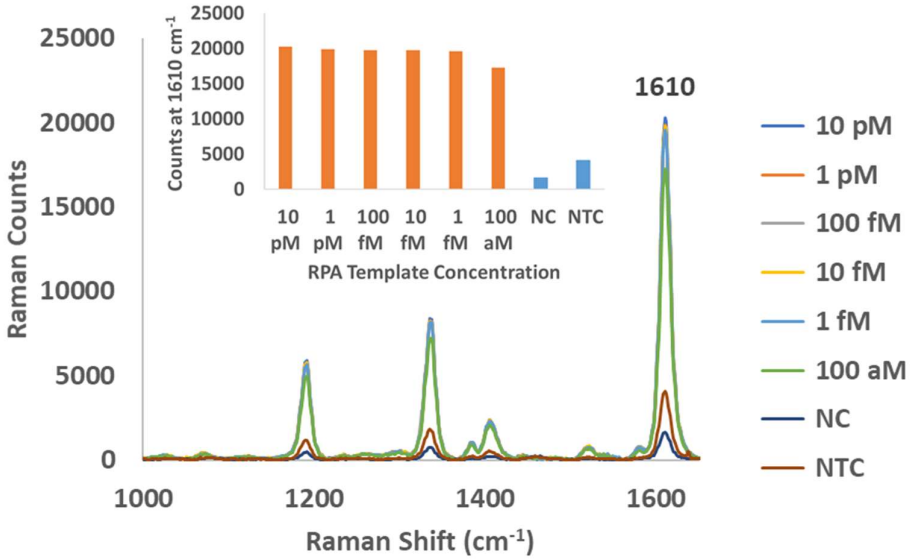

Figure 4.28. *Resonance Raman spectra of oxidised TMB following hybridisation of the HRP conjugate probe to 40 µL of RPA product amplified from a range of initial RPA template concentrations. RPA samples amplified with the inclusion of a purification step. Spectra accumulated with a 633 nm laser, 20 second acquisition time and 100 % (50 mW) laser power.*

The results confirmed significant discrimination of the target sequence. The colour change was more intense than observed previously, and this was reflected by the intense resonance Raman signal obtained. The RPA positive samples displayed ~ 20,000 counts whereas the RPA negative control samples < 5000 counts. The signal was generally equivalent for all the template concentrations investigated which correlated with the observed colour change. The signal obtained at 100 aM of template DNA was slightly lower than the other samples and this was representative of the slightly less intense band observed within the gel image. The highly comparable

signal intensities gained at higher concentrations may have indicated that the colour change had saturated prior to the addition of the stop solution, and therefore it may have been beneficial to stop the reaction sooner to provide a signal that was relative to the template concentration. Alternatively, the amplified products showed generally equivalent band intensities following purification as indicated within the gel image. Therefore, the results may have reflected a largely consistent yield of RPA product following purification. Further investigation of the reaction kinetics would be required to confirm the optimal time point for addition of the stop solution to samples that had been purified and detected using the 1x PBS buffer. The results indicated that significant discrimination of the RPA product was obtained using the resonance Raman assay method.

4.10 Conclusion of the Investigation

With completion of the investigation, it was concluded that the tailed RPA amplification product could be detected using a resonance Raman detection methodology with discriminatory value at the lowest concentration of 100 aM. Other methods were attempted although issues were encountered.

The SERS detection of the RPA product was initially investigated using DNA functionalised and dye-coded AgNPs, although the generation of a target -specific signal was not achieved. The assay format had been previously tried-and-tested using an HRP conjugate with the same capture and reporter probe sequences. The final step of the methodology was adapted by simply exchanging the HRP conjugate for a DNA functionalised and dye-coded AgNP conjugate. Upon addition of the AgNP reporter conjugate over a concentration range, virtually no SERS signal was obtained. At the highest concentration of 500 pM, some signal was evident, however this was demonstrated to be a non-specific signal when compared to the no template control which indicated a comparable signal intensity. The lack of a target-specific signal may be explained due to one of two likely reasons. Firstly, it is possible that the DNA functionalised and dye-coded AgNPs failed to hybridise to the surface due to steric repulsions that prevented the conjugates from interacting with the capture probe

upon the surface. Alternatively, it is likely that there was an insufficient density of the capture probe immobilised upon the surface of the maleimide activated plate to generate a detectable SERS response. To achieve an electromagnetic SERS response, the AgNPs would have to be positioned in close proximity to create a hotspot region that could significantly increase the magnitude of the SERS signal. As only a weak signal was obtained even with the addition of high concentrations of the AgNP conjugate, it was evident that hotspots were not formed. Therefore, it would be suggestible to attempt the same sandwich assay format upon an alternative surface, with the capacity to immobilise and concentrate the capture probe at a higher density than that of the maleimide activated plate. A potential alternative for future investigation may utilise an epoxy modified glass slide. Such surfaces are commonly utilised in combination with DNA probes that contain a terminal modified amino linker group for high density immobilisation and DNA microarray analysis using fluorophore chemistry. It is possible that this alternative surface may provide a detectable SERS signal using DNA functionalised and dye-coded AgNPs, although this would need to be investigated in future work.

The detection of the RPA product was further investigated in solution. The detection principle was based upon the controlled assembly of the AgNPs which may have been detectable by observing a red-shift or decrease in the plasmon peak of the AgNPs upon hybridisation to the tailed regions of the RPA product. It was thought that the interparticle distance would have been significant as each probe would have hybridised to the respective tail regions at each end of the RPA product. Therefore, it was likely that this approach may not have been appropriate to generate a significant electromagnetic SERS response as the interparticle distance may have been too great. However, if a shift in the plasmon peak could have been identified, it would confirm that the biological recognition event had occurred.

Upon attempting this strategy, a significant redshift and peak decrease was observed in the extinction spectrum and this was evident in both the complementary and no template control samples. The shift in the extinction spectrum was therefore

independent of the RPA DNA target sequence. Further investigation confirmed that this could not be resolved by denaturing the proteins within the RPA reaction mix or eliminating the magnesium acetate from the reaction mix. The conjugates were stable within PBS buffer; however, they were particularly unstable in the presence of the RPA product. This was accompanied by a total elimination of the SERS signal despite the RPA product inducing aggregation of the AgNPs. Ordinarily, this would be expected to increase the SERS signal intensity as the the reporter dye would be positioned within the hotspot regions of the aggregated AgNPs. As the signal was totally reduced, this indicated that the reporter dye was no longer present upon the surface. The presence of DTT within the RPA reaction mix was identified as the underlying issue. This was included within the manufacturers reagent composition and could not be readily removed or reproduced without the inclusion of the DTT. Furthermore, the RPA product is only available from one manufacturer (TwistDx) and alternative RPA products were not available. The experiment was attempted with NPs that were synthesised using the citrate reduction method (data not shown) and the same effect was observed. Therefore, the surface chemistry could not be altered to resolve the issue. This may explain the lack of available literature for the detection of RPA products using NPs in solution.

The final detection strategy investigated utilised a reporter probe that was conjugated with HRP as a substitute for the DNA functionalised and dye-coded AgNPs. This was performed upon the surface of a maleimide activated 96-well plate as previously attempted using the AgNP conjugates. The use of the HRP reporter probe was a necessary compromise due to the lack of signal obtained using the DNA functionalised and dye-coded AgNPs upon the surface, and the relative instability observed upon the attempted assembly in solution. If a colorimetric change could be produced, this would confirm the biological recognition event was obtained. Furthermore, this colorimetric change could be detectable and quantifiable using resonance Raman spectroscopy rather than SERS as a suitable alternative.

The resonance Raman detection strategy was demonstrated successfully. The RPA amplification product was readily discriminated from the negative control samples over the full detection range from 10 pM – 100 aM. The amplification of the tailed RPA product was highly efficient with detection confirmed visually at a concentration of just 100 aM in just 20 minutes and the reproducible discrimination of the positive samples from the negative samples. However, the signal obtained was non-linear at the upper limits of the detection range which was observed upon repeating the experiment. This was attributed to the efficiency of the RPA reaction which appeared to be saturated upon addition of higher concentrations of template DNA. This was supported by the intensity of the amplification bands that were analysed visually by gel electrophoresis. At high template concentrations, the band intensities generally appeared equivalent suggesting comparable yields of RPA amplification product. Therefore, this affected the detection range when analysed by resonance Raman spectroscopy following amplification which indicated a non-linear signal increase that was likely reflective of the saturated amplification yield.

The RPA reaction mix has been highly optimised prior to the application by the end-user. Therefore, there are minimal steps that the user can control to alter the amplification efficiency. One such step that is recommended is the mixing of the sample after four minutes of amplification. This improved the sensitivity of the assay; however, the detection range generated a uniform signal over the detection range. This was also apparent when analysing the purified samples. It is possible that an improved detection range could be obtained by reducing the incubation time upon the addition of the TMB substrate. The samples were analysed 30 minutes after the addition of the TMB substrate, in accordance with the guidelines of the substrate manufacturer. Future work may consider analysing the samples at earlier time points to identify if an improvement in the linearity of the detection range may be achieved in relation to the initial template concentration used to amplify the tailed RPA product.

Furthermore, the assay displayed some non-specific signal generated within the negative control samples. This was likely due to either non-specific binding of the HRP reporter conjugate upon the surface, or the presence of primer-dimer formations that contained both tailed regions at each end of the non-specific amplification product. This non-specific amplification product would therefore generate a non-specific signal upon hybridisation to the HRP reporter conjugate. Non-specific binding may be addressed in future work by investigating alternative blocking agents. The plates were blocked with 6-mercaptol-1-hexanol following functionalisation with the capture probe, however alternative blocking agents such as bovine serum albumin or casein may be investigated to identify if the non-specific signal in the negative controls can be reduced further. The formation of primer-dimers is a more significant issue as these were a product of the amplification process and contained both the tailed-regions that provide a means to cross-link the HRP reporter probe upon the surface. Typically, primer-dimers were amplified in the samples containing low concentrations of the template DNA, or within the no template control. This was confirmed by gel electrophoresis which indicated faint bands below the 50 bp DNA ladder marker. It may be possible to reduce these products by shortening the amplification time or increasing the reaction temperature, although these conditions had been preoptimized to ensure the maximum sensitivity. Altering these conditions would likely reduce the sensitivity of the assay. Future work may consider the addition of betaine within the RPA reaction mix, as this has recently been shown to improve both the specificity and sensitivity of the RPA reaction.[148] Betaine is a denaturant that can sharpen the melting transitions of dsDNA and shift the melting transition to a lower temperature with the additional benefit of having a proportionately greater effect on GC rich sequences which are prone to forming secondary structures.[149] The denaturant properties of DNA have thus been demonstrated in improving the amplification efficiency of amplification techniques including both PCR and RPA.[150, 148] It is likely that with the application of betaine, that the non-specific primer-dimers observed may be eliminated, and greater amplification sensitivities may be achievable. If the primer-dimers could be

eliminated, this may also reduce the non-specific signal observed within the no template control. Alternatively, future work may examine the possibility of reducing the primer concentration to potentially reduce the likelihood of primer dimer formation and subsequent amplification. A comparison of both approaches would be required to confirm the most effective approach to eliminating primer-dimer synthesis.

The RPA resonance Raman assay clearly discriminated between the positive and negative samples at the lowest concentration of 100 aM. The amplification of the RPA product with single-stranded tail regions provided a means to readily capture the amplification product and induce a colorimetric change upon hybridisation of the HRP conjugate with subsequent TMB addition. This avoided the necessity for the generation of a single-stranded DNA product for direct hybridisation and requires minimal sample processing steps prior to detection. The application of resonance Raman for the detection and quantification of an enzymatically catalysed colour change has been demonstrated previously within the group based upon the principles of an ELISA assay.[147] This utilised the molecular recognition properties of an antibody-antigen binding interaction. Laing et al., applied a quantitative resonance Raman (ELISA) for the detection of human tumour necrosis factor α, demonstrating that resonance Raman spectroscopy could be applied to achieve 50 times greater detection sensitivities as compared to conventional colorimetric methods.[147] The application of resonance Raman for the detection of an enzymatically catalysed colour change has not yet been demonstrated using a DNA amplification product. This investigation has demonstrated the feasibility of applying a novel and sensitive method for the detection of and RPA amplification product using resonance Raman spectroscopy. Future development may require optimisation of alternative blocking agents and application of betaine or primer concentration reduction to reduce non-specific amplification products, thus allowing for detection of RPA amplification products amplified from exceptionally low template concentrations. This may lead to the application of a resonance Raman method for the detection of isothermal

amplification products with greater sensitivities than that of traditional colorimetric detection.

4.11 Experimental

Nanoparticle Synthesis: AgNPs were synthesised using the same method as detailed within the experimental section of the *Candida krusei* proof-of-principle investigation (section 2.14).

Oligonucleotide Probe Design and Preparation: The oligo probes were designed by the project collaborators and the sequences were maintained for this investigation. The probe sequences used for the SERS plate-based assay and hybridisation assay in solution were modified with 3x hexaethylene glycol (HEG) spacer and a terminal dithiol. The probes were ordered pre-modified from IDT, Iowa, USA. The probe sequences used for the Resonance Raman plate-based assay were modified in accordance with prior research conducted by the project collaborators.[141] The capture probe was modified with a polyT_{15} spacer and the reporter probe was conjugated to HRP without inclusion of a spacer. The capture probe was supplied pre-modified by IDT, Iowa, USA. The HRP conjugated reporter probe was conjugated and supplied by Eurogentec, Liège, Belgium.

Buffer preparation: Buffers were prepared using the same methods as detailed within the experimental section of the *Candida krusei* proof-of-principle investigation (section 2.14). The resonance Raman plate-based assay utilised 1x PBS rather than 0.1 M PBS in accordance with prior research conducted by the project collaborators.[141] PBS tablets were supplied by Sigma-Aldrich, Dorset, UK. The PBS-Tween wash buffer was prepared with the addition of 0.05 % Tween 20.

Conjugate Preparation: The conjugates were prepared using the same method as detailed within the experimental section of the *Candida krusei* proof-of principle investigation (section 2.14) with further optimisation. AgNP concentrations were approximated using the Beer-Lambert law ($A = \varepsilon \times l \times C$) and the extinction coefficient 145 x 108 M^{-1} cm^{-1} for 30 nm AgNPs.[97] The oligo probes were added at an optimised

DNA: AgNP molar ratio of 1000: 1. The MGITC Raman reporter was added at an optimised MGITC: AgNP molar concentration ratio of 1000: 1.

Recombinase Polymerase Amplification: RPA reactions were performed on a Stratagene Mx3005P thermocycler (Agilent, California, USA) using a TwistAmp Basic® kit supplied by TwistDx, Maidenhead, UK. The RPA assay was performed using conditions that were optimised by the project collaborators. Reactions were performed in 50 µL volumes. The lyophilised reaction pellet was dissolved in 29.5 µL of rehydration buffer with gentle pipetting. The forward and reverse primers were then added at a standard concentration of 480 nM each and the reaction volume was increased to 46.5 µL with addition of MQ water. The reaction mix was spiked with 1 µL of *Legionella pneumophila* plasmid DNA. A plasmid (pUCIDT-AMP) containing the *wzm-1* gene within an 852 bp region of the *Legionella pneumophila* serogroup 1 lipopolysaccharide biosynthesis gene cluster (Genbank accession number JA223560.1) was utilised as the template material for RPA amplification. This was supplied by the project collaborator and originally manufactured by IDT (Iowa, USA). Magnesium acetate was added at a standard concentration of 14 mM. 2.5 µL of 280 mM magnesium acetate solution was pipetted into the lid of the RPA reaction tube prior to initiation of the reactions. When all samples were prepared, the samples were mixed vigorously by inverting the tubes 8 times to ensure even distribution of the reagents. The samples were then briefly centrifuged to ensure that none of the reaction mix remained within the lid of the reaction tube. Following mixing of the samples and initiation of the reaction, the samples were immediately placed within the thermocycler and the amplification reaction was left to proceed for 20 minutes at 37 °C. If required, the RPA samples were removed after 4 minutes of amplification and the inverting step was repeated prior to replacing within the thermocycler for the remaining 16 minute amplification time. Following amplification, the samples were immediately stored at 4 °C to terminate the reaction.

Purification of the RPA Product: The RPA product was purified using a Bioline Isolate II PCR purification kit (Bioline Reagents Ltd., London, UK), in accordance with the manufacturer guidelines.

SERS Plate-based Assay: The SERS plate-based assay was performed in Pierce maleimide activated black 96 well plates (Thermo Fisher Scientific, Massachusetts, USA). The capture probe was reduced using tris(2-carboxyethyl) phosphine hydrochloride (TCEP HCl) solution prior to addition to the maleimide activated well. The capture probe was reduced at room temperature for 1 hour using 50 µM of the capture probe and 10 mM of TCEP HCl solution. Following reduction, the capture probe was diluted to 200 nM in 0.1 M PBS. 100 µL of the reduced capture probe was then added to the well and left to incubate at 4 °C overnight. Following incubation, the wells were washed three times with 0.1 M PBS-Tween. The plate was then blocked with 200 µL of 100 µM 6-mercapto-1-hexanol which was added and left for 1 hour. Following blocking, the wells were washed three times with 0.1 M PBS-Tween. 40 µL of the RPA product was then added to the well and left to hybridise at room temperature with shaking for 30 minutes. The plate was then washed three times with 0.1 M PBS-Tween. The AgNP reporter conjugate was diluted in 0.1 M PBS and added at concentrations of 100 pM, 250 pM and 500 pM. The samples were left to hybridise for 30 minutes at room temperature without shaking. The wells were then washed three times with 0.1 M PBS-Tween. 100 µL of 0.1 M PBS was then added to the well prior to SERS analysis. SERS analysis was performed using the same method described within the *Candida krusei* proof-of-principle investigation. Spectral data was averaged, and baseline corrected using the SpectraGryph optical spectroscopy software.[122] Each spectrum was baselined using the adaptive baseline correction settings with the coarseness adjusted to 10 %.

Hybridisation Assay in Solution: Conjugates were hybridised in Eppendorf tubes containing 0.3 M PBS. The final volume for each sample was 500 µL per replicate. The 0.3 M PBS buffer was initially aliquoted, followed by addition of 50 pM of each conjugate and 40 µL of the RPA amplification product. Samples were briefly vortexed prior to hybridisation. The samples were then hybridised for 1 hour at room temperature.

Resonance Raman Plate-based Assay: The resonance Raman plate-based assay was performed using the same method as applied for the SERS plate-based assay, with

further modification. 1x PBS hybridisation buffer and 1x PBS Tween wash buffer was used rather than 0.1 M PBS as this was with prior research conducted by the project collaborators.[141] The capture probe was modified with a polyT_{15} spacer. The reporter probe was conjugated to HRP and 100 µL of the HRP probe was added to the well at a concentration of 10 nM and left to hybridise for 30 minutes at room temperature. The wells were then washed three times with 1x PBS-Tween prior to addition of 100 µL of TMB substrate (Abcam, Cambridge, UK). After 30 minutes, the reaction was stopped with the addition of 100 µL of 650 nm stop solution (Abcam, Cambridge, UK). Resonance Raman analysis was performed using a Renishaw Ramascope and 20x long-working distance objective (Renishaw Plc, Gloucestershire, UK). All data was gathered using a 633 nm laser wavelength and 100 % (50 mW) laser power. The analysis was performed in a black 96 well plate placed upon an adjustable platform. The optimal distancing was calibrated using an absolute ethanol standard prior to sample analysis. 200 µL of each sample was used for analysis. Spectra were gathered in 5x accumulations. All samples were analysed using a 20 second acquisition time. Spectral data was averaged, and baseline corrected using the SpectraGryph optical spectroscopy software.[122] Each spectrum was baselined using the adaptive baseline correction settings with the coarseness adjusted to 10 %.

5 Conclusion

The aim of this research was to progress the application of surface enhanced Raman spectroscopy (SERS) and resonance Raman spectroscopy for the detection of long-chain DNA fragments and amplification products. This was initially defined by the objective to answer two key research questions:

- Is it possible to apply SERS for the detection of long-chain DNA fragments by the controlled assembly of dye-coded and DNA functionalised AgNPs in solution?
- Is it possible to amplify a long-chain DNA fragment that is single-stranded and detectable by SERS based upon the controlled assembly of dye-coded and DNA functionalised AgNPs in solution?

The research succeeded in the primary objective to apply SERS for the detection of a synthetic, long-chain (100 base) DNA fragment by the controlled assembly of dye-coded and DNA functionalised AgNPs in solution. The assembly of the AgNP conjugates upon addition of the long-chain target sequence was not readily observable in the first instance upon analysis by UV-Vis extinction spectroscopy. However, the rate and extent of the AgNP conjugate assembly was significantly improved upon optimisation of the hybridisation conditions. This included addition of polyethylene glycol 10000 (PEG 10000) to the hybridisation buffer and the implementation of the hybridisations at an elevated temperature. These conditions were critical for the efficient assembly of the AgNP conjugates in solution. This confirmed that the long-chain DNA fragment could be detected based upon the principle of direct molecular recognition and assembly, thus negating the requirement for additional sample preparation or separation steps, or addition of non-specific aggregating agents.

Furthermore, the head-to-head probe orientation was identified as optimal for generating the maximum SERS response upon assembly. This was a key finding as the head-to-head probe orientation had not been previously attained or described within prior research regarding the SERS detection of long-chain DNA fragments. The

controlled assembly of dye-coded and DNA-functionalised AgNPs was applied for the SERS detection of 10 nM of a synthetic target DNA. This conclusively demonstrated that this strategy may be applied for the rapid and sensitive SERS detection of a long-chain DNA fragment, as confirmed by the 34: 1 SERS discriminatory enhancement ratio that was observed.

The research succeeded in the secondary objective to amplify a long-chain (383 base) ssDNA fragment, however, the SERS detection of this amplification product proved to be more complex than that of the synthetic target. Initially, a PCR assay was adapted and optimised for the asymmetric amplification of ssDNA. This required careful consideration of the primer properties and amplification conditions to ensure specific amplification. The asymmetric PCR assay was highly successful for the sensitive amplification of a biologically relevant target. A ssDNA target could be generated from a single copy of plasmid template material using the same number of amplification cycles as the standard PCR assay. This conclusively demonstrated that asymmetric PCR may be applied for the one-pot amplification of ssDNA with the same sensitivity and within the same timeframe as a standard PCR assay. This approach thereby eliminates the necessity for more complex methods of generating ssDNA such as alkali denaturation or enzymatic digestion.

The single-stranded asymmetric PCR amplification product was detectable by SERS based upon the controlled assembly of dye-coded and DNA-functionalised AgNPs in solution, however, this was not readily achievable without the addition of a heat-and-cool step. It was possible that this was due to the formation of secondary structures or target overhangs associated with length of the asymmetric PCR product which was significantly longer than that of the synthetic target. Furthermore, challenges associated with calculating the concentration of the asymmetric PCR product were identified. Further optimisation for the SERS detection of an asymmetric PCR product may be applied in future. Future work should consider the amplification of a shorter asymmetric PCR product to minimise the likelihood of secondary structure formation, and greater scrutiny of the potential for the target to form secondary structures based upon sequence complexity criteria such as the % GC content and distribution.

Such considerations may be applied prior to optimisation of the asymmetric PCR assay to increase the likelihood of detecting an asymmetric PCR product without the requirement for a heat-and-cool step. Furthermore, future work may apply a fluorescent molecular beacon and calibration curve for the quantitation of the single-stranded amplification product. Despite the challenges associated with the SERS detection of the asymmetric PCR product, a SERS discriminatory enhancement ratio of 5: 1 was conclusively achieved upon addition of an amplification product amplified from 10^4 copy numbers.

The newly found ability to detect long-chain DNA fragments and asymmetric PCR products by the controlled assembly of dye-coded and DNA-functionalised AgNPs in solution has significant implications for the SERS detection of DNA. Prior to this achievement, the SERS detection of long-chain DNA fragments or amplification products was generally limited to more complex methods that required sample separation steps and addition of non-specific aggregating agents for SERS detection. Renishaw Diagnostics Limited (RDL) were the commercial sponsor of the project and previously utilised a semiautomated method that required sample separation using streptavidin magnetic beads and addition of a non-specific aggregating agent for the multiplex detection of fungal pathogens.[82] However, this method was both costly, time-consuming and required the transfer of the samples during the preanalytical steps which increased the likelihood of sample contamination. Therefore, the findings described here confirmed that a simpler, faster, and more cost-effective method can be applied for the SERS detection of DNA by the controlled assembly of dye-coded and DNA-functionalised AgNPs in solution. Such a method can be further developed into a closed-tube, fully automated diagnostic system without requirement for preanalytical sample separation or preparation steps. This will likely have significant implications for the commercial development and simplification of the RDL diagnostic technology.

Furthermore, the use of SERS has significant potential for the multiplex detection of DNA. The research described here has confirmed the potential of a simplified detection strategy, and in future this may approach may be extended for the

multiplex detection of DNA. This could be achieved with the application of probe sequences specific to different target sequences, and multiple Raman reporters that correspond to the different target sequences. If the multiplex SERS detection of DNA based upon the controlled assembly of dye-coded and DNA-functionalised AgNPs can be demonstrated, this would have the potential to provide a method with a greater multiplexing capacity than traditional fluorophore chemistry. Such a method would be of great benefit for the detection of DNA in clinical, agricultural and forensic laboratories. This research represents an initial step in the direction of obtaining this long-term aim.

In addition to the ongoing development of novel SERS DNA detection methods, the field of molecular diagnostics continues to progress with the development of novel isothermal amplification techniques such as the recombinase polymerase amplification (RPA) technique. Whilst the polymerase chain reaction (PCR) has been widely accepted as a benchmark standard molecular diagnostic technique, it is likely that this will be replaced in future by an isothermal technique such as RPA. Isothermal techniques have the potential to eliminate the requirement for expensive equipment such as a thermocycler and enable the application of molecular diagnostics at the point-of-care. RPA has been applied here and shown to be both rapid and sensitive for the amplification of DNA. Due to the enzymatic mechanism of the RPA amplification reaction, it was not readily achievable to amplify a single-stranded amplification product in a manner that was analogous to the asymmetric PCR strategy that was applied previously. However, an alternative strategy was identified with the amplification of an RPA product using tailed primers. This provided a target with directly detectable single-stranded regions at each end of the target. The RPA reaction could amplify the tailed target sequence to the lowest visually observable concentration of 100 aM within 20 minutes.

In the first instance, the RPA amplification product was not readily detectable upon the surface of a maleimide activated 96-well plate using dye-coded and DNA-functionalised AgNPs. This was likely due to an insufficient density of the reporter conjugate hybridising to the surface. Therefore, further investigation will be required

for the detection of the RPA product using AgNP conjugates upon alternative surfaces, such as a glass slide spotted with a high density of the immobilised capture probe. If such a method could be demonstrated, the multiplex detection may be achieved upon the surface using differing primer tail sequences and capture probes immobilised in an array format upon the glass slide surface. With application of different probe sequences and multiple Raman reporters that correspond to the different primer tails, a multiplex SERS bio-barcode assay may be developed for the detection of RPA products. Furthermore, paper-based devices such as lateral flow devices may provide a suitable capture surface for the SERS detection of the RPA product using DNA functionalised and dye-coded NPs. The project collaborators have previously demonstrated the potential to detect tailed RPA products visually using DNA functionalised AuNPs and lateral flow devices.[141] However, this has not been demonstrated using DNA functionalised and dye-coded NPs with a SERS detection method. It is likely that this method could provide greater sensitivity and capacity for quantification than visual detection. A significant advantage of lateral flow diagnostic devices is the affordability and applicability at the point-of-care due to their small size and simplicity. Handheld Raman spectrometers are commercially available and therefore, the portability of lateral flow devices and hand-held Raman spectrometers would present an appropriate compatibility for the sensitive and quantitative detection or diagnosis at the point-of-care in resource limited settings.

An alternative detection strategy was demonstrated initially within the described research and resonance Raman spectroscopy was applied for the detection of a colorimetric change upon addition of a TMB substrate to an HRP conjugated reporter probe. This was analogous to the signal transduction mechanism of an enzyme-linked immunosorbent assay (ELISA), which is commonly performed as a benchmark standard diagnostic technique for the detection of protein biomarkers. The results indicated that this signal transduction strategy may also be applied for the detection of nucleic acid biomarkers using the RPA technique and tailed primers. Resonance Raman spectroscopy was successfully applied for the detection of the tailed amplification product with discriminatory value at the lowest concentration of 100

aM. Therefore, this method offers the potential to apply both immunoassays and nucleic acid molecular assays in parallel and apply quantitative analysis with the application of resonance Raman spectroscopy. This could prove to be advantageous in centralised diagnostic laboratories which generally utilise different detection methods for immunoassays and nucleic acid molecular assays. The application of resonance Raman spectroscopy to quantitatively analyse both enzyme-linked immunoassays and nucleic acid assays could present an opportunity to standardise the detection equipment by using a Raman spectrometer for analysis of both types of assay.

The research described here has demonstrated the potential to progress the application of SERS and resonance Raman spectroscopy for the detection of long-chain DNA fragments and amplification products. The results have shown that it is possible to detect long-chain DNA fragments using SERS and that by association, it should be possible to detect ssDNA amplification products with the same level of sensitivity and discrimination. Further challenges were identified upon the progression from synthetic target sequences to biologically relevant PCR amplification products. However, upon identification of these challenges, further optimisation may be applied to fully realise the potential of integrating SERS with nucleic acid amplification techniques. Moreover, different nucleic acid amplification techniques may require the development of novel detection strategies. Resonance Raman spectroscopy has been shown to be versatile alternative to SERS for detection of an RPA amplification product with the potential for quantitative analysis. The application of this detection method further validated the viability of utilising tailed primers, and in future these may be applied to alternative surface-based detection strategies such as glass slide arrays or paper-based devices in combination with a SERS detection method. It is hoped that the findings of the described research will encourage further development of novel strategies for the detection of DNA amplification products using Raman spectroscopy.

6 References

(1) Watson, J. D.; Crick, F. H. C. Molecular Structure of Nucleic Acids: A Structure for Deoxyribose Nucleic Acid. *Nature* **1953**, *171* (4356), 737–738.

(2) Dahm, R. Friedrich Miescher and the Discovery of DNA. *Dev. Biol.* **2005**, *278* (2), 274–288.

(3) Hargittai, I. The Tetranucleotide Hypothesis: A Centennial. *Struct. Chem.* **2009**, *20* (5), 753–756.

(4) Chargaff, E. Chemical Specificity of Nucleic Acids and Mechanism of Their Enzymatic Degradation. *Experientia* **1950**, *6* (6), 201–209.

(5) Franklin, R. E.; Gosling, R. G. Molecular Configuration in Sodium Thymonucleate. *Nature* **1953**, *171* (4356), 740–741.

(6) Pray, L. Discovery of DNA Structure and Function: Watson and Crick https://www.nature.com/scitable/topicpage/discovery-of-dna-structure-and-function-watson-397 (accessed May 14, 2019).

(7) Yakovchuk, P. Base-Stacking and Base-Pairing Contributions into Thermal Stability of the DNA Double Helix. *Nucleic Acids Res.* **2006**, *34* (2), 564–574.

(8) Fdardel. Hyperchromicity. https://commons.wikimedia.org/wiki/File:Hyperchromicity.svg (accessed Jul 8, 2019).

(9) Tan, Z.-J.; Chen, S.-J. Nucleic Acid Helix Stability: Effects of Salt Concentration, Cation Valence and Size, and Chain Length. *Biophys. J.* **2006**, *90* (4), 1175–1190.

(10) Owczarzy, R.; Moreira, B. G.; You, Y.; Behlke, M. A.; Walder, J. A. Predicting Stability of DNA Duplexes in Solutions Containing Magnesium and Monovalent Cations. *Biochemistry* **2008**, *47* (19), 5336–5353.

(11) Lipfert, J.; Doniach, S.; Das, R.; Herschlag, D. Understanding Nucleic Acid–Ion

Interactions. *Annu. Rev. Biochem.* **2014**, *83* (1), 813–841.

(12) Mullis, K. B. The Unusual Origin of the Polymerase Chain Reaction. *Sci. Am.* **1990**, *262* (4), 56–61, 64–65.

(13) Kornberg, A.; Lehman, I. R.; Bessman, M. J.; Simms, E. S. Enzymic Synthesis of Deoxyribonucleic Acid. *Biochim. Biophys. Acta* **1956**, *21* (1), 197–198.

(14) Lehman, I. R.; Bessman, M. J.; Simms, E. S.; Kornberg, A. Enzymatic Synthesis of Deoxyribonucleic Acid. I. Preparation of Substrates and Partial Purification of an Enzyme from Escherichia Coli. *J. Biol. Chem.* **1958**, *233* (1), 163–170.

(15) Bessman, M. J.; Lehman, I. R.; Simms, E. S.; Kornberg, A. Enzymatic Synthesis of Deoxyribonucleic Acid. II. General Properties of the Reaction. *J. Biol. Chem.* **1958**, *233* (1), 171–177.

(16) Saiki, R. K.; Scharf, S.; Faloona, F.; Mullis, K. B.; Horn, G. T.; Erlich, H. A.; Arnheim, N. Enzymatic Amplification of Beta-Globin Genomic Sequences and Restriction Site Analysis for Diagnosis of Sickle Cell Anemia. *Science* **1985**, *230* (4732), 1350–1354.

(17) Chien, A.; Edgar, D. B.; Trela, J. M. Deoxyribonucleic Acid Polymerase from the Extreme Thermophile Thermus Aquaticus. *J. Bacteriol.* **1976**, *127* (3), 1550–1557.

(18) Enzoklop. Polymerase Chain Reaction. https://commons.wikimedia.org/wiki/File:Polymerase_chain_reaction.svg (accessed May 18, 2019).

(19) Compton, J. Nucleic Acid Sequence-Based Amplification. *Nature* **1991**, *350* (6313), 91–92.

(20) Jonas, V.; Alden, M. J.; Curry, J. I.; Kamisango, K.; Knott, C. A.; Lankford, R.; Wolfe, J. M.; Moore, D. F. Detection and Identification of Mycobacterium Tuberculosis Directly from Sputum Sediments by Amplification of RRNA. *J. Clin. Microbiol.* **1993**, *31* (9), 2410–2416.

(21) Dean, F. B.; Hosono, S.; Fang, L.; Wu, X.; Faruqi, A. F.; Bray-Ward, P.; Sun, Z.; Zong, Q.; Du, Y.; Du, J.; et al. Comprehensive Human Genome Amplification Using Multiple Displacement Amplification. *Proc. Natl. Acad. Sci.* **2002**, *99* (8), 5261–5266.

(22) Notomi, T.; Okayama, H.; Masubuchi, H.; Yonekawa, T.; Watanabe, K.; Amino, N.; Hase, T. Loop-Mediated Isothermal Amplification of DNA. *Nucleic Acids Res.* **2000**, *28* (12), E63.

(23) Vincent, M.; Xu, Y.; Kong, H. Helicase-Dependent Isothermal DNA Amplification. *EMBO Rep.* **2004**, *5* (8), 795–800.

(24) Fire, A.; Xu, S. Q. Rolling Replication of Short DNA Circles. *Proc. Natl. Acad. Sci.* **1995**, *92* (10), 4641–4645.

(25) Wharam, S. D.; Marsh, P.; Lloyd, J. S.; Ray, T. D.; Mock, G. A.; Assenberg, R.; McPhee, J. E.; Brown, P.; Weston, A.; Cardy, D. L. Specific Detection of DNA and RNA Targets Using a Novel Isothermal Nucleic Acid Amplification Assay Based on the Formation of a Three-Way Junction Structure. *Nucleic Acids Res.* **2001**, *29* (11), E54-4.

(26) Piepenburg, O.; Williams, C. H.; Stemple, D. L.; Armes, N. a. DNA Detection Using Recombination Proteins. *PLoS Biol.* **2006**, *4* (7), e204.

(27) Guatelli, J. C.; Whitfield, K. M.; Kwoh, D. Y.; Barringer, K. J.; Richman, D. D.; Gingeras, T. R. Isothermal, in Vitro Amplification of Nucleic Acids by a Multienzyme Reaction Modeled after Retroviral Replication. *Proc. Natl. Acad. Sci.* **1990**, *87* (5), 1874–1878.

(28) Yong Zhang, D.; Brandwein, M.; Chun Hung Hsuih, T.; Li, H. Amplification of Target-Specific, Ligation-Dependent Circular Probe. *Gene* **1998**, *211* (2), 277–285.

(29) Walker, G. T.; Little, M. C.; Nadeau, J. G.; Shank, D. D. Isothermal in Vitro Amplification of DNA by a Restriction Enzyme/DNA Polymerase System. *Proc.*

Natl. Acad. Sci. U. S. A. **1992**, *89* (1), 392–396.

(30) James, A.; Macdonald, J. Recombinase Polymerase Amplification: Emergence as a Critical Molecular Technology for Rapid, Low-Resource Diagnostics. *Expert Rev. Mol. Diagn.* **2015**, *15* (11), 1475–1489.

(31) Zhao, Y.; Chen, F.; Li, Q.; Wang, L.; Fan, C. Isothermal Amplification of Nucleic Acids. *Chem. Rev.* **2015**, *115* (22), 12491–12545.

(32) Li, J.; Macdonald, J.; von Stetten, F. Review: A Comprehensive Summary of a Decade Development of the Recombinase Polymerase Amplification. *Analyst* **2019**, *144* (1), 31–67.

(33) Creighton, J. A.; Eadon, D. G. Ultraviolet–Visible Absorption Spectra of the Colloidal Metallic Elements. *J. Chem. Soc., Faraday Trans.* **1991**, *87* (24), 3881–3891.

(34) British Museum - Image Gallery: The Lycurgus Cup https://www.britishmuseum.org/join_in/using_digital_images/using_digital_images.aspx?asset_id=36154001&objectId=61219&partId=1 (accessed Jun 6, 2019).

(35) Faraday, M. X. The Bakerian Lecture. —Experimental Relations of Gold (and Other Metals) to Light. *Philos. Trans. R. Soc. London* **1857**, *147*, 145–181.

(36) Turkevich, J.; Stevenson, P. C.; Hillier, J. A Study of the Nucleation and Growth Processes in the Synthesis of Colloidal Gold. *Discuss. Faraday Soc.* **1951**, *11* (c), 55.

(37) Frens, G. Controlled Nucleation for the Regulation of the Particle Size in Monodisperse Gold Suspensions. *Nat. Phys. Sci.* **1973**, *241* (105), 20–22.

(38) Lee, P. C.; Meisel, D. Adsorption and Surface-Enhanced Raman of Dyes on Silver and Gold Sols. *J. Phys. Chem.* **1982**, *86* (17), 3391–3395.

(39) Pillai, Z. S.; Kamat, P. V. What Factors Control the Size and Shape of Silver Nanoparticles in the Citrate Ion Reduction Method? *J. Phys. Chem. B* **2004**,

108 (3), 945–951.

(40) Van Hyning, D. L.; Zukoski, C. F. Formation Mechanisms and Aggregation Behavior of Borohydride Reduced Silver Particles. *Langmuir* **1998**, *14* (24), 7034–7046.

(41) Heard, S. M.; Grieser, F.; Barraclough, C. G.; Sanders, J. V. The Characterization of Ag Sols by Electron Microscopy, Optical Absorption, and Electrophoresis. *J. Colloid Interface Sci.* **1983**, *93* (2), 545–555.

(42) Leopold, N.; Lendl, B. A New Method for Fast Preparation of Highly Surface-Enhanced Raman Scattering (SERS) Active Silver Colloids at Room Temperature by Reduction of Silver Nitrate with Hydroxylamine Hydrochloride. *J. Phys. Chem. B* **2003**, *107* (24), 5723–5727.

(43) Tem5psu. Nanoparticle LSPR. https://commons.wikimedia.org/wiki/File:Nanoparticle_lspr_2.png (accessed Jun 13, 2019).

(44) Mie, G. Beiträge Zur Optik Trüber Medien, Speziell Kolloidaler Metallösungen. *Ann. Phys.* **1908**, *330* (3), 377–445.

(45) Guo, L.; Jackman, J. A.; Yang, H.-H.; Chen, P.; Cho, N.-J.; Kim, D.-H. Strategies for Enhancing the Sensitivity of Plasmonic Nanosensors. *Nano Today* **2015**, *10* (2), 213–239.

(46) Smekal, A. Zur Quantentheorie Der Dispersion. *Naturwissenschaften* **1923**, *11* (43), 873–875.

(47) Raman, C. V.; Krishnan, K. S. A New Type of Secondary Radiation. *Nature* **1928**, *121* (3048), 501–502.

(48) Smith, E.; Dent, G. *Modern Raman Spectroscopy - A Practical Approach*; John Wiley & Sons, Ltd: Chichester, UK, 2004.

(49) Diem, M. *Modern Vibrational Spectroscopy and Micro-Spectroscopy*; John Wiley & Sons, Ltd: Chichester, UK, 2015.

(50) Fleischmann, M.; Hendra, P. J.; McQuillan, A. J. Raman Spectra of Pyridine Adsorbed at a Silver Electrode. *Chem. Phys. Lett.* **1974**, *26* (2), 163–166.

(51) Jeanmaire, D. L.; Van Duyne, R. P. Surface Raman Spectroelectrochemistry. *J. Electroanal. Chem. Interfacial Electrochem.* **1977**, *84* (1), 1–20.

(52) Albrecht, M. G.; Creighton, J. A. Anomalously Intense Raman Spectra of Pyridine at a Silver Electrode. *J. Am. Chem. Soc.* **1977**, *99* (15), 5215–5217.

(53) Mirkin, C. A.; Letsinger, R. L.; Mucic, R. C.; Storhoff, J. J. A DNA-Based Method for Rationally Assembling Nanoparticles into Macroscopic Materials. *Nature* **1996**, *382* (6592), 607–609.

(54) Thaxton, C. S.; Georganopoulou, D. G.; Mirkin, C. A. Gold Nanoparticle Probes for the Detection of Nucleic Acid Targets. *Clin. Chim. Acta* **2006**, *363* (1–2), 120–126.

(55) Alivisatos, A. P. Organization of "nanocrystal Groups" Using DNA. *Nature* **1996**, *382* (August), 609–611.

(56) Jin, R.; Wu, G.; Li, Z.; Mirkin, C. A.; Schatz, G. C. What Controls the Melting Properties of DNA-Linked Gold Nanoparticle Assemblies? *J. Am. Chem. Soc.* **2003**, *125* (6), 1643–1654.

(57) Elghanian, R.; Storhoff, J. J.; Mucic, R. C.; Letsinger, R. L.; Mirkin, C. A. Selective Colorimetric Detection of Polynucleotides Based on the Distance-Dependent Optical Properties of Gold Nanoparticles. *Science (80-.).* **1997**, *277* (5329), 1078–1081.

(58) Storhoff, J. J.; Elghanian, R.; Mucic, R. C.; Mirkin, C. A.; Letsinger, R. L. One-Pot Colorimetric Differentiation of Polynucleotides with Single Base Imperfections Using Gold Nanoparticle Probes. *J. Am. Chem. Soc.* **1998**, *120* (9), 1959–1964.

(59) Taton, T. A. Scanometric DNA Array Detection with Nanoparticle Probes. *Science (80-.).* **2000**, *289* (5485), 1757–1760.

(60) Nam, J.-M.; Stoeva, S. I.; Mirkin, C. A. Bio-Bar-Code-Based DNA Detection with PCR-like Sensitivity. *J. Am. Chem. Soc.* **2004**, *126* (19), 5932–5933.

(61) Taton, T. A.; Mucic, R. C.; Mirkin, C. A.; Letsinger, R. L. The DNA-Mediated Formation of Supramolecular Mono- and Multilayered Nanoparticle Structures. *J. Am. Chem. Soc.* **2000**, *122* (26), 6305–6306.

(62) Stoeva, S. I.; Lee, J.-S.; Thaxton, C. S.; Mirkin, C. A. Multiplexed DNA Detection with Biobarcoded Nanoparticle Probes. *Angew. Chemie Int. Ed.* **2006**, *45* (20), 3303–3306.

(63) Storhoff, J. J.; Lucas, A. D.; Garimella, V.; Bao, Y. P.; Müller, U. R. Homogeneous Detection of Unamplified Genomic DNA Sequences Based on Colorimetric Scatter of Gold Nanoparticle Probes. *Nat. Biotechnol.* **2004**, *22* (7), 883–887.

(64) Hill, H. D.; Vega, R. A.; Mirkin, C. A. Nonenzymatic Detection of Bacterial Genomic DNA Using the Bio Bar Code Assay. *Anal. Chem.* **2007**, *79* (23), 9218–9223.

(65) Bao, Y. P. SNP Identification in Unamplified Human Genomic DNA with Gold Nanoparticle Probes. *Nucleic Acids Res.* **2005**, *33* (2), e15–e15.

(66) Alhasan, A. H.; Scott, A. W.; Wu, J. J.; Feng, G.; Meeks, J. J.; Thaxton, C. S.; Mirkin, C. A. Circulating MicroRNA Signature for the Diagnosis of Very High-Risk Prostate Cancer. *Proc. Natl. Acad. Sci.* **2016**, *113* (38), 10655–10660.

(67) Cao; Jin, R.; Mirkin, C. A. DNA-Modified Core−Shell Ag/Au Nanoparticles. *J. Am. Chem. Soc.* **2001**, *123* (32), 7961–7962.

(68) Lee, J.-S.; Lytton-Jean, A. K. R.; Hurst, S. J.; Mirkin, C. A. Silver Nanoparticle−Oligonucleotide Conjugates Based on DNA with Triple Cyclic Disulfide Moieties. *Nano Lett.* **2007**, *7* (7), 2112–2115.

(69) Thompson, D. G.; Enright, A.; Faulds, K.; Smith, W. E.; Graham, D. Ultrasensitive DNA Detection Using Oligonucleotide−Silver Nanoparticle

Conjugates. *Anal. Chem.* **2008**, *80* (8), 2805–2810.

(70) Laing, S.; Gracie, K.; Faulds, K. Multiplex in Vitro Detection Using SERS. *Chem. Soc. Rev.* **2016**, *45* (7), 1901–1918.

(71) Wei, L.; Chen, Z.; Shi, L.; Long, R.; Anzalone, A. V.; Zhang, L.; Hu, F.; Yuste, R.; Cornish, V. W.; Min, W. Super-Multiplex Vibrational Imaging. *Nature* **2017**, *544* (7651), 465–470.

(72) Cao, Y. C.; Jin, R.; Mirkin, C. A. Nanoparticles with Raman Spectroscopic Fingerprints for DNA and RNA Detection. *Science* **2002**, *297* (5586), 1536–1540.

(73) Braun, G.; Lee, S. J.; Dante, M.; Nguyen, T.-Q.; Moskovits, M.; Reich, N. Surface-Enhanced Raman Spectroscopy for DNA Detection by Nanoparticle Assembly onto Smooth Metal Films. *J. Am. Chem. Soc.* **2007**, *129* (20), 6378–6379.

(74) Graham, D.; Thompson, D. G.; Smith, W. E.; Faulds, K. Control of Enhanced Raman Scattering Using a DNA-Based Assembly Process of Dye-Coded Nanoparticles. *Nat. Nanotechnol.* **2008**, *3* (9), 548–551.

(75) Graham, D.; Stevenson, R.; Thompson, D. G.; Barrett, L.; Dalton, C.; Faulds, K. Combining Functionalised Nanoparticles and SERS for the Detection of DNA Relating to Disease. *Faraday Discuss.* **2011**, *149*, 291–299.

(76) Thompson, D. G.; Faulds, K.; Smith, W. E.; Graham, D. Precise Control of the Assembly of Dye-Coded Oligonucleotide Silver Nanoparticle Conjugates with Single Base Mismatch Discrimination Using Surface Enhanced Resonance Raman Scattering. *J. Phys. Chem. C* **2010**, *114* (16), 7384–7389.

(77) Guerrini, L.; McKenzie, F.; Wark, A. W.; Faulds, K.; Graham, D. Tuning the Interparticle Distance in Nanoparticle Assemblies in Suspension via DNA-Triplex Formation: Correlation between Plasmonic and Surface-Enhanced Raman Scattering Responses. *Chem. Sci.* **2012**, *3* (7), 2262.

(78) Qian, X.; Zhou, X.; Nie, S. Surface-Enhanced Raman Nanoparticle Beacons Based on Bioconjugated Gold Nanocrystals and Long Range Plasmonic Coupling. *J. Am. Chem. Soc.* **2008**, *130* (45), 14934–14935.

(79) Zhang, Z.; Wen, Y.; Ma, Y.; Luo, J.; Jiang, L.; Song, Y. Mixed DNA-Functionalized Nanoparticle Probes for Surface-Enhanced Raman Scattering-Based Multiplex DNA Detection. *Chem. Commun.* **2011**, *47* (26), 7407.

(80) Donnelly, T.; Faulds, K.; Graham, D. Investigation of Silver Nanoparticle Assembly Following Hybridization with Different Lengths of DNA. *Part. Part. Syst. Charact.* **2016**, *33* (7), 404–411.

(81) Mabbott, S.; Thompson, D.; Sirimuthu, N.; McNay, G.; Faulds, K.; Graham, D. From Synthetic DNA to PCR Product: Detection of Fungal Infections Using SERS. *Faraday Discuss.* **2016**, *187*, 461–472.

(82) White, P. L.; Hibbitts, S. J.; Perry, M. D.; Green, J.; Stirling, E.; Woodford, L.; McNay, G.; Stevenson, R.; Barnes, R. A. Evaluation of a Commercially Developed Semiautomated PCR-Surface-Enhanced Raman Scattering Assay for Diagnosis of Invasive Fungal Disease. *J. Clin. Microbiol.* **2014**, *52* (10), 3536–3543.

(83) Enoch, D. A. Invasive Fungal Infections: A Review of Epidemiology and Management Options. *J. Med. Microbiol.* **2006**, *55* (7), 809–818.

(84) Brown, G. D.; Denning, D. W.; Gow, N. A. R.; Levitz, S. M.; Netea, M. G.; White, T. C. Hidden Killers: Human Fungal Infections. *Sci. Transl. Med.* **2012**, *4* (165), 165rv13-165rv13.

(85) Bassetti, M.; Mikulska, M.; Viscoli, C. Bench-to-Bedside Review: Therapeutic Management of Invasive Candidiasis in the Intensive Care Unit. *Crit. Care* **2010**, *14* (6), 244.

(86) Halliday, C. L.; Kidd, S. E.; Sorrell, T. C.; Chen, S. C. A. Molecular Diagnostic Methods for Invasive Fungal Disease: The Horizon Draws Nearer? *Pathology*

2015, *47* (3), 257–269.

(87) Wagner, K.; Springer, B.; Pires, V. P.; Keller, P. M. Molecular Detection of Fungal Pathogens in Clinical Specimens by 18S RDNA High-Throughput Screening in Comparison to ITS PCR and Culture. *Sci. Rep.* **2018**, *8* (1), 6964.

(88) Graham, D.; Mallinder, B. J.; Whitcombe, D.; Watson, N. D.; Smith, W. E. Simple Multiplex Genotyping by Surface-Enhanced Resonance Raman Scattering. *Anal. Chem.* **2002**, *74* (5), 1069–1074.

(89) Li, X.; Yang, T.; Li, C. S.; Wang, D.; Song, Y.; Jin, L. Detection of EGFR Mutation in Plasma Using Multiplex Allele-Specific PCR (MAS-PCR) and Surface Enhanced Raman Spectroscopy. *Sci. Rep.* **2017**, *7* (1), 4771.

(90) Li, X.; Yang, T.; Li, C. S.; Song, Y.; Lou, H.; Guan, D.; Jin, L. Surface Enhanced Raman Spectroscopy (SERS) for the Multiplex Detection of Braf, Kras, and Pik3ca Mutations in Plasma of Colorectal Cancer Patients. *Theranostics* **2018**, *8* (6), 1678–1689.

(91) Li, X.; Yang, T.; Li, C. S.; Jin, L.; Lou, H.; Song, Y. Prenatal Detection of Thalassemia by Cell-Free Fetal DNA (CffDNA) in Maternal Plasma Using Surface Enhanced Raman Spectroscopy Combined with PCR. *Biomed. Opt. Express* **2018**, *9* (7), 3167.

(92) Wee, E. J. H.; Wang, Y.; Tsao, S. C.-H.; Trau, M. Simple, Sensitive and Accurate Multiplex Detection of Clinically Important Melanoma DNA Mutations in Circulating Tumour DNA with SERS Nanotags. *Theranostics* **2016**, *6* (10), 1506–1513.

(93) Stokes, R. J.; Macaskill, A.; Lundahl, P. J.; Smith, W. E.; Faulds, K.; Graham, D. Quantitative Enhanced Raman Scattering of Labeled DNA from Gold and Silver Nanoparticles. *Small* **2007**, *3* (9), 1593–1601.

(94) Creighton, J. A.; Blatchford, C. G.; Albrecht, M. G. Plasma Resonance Enhancement of Raman Scattering by Pyridine Adsorbed on Silver or Gold Sol

Particles of Size Comparable to the Excitation Wavelength. *J. Chem. Soc. Faraday Trans. 2* **1979**, *75*, 790.

(95) Bhattacharjee, S. DLS and Zeta Potential – What They Are and What They Are Not? *J. Control. Release* **2016**, *235*, 337–351.

(96) Clogston, J. D.; Patri, A. K. Zeta Potential Measurement. In *Scientia Pharmaceutica*; 2011; Vol. 79, pp 63–70.

(97) Paramelle, D.; Sadovoy, A.; Gorelik, S.; Free, P.; Hobley, J.; Fernig, D. G. A Rapid Method to Estimate the Concentration of Citrate Capped Silver Nanoparticles from UV-Visible Light Spectra. *Analyst* **2014**, *139* (19), 4855.

(98) White, T. J.; Bruns, T.; Lee, S.; Taylor, J. AMPLIFICATION AND DIRECT SEQUENCING OF FUNGAL RIBOSOMAL RNA GENES FOR PHYLOGENETICS. In *PCR Protocols*; Elsevier, 1990; pp 315–322.

(99) Einsele, H.; Hebart, H.; Roller, G.; Löffler, J.; Rothenhofer, I.; Müller, C. A.; Bowden, R. A.; van Burik, J.; Engelhard, D.; Kanz, L.; et al. Detection and Identification of Fungal Pathogens in Blood by Using Molecular Probes. *J. Clin. Microbiol.* **1997**, *35* (6), 1353–1360.

(100) Klingspor, L.; Jalal, S. Molecular Detection and Identification of Candida and Aspergillus Spp. from Clinical Samples Using Real-Time PCR. *Clin. Microbiol. Infect.* **2006**, *12* (8), 745–753.

(101) Altschul, S. F.; Gish, W.; Miller, W.; Myers, E. W.; Lipman, D. J. Basic Local Alignment Search Tool. *J. Mol. Biol.* **1990**, *215* (3), 403–410.

(102) Owczarzy, R.; Tataurov, A. V.; Wu, Y.; Manthey, J. A.; McQuisten, K. A.; Almabrazi, H. G.; Pedersen, K. F.; Lin, Y.; Garretson, J.; McEntaggart, N. O.; et al. IDT SciTools: A Suite for Analysis and Design of Nucleic Acid Oligomers. *Nucleic Acids Res.* **2008**, *36* (Web Server), W163–W169.

(103) Prediger, E. Designing PCR primers and probes https://eu.idtdna.com/pages/education/decoded/article/designing-pcr-

primers-and-probes (accessed Apr 6, 2019).

(104) Demers, L. M.; Mirkin, C. A.; Mucic, R. C.; Reynolds, R. A.; Letsinger, R. L.; Elghanian, R.; Viswanadham, G. A Fluorescence-Based Method for Determining the Surface Coverage and Hybridization Efficiency of Thiol-Capped Oligonucleotides Bound to Gold Thin Films and Nanoparticles. *Anal. Chem.* **2000**, *72* (22), 5535–5541.

(105) Hurst, S. J.; Lytton-Jean, A. K. R.; Mirkin, C. a. Maximizing DNA Loading on a Range of Gold Nanoparticle Sizes. *Anal. Chem.* **2006**, *78* (24), 8313–8318.

(106) Zhang, X.; Servos, M. R.; Liu, J. Surface Science of DNA Adsorption onto Citrate-Capped Gold Nanoparticles. *Langmuir* **2012**, *28* (8), 3896–3902.

(107) Zhang, X.; Servos, M. R.; Liu, J. Instantaneous and Quantitative Functionalization of Gold Nanoparticles with Thiolated DNA Using a PH-Assisted and Surfactant-Free Route. *J. Am. Chem. Soc.* **2012**, *134* (17), 7266–7269.

(108) Zhang, X.; Servos, M. R.; Liu, J. Fast PH-Assisted Functionalization of Silver Nanoparticles with Monothiolated DNA. *Chem. Commun.* **2012**, *48* (81), 10114.

(109) Zhang, X.; Liu, B.; Dave, N.; Servos, M. R.; Liu, J. Instantaneous Attachment of an Ultrahigh Density of Nonthiolated DNA to Gold Nanoparticles and Its Applications. *Langmuir* **2012**, *28* (49), 17053–17060.

(110) Liu, B.; Liu, J. Methods for Preparing DNA-Functionalized Gold Nanoparticles, a Key Reagent of Bioanalytical Chemistry. *Anal. Methods* **2017**, *9* (18), 2633–2643.

(111) Doering, W. E.; Nie, S. Spectroscopic Tags Using Dye-Embedded Nanoparticles and Surface-Enhanced Raman Scattering. *Anal. Chem.* **2003**, *75* (22), 6171–6176.

(112) Qian, X.; Emory, S. R.; Nie, S. Anchoring Molecular Chromophores to Colloidal

Gold Nanocrystals: Surface-Enhanced Raman Evidence for Strong Electronic Coupling and Irreversible Structural Locking. *J. Am. Chem. Soc.* **2012**, *134* (4), 2000–2003.

(113) Lueck, H. B.; Daniel, D. C.; McHale, J. L. Resonance Raman Study of Solvent Effects on a Series of Triarylmethane Dyes. *J. Raman Spectrosc.* **1993**, *24* (6), 363–370.

(114) McKenzie, F.; Graham, D. Controlled Assembly of SERRS Active Oligonucleotide–Nanoparticle Conjugates. *Chem. Commun.* **2009**, No. 38, 5757.

(115) Zuker, M. Mfold Web Server for Nucleic Acid Folding and Hybridization Prediction. *Nucleic Acids Res.* **2003**, *31* (13), 3406–3415.

(116) Zhang, X.; Huang, P.-J. J.; Servos, M. R.; Liu, J. Effects of Polyethylene Glycol on DNA Adsorption and Hybridization on Gold Nanoparticles and Graphene Oxide. *Langmuir* **2012**, *28* (40), 14330–14337.

(117) Miyoshi, D.; Sugimoto, N. Molecular Crowding Effects on Structure and Stability of DNA. *Biochimie* **2008**, *90* (7), 1040–1051.

(118) Nakano, S.; Miyoshi, D.; Sugimoto, N. Effects of Molecular Crowding on the Structures, Interactions, and Functions of Nucleic Acids. *Chem. Rev.* **2014**, *114* (5), 2733–2758.

(119) Spink, C. H.; Chaires, J. B. Selective Stabilization of Triplex DNA by Poly(Ethylene Glycols). *J. Am. Chem. Soc.* **1995**, *117* (51), 12887–12888.

(120) Louie, D.; Serwer, P. Quantification of the Effect of Excluded Volume on Double-Stranded DNA. *J. Mol. Biol.* **1994**, *242* (4), 547–558.

(121) Knowles, D. B.; LaCroix, A. S.; Deines, N. F.; Shkel, I.; Record, M. T. Separation of Preferential Interaction and Excluded Volume Effects on DNA Duplex and Hairpin Stability. *Proc. Natl. Acad. Sci.* **2011**, *108* (31), 12699–12704.

(122) Menges, F. Spectragryph - Optical Spectroscopy Software. 2016.

(123) Gyllensten, U. B.; Erlich, H. A. Generation of Single-Stranded DNA by the Polymerase Chain Reaction and Its Application to Direct Sequencing of the HLA-DQA Locus. *Proc. Natl. Acad. Sci.* **1988**, *85* (20), 7652–7656.

(124) Sanchez, J. A.; Pierce, K. E.; Rice, J. E.; Wangh, L. J. Linear-After-The-Exponential (LATE)–PCR: An Advanced Method of Asymmetric PCR and Its Uses in Quantitative Real-Time Analysis. *Proc. Natl. Acad. Sci.* **2004**, *101* (7), 1933–1938.

(125) Pierce, K. E.; Sanchez, J. A.; Rice, J. E.; Wangh, L. J. Linear-After-The-Exponential (LATE)-PCR: Primer Design Criteria for High Yields of Specific Single-Stranded DNA and Improved Real-Time Detection. *Proc. Natl. Acad. Sci.* **2005**, *102* (24), 8609–8614.

(126) Dragan, A. I.; Pavlovic, R.; McGivney, J. B.; Casas-Finet, J. R.; Bishop, E. S.; Strouse, R. J.; Schenerman, M. A.; Geddes, C. D. SYBR Green I: Fluorescence Properties and Interaction with DNA. *J. Fluoresc.* **2012**, *22* (4), 1189–1199.

(127) Ririe, K. M.; Rasmussen, R. P.; Wittwer, C. T. Product Differentiation by Analysis of DNA Melting Curves during the Polymerase Chain Reaction. *Anal. Biochem.* **1997**, *245* (2), 154–160.

(128) Waterhouse, A. M.; Procter, J. B.; Martin, D. M. a; Clamp, M.; Barton, G. J. Jalview Version 2--a Multiple Sequence Alignment Editor and Analysis Workbench. *Bioinformatics* **2009**, *25* (9), 1189–1191.

(129) Vashist, S. K.; Luong, J. H. T. Bioanalytical Requirements and Regulatory Guidelines for Immunoassays. In *Handbook of Immunoassay Technologies*; Elsevier, 2018; pp 81–95.

(130) Shen, W.-H.; Hohn, B. DMSO Improves PCR Amplification of DNA with Complex Secondary Structure. *Trends Genet.* **1992**, *8* (7), 228.

(131) Gao, Y. Secondary Structure Effects on DNA Hybridization Kinetics: A Solution versus Surface Comparison. *Nucleic Acids Res.* **2006**, *34* (11), 3370–3377.

(132) Smith, B. D.; Dave, N.; Huang, P.-J. J.; Liu, J. Assembly of DNA-Functionalized Gold Nanoparticles with Gaps and Overhangs in Linker DNA. *J. Phys. Chem. C* **2011**, *115* (16), 7851–7857.

(133) Fields, B. S.; Benson, R. F.; Besser, R. E. Legionella and Legionnaires' Disease: 25 Years of Investigation. *Clin. Microbiol. Rev.* **2002**, *15* (3), 506–526.

(134) Albert-Weissenberger, C.; Cazalet, C.; Buchrieser, C. Legionella Pneumophila — a Human Pathogen That Co-Evolved with Fresh Water Protozoa. *Cell. Mol. Life Sci.* **2007**, *64* (4), 432–448.

(135) Fliermans, C. B.; Cherry, W. B.; Orrison, L. H.; Smith, S. J.; Tison, D. L.; Pope, D. H. Ecological Distribution of Legionella Pneumophila. *Appl. Environ. Microbiol.* **1981**, *41* (1), 9–16.

(136) Collins, S.; Jorgensen, F.; Willis, C.; Walker, J. Real-Time PCR to Supplement Gold-Standard Culture-Based Detection of Legionella in Environmental Samples. *J. Appl. Microbiol.* **2015**, *119* (4), 1158–1169.

(137) Mérault, N.; Rusniok, C.; Jarraud, S.; Gomez-Valero, L.; Cazalet, C.; Marin, M.; Brachet, E.; Aegerter, P.; Gaillard, J. L.; Etienne, J.; et al. Specific Real-Time PCR for Simultaneous Detection and Identification of Legionella Pneumophila Serogroup 1 in Water and Clinical Samples. *Appl. Environ. Microbiol.* **2011**, *77* (5), 1708–1717.

(138) Joda, H.; Beni, V.; Willems, A.; Frank, R.; Höth, J.; Lind, K.; Strömbom, L.; Katakis, I.; O´Sullivan, C. K. Modified Primers for Rapid and Direct Electrochemical Analysis of Coeliac Disease Associated HLA Alleles. *Biosens. Bioelectron.* **2015**, *73*, 64–70.

(139) Al-Madhagi, S.; Joda, H.; Jauset-Rubio, M.; Ortiz, M.; Katakis, I.; O'Sullivan, C. K. Isothermal Amplification Using Modified Primers for Rapid Electrochemical Analysis of Coeliac Disease Associated DQB1*02 HLA Allele. *Anal. Biochem.* **2018**, *556* (June), 16–22.

(140) Jauset-Rubio, M.; Svobodová, M.; Mairal, T.; McNeil, C.; Keegan, N.; El-Shahawi, M. S.; Bashammakh, A. S.; Alyoubi, A. O.; O'Sullivan, C. K. Aptamer Lateral Flow Assays for Ultrasensitive Detection of β-Conglutin Combining Recombinase Polymerase Amplification and Tailed Primers. *Anal. Chem.* **2016**, *88* (21), 10701–10709.

(141) Jauset-Rubio, M.; Svobodová, M.; Mairal, T.; McNeil, C.; Keegan, N.; Saeed, A.; Abbas, M. N.; El-Shahawi, M. S.; Bashammakh, A. S.; Alyoubi, A. O.; et al. Ultrasensitive, Rapid and Inexpensive Detection of DNA Using Paper Based Lateral Flow Assay. *Sci. Rep.* **2016**, *6* (1), 37732.

(142) Hermanson, G. T. The Reactions of Bioconjugation. In *Bioconjugate Techniques*; Elsevier, 2013; pp 229–258.

(143) Cazalet, C.; Jarraud, S.; Ghavi-Helm, Y.; Kunst, F.; Glaser, P.; Etienne, J.; Buchrieser, C. Multigenome Analysis Identifies a Worldwide Distributed Epidemic Legionella Pneumophila Clone That Emerged within a Highly Diverse Species. *Genome Res.* **2008**, *18* (3), 431–441.

(144) Piepenberg, O.; Armes, N. Recombinase Polymerase Amplification Reagents and Kits. 9,057,097 B2, 2015.

(145) Demers, L. M.; Mirkin, C. a; Mucic, R. C.; Reynolds, R. a; Letsinger, R. L.; Elghanian, R.; Viswanadham, G. A Fluorescence-Based Method for Determining the Surface Coverage and Hybridization Efficiency of Thiol-Capped Oligonucleotides Bound to Gold Thin Films and Nanoparticles. *Anal. Chem.* **2000**, *72* (22), 5535–5541.

(146) Li, Z.; Jin, R.; Mirkin, C. A.; Letsinger, R. L. Multiple Thiol-Anchor Capped DNA-Gold Nanoparticle Conjugates. *Nucleic Acids Res.* **2002**, *30* (7), 1558–1562.

(147) Laing, S.; Hernandez-Santana, A.; Sassmannshausen, J.; Asquith, D. L.; McInnes, I. B.; Faulds, K.; Graham, D. Quantitative Detection of Human Tumor Necrosis Factor α by a Resonance Raman Enzyme-Linked Immunosorbent Assay. *Anal. Chem.* **2011**, *83* (1), 297–302.

(148) Luo, G.; Yi, T.-T.; Jiang, B.; Guo, X.; Zhang, G. Betaine-Assisted Recombinase Polymerase Assay with Enhanced Specificity. *Anal. Biochem.* **2019**, *575* (February), 36–39.

(149) Rees, W. A.; Yager, T. D.; Korte, J.; Von Hippel, P. H. Betaine Can Eliminate the Base Pair Composition Dependence of DNA Melting. *Biochemistry* **1993**, *32* (1), 137–144.

(150) Henke, W.; Herdel, K.; Jung, K.; Schnorr, D.; Loening, S. A. Betaine Improves the PCR Amplification of GC-Rich DNA Sequences. *Nucleic Acids Res.* **1997**, *25* (19), 3957–3958.